UNIVERSIDAD NACIONAL AUTÓNOMA DE MÉXICO
POSGRADO EN CIENCIAS DE LA TIERRA
CENTRO DE GEOCIENCIAS
VULCANOLOGIA

ORIGEN Y EVOLUCIÓN DE LA CALDERA DE ILOPANGO, EL SALVADOR (CENTROAMÉRICA): UN SUPERVOLCÁN ACTIVO CON MÚLTIPLES ERUPCIONES EXPLOSIVAS CUATERNARIAS

Tesis con base en artículos científicos para optar por el grado de:

DOCTOR EN CIENCIAS DE LA TIERRA

PRESENTA

IVAN SUÑÉ PUCHOL

Director de Tesis:

Dr. Gerardo de Jesús Aguirre Díaz
POSGRADO EN CIENCIAS DE LA TIERRA

Juriquilla, Querétaro, Agosto 2019

Declaratoria de ética

Declaro conocer el Código de Ética de la Universidad Nacional Autónoma de México, plasmado en la Legislación Universitaria. Con base en las definiciones de integridad y honestidad ahí especificadas, aseguro mediante mi firma al calce que el presente trabajo es original y enteramente de mi autoría. Todas las citas de, o referencias a, la obra de otros autores aparecen debida y adecuadamente señaladas, así como acreditadas mediante los recursos editoriales convencionales.

Dedicatoria:

A toda la gran familia italo-catalana que estamos construyendo con el amor de mi vida…

A mis padres Joan y Marisa, por darme fuerza y confianza siempre, gracias por todo…

A mi hermano Xavi, la cunyi Nina y al nouvingut Victor, per compendrem i estar allí encara que hagi de ser massa per Skype…

Ai suoceri, fratelloni, cugini, zie e zii, grazie a tutti per volermi tanto bene…

A toda mi familia y amigos de México, El Salvador, Francia, Estados Unidos, Italia, Catalunya y España, gracias a todos por estar en mi vida y hacer posible toda esta aventura…

E sopratutto a te amore mio, grazie per essere la donna piú spettacolare del mondo mundial…ho hem tornat a fer, junts, com sempre and forever….

Agradecimientos

Primero que nada quiero agradecerle al Dr. Gerardo Aguirre todo lo que ha hecho por mi durante esta importante etapa de mi vida. Le doy las gracias por haber conseguido sacar lo mejor de mí y por la paciencia que ha necesitado para hacerlo. Gracias por su asesoramiento y por apoyar mi trabajo de campo y de laboratorio con el financiamiento de su proyecto de Ilopango "CONACYT-CB nº 240447. Gracias por la estancia en EUA, los congresos y los artículos que hemos conseguido.

Agradezco también a mi comité tutoral durante este doctorado: a la Dra. Lucia Capra, quien ha estado siempre disponible para aconsejarme y participar en todas las reuniones semestrales, y al Dr. Pablo Dávila Harris, quien a parte de asesorarme los 365 días del año, ha estado mil horas conmigo en el campo, me ha enseñado infinidad de cosas de valor incalculable y siempre ha estado listo para escucharme, como el buen amigo en el que se ha convertido para mí.

Quiero dar las gracias también al Consejo Nacional de Ciencias y Tecnología - CONACyT, por haberme concedido una de sus becas para estudiar doctorado en el programa de Posgrado de la UNAM, y por haber financiado el proyecto del Dr. Aguirre sobre la caldera de Ilopango (240447).

Mis más sincera gratitud a todo el personal del Ministerio de Medio Ambiente y Recursos Naturales – MARN y a la Policia Nacional Civil – PNC de El Salvador, porqué sin su apoyo en la logística y seguridad no se hubiera podido realizar el arduo trabajo de campo que se necesito para conseguir los objetivos de esta investigación. Gracias mi papá y mamá Salvadoreños Guayo y Guadalupe, a los hermanos Paco y Miguel, a la pequeña Emilia, a los tíos que me adoptaron para hacerme sentir como en casa en Sta. Tecla, a Luis, Walter, Demetrio, Fran, Douglas, Manuel, Celina, Victor, Willian, Fito, Jacky, Celia, J.A. Reyes, Don Angel, a todos, muchas gracias por la ayuda y el cariño.

Al mismo tiempo quiero agradecer a las personas que hicieron posible mi estancia en el Laboratorio Geocronológico en la Oregon State University de Corvallis (EUA). Muchas gracias a mi amigo el Dr. Dan Miggins por confiar en mi y brindarme esa oportunidad única. Gracias también al Dr. Anthony Koppers por permitirme usar uno de los más avanzados laboratorios de Ar/Ar del mundo. Gracias a Victoria, Anna, Seiko, Shan, Wolfang, James, Jake y a todos los demás colegas de la OSU.

Estoy muy agradecido con todos los co-autores que han participado en el trabajo y publicación de los artículos que conforman esta tesis, como mis grandes amigos Pierre Lacan, Dario Pedrazzi, Antonio Costa y Carlos Ortega, quienes me han ayudado en campo, en laboratorio y trabajo de gabinete, así como en la construcción y redacción de los artículos científicos.

A mis compañeros y amigos del CGEO que me ayudaron durante todos estos años y he podido compartir experiencias de vida irrepetibles, tanto a nivel académico como a nivel personal. Gracias especialmente a Gonzalo, que se animó a acompañarme en camioneta hasta San Salvador desde Querétaro para recoger las muestras de roca del Ilopango, gracias a Rorra, a Maria Isabel, Jaime, Berlaine, Diego, Gaby, Myrna, Mattia, Saul, Fito, Vania, Kurt, Eliseo, Paola, Paco, Walter, Rosario, Erik, y un largo etc., gracias por los asaditos, los partidos de fut, las fiestas y los follones que nos alegran la vida. Gracias también a todos los académicos y a toda la administración del CGEO, a los técnicos de laboratorio que me han ayudado, al Dr. Alex Iriondo, Manuel, Juan, Azucena, Blanca, Armando, Mariano, Carlos Mendoza, Dr. Juan Pablo Bernal, gracias a todos por haber hecho posible mi maestría y mi doctorado aquí con ustedes, y de una forma tan alegre, feliz e inolvidable. Quiero agradecer también a los doctores … por formar parte del comité de ésta tesis de Doctorado y por ayudarme a mejorar el trabajo.

Quiero agradecer también a todas las personas que he conocido en estos años en México y agradecerles, gracias a ti Migue y a toda tu familia Trujillo, gracias Cristian, Elvia, Carla, y a toda vuestra familia también, gracias a todos de todo corazón por tratarme como uno más de la familia. Gracias al grupo de viejetes del Padel con quien me lo pasaba tan bien jugando y riendo un rato, gracias a mi familia catalana de Quretaro: la Ester, Ferran, Joan, Aina, Jordi, Mireya, Abel amigo, Dario, Aldo, Berta y Arnau, Victor, Josep, Joan, Miquel, Oscar, gracies a tots per ser-hi.

Por último, quiero volver a agradecer a mi maravillosa familia, la qual he tenido tan lejos durante estos años, pero que gracias a Skype y Watsapp no se hace tan larga la distancia ni tan fuerte la anyoransa. Gracias a mis amigos de toda la vida, a la colla de Batea, al trenet de Masalio, ai amici di Perugia, al Edu, la Vane, a la Fanny, lo Mallo, a l'Agustí y especialmente gracias a mi esposa, al amor de mi vida, la persona más importante que tengo y con quien comparto esta aventura que es vivir, te amo Angela.

Índice

Resumen

La caldera de Ilopango es una estructura vulcano-tectónica con actividad en el Cuaternario, que causó grandes erupciones explosivas y afectando la parte central de El Salvador. Se originó hace 1.78 Ma, cuando el primer evento de colapso formó una caldera tipo graben, que dispersó una ignimbrita ~350 km^3 con un estilo eruptivo "*boiling-over*". Esta primera erupción formó la Ignimbrita Olocuilta, y cubre aproximadamente 2,000 km^2 de territorio con espesores de hasta 120 m. La cartografía geológica y levantamiento estratigráfico realizada en este estudio, complementada con correlación geoquímica y petrográfica, indican que la caldera de Ilopango produjo como mínimo 13 erupciones explosivas hasta la actualidad. La de mayor volumen fue la Ignimbrita Olocuilta. Las ignimbritas posteriores fueron de menor magnitud, pero todas con volúmenes superiores a 1 km^3 y VEI > 6. Cuatro de estas erupciones han ocurrido tan solo en los últimos 57 ka, siendo la última de todas la más conocida y mejor estudiada hasta el momento, la Tierra Blanca Joven (TBJ). Con esta investigación se ha definido por primera vez la historia volcánica explosiva de la caldera de Ilopango y la distribución de los depósitos piroclásticos asociados, así como un modelo sobre el posible origen vulcano-tectónico de la caldera y su evolución geológica.

La caldera de Ilopango es parte del Arco Volcánico de Centroamérica, el cual está asociado al magmatismo generado por la subducción de la placa de Cocos por debajo de la placa del Caribe. La caldera mide 17 x 13 km, está parcialmente ocupada por el lago de Ilopango y se localiza a lo largo de la Zona de Falla de El Salvador (ZFES), una franja estrecha y alargada de fallas laterales derechas, conectadas por cuencas "*pull- apart*". Concretamente, Ilopango se encuentra dentro de una de estas cuencas: el Pull- Apart de San Salvador. El origen y la evolución de la caldera está estrechamente ligado al desarrollo de éste *pull-apart*. Una prueba de esta posible relación vulcano-tectónica entre el Ilopango y las fallas regionales es la última erupción de la caldera, cuando se emplazó un domo intracratérico en el centro del lago (las Islas Quemadas) justo después de un terremoto tectónico ocurrido a finales del 1879.

El estudio geocronológico realizado en las 13 tobas identificadas, utilizando los métodos U/Pb, $^{238}U/^{230}Th$ y Ar^{39}/Ar^{40}, ha aportado nueva información para reconstruir la historia volcánica de la caldera de Ilopango. Acorde a la nomenclatura moderna en estratigrafía volcánica, se subdividió el Grupo Ilopango en tres formaciones: la Fm. Comalapa (tres erupciones, 1.78 – 1.34 Ma), la Fm. Altavista (6 erupciones, 918 – 257

ka), y la Fm. Tierras Blancas (4 erupciones, <57ka). Los depósitos producidos durante estas erupciones caldéricas son el producto de magmas calcoalcalinos ricos en Si y K (riodacitas), con plagioclasa, hornblenda y piroxeno. Los periodos de recurrencia son muy variables, desde más de 220 ka para las primeras erupciones, a ~100 ka en las erupciones intermedias, y ~20 ka para las últimas erupciones de la caldera. Destacan los largos tiempos de quietud entre las tres formaciones de hasta 400 ka, los cuales pueden estar relacionados a cambios en la tectónica regional de la ZFES.

El trabajo de vulcanología física realizado sobre el depósito de la TBJ, la última erupción explosiva de la caldera de Ilopango ocurrida hace tan solo unos 1500 años, detalla el tipo de procesos eruptivos que se originan en este volcán. El hidrovolcanismo producido por la interacción del magma con el agua del lago de Ilopango, determinó la intensa explosividad y la alta fragmentación durante la erupción de la TBJ, hasta tal punto que formó una nuve coignimbritica que envió ceniza hasta los 45 km de altitud. Los más de 30 km^3 DRE eyectados a la atmosfera durante esta erupción fueron catastróficos para las comunidades Mayas que vivían en la región.

Estudios geológicos completos en calderas volcano-tectónicas y multiepisódicas como la de Ilopango, son indispensables para evaluaciones futuras del peligro volcánico. Esta investigación describe la historia volcánica de la caldera y da una idea del potencial destructivo de la misma en caso de una nueva erupción. Los mapas de distribución obtenidos, así como la recurrencia estimada para las erupciones explosivas del Ilopango, brindan una primera aproximación a la amenaza que representa esta caldera, sobre todo para el área metropolitana de San Salvador y en general para Centroamérica y el sur de México.

Abstract

The Ilopango caldera is an active volcano-tectonic structure, which caused large explosive eruptions during the Quaternary affecting the central part of El Salvador. The first caldera collapse was at 1.78 Ma, and formed a graben-type caldera, producing a large ignimbrite-forming eruption of ~ 350 km^3. This first eruption formed the Olocuilta Ignimbrite, and covers approximately 2,000 km^2 with thicknesses up to 120 m. The geological cartography carried out in this study, complemented with geochemical and petrographic correlation, indicate that the Ilopango caldera produced at least 13 explosive eruptions until present day. The largest volume was that of the Olocuilta Ignimbrite. The later ignimbrites were of smaller magnitude, but all with volumes larger than to 1 km^3 and VEI> 6. Four of these eruptions have occurred in the last 57 ka, being the best known and most studied so far, as the last Tierra Blanca Joven (TBJ). This research has defined for the first time the explosive volcanic history of the Ilopango caldera and the distribution of the associated pyroclastic deposits, as well as a model on the possible vulcano-tectonic origin of the caldera and its geological evolution.

Ilopango caldera is part of the Central America Volcanic Arc, which is associated to the magmatism generated by the subduction of the Cocos plate beneath the Caribbean plate. The caldera′s size is 17 x 13 km, and is partially occupied by the Ilopango Lake. It is located along the El Salvador Fault Zone (ESFZ), a narrow and elongated strip of right lateral-faults, connected by *pull-apart* basins. Specifically, Ilopango is located within one of these basins: the *Pull-Apart* of San Salvador. The origin and evolution of the caldera is closely linked to the development of this pull- apart. A proof of this possible volcano-tectonic relationship with Ilopango and the regional faults is the last eruption of the caldera, when an intra-crateric dome was emplaced in the centre of the lake just after a tectonic earthquake occurred at the end of 1879 (the eruption of the Islas Quemadas, which means Burned Islands).

The geochronological study conducted on the 13 identified tuffs, using the U-Pb, $^{238}U/^{230}Th$ and Ar^{39}/Ar^{40} methods, has provided new information to reconstruct the volcanic history of the Ilopango caldera. According to the modern nomenclature in volcanic stratigraphy, the Ilopango Group was subdivided into three formations: the Comalapa Fm. (three eruptions, 1.78 - 1.34 Ma), the Altavista Fm. (6 eruptions, 918 - 257 ka), and the Tierras Blancas Fm. (4 eruptions, <57ka). The deposits formed during these calderic eruptions are the product of calc-alkaline magmas rich in Si and K (riodacites), with plagioclase, hornblende and pyroxene. The periods of recurrence are variable, from

more than 220 ka for the first eruptions, to ~ 100 ka in the intermediate eruptions, and ~ 20 ka for the last eruptions of the caldera. The long periods of quiescence between the three formations of up to 400 ka stand out, which may be related to changes in the regional tectonics of the ESFZ.

The physical volcanology work carried out on the TBJ deposit, the last explosive eruption of the Ilopango caldera that occurred only about 1500 years ago, describe the details of the eruptive processes originate in this volcano. The hidrovolcanism produced by the interaction of the magma with the water of the Ilopango Lake, determined the intense explosiveness and the high fragmentation during the eruption of the TBJ, to such an extent that the coignimbritic cloud reached more than 45 km of altitude. The more than 30 km^3 DRE ejected into the atmosphere during this eruption were catastrophic for the Mayan communities that lived in the region.

Complete geological studies in these multi-episodic volcano-tectonic calderas, such as Ilopango, are indispensable for future assessments of volcanic hazards. This research work describes the volcanic history of the caldera and provides an idea of the destructive potential of Ilopango in a probable future eruption. The distribution maps obtained, as well as the estimated recurrence for the explosive eruptions of Ilopango, provide a first approximation to the threat represented by this caldera, especially for the metropolitan area of San Salvador and in general for Central America and the south of Mexico.

1 Introducción

La caldera de Ilopango (CI) se localiza en la parte central de El Salvador, a menos de 10 km de la capital San Salvador, que con más de dos millones de habitantes, es la ciudad más poblada de Centroamérica (**Fig. 1**). La CI tiene una forma romboédrica, de 17 km de largo por 13 km de ancho, la cual está parcialmente rellenada por el lago de Ilopango, de casi 300 metros de profundidad. Esta caldera está activa y su último evento volcánico fue una erupción efusiva de un domo dacítico emplazado en el centro del lago, que formó las Islas Quemadas en 1879-1880 (Golombek y Carr, 1978; Richer et al., 2004). La última erupción explosiva de la CI ocurrió hace tan solo unos 1500 años y se conoce como la Tierra Blanca Joven (TBJ), la cual produjo un extenso depósito piroclástico blanco rio-dacítico (Williams y Meyer-Abich, 1955; Rose et al., 1999; Hernández, 2004; Kutterolf et al., 2008; Dull et al., 2001; Saxby et al., 2016; Aguirre- Díaz et al., 2017; Pedrazzi et al., 2018). La TBJ, con espesores de hasta 60 m de potencia y un volumen de emisión estimado de ~ 84 km^3 de material piroclástico (Dull et al., 2010), fue una de las erupciones más catastróficas del Holoceno en Centroamérica, cuyos efectos fueron devastadores para los asentamientos del imperio Maya ubicados en las cercanías de la caldera de Ilopango (Sheets, 1979; Dull et al., 2001). Aparte de la TBJ, la CI ha provocado otras tres grandes erupciones explosivas en los últimos 57,000 años (57 ka): la TB4, TB3 y TB2 (TB's; Rose et al., 1999; Hernández, 2004; Kutterolf et al., 2008). Otras ignimbritas más antiguas, estratigráficamente inferiores a las TB's, fueron reportadas en la zona por Hernandez et al., (2004).

Las calderas de colapso, como la de Ilopango, se forman por el hundimiento de bloques corticales dentro de una cámara magmática somera (Smith y Bailey, 1968; Lipman, 1997, 2000; Gottsmann y Martí, 2008). La subsidencia se produce a lo largo de fallas co-eruptivas, pero en algunos casos, las calderas utilizan fallas regionales preexistentes como discontinuidades corticales para colapsar, como sucedió durante el Oligoceno en la graben-caldera de Bolaños, en la Sierra Madre Occidental, México (Aguirre-Díaz y Labarthe- Hernández, 2003; Aguirre-Díaz et al., 2008). Algo así sucedió en el pasado, y sucede actualmente en la caldera de Ilopango, la cual fue formada en la Zona de Falla de El Salvador (ZFES, Martínez-Díaz, 2004), una franja

estrecha que cruza todo el país paralelamente al Arco Volcánico de El Salvador (AVES). Williams y Meyer-Abich (1955) describieron por primera vez la CI como una estructura vulcano-tectónica, la cual habría generado varias erupciones a lo largo de su actividad. Trabajos gravimétricos recientes de Saxby et al. (2016) confirman que la caldera de Ilopango tiene un control tectónico, donde las fallas verticales de la ZFES funcionan como una vía preferencial de extrusión de magma hasta la superficie (Tikoff y St. Blanquat, 1997).

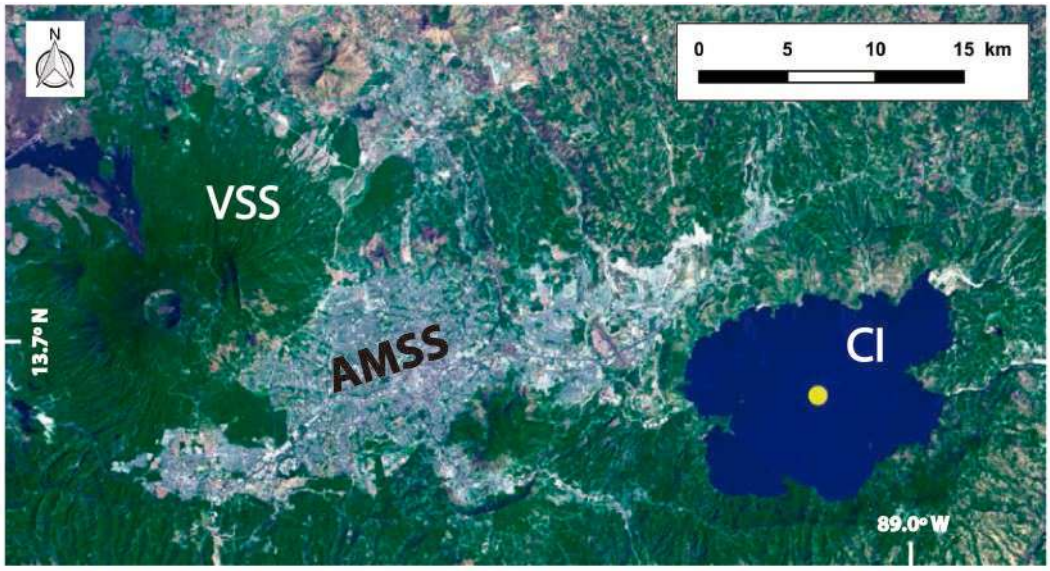

Fig. 1: Localización de la caldera de Ilopango (CI) junto al Área Metropolitana de San Salvador (AMSS), la cual se ubica entre ésta caldera y el volcán activo de San Salvador (VSS). Destaca la última colada de lava emitida por el VSS en 1917 (de color negro al nor-noreste del volcán). El punto amarillo en el centro del lago Ilopango representa la ubicación de las Islas Quemadas, producto de la última erupción de la caldera de Ilopango (1879-1880).

En este trabajo proponemos que Ilopango ha tenido grandes erupciones formadoras de extensas ignimbritas, asociadas a diferentes episodios de colapso caldérico (similar al complejo de Platoro en las montañas de San Juan, EUA, Lipman et al., 1996), y todas estas fases estarían relacionadas con la actividad y evolución de las fallas preexistentes de la ZFEZ (Soefield, 2004). La geomorfología del borde topográfico de la caldera de Ilopango, con varias bahías semicirculares, podría ser una evidencia de los múltiples eventos del colapso caldérico (Lexa et al., 2011). Durante esta investigación, se identificaron y caracterizaron todas estas erupciones y sus

respectivos depósitos generadas por la CI desde su formación, hace ~1.78 Ma, hasta la actualidad.

1.1. Marco teórico: calderas y supererupciones explosivas asociadas

Las calderas de colapso son las estructuras geológicas más peligrosas y las que han provocado las erupciones más voluminosas y catastróficas que se conocen en la Tierra, como por ejemplo la erupción de la caldera de Toba (Sumatra, Indonesia), cuya supererupción ocurrida hace 74 ka estuvo a punto de extinguir a los Homo Sapiens (Francis 1983; Rampino y Self, 1992). Estas superestructuras volcánicas se forman como consecuencia del colapso o subsidencia de grandes bloques corticales dentro de una cámara magmática somera, los cuales provocan la eyección explosiva y rápida de grandes volúmenes de material piroclástico a la atmosfera (Smith y Bailey, 1968; Druitt y Sparks, 1984; Cas y Wright, 1987; Lipman, 1997; Marti et al., 1994; Cole et al., 2005; Gottsmann y Martí, 2008). El resultado morfológico de este colapso caldérico es una depresión en el terreno de grandes dimensiones, rodeada por fallas sin-eruptivas que la bordean por donde se produce el hundimiento de los bloques, dejando a la vista la pared interna de la caldera y sobresaliendo el borde caldérico (**Fig. 2**). Los productos generados en este tipo de erupciones son mayormente depósitos de caída de pómez y ceniza, flujos piroclásticos formadores de ignimbritas, gases y emplazamientos de domos y coladas de lava post-colapso (Lipman 1984, 2000).

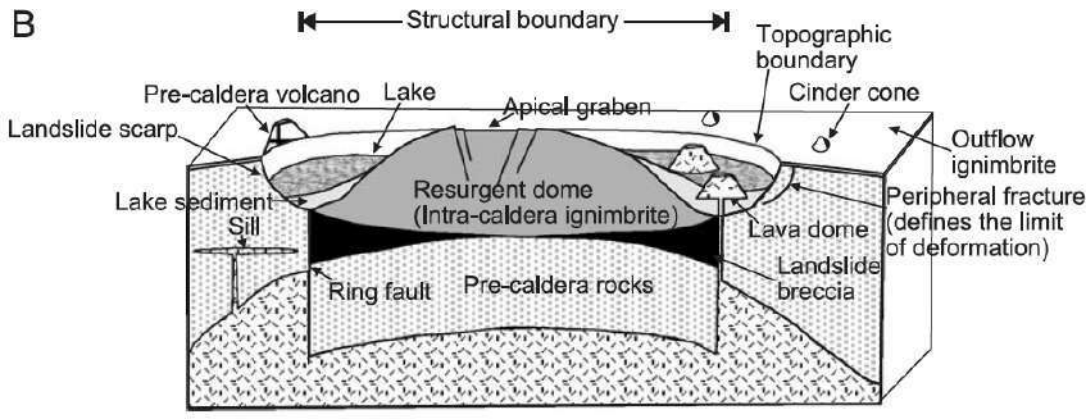

Fig. 2: Diagrama de una caldera de colapso tipo Pistón en 3D (Cole et al., 2005), donde se muestra esquemáticamente la estructura de estos complejos volcánicos.

Estas estructuras se encuentran en prácticamente todos los ambientes volcánicos de la tierra (Geyer y Martí, 2008; **Fig. 3**), como zonas de subducción (Toba; Francis 1983; Ilopango; Simkin y Siebert, 1994; Carr et al., 2007), *rifft* (Etiopia; Acocella et al., 2002) y *hot – spots,* tanto oceánicos (Las Cañadas, Islas Canarias, España; Schmincke, 1967; Marti y Gudmundsson, 2000), como continentales (Yellowstone, USA; Hildreth et al., 1984). La forma, génesis y el tamaño de una caldera es variable: algunas son circulares y con una sola fase de colapso (por ejemplo Reporoa, en Nueva Zelanda; Nairn et al., 1994; Beresford and Cole, 2000), mientras que otras son más alargadas, con tamaños que van de los pocos kilómetros hasta decenas de kilómetros (como Toba o La Garita, Colorado, USA; Lipmann 2000) y algunas forman parte de complejos caldéricos con varias fases de colapso (como el complejo Platoro, en San Juan Mountains; Lipman et al., 1996). Otras calderas están estrechamente ligadas a la tectónica, donde las fallas regionales condicionan desde la formación hasta el tipo de actividad volcánica de estas calderas (como la graben caldera de Bolaños, en la Sierra Madre Occidental de México, Jalisco; Aguirre- Díaz and Labarthe-Hernández, 2003; Aguirre-Díaz et al., 2008).

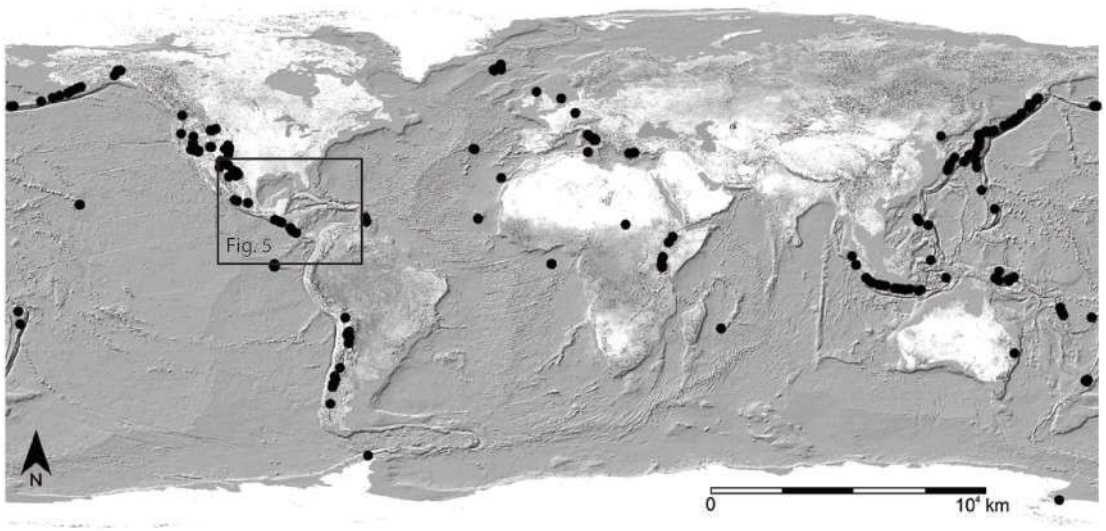

Fig. 3: Mapa mundial con la localización (circulo negro) de las calderas de colapso conocidas (modificado de Geyer y Martí, 2008).

Las erupciones en calderas pueden ser explosivas o efusivas; sin embargo, las más voluminosas y violentas son las explosivas, que pueden emitir grandes cantidades de material piroclástico a la atmosfera en cuestión de horas a pocos días (por ejemplo, Newhall y Dzurisin, 1988; Lipman, 1997; Cole et al., 2005; Gottsmann y Martí, 2008;

Costa et al., 2014). Las calderas se pueden clasificar por su composición (basálticas, peralcalinas, andesitico-daciticas o rioliticas; Cole et al., 2005) o también por su estilo y grado de subsidencia (Lipman 1995, 1997, 2000; Acocella 2007, 2008; **Fig. 4**): 1) *Downsag* es el primer paso en el colapso gravitacional de una caldera, con una subsidencia limitada donde las fallas anulares del borde no se han formado todavía o no han atravesado por completo el techo de la caldera, plegando y fracturando los materiales de la corteza litosférica (calderas basálticas no-explosivas como las de Hawaii o las Galapagos, Walker 1988); 2) *Trap-door* es el siguiente paso de madurez en el proceso de colapso caldérico, en donde solamente se ha hundido un sector del techo de la cámara mediante la formación de parte de las fallas inversas que conformarán el anillo del borde (p. ej. Valles caldera, Nuevo México, USA; Heiken et al., 1986); 3) Se conoce como *Plate/piston* cuando el colapso caldérico es producido por la subsidencia de un único bloque dentro de la cámara magmática, hundido gravitacionalmente una vez desarrolladas por completo las fallas periféricas del borde caldérico (Crater Lake, Oregón, USA; Bacon 1983); 4) Una caldera con avanzado grado de subsidencia también puede colapsar en estilo *Piecemeal*, en donde el techo de la cámara magmática se rompe en diferentes bloques (p. ej. Glencoe Caldera; Moore and Kokelaar, 1997, 1998); 5) las calderas tipo *Funnel* mayormente se relacionan a calderas pequeñas (< 2 – 4 km) que al colapsar adquieren una geometría de embudo por medio de un conducto central, con fallas internas empinadas y de fallas de borde ausentes (Guayabo caldera, Costa Rica; Hallinan 1993).

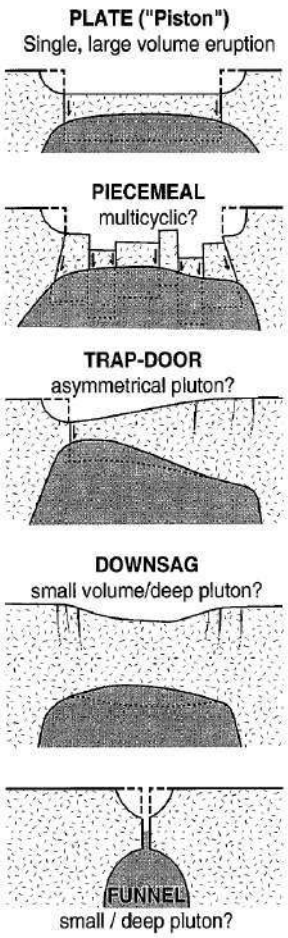

Fig. 4: Modelos de los cinco estilos de colapso propuestos por Lipman (1997)

Las calderas de colapso también se pueden clasificar dependiendo de su ubicación y relación con el contexto geológico regional donde se emplazó. La clasificación de Aguirre-Diaz (2008), define como caldera Somital, aquellas que se formaron en la parte alta de grandes estratovolcanes y asociadas a pequeños volúmenes emitidos de material

piroclástico (por ejemplo, Crater Lake en USA, el Somma – Vesubio en Italia o la caldera de San Pedro en volcán Temascalcingo, Estado de México; Roldán – Quintana y Aguirre – Díaz, 2006). Esta misma clasificación define como calderas Clásicas las que se forman en terrenos llanos, sin necesidad de la existencia de algún tipo de edificio volcánico anterior o estructuras tectónicas regionales (como por ejemplo Long Valley en USA o Los Humeros en el Estado de Puebla, México). El último tipo de caldera en la clasificación de Aguirre (2008), son las calderas tipo Graben, que son aquellas donde el techo de la cámara magmática colapsa a lo largo de fallas tectónicas regionales preexistentes en el terreno por donde se producen grandes erupciones fisurales (**Fig. 5**). Ejemplos de este tipo son varias calderas de Sierra Madre Occidental de México, como por ejemplo, el graben caldera de Bolaños (Aguirre-Díaz y Labarthe-Hernandez, 2003), o la misma caldera de Ilopango (El Salvador) como se define en este trabajo.

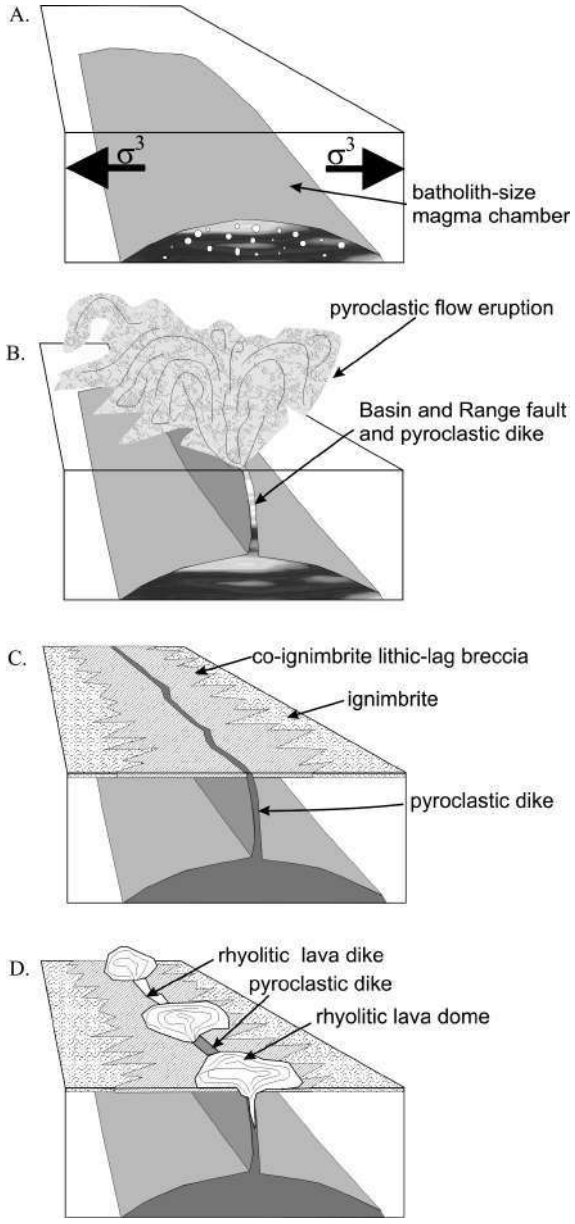

Fig. 5: Modelo esquemático que muestra el mecanismo de erupción fisural en las calderas del tipo Graben, en que los flujos piroclásticos salen a través de las fallas normales regionales (Aguirre-Díaz y Labarthe-Hernandez, 2003).

Las calderas de colapso de composición silícica son las únicas estructuras volcánicas capaces de provocar supererupciones explosivas, catalogadas como eventos que superan volúmenes emitidos de 450 km^3 DRE (Dense Rock Equivalent; Sparks et al., 2005; Self 2006), las cuales pueden llegar a VEI = 8 (el máximo Indice de Explosividad Volcánico; Newhal y Self,

1982). Este tipo de erupciones, aunque infrecuentes (una cada ~ 50,000 años), tienen un efecto catastrófico en las regiones circundantes a la caldera debido a lo destructivo que son sus productos (espesas caídas de pómez y enormes flujos piroclásticos), pudiendo incluso afectar a la estabilidad y el desarrollo de sociedades como ocurrió en la erupción de Santorini (Grecia, 1639-1530 a.C), la cual provocó el declive de la civilización Minoica (Nincovich y Hezzen, 1965; Sparks, 1979; Sigurdsson et al., 2006). Las supererupciones llegan a tener afectaciones globales, generando inviernos volcánicos que enfrían el clima terrestre. Inviernos volcánicos como el que ocurrió en la última gran erupción del Pinatubo en 1991 (Hansen et al. 1996), que sin llegar a niveles de supererupción, la ceniza fina y aerosoles dispersados en la estratosfera, provocaron absorción de la radiación solar y la consecuente bajada de temperatura (Self y Blake, 2008). Mucho más drásticos fueron los efectos de la supererupción de Toba, cuyas afectaciones climáticas pudieron acelerar y detonar el inicio de la última gran glaciación que ha sufrido el planeta Tierra (Rampino y Self, 1993).

Pero no todo son desventajas con las calderas volcánicas: son estructuras de alto interés económico, ya que la alta actividad geotérmica que producen las convierte en potenciales fuentes de energía renovable (p.ej. la Zona Volcánica de Taupo, Nueva Zelanda; Bibby et al., 1995). Además, son lugares favorables para la formación de depósitos minerales (Guillou – Frottier et al., 2000; Stix et al., 2003). En los últimos 25 años y gracias a la combinación entre el mapeo en calderas erosionadas (Lipman 1984, 1995, 2000a; Branney and Kokelaar, 1994; Aguirre – Díaz et al., 2003; 2007), al trabajo geodésico (Dvorak and Dzurisin, 1997) y al modelado analógico experimental (Marti et al., 1994; Acocella 2007, 2008), se ha adelantado mucho en el conocimiento y entendimiento de los procesos de formación y dinámica del colapso de las calderas volcánicas.

1.2. Marco geológico: tectónica, geodinámica y volcanismo en El Salvador

La caldera de Ilopango se ubica en la República de El Salvador y es uno de los volcanes más activos del Arco Volcánico Centroamericano (AVC), el cual se extiende desde la frontera México-Guatemala hasta Costa Rica y forma parte del Anillo de Fuego del Pacífico (Simkin y Siebert, 1994; Carr et al., 2007; Smithsonian Global Volcanism Program, 2013). El territorio salvadoreño se encuentra en la costa Pacífica de la placa del Caribe. A unos 200 km al norte de San Salvador, se encuentra el límite con la placa de

Norteamérica, donde las fallas laterales izquierdas del sistema Polochic-Motagua-Swan Islands están desplazando la placa del Caribe hacia el Este a una velocidad promedio de 8 mm/año (**Fig. 6a;** Agostini et al., 2006; DeMets, 2001; Funk et al., 2009; Guzmán-Speziale et al., 2005).

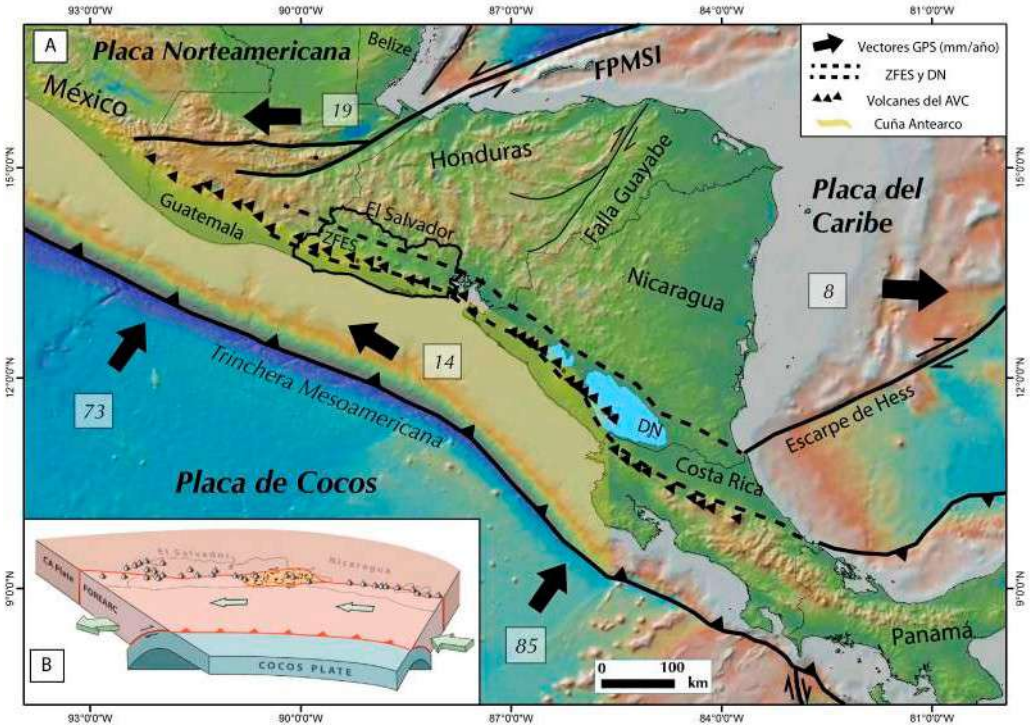

Fig. 6: A) Contexto geodinámico de El Salvador con las diferentes placas tectónicas que conforman Centroamérica. La Zona de Falla de El Salvador (ZFES) y la Depresión de Nicaragua (DN), asociadas a la subducción de la placa de Cocos por debajo de la placa Caribe, transcurren paralelamente al Arco Volcánico de Centroamérica (AVC). FPMSI: Fallas Polochic-Motagua-Swan Islands. B) Esquema 3D donde se muestra el desplazamiento lateral de la cuña trasarco entre la Trinchera Mesoamericana y el AVC, formando a su vez el pull-apart del golfo de Fonseca que separa El Salvador de Nicaragua (modificado de Alvarado et al., 2011).

El magmatismo de la caldera de Ilopango y del AVC en general, está relacionado con la subducción oblicua de Cocos por debajo de la placa del Caribe (LaFemina et al., 2009), desarrollada a lo largo de la trinchera mesoamericana a una velocidad promedio de 73 - 85 mm / año (Dixon, 1993; Mann, 2007). Esta subducción oblicua, junto con el efecto cremallera producido en el punto triple de Guatemala (Authemayou et al., 2011) y el desacople de la interfaz provocada

por el *roll-back* del *slab* de Cocos por debajo de la placa Caribe (Alonso-Henar, et al., 2015; 2017) habrían provocado el inicio del deslizamiento de la cuña *forearc* (o antearco) hacia el NW, paralela a la trinchera mesoamericana y con una velocidad actual de 8-14 mm/año con respecto a la placa Caribe (**Fig. 6**; Turner et al., 2007).

La combinación de estos dos movimientos relativos: 1) el movimiento hacia el Este de la placa del Caribe que provoca una extensión de trasarco, y 2) el desplazamiento hacia el Noroeste del antearco centroamericano, son aparentemente los responsables de la deformación trans-tensional a lo largo del AVC por medio de una serie de fallas laterales derechas *en-echelon* y conectadas por cuencas *pull-apart* (Montero y Dewey 1982; DeMets 2001, La Femina et al., 2002, Corti et al., 2005; Agostini et al., 2006, Turner et al., 2007; Funk et al., 2009; Canora et al., 2014), conocido como la Zona de Falla de El Salvador (ZFES, Martínez-Díaz, 2004). Uno de estos *pull-apart* es el del Golfo de Fonseca, que transfiere la deformación desde la ZFES hacia la Depresión de Nicaragua (Alvarado et al., 2011, **Fig. 6b**). La CI se encuentra dentro de una de estas cuencas tectónicas desarrollada en la parte central del país y conocida como el *Pull-Apart* de San Salvador (Garibaldi, et al., 2016), el cual se delimita al norte por la falla de Guaycume, la falla de la Cordillera del Bálsamo al sur, la falla de Zapotitan al Oeste y la de San Vicente al Este (**Fig. 7**). Esta última falla, con fuerte componente lateral derecho, está afectando la CI en su flanco oriental y es la causante del último gran terremoto de Mw 6.7 producido en la ESFZ en febrero de 2001 (Alvarenga et al. , 2001; Martínez Díaz et al., 2004; Canora et al., 2012; **Fig. 7**). Contextos tectónicos regionales como el que aporta el ZFES, el cual incluye fallas de desgarre, zonas de cizalla y cuencas *pull-apart*, favorecen el emplazamiento de centros magmáticos en niveles superficiales de la corteza y sirven como vías iniciales para el ascenso de magma (Hutton y Reavy, 1992).

Litológicamente, El Salvador está compuesto principalmente por rocas volcánicas de edades que van desde el Paleógeno superior hasta el presente (Donelly et al., 1990, Rose et al., 1999). Según el mapa geológico escala 1: 500,000 de El Salvador (Weber et al., 1974), el basamento está compuesto principalmente de calizas Jurásico-Cretácicas de la Formación Metapán, expuestas esporádicamente en la parte Noroeste del país y cubriendo menos del 5% de la superficie total de El Salvador. En el Oligoceno empezó el volcanismo, el cual se concentró en la parte más

septentrional del país formando la Montaña Fronteriza: una cordillera formada por los remanentes de los volcanes más antiguos de El Salvador y que delimita de forma natural, la frontera política del este país con Honduras (**Fig. 7**). Los productos de estos primeros volcanes que se emplazaron hace ~30 Ma, van desde ignimbritas silícicas hasta efusivas básicas a intermedias-acidas que constituyen las formaciones geológicas de Morazán y Chalatenango.

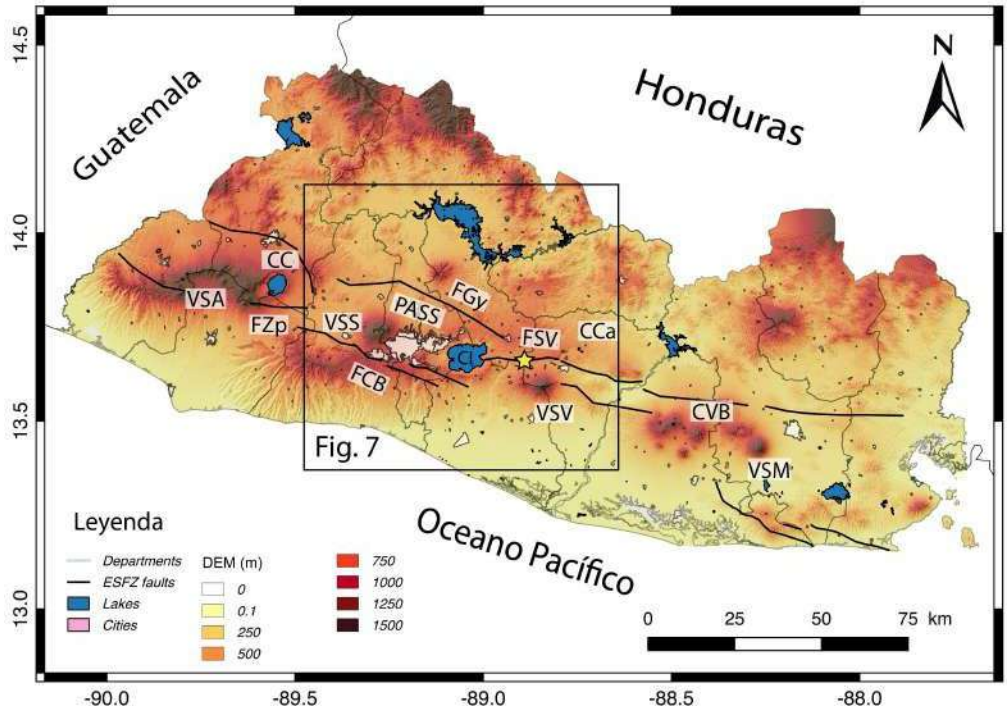

Fig. 7: Modelo Digital de Elevacion (DEM) de El Salvador donde se indican las fallas de la Zona de Falla de El Salvador (ZFES) y los principales volcanes del Arco Volcánico de El Salvador (AVES): Caldera de Coatepeque: CC, Volcán Santa Ana: VSA, Volcán San Salvador: VSS, Volcán San Vicente: VSV, Caldera Carboneras: CCa, Complejo Volcánico Berlín: CVB y Volcán San Miguel: VSM. El cuadrado negro nos indica la zona de estudio de esta investigación alrededor de la caldera de Ilopango (CI), la cual se localiza dentro del *Pull-Apart* de San Salvador, rodeado por la Falla San Vicente (FSV), la Falla Gaycume (FGy), la Falla de la Cordillera del Bálsamo (FCB) y la Falla del Zapotitán (FZp).

Desde el Mioceno, la actividad volcánica migró hacia el sur y se acercó a la Trinchera Mesoamericana, como consecuencia del *roll-back* de la placa subducida de Cocos (Carr 1976; Weinberg 1992, Alvarado et al, 2011, Alonso-Henar et al., 2015; 2017). El vulcanismo desde mediados del Mioceno hasta el Plioceno formó grandes estratovolcanes basálticos y andesíticos justo al sur del actual Arco Volcánico de El

Salvador (AVES); como el volcán Panchinmalco, el Jayaque o el mismo antiguo volcán de Ilopango, los cuales pertenecen a la Formación Bálsamo (Weber et al., 1974; Lexa et al., 2011). Durante el Plioceno-Pleistoceno, estos edificios volcánicos colapsaron gravitacionalmente asociados a la formación y evolución de la ZFES, formando las calderas de Plan de Renderos, Jayaque, la Carboneras y la CI (**Fig. 8**), cuyos productos piroclásticos fueron rellenando las depresiones tectónicas desarrolladas a lo largo de la ZFES y corresponden a la Formación Cuscatlán (Weber et al., 1974). Los relictos de estos grandes estratovolcanes antiguos forman la Cordillera de Bálsamo (**Fig. 8**, Williams y Meyer-Abich, 1955).

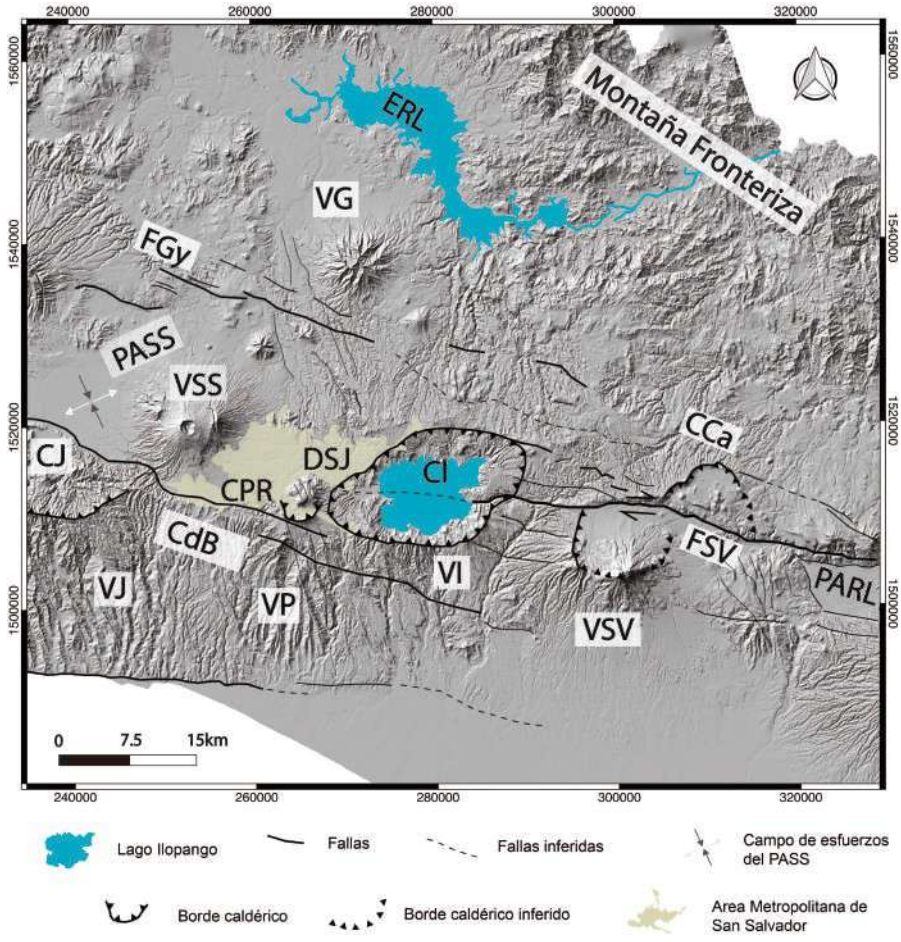

Fig. 8: Área de estudio con la caldera de Ilopango (CI) ubicada dentro del *Pull-Apart* de San Salvador (PASS) y rodeada por la mayor zona urbana del país. Volcán Panchinmalco: VP, volcán Jayaque: VJ, volcán de Ilopango: VI, volcán San Vicente: VSV, volcán Guasapa: VG, caldera de Plan de Renderos: CPR, caldera Jayaque: CJ, caldera la Carboneras: CCa, Cordillera de Bálsamo: CdB, falla San Vicente: FSV, falla Guaycume: FGy, Pull-Apart rio Lempa: PARL y ERL: embalse Rio Lempa.

Actualmente el AVES comprende 21 volcanes activos, tres de los cuales han hecho erupción en el último siglo, el Santa Ana, el San Salvador y el San Miguel (**Fig. 7**; Siebert and Simkin, 2002). Los productos de estos volcanes, así como los de la caldera de Coatepeque y los materiales más recientes de la CI (TB4, TB3, TB2, TBJ y domos efusivos), abarcan desde el Pleistoceno superior hasta el Holoceno y forman parte de la Formación San Salvador (Weber et al., 1974; Reynolds, 1987; CEL, 1992; Rose et al., 1999; Mann, 2007; Hernández, 2004, 2010; Kutterolf et al., 2008; Lexa et al., 2011).

El marco tectónico de El Salvador es una pieza clave para la descripción de los procesos magmáticos y geoquímicos en la región. La mayoría de los volcanes basáltico-andesíticos activos de la zona se concentran dentro de las cuencas *pull-apart*, mientras que las calderas, de composiciones más silícicas, se localizan mayormente en la traza de las principales fallas laterales derechas del ESFS (Garibaldi et al., 2016), como es el caso de la caldera de Ilopango (Martínez-Díaz et al., 2004; Mann, 2007; Lexa et al., 2011; Saxby et al., 2016). Tal como ocurre en el AVC, en el AVES los volcanes se agrupan en diferentes centros eruptivos compuestos por varios conductos por donde se emplazaron volcanes, domos, conos y calderas. Los productos volcánicos emitidos a lo largo del AVES constituyen una asociación típicamente calcoalcalina de subducción, con composiciones que van desde basálticas a riolíticas (Carr et al., 2007).

1.3. Motivación, hipótesis y objetivos

El principal motivo para investigar la CI es que se trata de una estructura vulcano-tectónica activa y peligrosa para la población salvadoreña, de la cual no se habían estudiado con detalle las diferentes fases eruptivas. Prácticamente todos los estudios geológicos previos realizados sobre la caldera de Ilopango, se habían centrado en la última erupción explosiva TBJ. Por ahora existen pocas publicaciones que reporten detalles sobre las erupciones previas (como la TB4, TB3 y TB2), y no hay ningún trabajo vulcanológico que caracterice las ignimbritas relacionadas a las etapas de formación de la caldera. Con esta falta de información se desconocía el origen y la evolución de la caldera, así como la relación entre la actividad volcánica de la caldera y la actividad tectónica de las estructuras regionales de la ZFES, las cuales propongo son el mecanismo disparador de las erupciones de una caldera tipo *pull-apart*/graben.

La hipótesis de este trabajo es que la caldera de Ilopango pudo haber provocado

más de una docena de grandes erupciones explosivas por colapso en los últimos 2 Ma, muchas de ellas siendo incluso mayores en magnitud que la última erupción TBJ, a juzgar por los depósitos que afloran en sus alrededores. Es por eso que definir las múltiples fases volcánicas generadas desde su inicio, cuantificar la extensión y el volumen de los productos asociados, fecharlos para poder establecer los tiempos de recurrencia y determinar sus características físico-químicas, aportarían los datos geológicos necesarios para conocer mejor la naturaleza de la caldera de Ilopango y evaluar el riesgo que supondrían futuras erupciones paroxismales similares a la reciente TBJ.

Cabe señalar que, a pesar de que la TBJ es la unidad mejor estudiada de la caldera, antes de este estudio no se habían realizado mapas de isopacas e isopletas con suficientes puntos de medición y secciones estratigráficas, para así poder determinar de manera más confiable la distribución espacial, espesores y volumen de los productos piroclásticos asociados. Es por eso que en esta investigación se realizó un trabajo sistemático de la TBJ, para así poder definir su alcance más allá de las fronteras de El Salvador. Sin duda alguna, la caldera de Ilopango es uno de los volcanes más complejos y peligrosos del AVES, siendo la erupción TBJ uno de los eventos más grandes del Holoceno y finales del Pleistoceno en la zona de Centroamérica. Si ocurriera una nueva erupción tipo TB's hoy en día, afectaría de manera fatal a la sociedad salvadoreña, pudiendo perturbar en gran medida a la población de Centroamérica y México.

Objetivos específicos:

- Identificar el número de erupciones volcánicas explosivas de la caldera de Ilopango, para completar la historia volcánica junto con las últimas 4 erupciones piroclásticas conocidas como las Tierras Blancas (TB's < 57 ka).
- Caracterizar cada erupción explosiva identificada y sus depósitos asociados, determinar la distribución de los flujos piroclásticos, la composición química y mineralógica, sus edades, los estilos eruptivos y mecanismos de emplazamiento, etc.
- Calcular volúmenes de material eyectado de todas las unidades posibles y determinar la dispersión de la pómez /ceniza de caída de la TBJ mediante modelado numérico.
- Estimar el periodo de recurrencia y una evaluación preliminar de la peligrosidad volcánica que representa la caldera.

- Determinar el origen y la evolución vulcano-tectónica de la caldera.
- Publicar los resultados en revistas científicas, así como presentarlos en foros nacionales e internacionales.

1.4. Contenido de la tesis

En el Capítulo 1 se presenta una introducción de la tesis y el estado del arte de la caldera de Ilopango, además de los objetivos y motivos de la investigación. El Capítulo 2 describe la metodología utilizada, tanto para la recolección de datos de campo, incluyendo mapeo geológico, levantamiento estratigráfico y muestreo, como en el procesamiento, análisis e interpretación de datos de laboratorio, incluyendo los análisis geoquímicos, geocronológicos, petrográficos, y modelado numérico. En el último apartado de este capítulo se explica cómo se presentaron los resultados de estos análisis.

En el Capítulo 3 se presenta el trabajo geológico realizado para caracterizar las tres primeras grandes erupciones explosivas de la caldera de Ilopango. El análisis detallado y desde una perspectiva multidisciplinaria de las extensas ignimbritas formadas por estas tres primeras erupciones de la CI nos permite proponer un modelo conceptual sobre la formación y evolución de esta caldera desde un punto de vista vulcano-tectónico. En este capítulo se presentan datos (geocronológicos, petrológicos, estratigráficos, estructurales, etc.) que soportan las primeras interpretaciones de otros autores en que se sugiere que la actividad de caldera de Ilopango está estrechamente ligada a la actividad tectónica regional ZFES. El primer colapso de la CI fue del tipo graben caldera en un contexto extensional a lo largo del trasarco salvadoreño, y posteriormente, a medida que la ZFES evolucionaba hacia la provincia transtensiva que es hoy en día, fue colapsando como una *pull-apart* caldera vinculada al sistema de fallas laterales derechas (strike-slip) de la ZFES. Las primeras erupciones fueron las de mayor volumen de toda la historia volcánica de esta caldera poligenética, pudiendo llegar hasta los valores de las supererupciones (~350 km^3 DRE, Suñe-Puchol et al., 2019). Químicamente estos depósitos provienen de magmas calcoalcalinos muy evolucionados típicos de zonas de subducción, riolítas con alto contenido en potasio, con periodos de recurrencia largos de hasta 220 ka entre erupciones.

En el Capítulo 4 se presenta una revisión completa de la estratigrafía volcánica de la caldera Ilopango. Se propone una nueva nomenclatura de las unidades siguiendo las recomendaciones de Marti et al. (2018). Se define el Grupo Ilopango, subdividido en tres formaciones: 1) la Formación Comalapa (1.785 – 1.34 Ma), que incluye las tres primeras ignimbritas, presentadas en el capítulo anterior; 2) la Formación Altavista (918 – 257 ka), que incluye seis depósitos piroclásticos recién identificados y caracterizados, los cuales se presentan en este capítulo; y 3) la Formación Tierras Blancas (últimos 57 ka), que incluye a las últimas 4 erupciones explosivas, y las únicas que se habían documentado antes de esta tesis. Además, en el Capítulo 4 se presentan los datos detallados sobre las 6 erupciones de la Fm. Altavista, incluyendo datos estratigráficos, químicos, físicos, y geocronológicos, que nos permiten estimar la magnitud de cada erupción, los estilos eruptivos y procesos volcánicos, así como elaborar una historia volcánica detallada de la CI, así como los periodos de recurrencia de las grandes erupciones explosivas.

En el Capítulo 5 se presenta un trabajo centrado en la última erupción explosiva de la CI, la unidad conocida como Tierra Blanca Joven (TBJ), la cual cubre la parte central de El Salvador con gruesas capas de ceniza. En este capítulo se presenta los datos estratigráficos y vulcanológicos de los depósitos asociados a la TBJ, utilizados para describir las fases y los procesos eruptivos ocurridos a lo largo de esta gran erupción, así como para estimar el volumen aproximado (> 30 km^3 DRE) y modelar la dispersión de las cenizas y la distribución de los flujos piroclásticos. Durante este trabajo se encontraron las cenizas de la TBJ a distancias mayores de 120 km, tanto hacia el sureste (Golfo de Fonseca, frontera con Nicaragua y Honduras), como hacia el noroeste (en las pirámides de Tazumal, en la localidad de Chalchuapa).

Para cerrar la tesis, en el capítulo 6 se presenta una discusión integrando los resultados obtenidos y planteando futuros trabajos para, una vez establecida la geología general de caldera, se pueda abordar el tema del peligro volcánico bajo el que vive la población salvadoreña.

El Capítulo 7 presenta las conclusiones de este estudio involucrando el trabajo geológico, volcánico y estructural realizado en la CI.

2. Metodología

Para la realización del estudio geológico, vulcanológico y estructural llevado a cabo durante esta tesis sobre la caldera de Ilopango y sus productos eruptivos, la metodología utilizada se basó en trabajo de campo, análisis de laboratorio y posterior interpretación de resultados. Para ello, y antes de ir campo, se recopiló toda la bibliografía disponible de la zona. Los datos obtenidos, tanto de campo como de laboratorio se integraron en mapas y manuscritos, productos elaborados en una fase de gabinete para posterior publicación. En este capítulo se presentan todas las técnicas usadas y el procedimiento del trabajo subdivididos en 4 apartados donde se abarcan las metodologías en teledetección, campo, laboratorio y gabinete.

2.1. Recopilación bibliográfica y análisis del terreno por teledetección

En primer lugar, se realizó un trabajo exhaustivo para recopilar todos los datos geológicos, geoquímicos, geocronológicos, estructurales y de vulcanología en general publicados previamente sobre la CI. Se leyeron los primeros reportes sobre geología hechos en El Salvador como los de Williams y Meyer – Abich (1955) o Weyl (1957), para posteriormente centrarnos en los depósitos del Ilopango como es la TBJ (Hart y Steen – McIntyre, 1983; Vallance y Houghton, 1988; Dull et al., 2010), el resto de las TB's (Rose et al., 1999; Kutterolf et al., 2008;) y de las ignimbritas más antiguas emitidas por esta caldera (Hernández, 2004; Lexa et al., 2011). Se examinaron otros trabajos más enfocados en la estructura de la caldera de Ilopango, como la gravimetría de Saxby et al. (2016), los modelos analógicos de las strike-slip caldera de Holohan et al. (2008) y el estudio estructural en el *Pull-Apart* de San Salvador de Garibaldi et al. (2016). Además, se inspeccionó la extensa literatura existente que trata sobre el contexto geodinámico y tectónico de Centroamérica y El Salvador en general (De Mets, 2001; Martínez – Díaz et al., 2004; Corti et al., 2005; Funk et al., 2006; Carr et al., 2007; Alvarado et al., 2011; Alonso-Henar et al., 2015, 2017), para comprender mejor lo que está sucediendo actualmente en la zona de Ilopango y poder plantear hipótesis sobre el origen de esta caldera desde una perspectiva vulcano-tectónica.

Una vez familiarizados con la caldera de Ilopango y considerando todos los trabajos existentes hasta la fecha, delimitamos la zona de estudio en base al mapa geológico 1:500,000, realizado por la Misión alemana en los años 70 (Weber et al., 1974). Gracias a ese documento, pudimos acotar preliminarmente la extensión de los productos piroclásticos antiguos de la caldera de Ilopango. Es importante mencionar que en ese trabajo pionero de cartografía que abarcó todo el territorio salvadoreño, no se identificaron el número de erupciones explosivas que tuvo la CI previamente a las 4 TB's. Los productos piroclásticos más antiguos de la caldera de Ilopango se clasificaron en un mismo miembro, el "c1", dentro de la Formación Cuscatlán (colores beige en el mapa de la **Fig. 9**). Esta formación incluye todos los depósitos desde la formación de la CI hasta la erupción TB4, emitida hace ~57 ka por Ilopango y que sirve de marcador para el inicio de la formación San Salvador "S3" (en amarillo, **Fig. 9**).

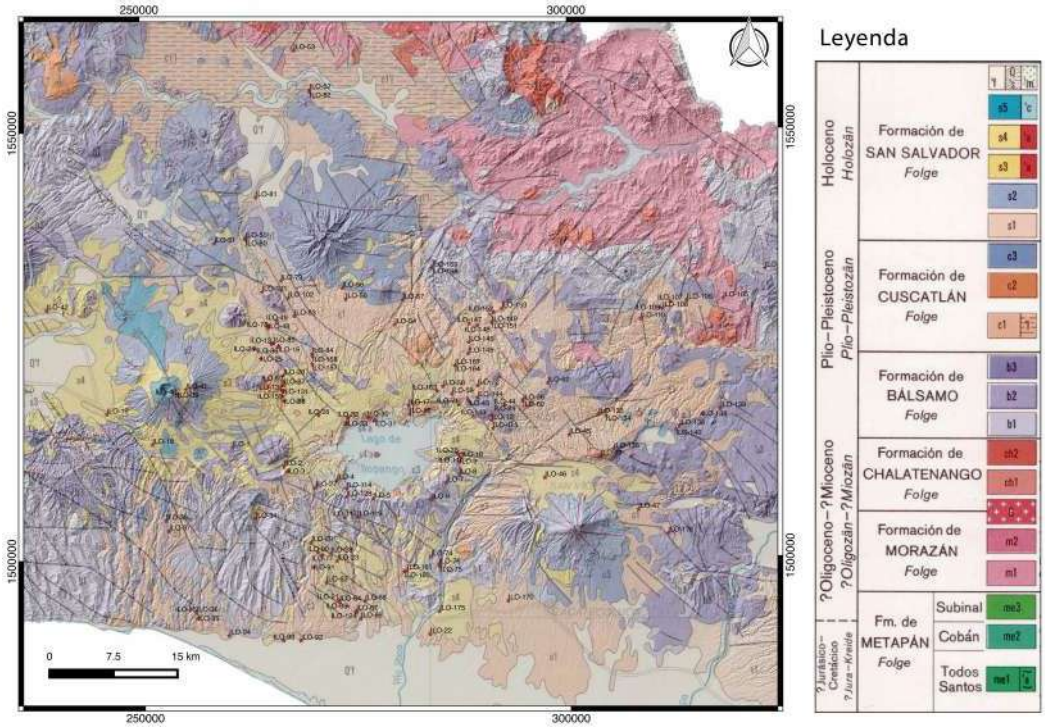

Fig. 9: Mapa geológico de la zona de estudio sobre el Modelo de Elevación Digital de 10 m (modificado de Weber et al., 1974).

El mapa geológico de Weber et al., (1974), originalmente analógico, se rasterizó y se georeferenció en un Sistema de Información Geográfica libre como es el QGis v. Las Palmas. Posteriormente se sobrepuso al Modelo de Elevación Digital terrestre de El Salvador, de 10 metros de precisión (DEM, **Fig. 9**), para así poder observar

conjuntamente la geomorfología de la zona y las formaciones litoestratigráficas. De esta manera elaboramos un primer mapa base donde poder organizar las salidas de campo y clasificar los datos ordenadamente. Concretamente el área de estudio delimitada ocupa unos 3,000 km^3 de territorio, localizada en la parte central de El Salvador. Por otro lado, utilizamos imágenes de satélite para determinar afloramientos potencialmente útiles, así como para identificar las principales vías de acceso y comunicación. Esto se hizo antes y durante el trabajo de campo, por medio de una Tablet con GPS para estar localizados en todo momento y hacer más efectivo el tiempo en el campo.

2.2. Trabajo de campo: levantamiento estratigráfico, mapeo y muestreo

Una vez establecida la zona de estudio y la posible distribución de los productos piroclásticos de la CI (**Fig. 9**), se procedió a organizar el trabajo de campo. El objetivo principal de esta fase del trabajo era realizar el mapeo geológico de la zona de estudio al completo y el levantamiento estratigráfico de todos los productos de interés de la caldera, para que una vez determinado el número de depósitos/erupciones y su distribución espacial mediante correlación, se pudiese proceder al muestreo ordenado de todas las unidades reconocidas y su posterior caracterización en laboratorio (geocronología, geoquímica, petrografía, etc.). Para ello se programaron hasta 8 campañas de trabajo de campo, que duraron entre 2 a 5 semanas cada una, y se extendieron desde 2015 a 2017. Aún con las dificultades que representa hacer campo en una zona tropical y muy cubierta por vegetación como es El Salvador, encontramos los suficientes afloramientos útiles para completar los propósitos de esta investigación. En total se realizaron alrededor de 350 puntos de observación, de los cuales se levantaron unas 200 secciones estratigráficas y se muestrearon todas las unidades litoestratigráficas necesarias para completar el estudio: desde las 13 ignimbritas emitidas por el Ilopango, hasta algunas de sus lavas y otras unidades procedentes de otros centros eruptivos (como el Volcán San Salvador, la caldera Carboneras o otras lavas viejas de la cordillera del Bálsamo). Cabe destacar que para realizar el trabajo de campo fue necesaria la colaboración logística por parte del Ministerio de Medio Ambiente y Recursos Naturales – MARN de El Salvador (vehículos y gente conocedora de la zona) y de la Policía Nacional Civil - PNC, quien nos aportó seguridad a la hora de trabajar en lugares conflictivos.

Parte de estas campañas de campo se dedicaron también para trabajar otros aspectos del proyecto de investigación dirigido por el Dr. Gerardo Aguirre, titulado "Peligrosidad para México de super-erupciones originadas en Centroamérica: El caso de

la caldera de Ilopango, El Salvador, y su influencia en el declive del Imperio Maya". Por ejemplo, conjuntamente con el Dr. Dario Pedrazzi y otros miembros del equipo, se realizó un trabajo sistemático de vulcanología física sobre la TBJ, con el objetivo de describir a detalle los procesos volcánicos de ésta última erupción explosiva ocurrida hace unos 1500 años (ver **capítulo 5** para más detalles). Además, se visitaron excavaciones en sitios arqueológicos como las pirámides de Tazumal o la de San Andrés (**Fig. 10a**), donde se pudo observar directamente la relación entre las cenizas de la TBJ y estas construcciones Mayas.

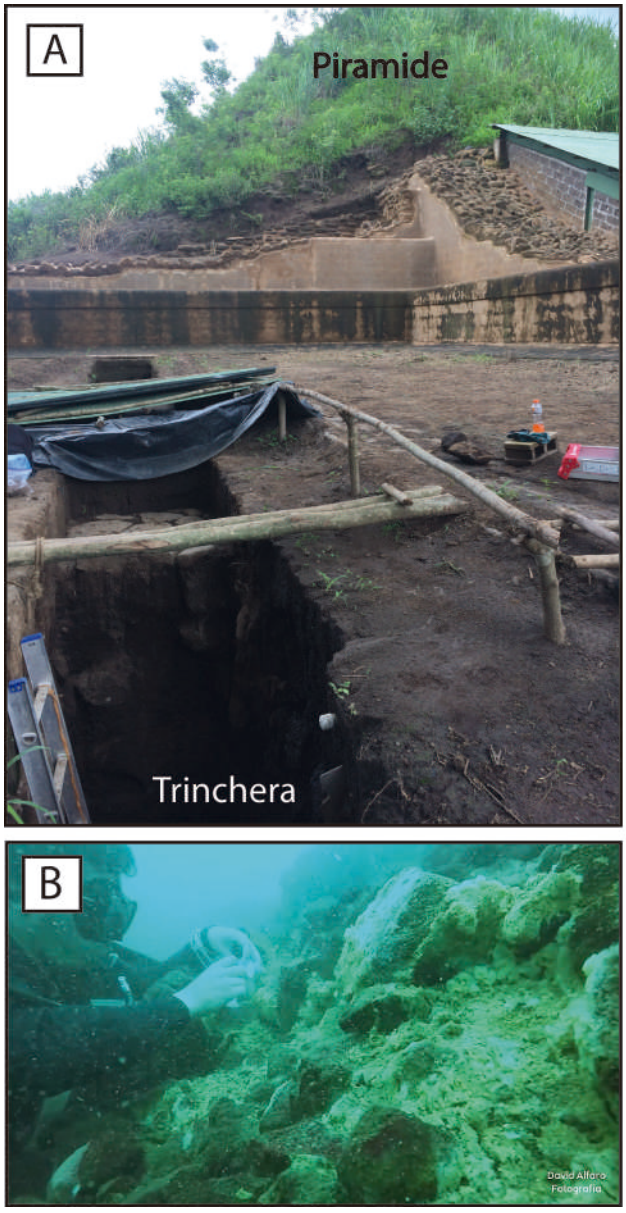

Fig. 10: a) Excavación al pie de la pirámide principal del sitio arqueológico de San Andrés, y **b)** muestreo de fluidos hidrotermales en el fondo del lago Ilopango (foto de David Alfaro).

En la última campaña de campo, y gracias a la disponibilidad de José Bairés y David Alfaro (buzos profesionales y expertos conocedores del Lago de Ilopango), nos sumergirnos a muestrear fluidos hidrotermales que emanan de forma continuada desde el fondo del lago de Ilopango (**Fig. 10d**). Todos estos datos de campo se recopilaron en varios formatos digitales: desde reportes de campo en documentos Word, tablas Excel, soporte en el Google Earth, etc. Las coordenadas geográficas se grabaron con un GPS portátil tipo Garmin, en sistema de proyección UTM (Datum: D_WGS_1984, zona 16P).

2.3. Envío de muestras y análisis en laboratorio

Las muestras recolectadas en campo se organizaron y clasificaron en las instalaciones del Observatorio Ambiental de El Salvador. Des de allí se enviaron las muestras más importantes y urgentes por paquetería hasta Querétaro (UPS y Correos de El Salvador), y así poder empezar los primeros análisis en los laboratorios del Centro de Geociencias (CGEO). El resto de muestras se fueron acumulando en un almacén del MARN hasta que nosotros mismos las fuimos a buscar por vía terrestre. Con una camioneta de la UNAM-CGEO, atravesamos las fronteras de Guatemala hasta llegar a San Salvador, donde cargamos unas 30 cajas de muestras de rocas y cenizas para llevárnoslas de regreso con nosotros hasta el campus Juriquilla. Una vez en Querétaro, la mayoría de muestras fueron analizadas en los laboratorios del CGEO (geocronología por circones, geoquímica de roca total, laminación para observación petrográfica, etc.), pero otras muestras fueron enviadas por DHL al campus de la Oregon State University (OSU) de Corvallis (EUA), en donde se analizaron para conseguir fechamientos por el método de $^{39}Ar/^{40}Ar$. Otras muestras de carbón se enviaron al laboratorio comercial Beta Analitic de Texas (EUA), para el fechamiento por el método del ^{14}C. También se enviaron muestras de vidrio de la TBJ a la Universidad de Oxford (UK) para realizar análisis por microsonda electrónica. A continuación se explican todos los métodos del trabajo de laboratorio utilizados en este estudio.

Geocronología: U/Pb, $^{238}U/^{230}Th$ y Ar^{39}/Ar^{40}

Un aporte destacable de esta tesis de doctorado es el estudio geocronológico realizado sobre los productos piroclásticos de la CI. Gracias a los fechamientos llevados a cabo usando métodos radiométricos como son el U/Pb, $^{238}U/^{230}Th$ y Ar^{39}/Ar^{40}, se ha podido descifrar, por primera vez, una historia volcánica más completa de la que se

conocía para esta caldera activa. En cuanto a la técnica del U/Pb y $^{238}U/^{230}Th$, el mineral utilizado para medir esta relación isotópica es el Circón ($ZrSiO_4$). Los circones son cristales muy resistentes a la intemperización, y por ello conforman un sistema cristalino prácticamente cerrado desde su formación. Es por eso que resultan muy útiles para medir la edad de las rocas que los contienen por medio del conteo isotópico U/Pb, o $^{238}U/^{230}Th$ para rocas más jóvenes de 350 ka.

En este caso, los circones se separaron a partir de fragmentos juveniles de pómez de cada ignimbrita o depósito de caída asociado a las diferentes erupciones de la caldera. Este trabajo se realizó en los laboratorios de Molienda y Separación de Minerales del CGEO, en donde se removieron los líticos pegados a los clastos de pómez para evitar fechar circones heredados. Luego se trituraron las pómez y se tamizaron hasta la fracción 74-44 μm (las dimensiones de la mayoría de circones de origen volcánico se encuentran en ese rango). Esa fracción pulverizada se lavó y se bateó para concentrar los minerales pesados (**Fig. 11a**). Después de secar ese concentrado a 70º C en el horno, se pasó la muestra por el Electroimán Frantz para separar los minerales magnéticos (**Fig. 11b**). La porción de minerales no magnéticos, reducida notablemente después de todo el proceso de separado, se introduce en una placa de Petri y se pican los circones uno a uno con la ayuda de una lupa binocular.

Una vez montados los suficientes circones en una probeta con resina endurecida (unos 50 para rocas volcánicas), se comprobó su pureza por catodoluminiscencia en el ELM-3R (Marshall, 1988) y luego fueron analizados por el técnico del Laboratorio de Estudios Isotópicos-LEI del CGEO, el Dr. Carlos Ortega Obregón, quien me supervisó y asesoró en todo el proceso de separación de circones. Para los fechamientos U/Pb se utilizó el espectrómetro Thermo ICAP Qc (LA-ICP-MS), con una resolución de 193 nm (Solari et al., 2010), y para los análisis U-Th el Thermo Neptune plus (Bernal et al. (2014). Una vez analizados los circones, se redujeron los datos usando el Isoplot software (v. 3. 7) para los análisis U-Pb (Ludwig, 2008) y el IntCal09 software para calibrar las edades U- Th (Reimer et al., 2009). Ver **capítulos 3 y 4** para más detalles y ejemplos de edades obtenidas en circones.

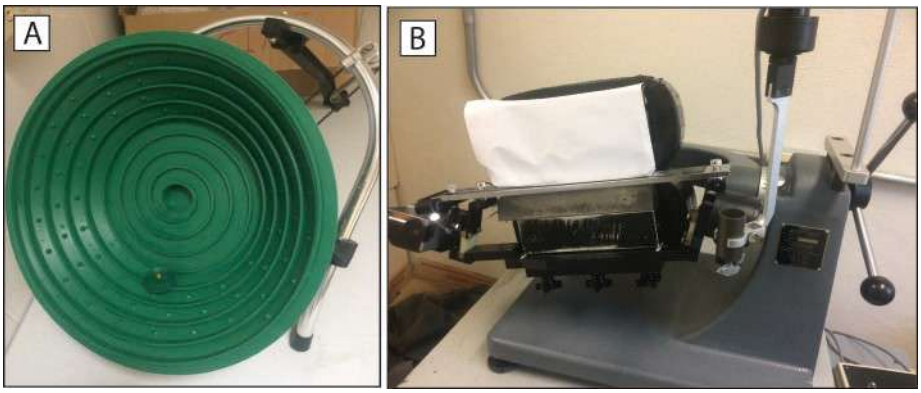

Fig. 11: a) Batea de plástico en espiral para lavar y concentrar mineral pesado, y **b)** Electroimán Frantz para separar minerales magnéticos.

Con la intención de complementar el estudio geocronológico y reforzar las edades obtenidas por el método U-Th-Pb, se realizó una estancia académica de 5 meses en el Laboratorio de Geocronología de la Oregon State University - OSU (Corvallis, EUA) para obtener edades $^{39}Ar/^{40}Ar$ de toda la secuencia piroclástica de la CI. En esta técnica, al igual que en el caso de los circones, se trituraron clastos de pómez juvenil para poder separar cristales apropiados en este tipo de fechamientos. Aunque los sanidinos son la fase mineral preferencial para este tipo de análisis en rocas jóvenes debido a su alto contenido en K y Ar, lamentablemente no se encontraron este tipo de cristales en ninguna unidad del Ilopango, así que básicamente se usaron plagioclasas y hornblendas.

La pómez triturada se tamizó y se lavó la fracción de 500-177 µm. Usando un ultrasonido se removió todo el polvo pegado al concentrado mineral. Los feldespatos fueron separados magnéticamente de los anfíboles y piroxenos usando un Frantz (como el de la **Fig. 11**), y luego fueron bañados en ácidos (HF, $HN0_3$ y HCL) para eliminar restos de vidrio pegados a los cristales (Koppers et al., 2011). Una vez secos se seleccionaron los mejores cristales (por tamaño, forma y pureza) y se empaquetaron para ser irradiados en el reactor nuclear TRIGA CLICIT de la Oregon State University conjuntamente con los sanidinos *Fish Canyon Tuff* de edad conocida (28.201 ± 0.023 Ma, 1σ; Kuiper et al. 2008), que sirvieron como estándares. Los concentrados minerales fueron analizados con la técnica "Incremental Heating" debido a que en cristales individuales de plagioclasa o de hornblenda no hay suficiente argón radiogénico para obtener resultados confiables (Rose et al., 1999). Los analisis se efectuaron con el espectrómetro de masas ARGUS-VI (**Fig. 12**), que con su láser de CO_2 y su multicolector de gases es capaz de medir los cinco isotopos de Ar simultáneamente (el

36, 37, 38, 39 y 40). Para conseguir la mayor precisión posible en cada fechamiento, se efectuaron un gran numero de pasos o "heating steps" (hasta 22-23 por muestra), en donde se median cada vez los 5 gases del argón subliminados durante el calentamiento del concentrado mineral por láser. Las edades se obtuvieron al reducir los datos con el software ArArCALC v2.5.1 (Koppers, 2002). Todo el proceso fue supervisado por el Dr. Dan Miggins, gerente del laboratorio del OSU. Para más detalles de esta técnica y ejemplos de edades $^{39}Ar/^{40}Ar$, ver **capítulos 3 y 4** de esta tesis.

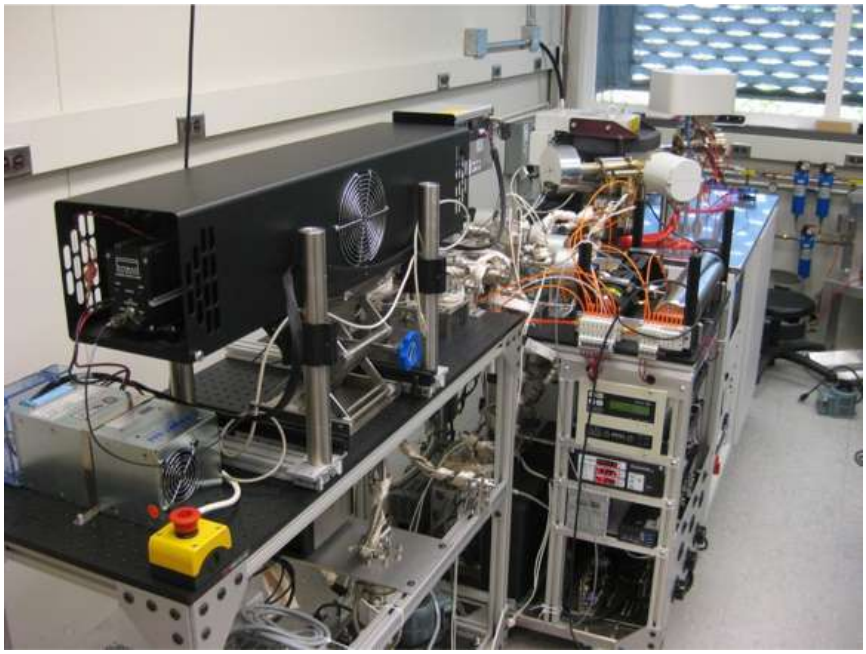

Fig. 12: Espectrómetro ARGUS VI con laser de CO2 y línea de extracción con multicolector (isótopos 36, 37, 38, 39 y 40 de Ar).

Geoquímica y Petrografía

Con el propósito de caracterizar químicamente y soportar la correlación estratigráfica de los productos piroclásticos de la CI, se llevaron a cabo análisis de roca total utilizando clastos de pómez juvenil, previamente secada en el horno a 80º C y limpiada cuidadosamente a mano para evitar contaminación. Las muestras se pulverizaron manualmente en un mortero de Ágata hasta homogenizar todo a 74 µm, usando una malla plástica del 200 nueva para cada muestra. Los elementos mayores fueron medidos por la Dr. Patricia Girón mediante el método de Fluorescencia de Rayos X en el Departamento de Geoquímica del Instituto de Geología de la UNAM (Ciudad de México), usando el espectrómetro X RIGAKU ZSX Primus II. Las Tierras Raras

(REE) y los elementos traza los midió la M. en C. Ofelia Pérez Arvizu en el Laboratorio de Estudios Isotópicos y utilizando el cuarto ultralimpio del CGEO. Los métodos y manejo de las muestras se describen en Bernal y Lozano-Santacruz (2005). Todos estos datos se ilustran en graficas tipo TAS (Total-Alkali-Silica, LeBas et al., 1986), Spider-multielements (tierras raras normalizadas al MORB, Sun and McDonough, 1989) y Harker (donde se plotea la concentración de varios elementos químicos en frente del SiO_2, como es el K; Pecerillo and Taylor, 1976). Para más detalles sobre estos análisis ver **capítulos 3 y 4.**

En cuanto a los análisis químicos en la TBJ, además de hacer los de roca total, se efectuaron otros estudios para conocer la composición del vidrio y así poder cuantificar la abundancia en elementos como el S^{-2}, el F^- y el Cl^- emitidos durante esa erupción y así evaluar su impacto ambiental. Estos nuevos análisis los realizó la Dra. Victoria Smith en el laboratorio de Arqueología e Historia del Arte de la Universidad de Oxford con el método de microsonda EPMA (wavelength-dispersive electron probe microanalysis). La sonda de electrones utilizada fue calibrada para cada elemento utilizando un mineral bien conocido como estándar, y se verificó este calibrado analizando el vidrio de referencia MPI-DING (Jochum et al., 2006). Para más detalles de este método ver **capítulo 5**.

En el taller de laminación del CGEO y bajo la supervisión del técnico Juan Vázquez, se prepararon láminas delgadas para observación petrográfica de los productos de la CI, y así poder caracterizar las texturas y la mineralogía de los depósitos volcánicos del Ilopango. Con una cámara incorporada a un microscopio del Laboratorio de Petrografía del CGEO, y con la colaboración del Dr. Alexander Iriondo, se sacaron microfotografías de todas las unidades de interés.

Otros análisis de laboratorio: Granulometría, 14C y dendrocronología

Como parte del estudio de vulcanología física sobre la TBJ, se realizaron análisis granulométricos en las muestras de pómez y ceniza recolectadas en campo con Dario Pedrazzi. Parte de estos análisis se efectuaron en los laboratorios del Observatorio Ambiental del MARN-El Salvador, donde se tamizaron en seco más de 141 muestras proximales, medias y distales, para así obtener la distribución del tamaño de grano y el porcentaje de componentes (rango de apertura de tamices desde −6 Φ a 3 Φ, donde Φ = – log2 □; d es el diámetro en mm). En el Laboratorio de Vulcanología Física del CGEO

se realizó la otra parte del análisis granulométrico. Con la ayuda de un MicroTec Analisette22 Fritsch, se hizo el tamizado húmedo, separando las fracciones de ceniza más fina (4 Φ a >10 Φ). El porcentaje de peso de cada fracción tamizada se calculó y se ploteó en curvas acumulativas (ver detalles en **capitulo 5**). Se hizo el conteo de los juveniles entre -5 a 0 Φ con la ayuda de una microscopio binocular, se fotografiaron y se identificaron los diferentes componentes. De esta manera, gracias al mapeo, al levantamiento estratigráfico, a estos resultados granulométricos y a los modelos numéricos posteriores que se presentan en la siguiente sección y en el **capítulo 5**, se pudieron determinar parámetros físicos de la erupción de la TBJ como son la altura de la columna eruptiva, la tasa de emisión, duración y dispersión de cenizas.

En el Laboratorio de Vulcanología Física del CGEO también se prepararon muestras de carbono que se encontraron incluidos en el depósito de la TBJ. Éstas se enviaron al laboratorio comercial de Beta Analitic (calidad ISO 17025) en Texas (EUA), para el fechamiento de esa erupción mediante el método de ^{14}C y AMS (Accelerator Mass Spectrometry).

2.4. Trabajo de gabinete: elaboración de mapas, digitalización de series estratigráficas, modelado numérico y estimación de parámetros físicos

En una etapa posterior al campo y los análisis de laboratorio, e integrando todos los datos obtenidos previamente, se generaron productos relevantes que se aportan en esta investigación y que forman parte de publicaciones en congresos y revistas indexadas. Estos son, por ejemplo, nuevos mapas georeferenciados en Qgis v. Las Palmas, donde se despliega la distribución espacial de todas las unidades piroclásticas identificadas de la CI, o series estratigráficas digitalizadas con el programa Adobe Ilustrator CS6, que además incluyen datos geocronológicos, estructurales y granulométricos (ver ejemplos en los **capítulos 3, 4 y 5**). En esta etapa de gabinete también se calcularon los volúmenes de los flujos piroclásticos del Ilopango por medio del método de Triangulación Deleuriana de Macedonio and Pareschi (1991), el cual utiliza el área ocupada por las ignimbritas, el espesor de la capa medida en diferentes puntos bien distribuidos espacialmente y el nivel 0 en los bordes del flujo, para así estimar un volumen de piroclastos por interpolación (ver **capítulo 3**). Estos volúmenes, los cuales se obtuvieron con la ayuda del Dr. Antonio Costa (miembro del proyecto Ilopango), después fueron transformados a Dense Rock Equivalent (DRE) siguiendo la metodología de Quane and Russell (2005). Para estimar el volumen de las caídas de

tefra de la erupción TBJ, el Dr. Dario Pedrazzi (miembro del proyecto Ilopango) reconstruyó los mapas de isopacas a partir de los datos recolectados en campo y los resultados de análisis granulométricos. Posteriormente se utilizaron métodos basados en adelgazamiento logarítmico de los depósitos (Bonadonna y Costa, 2012; 2013). Para modelar la dispersión de las cenizas de esta erupción TBJ el Dr. Antonio Costa utilizó el software HAZMAP (Macedonio et al., 2005). A partir de la inversa del volumen se pudo estimar la altura de la columna (Costa et al., 2009) y la tasa eruptiva (Mastin et al., 2009). Ver **capitulo 5** para más detalles.

3. Descripción de las primeras erupciones formadoras de extensas ignimbritas por la caldera de Ilopango, una estructura vulcano-tectónica tipo graben/pull-apart en El Salvador.

Artículo: Suñe-Puchol, I., Aguirre-Díaz, G.J., Dávila-Harris, P., Miggins, D.P., Pedrazzi, D., Costa, A., Ortega-Obregón, C., Lacan, P., Hernández, W., Gutiérrez, E., 2019. The Ilopango caldera complex , El Salvador : Origin and early ignimbrite-forming eruptions of a graben / pull-apart caldera structure. J. Volcanol. Geotherm. Res. 371, 1–19. doi:10.1016/j.jvolgeores.2018.12.004

Contribuciones individuales de los autores:

- **Ivan Suñé Puchol:** diseño y organización del estudio, trabajo de campo y de laboratorio, procesamiento, análisis e interpretación de datos, redacción del artículo.
- **Gerardo Aguirre Díaz:** financiamiento, concepción y plan de trabajo, supervisión, trabajo de campo, interpretación de los datos, revisión del artículo.
- **Pablo Dávila Harris:** diseño y supervisión del estudio, trabajo de campo, interpretación de datos y corrección del artículo.
- **Dan Miggins:** supervisión en laboratorio y en procesamiento e interpretación de fechamientos Ar/Ar, corrección del artículo.
- **Dario Pedrazzi:** trabajo de campo, interpretación de datos y corrección del artículo.
- **Antonio Costa:** trabajo de campo y cálculo de volumen de la ignimbritas mediante modelos numéricos.
- **Carlos Ortega Obregón:** supervisión en laboratorio y fechamientos U-Pb, procesamiento e interpretación de datos geocronológicos.
- **Pierre Lacan:** trabajo de campo e interpretación de datos vulcano-tectónicos.
- **Walter Hernández:** trabajo de campo e interpretación de la geología de la zona.
- **Eduardo Gutiérrez:** apoyo logístico y trabajo de campo.

Journal of Volcanology and Geothermal Research 371 (2019) 1-19

Contents lists available at ScienceDirect

Journal of Volcanology and Geothermal Research

jour nal homepage: www.elsevier. com/ locate/ jvolgeores

The Ilopango caldera complex, El Salvador: Origin and early ignimbrite-forming eruptions of a graben/pull-apart caldera structure

Ivan Suñe-Puchol [a,*], Gerardo J. Aguirre-Díaz [a], Pablo Dávila-Harris [b], Daniel P. Miggins [c], Dario Pedrazzi [d], Antonio Costa [e], Carlos Ortega-Obregón [a], Pierre Lacan [a], Walter Hernández [f], Eduardo Gutiérrez [f]

[a] Centro de Geociencias, Universidad Nacional Autónoma de México, Blvd. Juriquilla 3001, Campus UNAM-Juriquilla, Querétaro, 76230, Mexico
[b] División de Geociencias Aplicadas, IPICYT, San Luis Potosí 78216, Mexico
[c] College of Earth, Ocean and Atmospheric Sciences, Oregon State University, 104 CEOAS Administration Building, 101 SW 26th St, Corvallis, OR 97331, USA
[d] ICTJA, CSIC, Group of Volcanology, SIMGEO UB-CSIC, Institute of Earth Sciences Jaume Almera, Lluis Sole i Sabaris s/n, 08028 Barcelona, Spain
[e] Istituto Nazionale di Geofisica e Vulcanologia, INGV-Bologna, Via Donato Creti, 12, 40100 Bologna, Italy
[f] Gerencia de Geología del Observatorio Ambiental, Ministerio de Medio Ambiente y Recursos Naturales MARN, San Salvador 76230, El Salvador

a r t i c l e i n f o

Article history:
Received 3 August 2018
Received in revised form 4 December 2018
Accepted 6 December 2018
Available online 17 December 2018

Keywords:
Central America Volcanic Arc
Tectono-volcanism
El Salvador Fault Zone
Fissure eruption
Hydromagmatism

a b s t r a c t

The Ilopango caldera is located in the central part of El Salvador, within the right-lateral El Salvador Fault System (ESFZ) and adjacent to the capital city of San Salvador. The caldera has a polygonal shape of 17 × 13 km and hosts an intra-caldera lake. Ilopango caldera had multiple collapse eruptions that formed widespread and voluminous silicic ignimbrites. Volcanic activity of the caldera has been controlled by strike-slip faults of the ESFZ. In this work we present the geological characteristics of the first three ignimbrite-forming eruptions of Ilopango caldera, providing an interpretation of the origin and initial stages of the volcanic evolution of this caldera complex. An initial extensional regime of the ESFZ possibly developed a graben at or near the actual Ilopango caldera, where the graben's master faults worked as fissure vents during the first caldera collapse. The Olocuilta Ignimbrite was emplaced at 1.785 ± 0.01 Ma BP, with a Dense Rock Equivalent (DRE) volume N 50 km³ (probably ~300 km³). The ESFZ stress gradually changed from extensive to transtensive, inducing the second collapse associated with a pull-apart caldera, producing the Colima Ignimbrite at 1.56 ± 0.01 Ma BP, with a DRE volume of N11 km³. The transtensive regime increased along the ESFZ, producing the third collapse in the pull-apart graben caldera apparently affected by the newly formed strike-slip San Vicente Fault. This phase corresponds to the explosive eruption that formed the Apopa Ignimbrite at ~1.34 Ma BP, with N9 km³ DRE volume. The latter ignimbrite marks a change in the eruptive style producing hydromagmatic pyroclastic flows followed by a dense ignimbrite with coignimbrite lithic breccias. These features suggest the involvement of water that could come from a paleollopango lake within the caldera depression associated with the second caldera collapse at 1.56 Ma BP. Ilopango is thus a multistage caldera system associated with the largest explosive events registered in El Salvador so far.

1. Introduction

Collapse calderas are formed by the subsidence of crustal blocks along bounding faults into a shallow chamber during the fast evacuation of magma (Smith and Bailey, 1968; Druitt and Sparks, 1984; Lipman, 1997, 2000; Gottsmann and Martí, 2008). Caldera eruptions can be explosive or effusive; but, the most catastrophic and voluminous are the explosive ones that can erupt massively large volumes of pyroclastic material within hours to few days (e.g., Newhall and Dzurisin, 1988; Lipman, 1997; Cole et al., 2005; Gottsmann and Martí, 2008; Costa et al., 2014; Costa and Marti, 2016). Silicic collapse calderas are associated with infrequent but catastrophic explosive supereruptions and are considered a major geohazard (e.g., Toba at ca. 74 ka, Francis et al., 1983; Rampino and Self, 1993; Self, 2006).

In collapse calderas, the subsidence of the chamber roof is produced by syn-collapse faults formed during the collapse phase (e.g., Sparks et al., 1985; Marti et al., 1994; Smith and Braile, 1994; Bacon and Lanphere, 2006; Acocella, 2007). In some cases, collapse calderas used pre-existing tectonic faults as cortical discontinuities to collapse, such as calderas associated with the Sierra Madre Occidental in Mexico (Aguirre-Díaz and Labarthe-Hernández, 2003; Aguirre-Díaz et al., 2008; Gottsmann et al., 2009; Sunye-Puchol et al., 2017), the Cañas Dulces caldera in Costa Rica (Molina et al., 2014), as well as several calderas within the Ethiopian Rift (Acocella et al., 2002; Robertson et al., 2015). The Ilopango caldera (IC) apparently corresponds to this last

* Corresponding author.
E-mail address: ivansp@geociencias.unam.mx (I. Suñe-Puchol).

https://doi.org/10.1016/j.jvolgeores.2018.12.004
0377-0273/

type, which is known as pull-apart/graben calderas (Aguirre-Díaz, 2008; Aguirre-Díaz et al., 2008) and related to extensional and/or trans-tensional tectonic regimes. Williams and Meyer-Abich (1955) first described IC as a volcano-tectonic depression with several eruptions. Recently, Saxby et al. (2016) interpreted Ilopango as a strike-slip caldera, in the same sense as Aguirre-Díaz and Martí (2015), where the vertical faults of the El Salvador Fault Zone (ESFZ) worked as a preferential pathway for magma ascension to the surface (Tikoff and de Saint Blanquat, 1997). Other examples with reports of association between large calderas and pull-apart basins are from Las Sierras-Masaya volcanic complex in Nicaragua (Girard and van Wyk de Vries, 2005; Holohan et al., 2008) and the Toba caldera in Indonesia, within the Great Sumatran Fault Zone (Bellier and Sébrier, 1994). The aim of this work is to study the origin of IC and the first ignimbrite forming eruptions and clarify the relationships between volcanism and the regional transtensive tectonics.

IC is located in the central part of El Salvador, next to the capital city of San Salvador (Fig. 1, index map) and it has a rectangular-rhombohedral shape with 17 × 13 km. The caldera hosts the Ilopango Lake, which is 231 m deep, has an area of 70.5 km² and contains ~12 km³ of water (Sánchez-Esquivel, 2016). The last volcanic event of the caldera is marked by the Islas Quemadas eruption at 1879-1880 (Fig. 2) that formed an intra-lake lava dome (Golombek and Carr, 1978; Richer et al., 2004). The youngest ignimbrite eruption formed by IC has been the historic Tierra Blanca Joven (TBJ) eruption (Williams and Meyer-Abich, 1955; Rose et al., 1999; Hernández, 2004; Kutterolf et al., 2008; Dull et al., 2001; Saxby et al., 2016; Aguirre-Díaz et al., 2017; Pedrazzi et al., 2018), approximately 1500 years ago and that apparently devastated the Mayan civilization in the region (Dull et al., 2010). Prior to TBJ eruption, there were 3 large explosive eruptions during the last 57 ka: TB4, TB3 and TB2 (Rose et al., 1999; Hernández, 2004; Hernández et al., 2010; Kutterolf et al., 2008).

In this work, we show that IC had multiple large-volume ignimbrite eruptions associated with collapse episodes (similar to the Platoro complex in San Juan Mountains; Lipman et al., 1996), and all of them were related to pre-existing regional structure faults associated with the ESFZ. This paper focuses on the ignimbrites of the three earliest volcanic eruptions related to IC, which have not been previously described and interpreted. These are the Olocuilta Ignimbrite (OI), Colima Ignimbrite (CoI), and Apopa Ignimbrite (ApI). For these three newly mapped ignimbrite sheets, we present their stratigraphic and chemical characteristics as well as a robust geochronological framework, and their link with the coeval tectonics of the region.

2. Tectonic and geologic setting of Ilopango caldera (IC)

2.1. Central America tectonic framework

IC is the largest active volcano in El Salvador, a Central American country that lies on the Pacific shore of the Caribbean plate (Fig. 1). About 200 km to the north of San Salvador City is the boundary with the North American plate, represented by the left strike-slip system of Polochic-Motagua-Swan Island Fault (PMSIF), which is the source of the eastward displacement of the Caribbean plate at an average speed

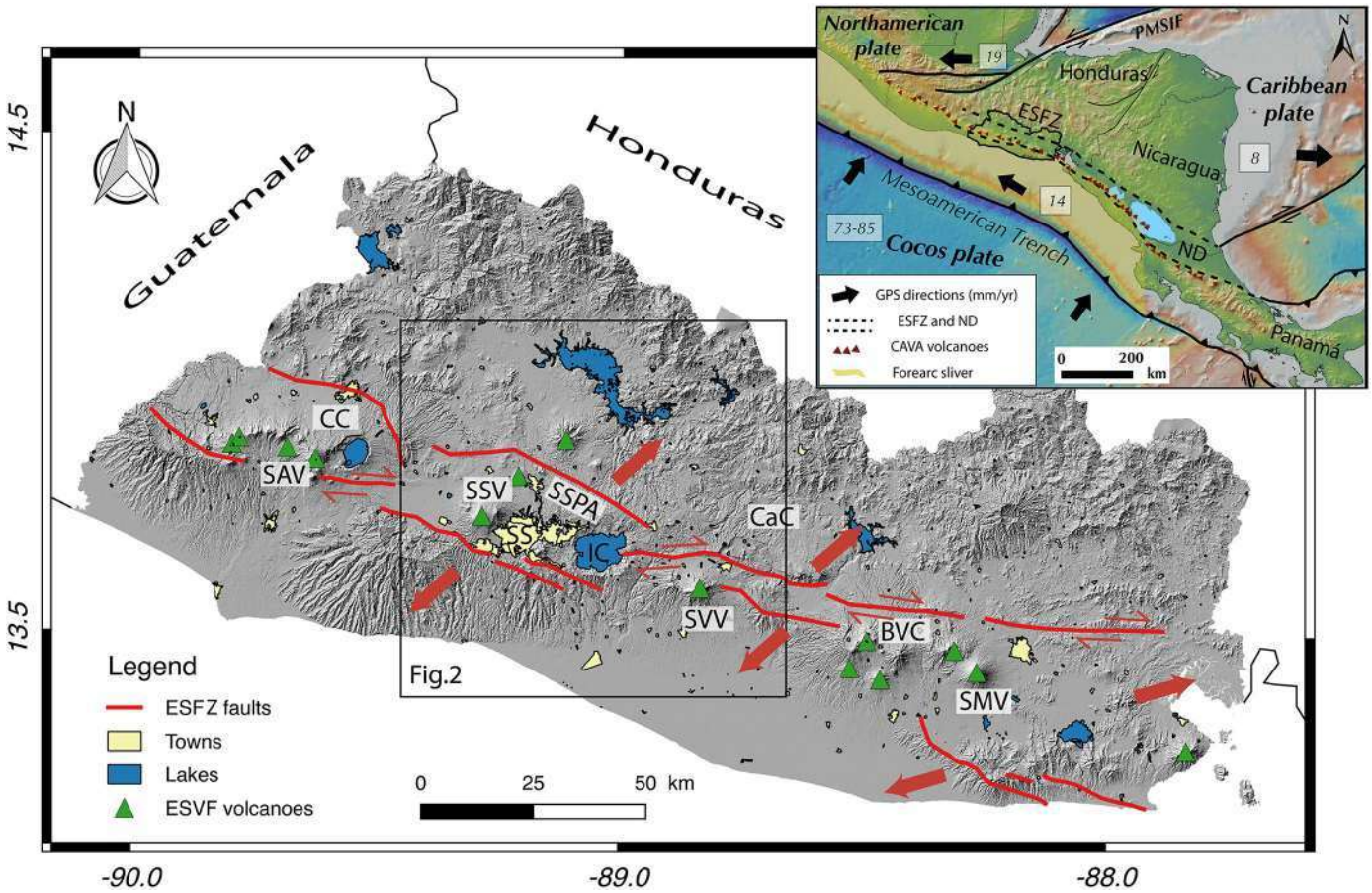

Fig. 1. Index map of main volcanoes and faults of El Salvador indicating location of Ilopango caldera and the study area shown in Fig. 2 (inset map). ESFZ: El Salvador Fault Zone, ESVF: El Salvador Volcanic Front, SS: San Salvador City, SAV: Santa Ana Volcano, CC: Coatepeque Caldera, SSV: San Salvador volcano, IC: Ilopango caldera, SVV: San Vicente Volcano, BVC: Berlin Volcano Complex, and SMV: San Miguel Volcano. Red arrows indicate the actual kinematic within pull-apart basins along ESFZ (after Staller et al., 2016). The inset map shows the continental-scale location of El Salvador in Central America and its regional tectonic setting indicating the main fault systems along the Central American Volcanic Arc - CAVA (after Funk et al., 2009). (For interpretation of the references to colour in this figure legend, the reader is referred to the web version of this article.)

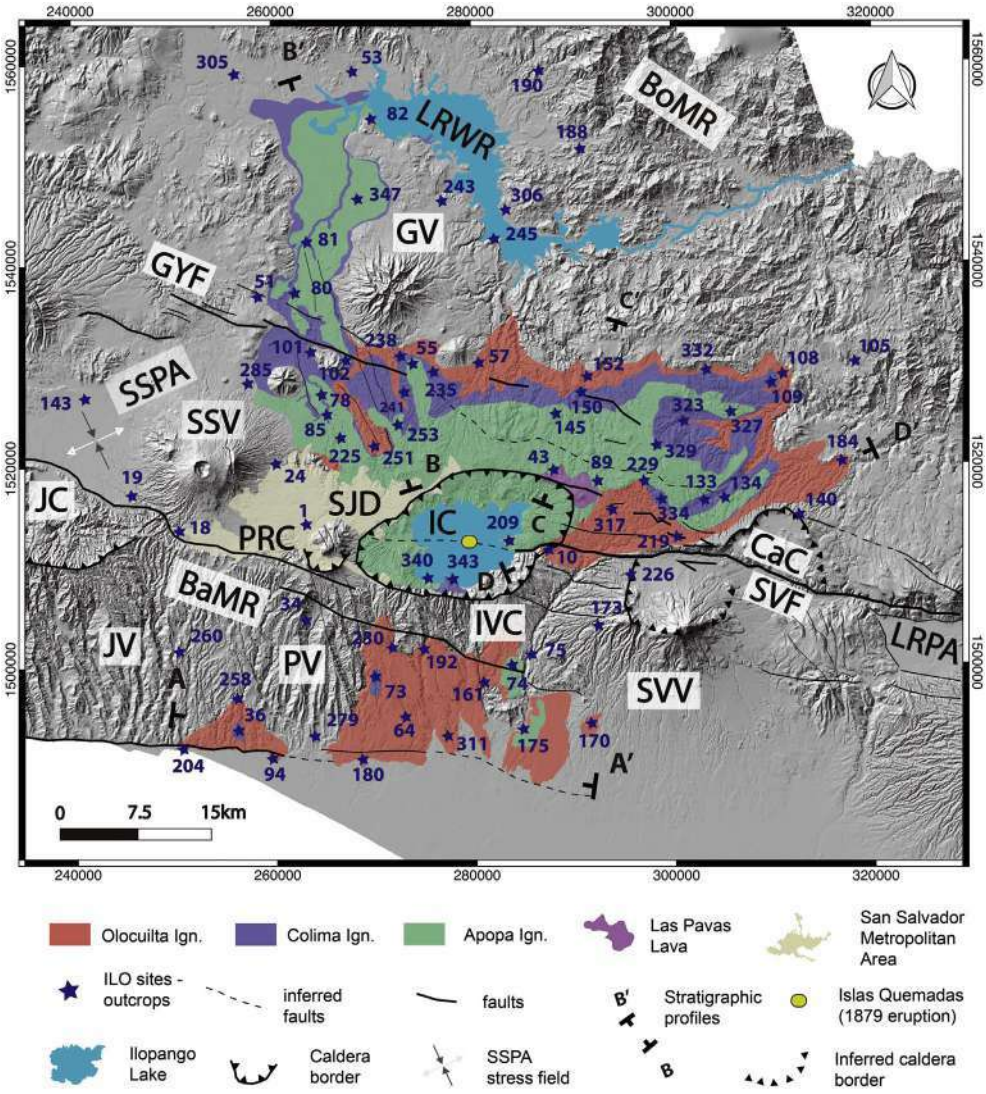

Fig. 2. Index map of the area covered in this study at central El Salvador, showing the distribution of the first three ignimbrites of Ilopango caldera (IC), Olocuilta Ignimbrite (OI, red), Colima Ignimbrite (CoI, blue) and Apopa Ignimbrite (ApI, green). Other features mentioned in main text are also indicated, including sampling location sites (blue stars, sample number with prefix ILO-), Las Pavas Lava (LPL, purple), main tectonic structures and other volcanoes and calderas. IVC: Ilopango Volcanic Complex, JC: Jayaque Caldera, JV: Jayaque Volcano, PV: Panchinmalco Volcano, PRC: Planes de Renderos Caldera, SJD: San Jacinto Dome, SSV: San Salvador volcano, SVV: San Vicente Volcano, CaC: Carbonera caldera, GV: Guasapa Volcano, SSPA: San Salvador Pull-Apart, BaMR: Balsamo Mountain Range, BoMR: Border Mountain Range, LRPA: Lempa River Pull-Apart, SVF: San Vicente Fault, GYF: Guaycume Fault; LRWR: Lempa River Water Reservoir. In yellow is the San Salvador Metropolitan Area (SSMA, ~3 million population). (For interpretation of the references to colour in this figure legend, the reader is referred to the web version of this article.)

of 8 mm/year (Fig. 1; DeMets, 2001; Guzmán-Speziale et al., 2005; Agostini et al., 2006; Funk et al., 2009). Ilopango is a caldera of the Central American Volcanic Arc (CAVA), which extends from Guatemala to Costa Rica (e.g., Simkin and Siebert, 1994; Carr et al., 2007; Sitemap et al., 2014). The CAVA magmatism is related to the oblique subduction of Cocos under Caribbean plate, developed along the Mesoamerican trench since the early Tertiary until the present day, at an average speed of 73-85 mm/year (Fig. 1; Dixon, 1993; Mann, 2007; DeMets, 2001). Oblique subduction (LaFemina et al., 2009), together with a zipper effect produced at the triple junction in Guatemala (Authemayou et al., 2011), and the decoupled interface initiated by the rollback of the Cocos slab (Alonso-Henar et al., 2015, 2017), might be the causes of the forearc sliver displacement of the El Salvador and Nicaragua to the NW (8-14 mm/year; Fig. 1; Corti et al., 2005; Turner et al., 2007; Alvarado et al., 2011).

The eastward motion of Caribbean plate and the northwestward displacement of the Central American forearc are responsible for the transtensional deformation along the CAVA in a series of en-echelon right-stepping, dextral faults connected by pull-apart basins along fault step-overs (Montero and Dewey, 1982; DeMets, 2001, LaFemina et al., 2009; Corti et al., 2005; Agostini et al., 2006, Turner et al., 2007; Funk et al., 2009; Canora et al., 2014), known as El Salvador Fault Zone (ESFZ; Martínez-Díaz et al., 2004). The ESFZ crosses all of El Salvador with a WNW-ESE trend (Figs. 1 and 2), and results in the opening of the San Salvador Pull-Apart (Garibaldi et al., 2016), where IC is emplaced (Figs. 1 and 2). Carr (1976) mentions a pure extensional regime previous to the actual transtensional regime along the ESFZ, induced by the rollback of the Cocos slab started during the Pliocene (Canora et al., 2014; Alonso-Henar et al., 2015, 2017). Weinberg (1992) proposed a similar geodynamic evolution for the Nicaragua graben, where the present-day deformation is controlled by a right-lateral transtensional regime, localized along the Nicaragua volcanic front and superimposed to a previous rift.

The last fault-slip offset of ESFZ occurred during a Mw 6.7 earthquake on February 13 of 2001, indicating a dominant transcurrent stress field along the San Vicente Fault (Fig. 2; Martínez-Díaz et al., 2004; Alvarenga et al., 2001; Canora et al., 2012). This structure, which is affecting the IC volcanism (Saxby et al., 2016), has totally displaced an

older caldera located 12 km to the east: the Carbonera caldera (Fig. 2; Canora et al., 2014). Since the formation of Carbonera caldera about 2.1 Ma ago (Rotolo and Castorina, 1998), strike-slip tectonics along the San Vicente Fault has been active with dextral sense and an average slip rate of ~5 ± 0.5 mm/yr, (Canora et al., 2014). This regional tectonic framework including strike-slip faults, shear zones, pull-apart basins, releasing bends and step-overs, favored the initial pathways for ascension of magma and the emplacement of magmatic centers at shallow levels of the crust (Hutton and Reavy, 1992).

2.2. Geologic setting of Ilopango caldera

El Salvador is predominantly made up of volcanic rocks with ages ranging from the Eocene to the present (Donnelly et al., 1990; Rose et al., 1999). The basement is mainly composed of Jurassic-Cretaceous limestone, represented by the Metapán Formation (Weber et al., 1974), which is sporadically exposed in the NW part of the country. During the Oligocene, volcanism formed the Border Mountain Range at the northernmost part of the country and corresponds to the Morazán and Chalatenango formations. This range marks the geographical border between El Salvador and Honduras (Fig. 2). Since the Miocene, volcanic activity migrated southward and approached the Mesoamerican trench. Volcanism from mid-Miocene to Pliocene formed large basaltic and andesitic stratovolcanoes just south of the actual El Salvador Volcanic Front, such as Panchinmalco Volcano, Jayaque Volcano and the oldest sequence of the Ilopango Volcanic Complex, represented by the Balsamo Formation (Lexa et al., 2011; Fig. 2). The cores of these eroded volcanoes form the Balsamo Mountain Range (Figs. 1 and 2; Williams and Meyer-Abich, 1955). During the Pliocene-Pleistocene, several volcanic edifices collapsed gravitationally apparently associated with the ESFZ structures, forming the calderas of Plan de Renderos and Jayaque both belonging to the Balsamo formation (Lexa et al., 2011), and the Carbonera caldera and early volcanic rocks of the IC that form part of the Cuscatlán Formation (Fig. 2; Weber et al., 1974).

The currently active volcanic belt forms the El Salvador Volcanic Front, which is part of the CAVA (Fig. 1; Carr et al., 2007). Products associated with these volcanic centers from late Pleistocene to Holocene comprise the San Salvador Formation (Weber et al., 1974; Reynolds, 1987; Lexa et al., 2011). The Coatepeque Caldera deposits and late Ilopango Tierras Blancas (TB4, TB3, TB2 and TBJ) are part of this last formation (CEL, 1992; Rose et al., 1999; Hernández, 2004; Hernández et al., 2010; Kutterolf et al., 2008).

3. Methodology

3.1. Field work

Geologic work was based initially on the El Salvador 1: 500,000 geological map of Weber et al. (1974), as well as on previous maps and stratigraphy reported by other authors (Hernández, 2008; Lexa et al., 2011; Garibaldi et al., 2016). Through this data and several fieldwork campaigns between 2015 and 2017, a new stratigraphic framework and a new geologic map for the Ilopango caldera complex and its surroundings were built. This new map covers around 3000 km² of the central part of El Salvador, from Border Mountain Range at north, to the Pacific coast at the south, and from the Lempa River Pull-Apart basin at the east, to Jayaque Caldera at the west (Fig. 2).

Prior to, and during fieldwork, outcrops were identified via satellite images to determine the available access. Once identified and reached, exposures were described geologically, measured for stratigraphic sections, and samples were collected. Despite the difficulties of fieldwork in the El Salvador tropical area, we found the necessary outcrops to fulfill the goals of this study. A Digital Elevation Model (DEM) with 10 m precision was used as a topographic base map. Nearly 85 stratigraphic sections were measured, and several samples were collected for $^{40}Ar/^{39}Ar$ and U-Pb dating, for petrographic analysis in thin sections, and for major and trace element analyses. Geographic coordinates were recorded with a portable GPS (UTM projection system, Datum: D_WGS_1984, zone 16P). Samples were organized and classified in the Observatorio Ambiental of the Ministerio de Medio Ambiente y Recursos Naturales (MARN) of El Salvador, packed and sent to the Centro de Geociencias (CGEO) of the Universidad Nacional Autónoma de México (UNAM) in Querétaro, Mexico. Results of the geochronologic, petrographic and geochemical analyses are described in Section 4. Prior to sample preparation for both chemical and geochronological analysis, samples were inspected for purity and freshness with the binocular microscope, and then in thin sections for petrographic analysis.

3.2. Geochronology techniques

Zircon crystals were separated and dated by U-Pb isotopic analysis at the Laboratorio de Estudios Isotópicos (LEI) of CGEO-UNAM, using a 193 nm Resolution M50 laser ablation inductively coupled plasma mass spectrometer (LA-ICP-MS) Thermo ICAP Qc following the method described in Solari et al. (2010) and Ortega-Obregón et al. (2013). Pumice fragments were separated from the different units, removing altered surfaces and then crushed and sieved to fractions of 74-44 μm. This fraction was then washed using a plastic pan to concentrate the heavy crystals from the lighter glass. Mineral concentrates were magnetically separated by means of a Frantz Isodynamic Separator to further concentrate the zircons. Representative zircons were handpicked under a binocular microscope and checked for purity and zoning using an ELM-3R luminoscope by cathodoluminescence, before and after the ICP-MS laser ablation analysis. About 50 zircon grains per sample were selected in order to obtain a statistically representative age.

Samples for $^{40}Ar/^{39}Ar$ dating were sent directly to the Oregon State University, Corvallis, U.S.A., for analysis in the OSU Argon Geochronology Laboratory. As with zircons, clean pumice clasts were separated and crushed to obtain mineral concentrations. Crushed samples were sieved to 500-177 μm fractions and washed with deionized water using an ultrasonic bath to remove dust. Feldspars were magnetically separated from amphiboles and pyroxenes, and all phases were acid-leached following methods of Koppers et al. (2011). Sanidine or orthoclase is the preferred mineral phase in $^{40}Ar/^{39}Ar$ dating of young tephras. Unfortunately, no high-potassium feldspar was found in any of the IC samples. The only available phases to date were plagioclase and hornblende (ultra-pure separates picked clean of melt inclusion-rich crystals) and groundmass concentrations (lava samples). Incremental heating technique on bulk samples was employed to examine each phase analyzed. We used concentrates of the minerals since individual grains do not yield enough radiogenic argon for accurate single-crystal total fusion analyses (Rose et al., 1999). To achieve the highest possible precision in the $^{40}Ar/^{39}Ar$ age determinations, a large number of heating steps (22-33 heating steps) were carried out for each sample (Koppers et al., 2011). Age plateaus were chosen including as many contiguous and concordant step ages as possible. Before analyzing a sample, and after every three heating steps, system blanks were measured. In this way, after the first 7 to 14 low temperature steps, an adequate amount of discordant gases was released from alterations remaining and atmospheric contamination. To get the appropriate eruption timing it was necessary to recalculate the ages using the Kuiper et al. (2008) age for the Fish Canyon Tuff as flux monitor, reducing the data with the ArArCALC v2.5.1 software from Koppers (2002). All $^{40}Ar/^{39}Ar$ age errors reported here are 2σ. More details of the techniques employed in the dating process are provided in Appendix B and in Koppers et al. (2011).

3.3. Geochemistry

Chemical analyses were performed on whole-rock pumices that were previously dried in an oven at 90 °C for 24 h and hand-cleaned

by removing the weathered surface under careful clean conditions to avoid contamination. Samples were crushed and grinded by hand using an agate ceramic mortar, until a homogenous powder with −200 mesh size was obtained using new plastic mesh for research standards in each sample. Major, trace, and Rare Earth-Elements (REE) were obtained. Major and some trace elements were measured by means of X-Ray Fluorescence (XRF) technique in the laboratory of Instituto de Geología, UNAM (Mexico), using a X RIGAKU ZSX Primus II spectrometer. REE and other trace element analyses were obtained by ICP-MS in the LEI of CGEO. Method of sample handling and analyses techniques are described in Bernal and Lozano-Santacruz (2005).

4. Results

4.1. Stratigraphy and distribution of the early Ilopango caldera ignimbrites

The systematic geologic mapping and volcanic stratigraphy carried out on IC deposits has allowed for the identification and characterization of the three lowermost explosive eruptions from IC. They comprise broadly distributed Quaternary pyroclastic deposits, from oldest to youngest: Olocuilta, Colima and Apopa ignimbrites. They consist of widespread ignimbrite sheets covering the central portion of El Salvador (Fig. 2).

4.1.1. Olocuilta Ignimbrite (OI)

The first volcanic eruption from IC occurred at 1.785 ± 0.006 Ma BP (Ar/Ar age, Section 4.3 of geochronology results) and produced the high-K rhyolitic OI (Table 1). This pyroclastic deposit consists mostly of large pumice (40% vesicles), and lithics (15–25% total volume) in an ash matrix. In general, the pumices contain phenocrysts of plagioclase, quartz, pyroxenes and Fe-Ti oxides with accessory zircon and apatite. OI overlies a sequence of volcano-clastic sediments deposited over the Zaragoza Ignimbrite (Weyl, 1957), which is an older andesitic-dacitic tuff from Jayaque Caldera (Fig. 3). OI is light red to pink due to the alteration of the ferromagnesian components. At ILO-73, near the town of Olocuilta, the contact between the top of OI and the base of CoI is exposed (Figs. 2, 3 and 4d).

OI shows a basal thin layer of pumice-lapilli fall between 30 and 25 cm overlaid by tens of meters of a massive ignimbrite unit (Fig. 4a), forming a thick deposit observable at distances of up to 30 km from the caldera (e.g., at ILO-184, Fig. 2). Diffuse internal stratification is marked by lenses of pumice (PlensL, Figs. 3 and 4e). The ignimbrite shows a 1-3 m thick basal pumice breccia (PmBr, Fig. 3), containing pumice up to 20 cm in diameter. The middle zone of the OI is a lithic-rich, massive lapilli tuff (mLTl, Fig. 3), at the medial to proximal facies on the northern flank of IC, with lithics of 15 cm (ILO-251, ILO-10 and ILO-219, Fig. 2). At the top of OI and in particular in the southern outcrops, it is welded 8-10 m thick, with columnar jointing (Fig. 4b). Welding reaches from partially (eutaxitic texture, with pumice lapilli collapse, ILO-64; Figs. 2, 4f and 6a), to densely welded (with fiammes, ILO-96; Figs. 2 and 6b), being IV–V of Quane and Russell (2005) rank. The welded top of OI acted as a resistant caprock that protected the unconsolidated lower zones of this ignimbrite from erosion and formed an extensive plateau that dominates the geomorphology of the Balsamo Mountain Range (Figs. 2 and 4c). Perennial streams have incised deeply this plateau reaching the basement rocks (lavas and volcanic breccias of the Balsamo formation). Some of these canyons expose entire stratigraphic sections of the OI up to 100 m thick such as exposures in ILO-192 (Figs. 2 and 4c). Above the welded level, there is an additional 25 m of non-welded ignimbrite that is indurated by vapor-phase silicification (ILO-180; Fig. 2), indicating a total thickness of ~125 m for OI.

Table 1
Whole-rock chemistry of OI, CoI and ApI pumices.

Sample	ILO-199	ILO-313	ILO-21	ILO 36-A	ILO-64	ILO-184	ILO-36-B	ILO-82	ILO-73	ILO-134	ILO-78
Unit	OI	OI	OI	OI	OI	OI	CoI	CoI	CoI	ApI	ApI
SiO_2	74.9	76.3	75.0	74.6	75.9	74.8	71.9	72.5	72.2	71.9	71.8
TiO_2	0.13	0.11	0.13	0.16	0.13	0.12	0.35	0.35	0.39	0.30	0.29
Al_2O_3	14.9	13.0	14.1	14.9	13.7	14.8	14.9	14.5	15.3	15.3	14.3
FeO*	1.48	1.27	1.54	1.71	1.42	1.70	2.45	2.36	2.76	3.09	3.19
MnO	0.08	0.06	0.06	0.06	0.06	0.06	0.09	0.10	0.10	0.11	0.10
MgO	0.28	0.30	0.41	0.34	0.28	0.32	0.51	0.55	0.55	0.60	0.83
CaO	1.14	1.12	1.21	1.14	1.11	1.16	1.63	1.54	1.54	2.20	2.85
Na_2O	2.38	2.06	2.30	2.43	2.14	2.87	2.64	2.66	2.56	3.53	3.71
K_2O	4.69	5.72	5.22	4.60	5.22	4.05	5.30	5.35	4.57	2.87	2.84
P_2O_5	0.03	0.03	0.03	0.03	0.03	0.03	0.06	0.07	0.07	0.08	0.09
LOI	3.27	2.56	4.58	2.22	3.87	4.24	4.25	3.89	5.34	4.19	5.54
SUM	99.9	99.9	100.1	99.8	99.9	99.8	100.1	99.9	99.9	99.9	99.7
Rb	87	107	106	94	105	85	126	117	125	48	43
Sr	114	111	123	119	114	117	180	160	179	208	190
Ba	1212	1146	1297	1200	1322	1242	1163	1211	1172	1100	956
Y	17	19	17	15	15	18	37	32	36	19	11
Zr	104	89	114	123	106	102	301	273	323	210	92
Nb	5	5	4	3	2	5	7	5	6	5	3
V	5	4	8	11	19	6	17	12	15	15	23
Cr	0	0	b3	4	9	0	0	b3	b3	1	b3
Co	2	2	5	8	3	3	4	7	8	5	8
Ni	7	7	10	10	10	8	7	9	10	7	8
Cu	5	7	20	13	12	12	7	10	10	19	10
Zn	29	13	35	30	34	28	51	54	58	54	43
Th	7	6	8	7	8	7	7	8	10	3	3
Pb	11	7	8	7	9	9	14	12	15	8	5
X (m)	274,665	275,498	272,823	256,099	272,901	316,801	256,099	269,885	270,915	304,297	264,763
Y (m)	1,501,091	1,493,097	1,495,122	1,493,793	1,494,947	1,520,480	1,493,793	1,554,548	1,500,438	1,516,540	1,526,998

OI: Olocuilta Ignimbrite, CoI: Colima Ignimbrite, ApI: Apopa Ignimbrite.
Major elements in wt% and trace elements in ppm.
Samples analyzed by X-Ray Fluorescence in the Insituto de Geología (UNAM) by Patricia Girón.
Coordinates in WGS84 system (zone 16P).
FeO*-total iron; LOI: Lost of ignition.

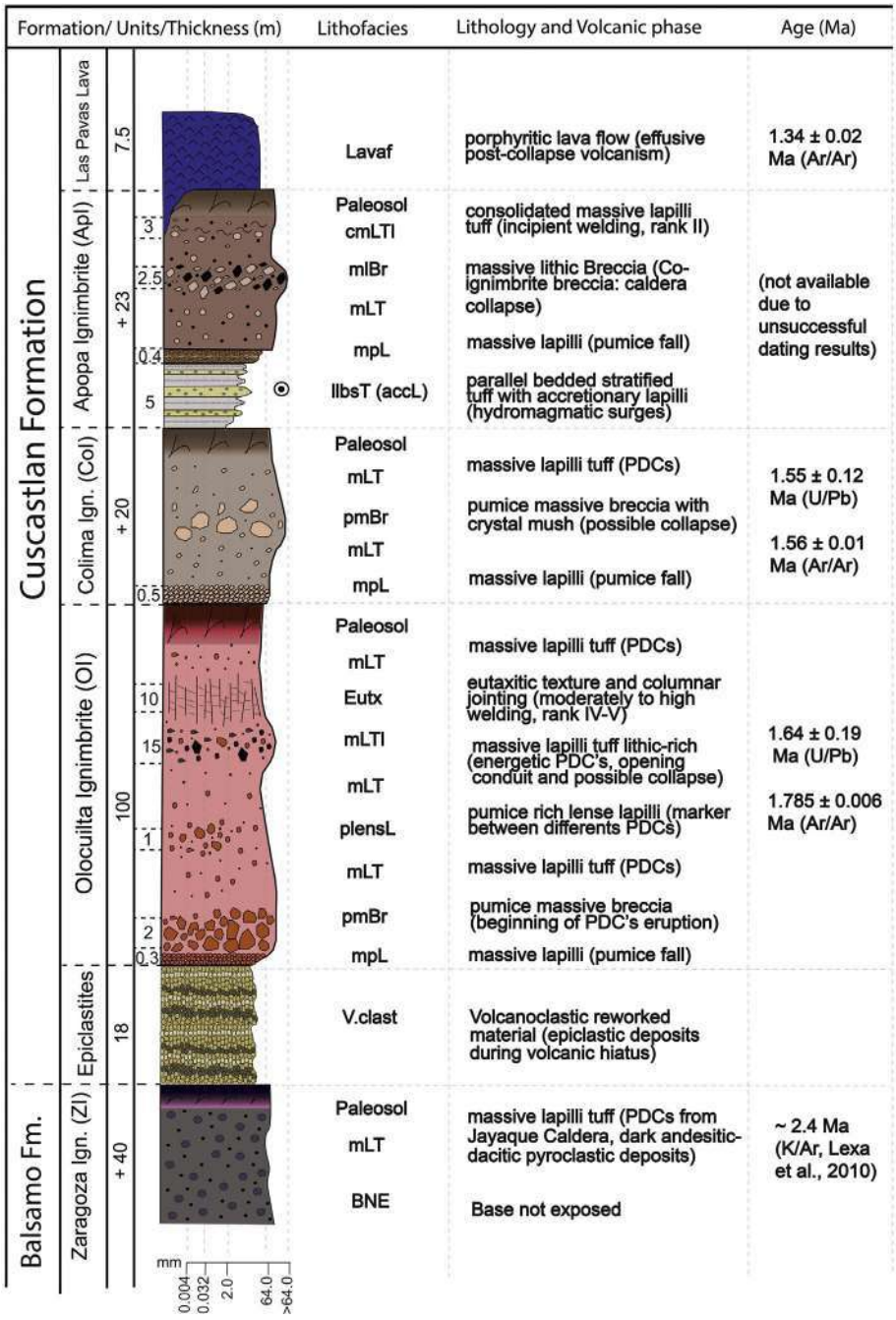

Fig. 3. Composite stratigraphic section of the early Ilopango caldera products, showing lithofacies type (following nomenclature of Branney and Kokelaar, 2002 and Brown and Branney, 2004), interpretation and age for each deposit. (For interpretation of the references to colour in this figure legend, the reader is referred to the web version of this article.)

4.1.2. Colima Ignimbrite (CoI)

The second large explosive eruption from IC occurred at 1.57 ± 0.01 MaBP (Ar/Arage, see Section 4.3 of geochronology results) producing the CoI, which is a high-K rhyolitic unit (Table 1) with plagioclase, hornblende, and accessory minerals of apatite, zircon and Fe-Ti oxides. This ignimbrite, like the previous one, starts with a thin layer of pumice-lapilli fallout overlying the paleosol developed at the top of OI (e.g. ILO-73 and ILO-36; Figs. 2, 3, 4d and 5b). Above this basal layer, there is a sequence of pyroclastic density currents (PDC) deposits composed mostly of a pale grey ash matrix with large white and highly vesiculated pumice (50 vol%), and minor amounts of lithics. This ignimbrite traveled distances of up to 40 km to the north of the caldera, reaching the Lempa River Water Reservoir (ILO-82; Figs. 2 and 5a). In proximal facies of the caldera it is very difficult to find outcrops where the CoI stratigraphic section is completely exposed due to the heavy vegetation and because this unit is covered by younger Ilopango tuffs. However, in medial facies like at the ILO-150 (Fig. 2), there are at least 19 m of this deposit are observable.

There is no evidence of lithic breccias or welded zones in the CoI and, in general, it is an unconsolidated tuff easily eroded by the tropical rains of El Salvador's weather, mainly on the steep slopes of the southern flank of IC, where the ignimbrite is sporadically exposed. The CoI is relatively massive, with large pumices concentration zones, generally at the base and middle part of the unit forming pumiceous breccias (pmBr in Fig. 3, pumice of ~20 cm). Within these breccias there are pieces of intrusive cognate blocks among the components (e.g., at ILO-101; Figs. 2 and 5c). These are vesiculated fragments of crystalline igneous rock with 50% total volume in crystals with a non-fragmented

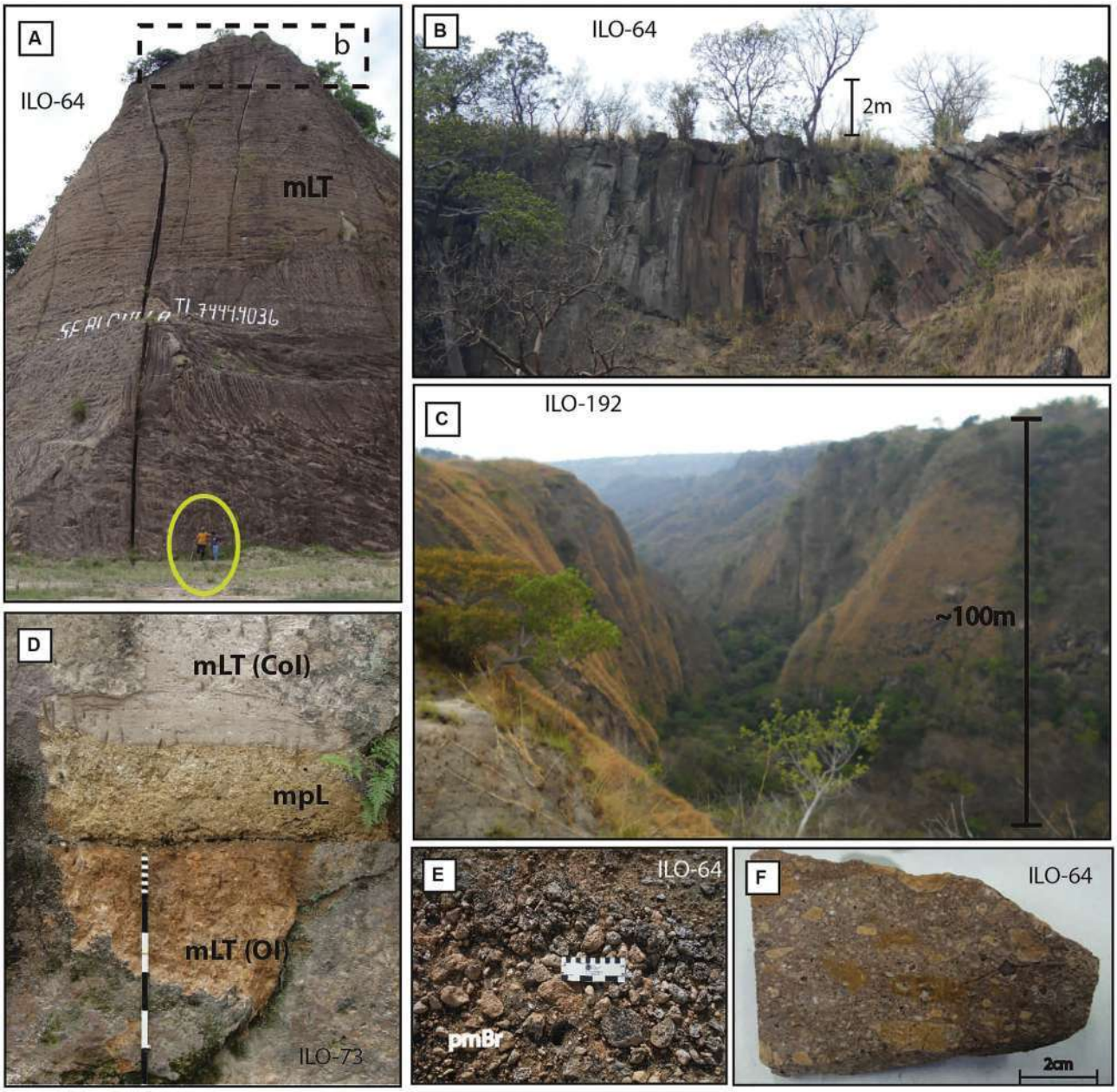

Fig. 4. Field and sample photographs of OI. a) Quarry at ILO-64 (Fig. 2) exposing 50 m of OI (note geologist for scale). b) Top of OI showing moderate to dense welding with columnar jointing (ILO-64, Fig. 2). c) View to the south from ILO-92 (Fig. 2), where the Tapalhuaca canyon cuts the plateau formed by the welded OI and exposes at least 100 m of this ignimbrite. d) Basal pumice fall (mpL) of the CoI above OI at ILO-73 (Fig. 2). e) Pumice massive Breccia (PmBr) indicating PDC pulses within OI. f) Hand specimen of OI with eutaxitic texture sampled at ILO-64 (Rank IV of welding intensity scale, Quane and Russell, 2005; Fig. 2).

vesiculated glass matrix (Fig. 6c). Polished thin sections of these enclaves show glomeroporphyritic texture with plagioclase and hornblende (Fig. 6d), and poikilitic texture with small hornblende within plagioclase large phenocrysts (Fig. 6e). We infer that these cognate blocks are *crystal mush* clasts, which correspond to broken pieces of the subcaldera magma chamber wall.

4.1.3. Apopa Ignimbrite (ApI)

The third large explosive eruption associated with IC produced the ApI at ~1.34 Ma BP (age of a overlaying lava, see Section 4.3). This ignimbrite is a medium-K rhyolitic tuff (see Table 1) with plagioclase and hornblende as principal phases and minor amounts of biotite and clinopyroxene, with accessory zircon, apatite and Fe-Ti oxides. At the base of ApI there is a sequence of sub-parallel dilute PDC deposits (llbsT, surge deposits; Fig. 3) mostly composed of fine, yellow-white ash and accretionary lapilli, and small fragmented clasts of pumice (ILO-175; Figs. 2, 5d and e). The matrix is highly fragmented ash tuff, with sparse complete glass shards, and fine interstitial ash-dust and tiny fragments of the mineral assemblage (Fig. 6f). These fine-grained deposits of the ApI eruption resemble soft clay, probably due to the content of zeolites or other alteration minerals. They reach up to 5 m in thickness, with diffuse cross-lamination and load structures (f*lames* in ILO-327, Figs. 2 and 5g).

Directly above these laminated deposits there are: 1) a thin layer of orange pumice-lapilli (mpL), rich in crystals (10-15 vol%), with mostly hornblende and plagioclase, and 2) a sequence of denser lithic-rich PDCs deposits (mLT, Fig. 5d). These PDCs of the upper part of the ApI show a diffuse internal stratification with several pumice-rich horizons (plensL) and a lithic breccia layer (mlBr). This breccia can be correlated in several proximal outcrops to the north of IC and it is also observed

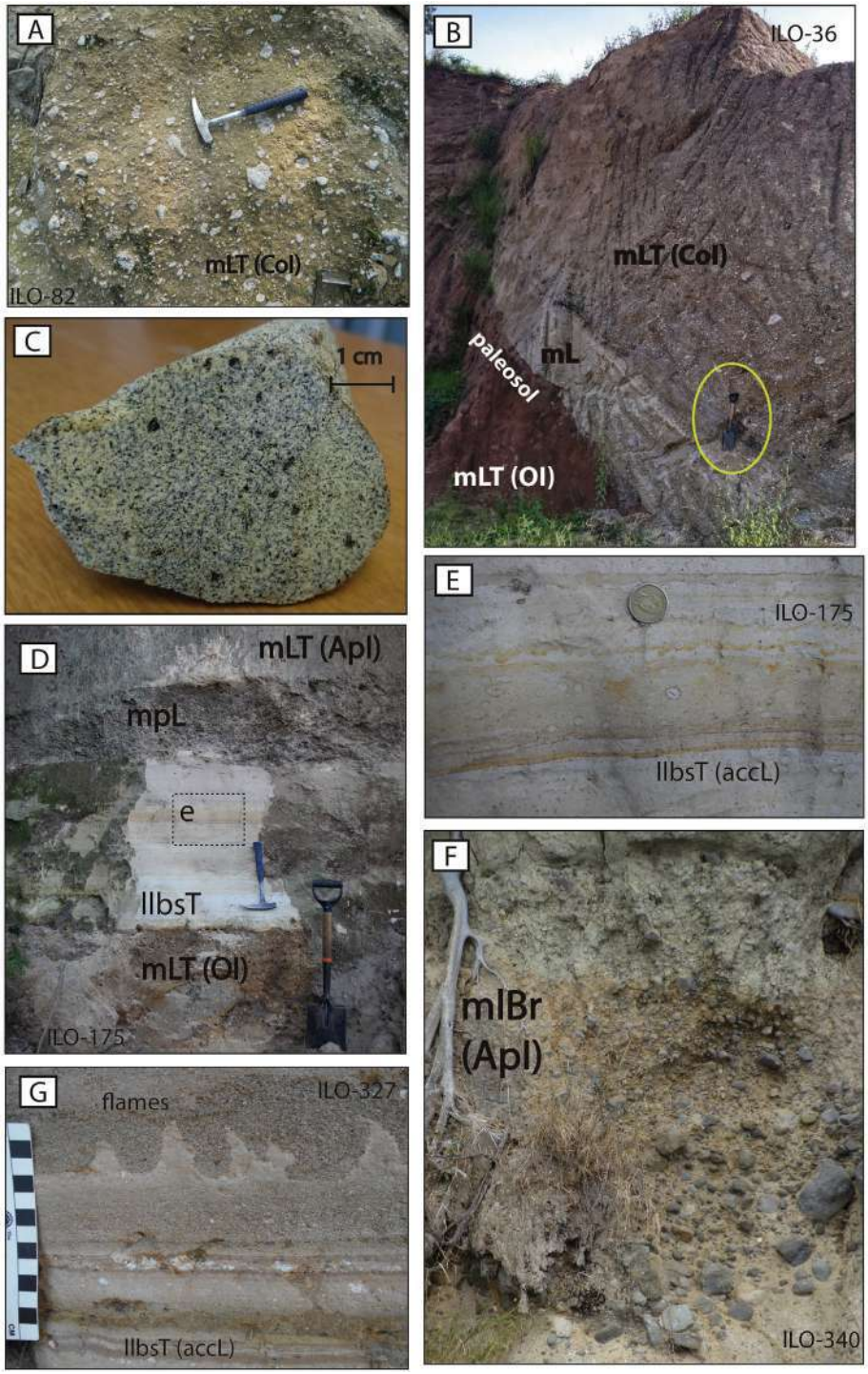

Fig. 5. Field and samples photographs of CoI and ApI. a) CoI at ILO-82 (Fig. 2) mostly composed of white pumice and pale grey glass shards matrix. b) Contact of CoI and OI at ILO-36 (Fig. 2). c) Hand-size sample of a piece of *crystal mush* found in the pumice breccia of CoI at ILO-101 (Fig. 2): this clast is an intrusive cognate lithic from the magma chamber wall. d) Complete sequence of ApI above a paleosol at ILO-175 (Fig. 2) showing dilute hydromagmatic PDC deposits at the base (llbsT), a pumice fall layer in the middle (mpL) and denser PDC deposits at the top (mLT). e) Detail of the basal dilute PDCs deposits of ApI showed in the previous photo, where stands out the accretionary lapilli and internal lamination. f) Proximal facies of ApI along the Ilopango Lake shore (ILO-340, see Fig. 2) showing a coignimbritic lithic lag breccia zone. g) Load and flame structures within the dilute PDC deposits at the base of ApI at ILO-327 (Fig. 2).

also along the shore of the Ilopango Lake, where angular lithics can be as large as 50 cm in diameter (ILO-145, ILO-225 and ILO-340, Figs. 2 and 5f). The ApI is the first IC ignimbrite that contains a heterolithological lithic breccia, with lava and plutonic lithic clasts, interpreted as a coignimbrite lithic lag breccia (ILO-89; Figs. 2 and 5g). The ApI reaches as far as the Lempa River Water Reservoir (ILO-82; Fig. 2), throughout a valley to the north for ~40 km. The accumulation of hot material filling this valley caused the incipiently welding of the top of ApI, with adhesion between clasts but remaining undeformed (rank II, Quane and Russell, 2005). At ILO-102, located about 20 km to the NW of IC (Fig. 2), this welded top level protected the underlying and unconsolidated tuff of ApI from erosion. At this site the ignimbrite reaches about 14 m of thickness. On the southern facies, as with the CoI, the ApI is sporadically exposed due to erosion. At some locations,

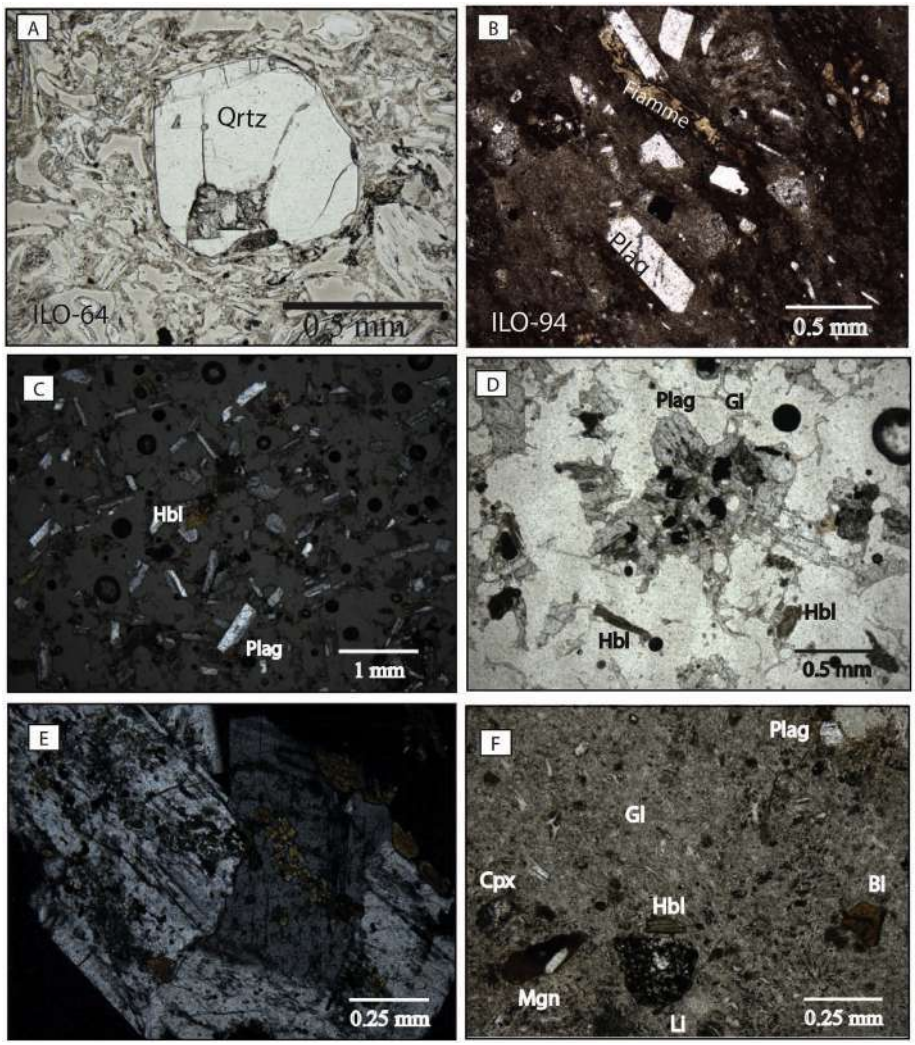

Fig. 6. Microscopic characteristics of the OI, CoI and ApI. a) Phenocryst of Quartz (Qrtz) within the welded zone of OI, showing resorption embayment and glassy shards matrix (thin section polished from Fig. 4f). b) Microtexture of the dense welded OI at ILO-96 site (Rank V, Quane and Russell, 2005; Fig. 2) showing collapsed glass shards and fiammes (in yellow), around rigid plagioclase phenocrysts. c) Interlocking texture of the crystal mush piece from CoI (Fig. 5c), with vesiculated and non-fragmented glass matrix (Gl). The mineralogy of this cognate includes hornblende (Hbl) and plagioclase (Plag). d) Glomeroporphydic texture presented in the same crystal mush piece (grouped plagioclase and hornblende crystals). e) Poikilitic texture in the CoI crystal mush piece (small hornblende in large plagioclase crystals). f) Thin section of the basal surges deposits of ApI with very fragmented glass shards matrix (Gl), crystals of clinopyroxene (Cpx), biotite (Bi), plagioclase (Plag), hornblende (Hbl) and Fe-Ti oxides (Mgt), and lithics (Li). (For interpretation of the references to colour in this figure legend, the reader is referred to the web version of this article.)

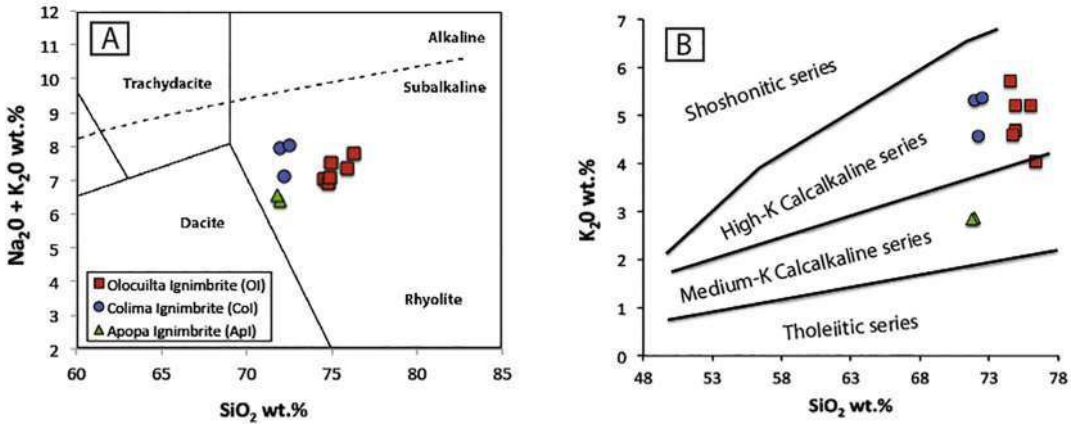

Fig. 7. Geochemical classification of OI, CoI and ApI. a) Total-Alkali-Silica (TAS) diagram with classification of LeBas et al. (1986) showing that the three ignimbrites are subalkaline rhyolites, but each with a well-defined cluster in the plot. b) SiO_2-K_2O plot with classification of Peccerillo and Taylor (1976) showing that OI and CoI are in the High-K calcalkaline suite, and ApI in the Medium-K suite.

(e.g., ILO-175, Fig. 2), the ApI is only covered by a consolidated lahar deposit that protected this ignimbrite from fluvial erosion (Fig. 5d).

4.2. Geochemistry

Whole-rock chemical analyses were carried out on pumice fragments collected from the three ignimbrites (Table 1) in order to obtain the geochemical characteristics of the earliest volcanic products of IC. The pyroclastic products of the IC are all subalkaline rhyolites with high SiO_2 content (Fig. 7a), and high-K_2O values for the first two eruptions (OI and CoI), and medium content for the third one (ApI, Fig. 7b). Harker variation diagrams (Fig. 8) show evolved magmas for the three ignimbrites, with OI as the most evolved, which is the richest in SiO_2 and the poorest in total FeO and MgO. From OI to CoI to ApI there is a tendency for a slightly less evolved magma. The three ignimbrites show the typical calcalkaline nature of subduction type magmas along continental margins, as elsewhere in CAVA (Arculus and Curran, 1972; Morris and Ryan, 2004; Murphy, 2007).

Abundances of the Rare Earth Elements (REE) and other key trace elements are displayed in a *spider* diagram (Fig. 9), in which the elements are arranged from left to right in order of increasing compatibility, and values normalized to Mid-Ocean Ridge Basalt values (MORB, Sun and McDonough, 1989). This diagram confirms the comagmatic origin for the three ignimbrites, with some features that can be used for correlation purposes. For example, the CoI generally has higher concentrations of REE than the other two ignimbrites and a notable negative anomaly in the Sr and Eu. OI also has a negative anomaly in Sr but not in Eu. Finally, ApI has no Eu anomaly, and a positive Sr anomaly (Fig. 9). Negative Eu anomalies probably reflect plagioclase fractionation (Wilson, 1989). Plagioclase is the most abundant phenocryst in calcalkaline magmas, typically dominated over alkali feldspar (Murphy, 2007), as occurs in the Ilopango ignimbrites here described.

4.3. Geochronology

4.3.1. U/Pb dating in zircon

Four samples from the three first IC ignimbrites were collected for radiogenic U-Pb zircon analyses, with a single sample from OI (ILO-64, Figs. 2 and 10a), two from CoI (ILO-73 and ILO-82, Figs. 2, 10b and c), and one from ApI (ILO-78 site, Fig. 2). Analytical data are summarized in Appendix A. The U-Pb zircon ages were obtained from the intersection of the Concordia curve with the normal isochron (Fig. 10a, b and c) using the Isoplot software (v. 3.7) and methods of Ludwig (2008). To obtain the best possible results, we discarded the most discordant zircons (largest ellipsoids in the isochron diagram). U/Pb zircon age for OI yielded 1.64 ± 0.19 Ma (1.45–1.83 Ma range). The large error is caused probably because most zircons analyzed were too small (b80 μm), which have xenocrystic cores with concentric zoning (Fig. 10d and e), and due the limitations of the U-Pb method in such young zircons (all the errors of U/Pb reported in this study refer to 2σ standard deviation). The most probable age of the crystallization of this zircon age is close to 1.8 Ma.

The two samples of zircon analyzed for the CoI were collected from the proximal facies to the south of IC (ILO-73, Fig. 2) and at 40 km to the north of IC (ILO-82, Fig. 2). The zircon ages are 1.53 ± 0.28 Ma and 1.55 ± 0.12 Ma, for southern and northern sites respectively, supporting the correlation of this ignimbrite between the proximal and distal facies (Fig. 10b and c). No age for ApI could be obtained possibly because of the low content in U and Pb for this ignimbrite (see the relative concentrations in the spider diagram of Fig. 9). Most ApI zircons were inherited from an old basement of around 70 Ma.

Zircon analyses in such young products as the IC ignimbrites yield imprecise results, so it was necessary to use another geochronological method trying to better constrain the timing of each ignimbrite. We thus estimated $^{40}Ar/^{39}Ar$ ages.

4.3.2. $^{40}Ar/^{39}Ar$ dating

Five new $^{40}Ar/^{39}Ar$ ages (Table 2 and Fig. 11) were obtained by incremental heating methods using the ARGUS-VI mass spectrometer. Five high-purity plagioclase concentrates were analyzed for the OI (ILO-64 site; Fig. 2), which were then stacked to produce a new plateau age of 1.785 ± 0.006 Ma (Fig. 11a). This high-precision age of OI is within the analytical error of previous reported ages for this unit (1.77 ± 0.4 Ma, 1σ; Lexa et al., 2011) and within the U-Pb zircon age reported above (1.64 ± 0.19 Ma 2σ). The CoI samples were analyzed by plagioclase and hornblende separates from the same site

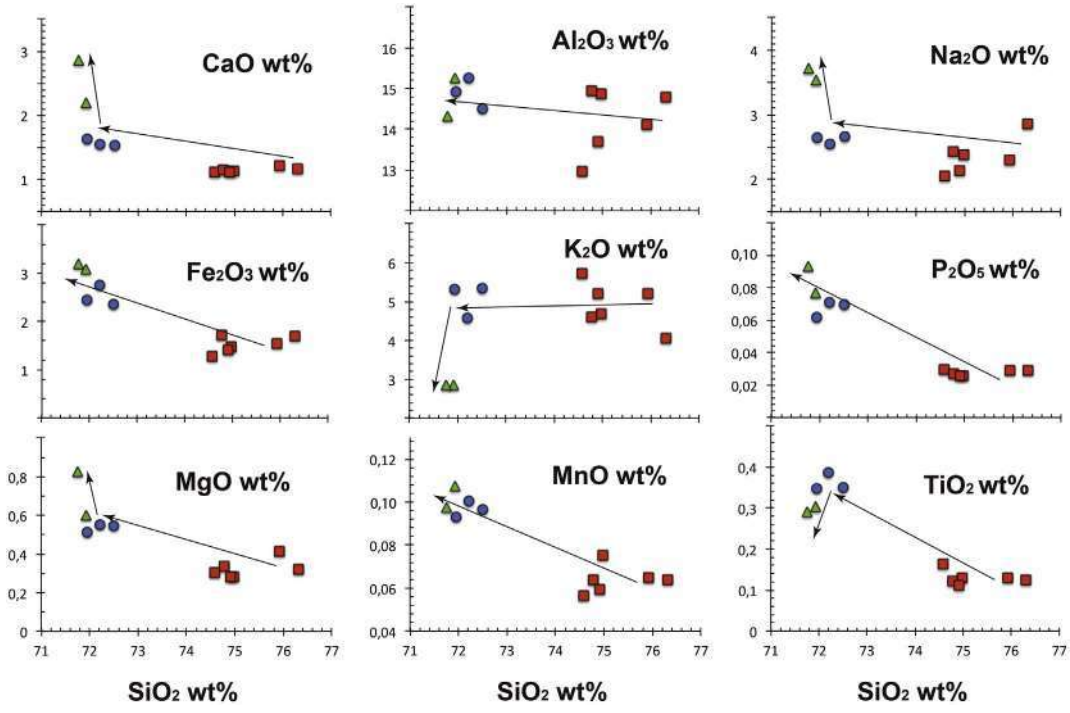

Fig. 8. Harker variation plots of OI, CoI and ApI. Note well-defined groups of each ignimbrite. Arrows indicate possible evolving trends (symbols as in Fig. 8).

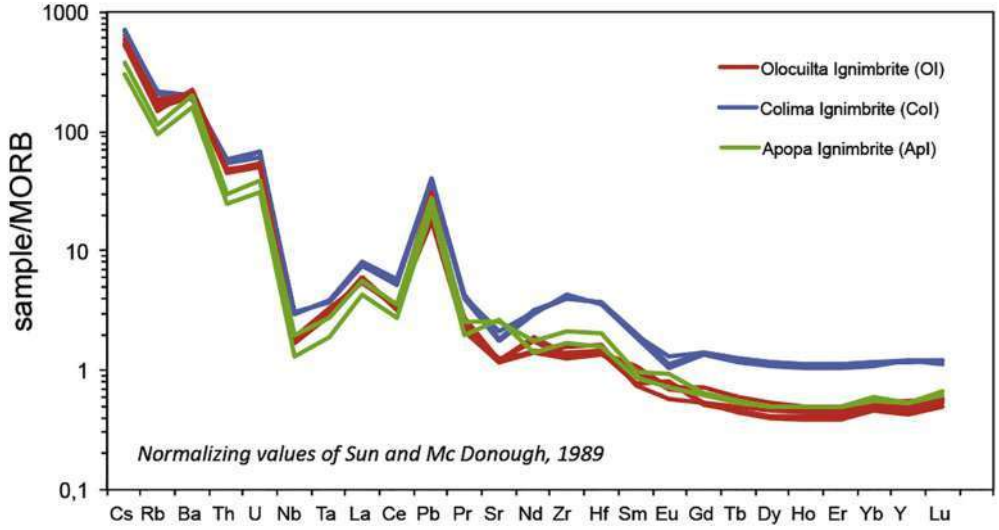

Fig. 9. Spider diagrams of OI, CoI and ApI normalized to MORB (Sun and McDonough, 1989) showing the REE abundances.

(ILO-73, Fig. 2), yielding 1.57 and 1.56 ± 0.01 Ma, respectively (Fig. 11b and c). This result agrees with the U-Pb zircon ages of this work (Fig. 10b and c).

No $^{40}Ar/^{39}Ar$ ages were obtained for the ApI because the hornblende and plagioclase yielded too much atmospheric argon to obtain reliable ages. Since these analyses were unsuccessful, we sampled the unit overlying ApI: Las Pavas Lava (LPL, Fig. 3), a post-caldera dome emplaced just after the eruption of ApI (ILO-43 site, Fig. 2). Plagioclase and a groundmass separates were analyzed for this lava (Fig. 11d and e), yielding ages of 1.34 ± 0.02 Ma and 1.22 ± 0.02 Ma respectively. The LPL groundmass yielded a slightly younger age than the plagioclase age due to excess atmospheric argon. There is no well-developed

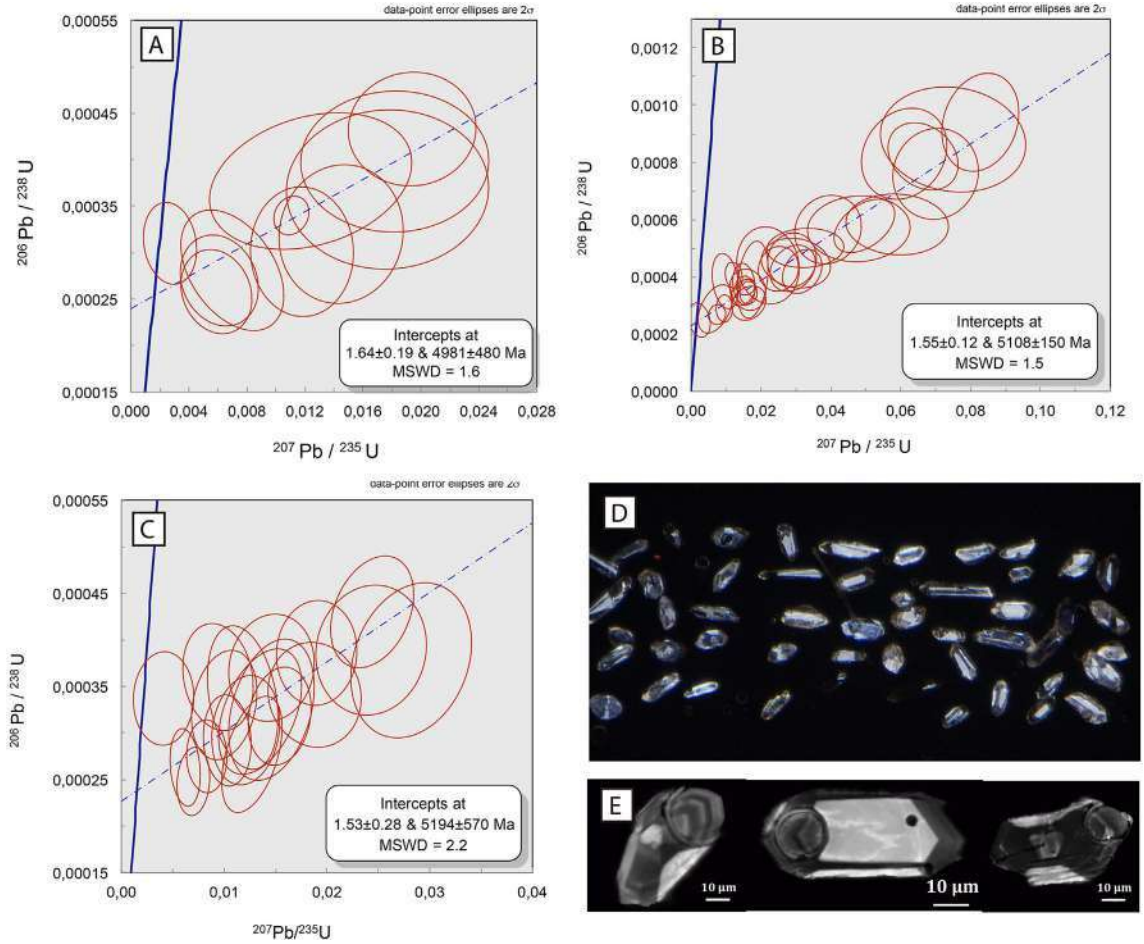

Fig. 10. U-Pb zircon age concordia and isochron diagrams of OI and CoI including images of the analyzed zircons by means of LA-ICPMS. ApI results were discarded (see Section 4.3.1). a) OI (ILO-64). b) CoI (ILO-82). c) CoI sample (ILO-73). d) Cathodoluminescence image of the analyzed zircons from OI's ILO-64 sample. e) Scanning Electron Microscope (SEM) image of zircons from OI's ILO-64 sample after laser ablation ICP-MS analyses.

Table 2
Summary of incremental heating $^{40}Ar/^{39}Ar$ analyses on early Ilopango caldera products.

Sample information					Age spectrum						Total fusion		Inverse isochron analyses		
Unit	Sample	X (m)	Y (m)	Material	Age ± 2σ (Ma)	^{39}Ar (%)	K/Ca	MSWD	n	N	Age ± 2σ (Ma)	K/Ca	Age ± 2σ (Ma)	40/36 intercept	MSWD
Olocuilta Ign.	ILO-63	271,353	1,497,223	Plagioclase	1.785 ± 0.006	86.37	0.072	1.10	87	124	1.792 ± 0.06	0.073	1787 ± 0,006	291.80 ± 3.46	1.05
Colima Ign.	ILO-73-P	270,915	1,500,438	Plagioclase	1.57 ± 0.01	100	0.058	2.77	22	22	1.56 ± 0.01	0.058	1,58 ± 0,01	276,71 ± 8,18	1.47
Colima Ign.	ILO-73-H	270,915	1,500,438	Hornblende	1.56 ± 0.01	100	0.058	1.38	22	25	1.55 ± 0.01	0.058	1.57 ± 0.02	294.05 ± 3.21	1.39
Las Pavas Lava	ILO-43-P	288,141	1,518,462	Plagioclase	1.34 ± 0.02	92	0.030	1.39	19	28	1.37 ± 0.01	0.028	1.33 ± 0.04	303.55 ± 21.24	1.42
Las Pavas Lava	ILO-43-G	288,141	1,518,462	Groundmass	1.22 ± 0.03	41	0.345	1.97	11	33	1.27 ± 0.01	0.345	1.22 ± 0.04	295.36 ± 1.40	2.18

K/Ca values are calculated as weighted means for the age spectra or as total fusion K/Ca values by combining the gas analyses. Both the number of steps (n) included in the age plateau and isochron calculations and the total number of incremental heating steps (N) have been listed. MSWD values for the age plateaus and inverse isochrons are calculated using n − 1 and n − 2 degrees of freedom, respectively. All samples from this study where monitored against FCT-FM sanidine (28.03 ± 0.18 Ma) as calibrated by Kuiper et al. (2008). Reported errors on the $^{40}Ar/^{39}Ar$ ages are at the 95% confidence level (2σ) including 0.3–0.4% standard deviation in the J-value.

paleosol at the top of this ignimbrite that contacts directly with the base of LPL, so the most probably age for the ApI is close to 1.34 Ma. Tables with all the analytical data of these Ar/Ar measurements are given in Appendix C.

4.4. Stratigraphic correlation

Stratigraphic descriptions, geological mapping and analytical results have allowed us to make a spatial and temporal correlation for the first 3

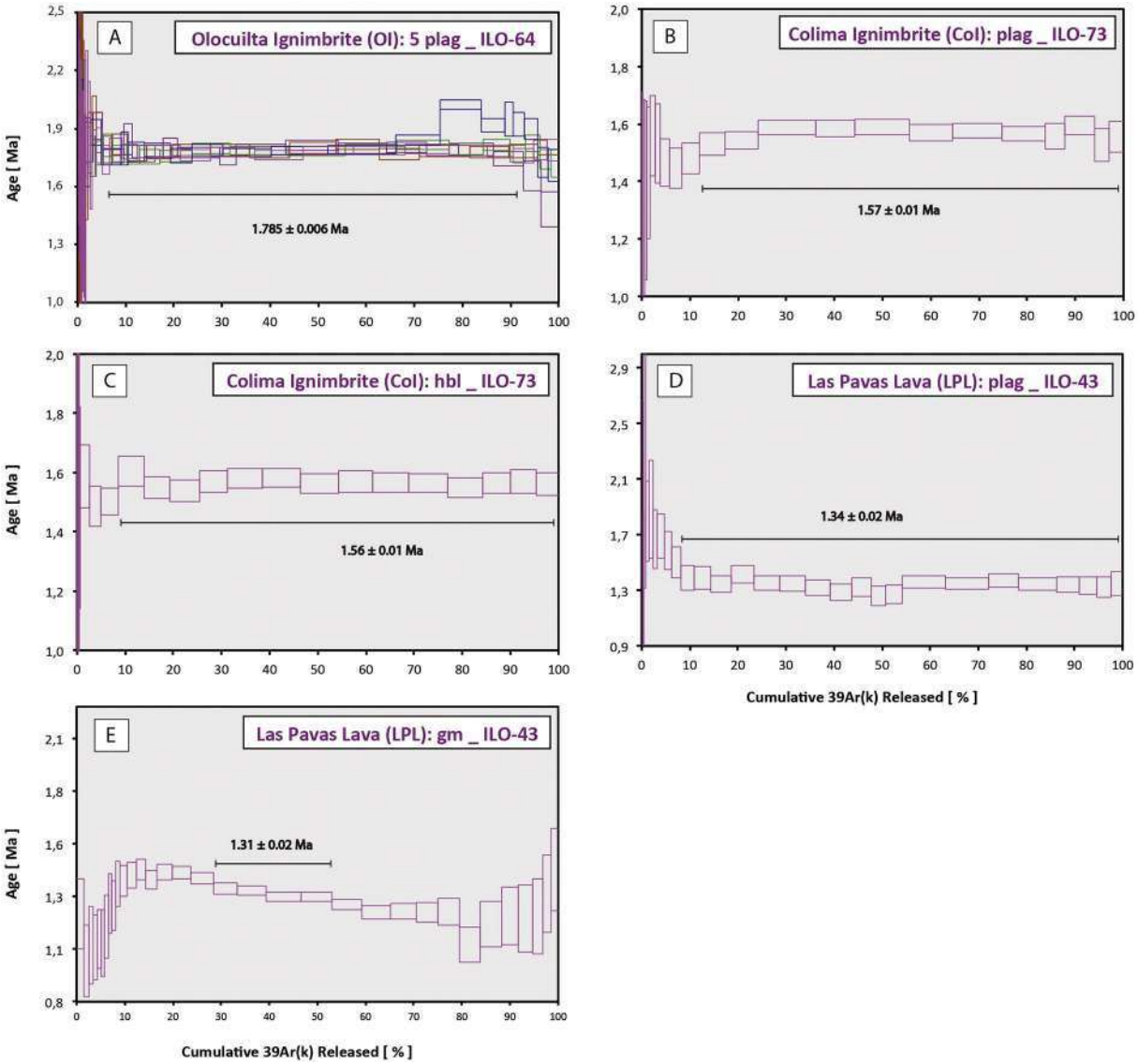

Fig. 11. $^{40}Ar/^{39}Ar$ age spectra showing high-resolution incremental heating steps for OI, CoI and LPL. Results of ApI were discarded and instead LPL was used to constrain the age of ApI (see Section 4.3.2). The weighted average age or plateau age (±2σ) is indicated. a) 5 stacked runs of plagioclases with different crystal sizes from OI. b) 1 plagioclase run from CoI. c) 1 hornblende run from the same CoI sample shown in b). d) 1 plagioclase run of LPL. e) 1 groundmass run of the same LPL sample of d).

ignimbrites of IC (Fig. 12). Four profiles (A, B, C and D) containing representative measured stratigraphic sections (logs) show the thickness and distribution of the early IC ignimbrites, as well as the lithofacies changes from proximal to distal deposits from the caldera.

5. Discussion

5.1. Volcanic phases of early ignimbrite-forming eruptions of Ilopango caldera

OI represents the first and largest explosive eruption of IC, which began with a brief eruption column that deposited a thin layer of pumice-lapilli fall. This column collapsed apparently by depressurization due to the sudden opening and widening of the vent, from a central vent to a larger fissure vent possibly related to the extensional tectonics of the area (e.g., Aguirre-Díaz and Labarthe-Hernández, 2003; Costa et al., 2011 and Section 5.3). The eruption then changed to extrusion of dense PDCs from the wider and larger fissure vent probably with a boiling-over style (e.g., Pacheco-Hoyos et al., 2018), as indicated by the pumice-rich nature of the OI and the long runout distances (Roche et al., 2016), which suggest lower explosivity and fragmentation of magma during eruption. At least 74 km^3 of pyroclastic material equivalent to 50 km^3 DRE came out of the vent (Section 5.2), filling the paleotopographic lows and covering a total area of about 3000 km^2, with runouts of at least 40 km. These PDCs were deposited continuously forming one single cooling unit, the massive OI. To the south of the

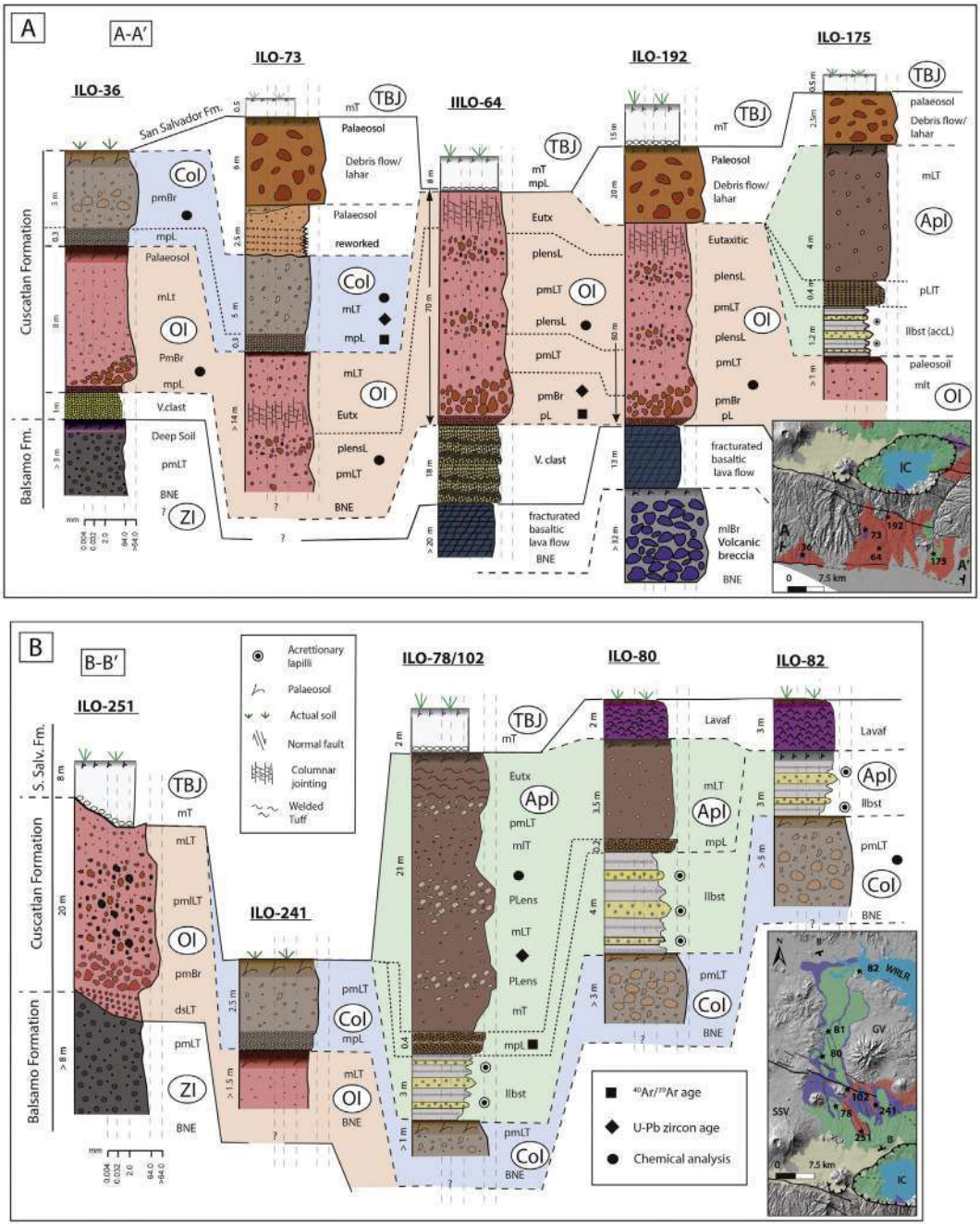

Fig. 12. Representative stratigraphic sections of OI, CoI and ApI overlying the Balsamo Formation materials, including lavas, volcanic breccias and dacitic-andesitic ignimbrites (note inset with index map showing location of each log site). a) Representative logs to the south of IC. b) Representative logs to the north of IC (Tierra Blanca Joven-TBJ is the youngest explosive event of IC at about 1500 BP). c) Representative logs to the northeast of IC (the 1.34 Ma LPL is covering ApI in ILO-43 with no paleosol between). d) Representative logs to the east of IC (note the San Vicente strike-slip Fault affecting the Carbonera caldera rim).

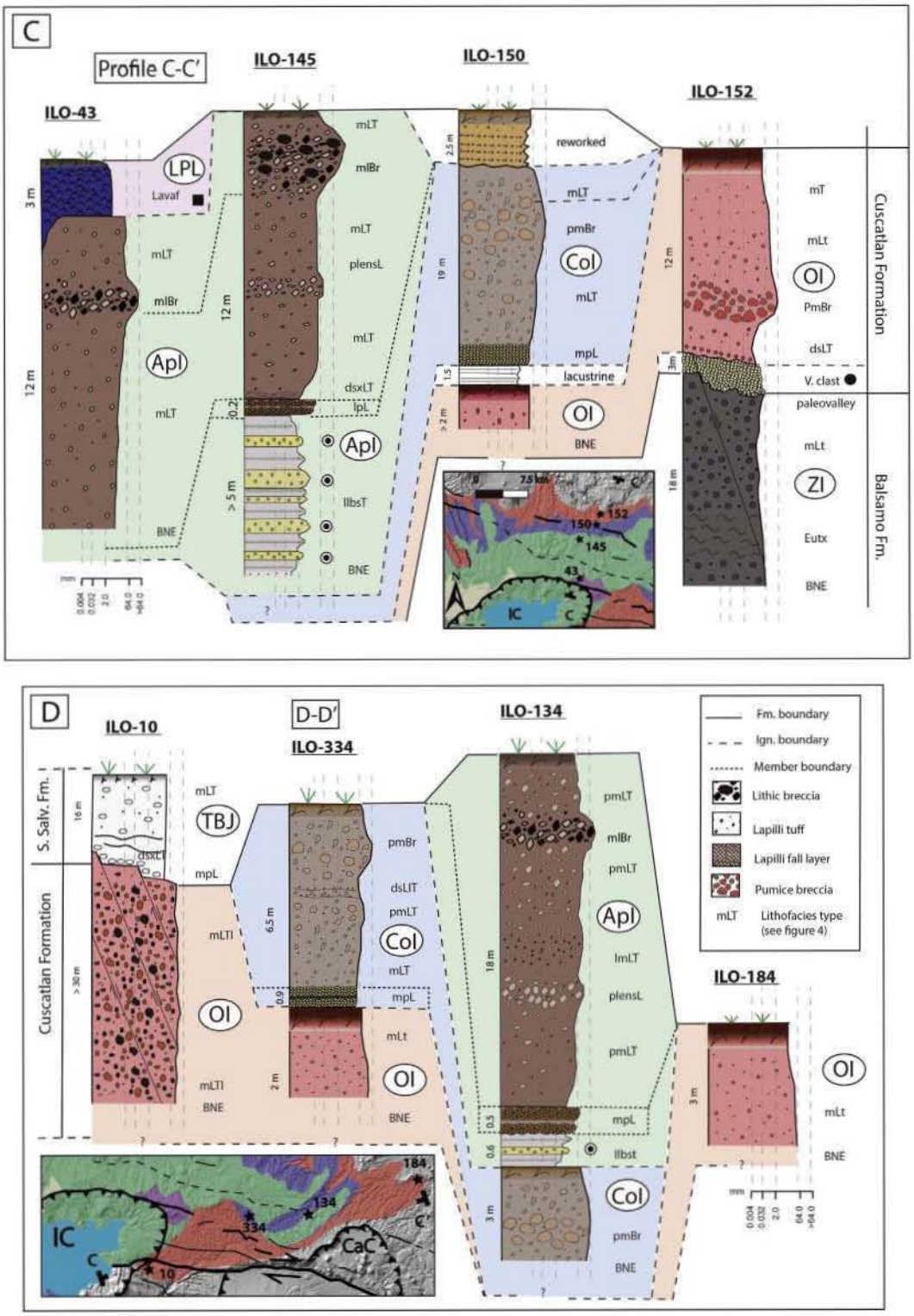

Fig. 12 (*continued*).

caldera this ignimbrite reached a thickness of N100 m (ILO-192, Figs. 2 and 4c), forming a medium to intensely welded level and building a plateau that stands out in the geomorphology: the Balsamo Mountain Range (Figs. 2 and 4c). To the north, this ignimbrite is only slightly welded (ILO-251; Fig. 2), probably because OI in this lithofacies (Fig. 12b) is very rich in lava lithics that tend to cool the PDC deposit more rapidly (Marti et al., 1991). Lithic-rich proximal facies of the OI can be interpreted as coignimbritic lithic lag breccias (Branney and

Kokelaar, 1997), indicating the proximity to the assumed fissure vent at or near the actual Ilopango lake.

The CoI is the result of the second large explosive eruption of IC. Similarly to OI, this eruption began with a brief eruptive column that formed a pumice fallout deposit of about ~50 cm thick. The initial column was followed by PDCs erupted from the caldera as boiling-over, produced during the second collapse phase of IC. These PDCs moved over the surface filling the lower parts of the paleotopography at San Salvador Pull-Apart (Fig. 2). PDCs traveled in all directions from the caldera with high mobility. The CoI spread north as far as the Lempa River Water Reservoir, with a runout of about 40 km (ILO-82, Fig. 2). To the southwest CoI's PDCs reached La Libertad Port, at 26 km from the caldera (ILO-36, Fig. 2). This unit consists of a lithics-poor, non-welded ignimbrite, with zones of large-pumice breccia lenses and intrusive cognate blocks (Fig. 5c) that we interpret as pieces of the subcaldera magma chamber, which suggests changes in the magmatic mass rate and the break apart of the magma chamber wall during caldera collapse. Both high-particle concentrations in the PDCs and the long runout distances were maintained because of the continuous supply of dense currents at the vent (Roche et al., 2016).

The third eruption of the IC that formed the ApI started differently than the two previous ones. Instead of pumice fallout deposits, there is a sequence of dilute fine-ash PDC deposits with accretionary lapilli at the base of this ignimbrite, suggesting that the eruption started with a hydromagmatic phase. Magma-water interaction increases the explosivity (i.e., fragmentation), and the PDCs become more turbulent leaving local cross-bedded deposits (Brown et al., 2010). As the eruption continued, and once the ratio of water-magma in the system decreased, the eruption switched to magmatic style where a brief eruptive column was generated producing a layer of 40-50 cm of pumice fall deposit. This was followed by the eruption of sustained large-volume denser PDCs, which thickened the overall volume of the ApI. Throughout this quasi-steady sequence of dense PDCs, there is a horizon of coignimbritic lithic lag breccias observable in the proximity of IC, which includes lava lithics up to 50 cm in diameter probably indicating the third caldera collapse episode (Aguirre-Díaz and Labarthe-Hernández, 2003; ILO-145 and ILO-43, Figs. 2 and 12c). The top of ApI is locally slightly welded, due to the accumulation of hot pyroclastics along the valley where is located ILO-78/102 (Rank II-III, Quane and Russell, 2005; Fig. 12b).

Water driving the hydromagmatic eruptions of the ApI was probably derived from a paleolake that filled the Ilopango depression formed after the second caldera collapse at 1.56–1.34 Ma (during the CoI eruption), similarly to the Taal caldera lake eruption in Philippines at 1965 (Moore et al., 1966). In some cases, dilute PDCs generated by hydromagmatism can travel farther than denser PDCs, like in ApI, where the basal dilute surges are observable at the Lempa River Water Reservation shore and the denser PDC's did not (ILO-81 and 82; Figs. 2 and 12b). A similar scenario occurred at the NE of the caldera (ILO-327; Figs. 2 and 3), where dilute PDCs deposited ~1 m of cross-stratified surges with no presence of massive and denser facies of ApI.

5.2. Volumes and magnitudes of early explosive eruptions of the Ilopango caldera

As the widespread distribution of the pyroclastic products of OI, CoI and ApI indicates (Fig. 2), the first volcanic phases of IC were large-volume explosive eruptions, with OI being the largest reported so far, even larger than the TBJ (the last explosive eruption of IC with 39 km^3 DRE; Dull et al., 2010). In order to characterize the magnitude and assess the minimum Volcanic Explosivity Index (VEI) of the three early IC eruptions, we estimated the deposit volumes of OI, CoI and ApI. The volumes were calculated employing the Delaunay triangulation method (Macedonio and Pareschi, 1991), particularly suitable for the reconstruction of volume between geological horizons and about the interpolation of bivariate data, when function values are available at irregularly-spaced data points, like in our case. This method uses the area occupied by the tuff, the local thickness of several sites (sampling and data sites ILOs, Fig. 2), and the zero-thickness boundary points. All data were processed in an attribute table with ArcGIS 10.2 by ESRI©, following the method described in Pitcher et al. (2017). The estimated deposits volumes were then transformed into DRE volume using the density ranks table of Quane and Russell (2005).

The welding of OI favored better preservation of this deposit that allowed several data collection sites for OI volume estimation. In some sites either the base or the roof of the unit is missing (see table in Appendix D), so conservative estimations for the OI volume range from 78 to 64 km^3 of PDC deposit and ~50 km^3 of DRE, indicating an eruption magnitude of 7.2 (Pyle, 2000) and a VEI ~ 7 (Newhall and Self, 1982). These estimates do not include tephra fall deposits and the graben-caldera fill, which may be significant. If we assume a ratio of 1:1:1 of intracaldera ignimbrite, outflow ignimbrite and distal ashfall deposits, as proposed by Mason et al. (2004), the total volume would increase to ~150 km^3 DRE, reaching a VEI N 7. In addition, the outflow sheets of OI probably reached the Pacific Ocean to the south as the smaller TBJ eruption did, and thus, an unknown amount of material, not-included in the volume estimates, may have gone out to sea. To the north, OI should have reached the Lempa River Water Reservoir area as CoI and ApI did (ILO-82; Fig. 2), since OI is much larger than the earlier eruptions deposit. The OI is presumably beneath these two younger ignimbrites and/or the recent lacustrine deposits in the distal zone. To the west, the PDCs of OI apparently traveled within an originally flat San Salvador Pull-Apart topography (Fig. 2), because at that period the San Salvador volcano did not exist as a topographic barrier (this volcano is ~70 ka; Sofield, 2004). Therefore, we interpret that PDCs of this first explosive eruption traveled radially from the vent. Assuming the possible original distribution of OI (Fig. 13), this ignimbrite volume might increase to of ~300 km^3 DRE. This order of magnitude corresponds to a VEI ~ 8, similar to the lower range of the supereruptions (Sparks et al., 2005; Self, 2006).

CoI and ApI outcrops showing complete thicknesses are scarce (table in Appendix D), and thus it was difficult to calculate an accurate volume of the second and third eruptions. Very conservative minimum volumes for these ignimbrites result in 16 km^3 and 13 km^3 of tephra respectively, and N11 km^3 and 9 N km^3 as DRE. More realistic volume estimates would give volumes between the OI minimum volume (~50 km^3 DRE) and the TBJ volume (39 km^3 DRE, Dull et al., 2010), because the deposit distributions of CoI and ApI are generally thicker and widespread than TBJ. For these reasons, the volume of these two eruptions should be higher than 40 km^3 DRE (VEI ≥ 6).

5.3. Origin and geologic evolution of IC in relation with the regional tectonics

The geodynamic evolution of the Ilopango area since 2 to 1 Ma includes the initial major volcanic explosive eruptions of IC (Fig. 13). These events began with the caldera collapse episodes associated with OI (1.785 ± 0.006 Ma), CoI (1.56 ± 0.01 Ma) and ApI (~1.34 Ma). A key factor to be considered in the origin of these eruptions is the regional and local tectonics in Ilopango area. A schematic model of the volcano-tectonic evolution during the early explosive eruptions of IC is explained below and illustrated in Fig. 13:

1) The first major eruption, represented by the OI, lacks pre-ignimbrite thick pumice fallouts (Plinian) deposits, which is a characteristic of fissure ignimbrite-forming eruptions related to regional faults (e.g., Aguirre-Díaz and Labarthe-Hernández, 2003; Aguirre-Díaz et al., 2008) and corresponds to overpressure type caldera eruptions (Geyer and Martí, 2008). Close to the timing of the OI eruption (1.785 Ma) there was an extensional setting within the ESFZ (Carr, 1976; Canora et al., 2014; Alonso-Henar et al., 2015, 2017). This extension could have produced a graben at or near the site of the actual IC (Fig. 13a). At the same time, the extension favored the continued ascension of an elongate magma chamber to shallower levels

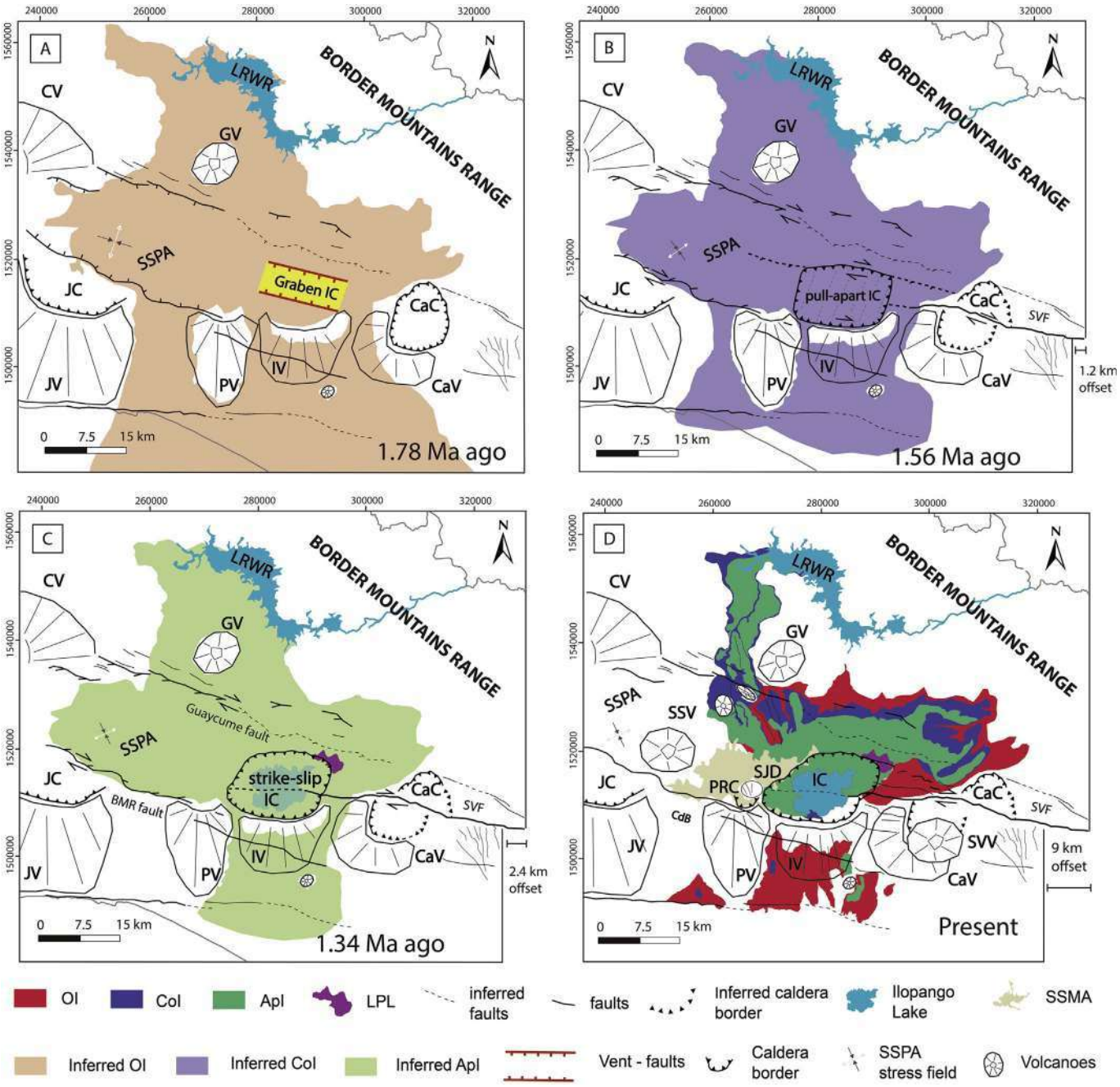

Fig. 13. Schematic geological model of the IC origin and its evolution through OI, CoI and ApI caldera collapse eruptions. a) First IC collapse related to a graben type caldera during an extensional phase along ESFZ and eruption of OI at about 1.78 Ma. b) Second IC collapse related to a pull-apart graben during the transition from extensional to transtensional tectonic regime along ESFZ and eruption of CoI at about 1.56 Ma. Note the initial offset of CaC associated to the strike-slip San Vicente Fault (SVF) to the east of IC. c) Third collapse of IC related to the already formed pull-apart graben and ApI eruption at about 1.34 Ma. The San Vicente Fault continues the offset of CaC. d) Actual features in IC showing main faults and distribution of OI, CoI and ApI.

(e.g., Aguirre-Díaz and Labarthe-Hernández, 2003; Costa and Marti, 2016) until the magmatic system suddenly opened along the graben's faults and the OI eruption occurred as fissure vents and producing the first IC collapse. This graben was capable of erupting massively the pumiceous pyroclastic currents that formed OI (the largest of the three ignimbrites reported here). Analogue models of Holohan et al. (2008) revealed a "graben localized above magma chamber" during an initial stage of extensional deformation in strike-slip calderas, the type of tectonic caldera that suggested Saxby et al. (2016) for the current IC.

2) During the timing among the first and the second explosive eruption of IC (a time span of 1.78 to 1.56 Ma BP), the tectonic regime along the ESFZ changed gradually from extensional to transtensional, provoking the development of strike-slip faults and pull-apart structures along the El Salvador Volcanic Front (Correa-Mora et al., 2009; LaFemina et al., 2009; Alonso-Henar et al., 2015, 2017; Garibaldi et al., 2016). At the moment of CoI (the second eruption of IC at ~1.56 Ma BP), the San Vicente Fault already existed and it had displaced the Carbonera caldera rim with a dextral offset of N1 km (CaC, Fig. 13b). Offset started at ~1.70 Ma BP with an average slip rate of ~5 ± 0.5 mm/yr (Canora et al., 2014; Rotolo and Castorina, 1998). This new input of laterally component in ESFZ could have changed the IC dynamics between the OI and CoI eruptions, evolving from a graben-caldera type to a pull-apart caldera

type (Fig. 13a and b). Similar processes from extensional to transtensional settings in areas with calderas are the cases of the Suwoh, Ranau and Toba calderas along the Great Sumatran Fault Zone, in Indonesia (Bellier and Sébrier, 1994) and the calderas in the Sierra Madre Occidental, in Mexico (Aguirre-Díaz et al., 2008).

3) During the third explosive eruption of IC (ApI, at ~1.34 Ma BP) the resulting caldera was apparently affected by the strike-slip activity along the San Vicente Fault, which by then had already displaced the Carbonera caldera rim by N2.3 km (Fig. 13c). Regionally, between the second and third caldera eruptions (time span of 1.56-1.34 Ma), the lateral component of the ESZF increases in detriment of the extensional (Canora et al., 2014; Alonso-Henar et al., 2015, 2017). The IC framework of a pull-apart caldera continued during this eruption, but with a higher lateral component due to the effect of the San Vicente Fault prolongation westward (Fig. 13b and c). The presence of a coignimbritic lithic lag breccia within the ApI indicates that the third caldera collapse onset could have been in a setting of higher compression between blocks, caused probably by lateral stretching (Holohan et al., 2008). Calderas in strike-slip zones are often elongated by the regional faulting control, and apparently formed from noncircular but rather elongated magmatic reservoirs, for example the Rannoch Moor granite in Scotland (Jacques and Reavy, 1994), or the Ardara pluton, Ireland (Molyneux and Hutton, 2000). These complexes were deformed and elongated by transtensive regional faults prior to full crystallization. This kind of stretching that increase compression locally is currently occurring in IC area (Garibaldi et al., 2016), where recent gravimetric studies classified it as a strike-slip caldera (Saxby et al., 2016; Fig. 13d).

As with the possible proto-graben related to the OI eruption, there is no clear geomorphologic evidence that IC was a pull-apart caldera type during the CoI and ApI eruptions. However, it is possible that this old pull-apart basin is being cut by the strike-slip San Vicente Fault. In general, the obliteration of a pull-apart/graben appears to be the consequence of the new strike-slip faulting that develops and propagates across the pre-basin through its center (e.g., Bellier and Sébrier, 1994). An important consequence of this type of tectonic evolution is that pull-apart grabens could be ephemeral structures within strike-slip faults (Holohan et al., 2008).

The potential volumes reported here for the three early caldera collapse eruptions make IC the largest active eruptive center of the El Salvador Volcanic Front since about 1.75 Ma. A high magma production was necessary to generate these amounts of pyroclastic products of the early IC's stages. The primary control for the production of great amounts of silicic magma at continental-margin systems is the flux of basaltic magma from the mantle (Smith, 1979; Hildreth, 1981; de Silva and Gosnold, 2007). This high flux of magma in the CAVA was apparently possible during the rollback of the subducted plate of Cocos beneath Central America since the late Miocene (Alonso-Henar et al., 2015, 2017), which may have caused the opening of a mantle wedge and the consequent process of flare-up (Aguirre-Díaz et al., 2008). Continued rise of magma to shallow levels was favored by the extensional and transtensional tectonics, where the regional strike-slip faults and local pull-apart basins worked out as the principal magma pathways.

6. Conclusions

The Ilopango caldera (IC) had multiple caldera collapse eruptions during its eruptive history. The first three caldera-forming eruptions from Ilopango produced the OI at 1.785 ± 0.006 Ma, the CoI at 1.56 ± 0.01 Ma, and the ApI at ~1.34 Ma. They all are rhyolitic and calcalkaline tuffs, which is common for magmas at continental margins subduction zones, such as the Central American Volcanic Arc. OI was the largest eruption of Ilopango caldera complex, probably generated from a graben-type caldera related to the extensional tectonics at central El Salvador. This deposit covered an area of ~3000 km² with a minimum DRE volume of 50 km³, likely up to 300 km³ DRE considering the coignimbritic ash cloud, the intracaldera fill and eroded deposits, corresponding to a VEI ≥ 7. Both the CoI and ApI have smaller volumes than OI, but similar or even larger than TBJ deposit, which is more than ~40 km³ DRE. We suggest that the caldera structure changed from pure extensional graben during the OI eruption to a pull-apart during the CoI and ApI eruptions, with higher lateral component for the last one. All three caldera-forming episodes are related to the evolution of the ESFZ, which actually involves large strike-slip faults and pull-apart basins. Ilopango caldera complex represents the largest, highly explosive, and active long-lived caldera structure in El Salvador. Activity related to ignimbrite-forming eruptions at Ilopango started at 1.785 Ma BP and it is still producing large ignimbrites sheets like the TBJ, emplaced ~1500 years ago.

Acknowledgements

This study was financed by CONACYT-CB grant 240447 to GAD. We appreciate the logistical support of the Ministerio de Medio Ambiente y Recursos Naturales – MARN, and of the Policia Nacional Civil – PNC, of El Salvador. We thank the doctoral scholarship grant to the first author from CONACYT-Mexico. We want to be grateful to Juan Vazquez for thin section elaboration, to Lozano Santacruz and Patricia Girón for XRF analyses, Ofelia Perez for the REE and trace elements analyses, and Alex Iriondo for SEM and petrographic analyses. We acknowledge to Anthony Koppers for his help and support in the Ar/Ar geochronology laboratory at Oregon State University (OSU). This manuscript was greatly improved by comments and suggestions from the editor Joan Martí and the reviewers Valerio Acocella and Jim Cole.

Appendix A. Supplementary data

Supplementary data to this article can be found online at https://doi.org/10.1016/j.jvolgeores.2018.12.004.

References

Acocella, V., 2007. Understanding caldera structure and development: an overview of analogue models compared to natural calderas. Earth-Sci. Rev. 85, 125-160.

Acocella, V., Korme, T., Salvini, F., Funiciello, R., 2002. Elliptic calderas in the Ethiopian Rift: control of pre-existing structures. J. Volcanol. Geotherm. Res. 119, 189–203. https://doi.org/10.1016/S0377-0273(02)00342-6.

Agostini, S., Corti, G., Doglioni, C., Carminati, E., Innocenti, F., Tonarini, S., Manetti, P., Di Vincenzo, G., Montanari, D., 2006. Tectonic and magmatic evolution of the active volcanic front in El Salvador: insight into the Berlín and Ahuachapán geothermal areas. Geothermics 35, 368–408. https://doi.org/10.1016/j.geothermics.2006.05.003.

Aguirre–Díaz, G., 2008. Types of collapse calderas. IOP conf. Series: Earth an Environmental Science. 3 (012021).

Aguirre-Díaz, G.J., Labarthe-Hernández, G., 2003. Fissure ignimbrites: fissure source origin for voluminous ignimbrites of the Sierra Madre Occidental and its relationship with Basin and Range faulting. Geology 31, 773-776.

Aguirre-Díaz, G.J., Martí, J., 2015. Graben calderas: examples from Mexico, Central America, and the Andes. 26th IUGG General Assembly, Prague, Czech Republic, June 22–July 2, 2015; Abstracts https://www.czech-in.org/cm/IUGG/CM.NET.WebUI/CM.NET.WEBUI.scpr/SCPRfunctiondetail.aspx?confID=05000000-0000-0000-0000-000000000053&sesID=05000000-0000-0000-0000-000000002536&absID=07000000-0000-0000-0000-000000022205.

Aguirre-Díaz, G.J., Labarthe-Hernández, G., Tristán-González, M., Nieto-Obregón, J., Gutiérrez-Palomares, I., 2008. Ignimbrite flare-up and graben-calderas of the Sierra Madre Occidental, Mexico. In: Gottsmann, J., Martí, J. (Eds.), Caldera Volcanism: Analysis, Modelling and Response. Developments in Volcanology vol. 10. Elsevier, Amsterdam. ISBN: 978-0-444-53165-0. https://doi.org/10.1016/S1871-644X(07)00004-6 (492 pp., (143-180 pp.)).

Aguirre-Díaz, J.G., Suñe-Puchol, I., Davila-Harris, P., Pedrazzi, D., Hernandez, W., Gutierrez, E., 2017. Volcanic history of the Ilopango caldera, Central American Volcanic Arc. 113th Annual Meeting, 2017 GSA Cordilleran Section, Hawaii, USA.

Alonso-Henar, J., Schreurs, G., Martinez-Díaz, J.J., Álvarez-Gómez, J.A., Villamor, P., 2015. Neotectonic development of the El Salvador Fault Zone and implications for deformation in the Central America Volcanic Arc: insights from 4-D analog modeling experiments. Tectonics 34, 133–151. https://doi.org/10.1002/2014TC003723.

Alonso-Henar, J., Álvarez-Gómez, J.A., Martinez-Díaz, J.J., 2017. Neogene-quaternary evolution from transpressional to transtesional tectonics in Northern Central America controlled by cocos: Caribbean subduction coupling change. J. Iber. Geol. https://doi.org/10.1006/s415113-017-0034-2.

Alvarado, D., DeMets, C., Tikoff, B., Hernandez, D., Wawrzyniec, T.F., Pullinger, C., Mattioli, G., Turner, H.L., Rodriguez, M., Correa-Mora, F., 2011. Forearc motion and deformation between El Salvador and Nicaragua: GPS, seismic, structural, and paleomagnetic observations. Lithosphere 3, 3–21. https://doi.org/10.1130/L108.1.

Alvarenga, E.R., Hernández, D.A., Hernández-Flores, D.A., 2001. Cronología de sismos destructivos en El Salvador: Servicio Geológico Nacional, Área de Sismología.

Arculus, R.J., Curran, E.B., 1972. The genesis of the calc-alkaline rock suite. Earth Planet. Sci. Lett. 15, 255–262.

Authemayou, C., Brocard, G., Teyssier, C., Simon-Labric, T., Guttiérrez, A., Chiquín, E.N., Morn, S., 2011. The Caribbean-North America-Cocos Triple Junction and the dynamics of the Polochic-Motagua fault systems: pull-up and zipper models. Tectonics 30, 1–23. https://doi.org/10.1029/2010TC002814.

Bacon, C.R., Lanphere, M.A., 2006. Eruptive history and geochronology of Mount Mazama and the Crater Lake region, Oregon. Geol. Soc. Am. Bull. 118, 1331–1359. https://doi.org/10.1130/B25906.1.

Bellier, O., Sébrier, M., 1994. Relationship between tectonism and volcanism along the Great Sumatran Fault Zone deduced by spot image analyses. Tectonophysics 233, 215–231. https://doi.org/10.1016/0040-1951(94)90242-9.

Bernal, J.P., Lozano-Santacruz, R., 2005. Characterization of a new set of eight geochemical reference materials for XRF major and trace element analysis. Rev. Mex. Cienc. Geol. 22 (3), 329-344.

Branney, M.J., Kokelaar, P., 1997. Giant bed from a sustained catastrophic density current flowing over topography: Acatlán ignimbrite, Mexico. Geology 25, 115–118. https://doi.org/10.1130/0091-7613(1997)025b0115:GBFASCN2.3.CO;2.

Branney, M.J., Kokelaar, P., 2002. Pyroclastic density currents and the sedimentation of ignimbrites. Geol. Soc. Lond. Mem. 27 (152 pp.).

Brown, R.J., Branney, M.J., 2004. Event stratigraphy of a caldera-forming ignimbrite eruption on Tenerife: the 273 ka Poris Formation. Bull. Volcanol. 66, 392-416.

Brown, R.J., Branney, M.J., Maher, C., Dávila-Harris, P., 2010. Origin of accretionary lapilli within ground-hugging density currents: evidence from pyroclastic couplets on Tenerife. Bull. Geol. Soc. Am. 122, 305–320. https://doi.org/10.1130/B26449.1.

Canora, C., Villamor, P., Martínez-Díaz, J.J., Berryman, K.R., Álvarez-Gómez, J.A., Capote, R., Hernández, W., 2012. Paleoseismic analysis of the San Vicente segment of the El Salvador Fault Zone, El Salvador, Central America. Geol. Acta 10, 103-123. https://doi.org/10.1344/105.000001700.

Canora, C., Martínez-Díaz, J.J., Villamor, P., Staller, A., Berryman, K., Álvarez-Gómez, J.A., Capote, R., Diaz, M., 2014. Structural evolution of the El Salvador Fault Zone: an evolving fault system within a volcanic arc. J. Iber. Geol. 40, 471-488.

Carr, M.J., 1976. Underthrusting and Quaternary faulting in northern Central America. Geol. Soc. Am. Bull. 87, 825-829. https://doi.org/10.1130/0016-7606(1976)87b825:UAQFINN2.0.CO;2.

Carr, M., Patiño, L., Feingenson, M., 2007. Chapter 22: petrology and geochemistry of lavas. Cent. Am. Geol. Resour. Hazards, pp. 1–26.

CEL (Comision Ejecutiva Hidroelectrica del Rio Lempa), 1992. Desarrollo de los Recursos Geotermicos del Area Centro-Occidental de El Salvador. Prefactibilidad Geotermica del Area de Coatepeque. Reconocimiento Geotermico. Informe Final. Internal Report.

Cole, J.W., Milner, D.M., Spinks, K.D., 2005. Calderas and caldera structures: a review. Earth-Sci. Rev. 69, 1–96.

Correa-Mora, F., DeMets, C., Alvarado, D., Turner, H.L., Mattioli, G., Hernandez, D., Pullinger, C., Rodriguez, M., Tenorio, C., 2009. GPS-derived coupling estimates for the Central America subduction zone and volcanic arc faults: El Salvador, Honduras and Nicaragua. Geophys. J. Int. 179, 1279–1291.

Corti, G., Carminati, E., Mazzarini, F., Garcia, M.O., 2005. Active strike-slip faulting in El Salvador, Central America. Geology 33, 989–992.

Costa, A., Marti, J., 2016. Stress field control during large caldera-forming eruptions. Front. Earth Sci. 4, 92. https://doi.org/10.3389/feart.2016.00092.

Costa, A., Gottsmann, J., Melnik, O., Sparks, R.S.J., 2011. A stress-controlled mechanism for the intensity of very large magnitude explosive eruptions. Earth Planet. Sci. Lett. 310, 161–166. https://doi.org/10.1016/j.epsl.2011.07.024.

Costa, A., Smith, V., Macedonio, G., Matthews, N., 2014. The magnitude and impact of the Youngest Toba Tuff super-eruption. Front. Earth Sci. 2, 16. https://doi.org/10.3389/feart.2014.00016.

DeMets, C., 2001. A new estimate for present-day Cocos-Caribbean plate motion: Implications for slip along the Central American volcanic arc. Geophys. Res. Lett. 28, 4043–4046. https://doi.org/10.1029/2001GL013518.

Dixon, T.H., 1993. GPS measurement of relative motion of the Cocos and Caribbean plates and strain accumulation across the Middle America Trench. Geophys. Res. Lett. 20, 2167–2170. https://doi.org/10.1029/93GL02415.

Donnelly, T.W., Horne, G.S., Finch, R.C., Lopez-Ramos, E., 1990. Northern Central America: the Maya and Chortis blacks. In: Dengo, G., Case, J.E. (Eds.), The Geology of North America: The Caribbean Region, pp. 37–76.

Druitt, T.H., Sparks, R.S.J., 1984. On the formation of calderas during ignimbrite eruptions. Nature 310, 679-681.

Dull, R.A., Southon, J.R., Sheets, P., 2001. Volcanism, ecology and culture: a reassessment of the Voclán Ilopango TBJ eruption in the southern Maya realm. Lat. Am. Antiq. 12 (1), 25–44.

Dull, R.A., Southon, J.R., Kutterolf, S., Freundt, A., Wahl, D., Sheets, P., 2010. Did the TBJ Ilopango eruption cause the AD 536 event? AGU Fall Meet. Abstr.. vol. 1, p. 2370

Francis, P.W., O'Callaghan, L., Kretzschmar, G.A., Thorpe, R.S., Sparks, R.S.J., Page, R.N., 1983. The Cerro Galan ignimbrite. Nature 301, 51–53.

Funk, J., Mann, P., McIntosh, K., Stephens, J., 2009. Cenozoic tectonics of the Nicaraguan depression, Nicaragua, and Median Trough, El Salvador, based on seismic-reflection profiling and remote-sensing data. Bull. Geol. Soc. Am. 121, 1491-1521. https://doi.org/10.1130/B26428.1.

Garibaldi, N., Tikoff, B., Hernández, W., 2016. Neotectonic deformation within an extensional stepover in El Salvador magmatic arc, Central America: implication for the interaction of arc magmatism and deformation. Tectonophysics 693, 327-339. https://doi.org/10.1016/j.tecto.2016.05.015.

Geyer, A., Martí, J., 2008. The new worldwide collapse caldera database (CCDB): a tool for studying and understanding caldera processes. J. Volcanol. Geotherm. Res. 175, 334–354. https://doi.org/10.1016/j.jvolgeores.2008.03.017.

Girard, G., van Wyk de Vries, B., 2005. The Managua Graben and Las Sierras-Masaya volcanic complex (Nicaragua); pull-apart localization by an intrusive complex: results from analogue modeling. J. Volcanol. Geotherm. Res. 144, 37–57. https://doi.org/10.1016/j.jvolgeores.2004.11.016.

Golombek, M.P., Carr, M.J., 1978. Tidal triggering of seismic and volcanic phenomena during the 1879-1880 eruption of Islas Quemadas volcano in El Salvador, Central America. J. Volcanol. Geotherm. Res. 3, 299–307. https://doi.org/10.1016/0377-0273(78)90040-9.

Gottsmann, J., Martí, J., 2008. Caldera volcanism: analysis, modelling and response. Developments in Volcanology. vol. 10. Elsevier, Amsterdam (492 pp.).

Gottsmann, J., Lavallée, Y., Martí, J., Aguirre-Díaz, G., 2009. Magma-tectonic interaction and the eruption of silicic batholiths. Earth Planet. Sci. Lett. (ISSN: 0012-821X) 284, 426–434. https://doi.org/10.1016/j.epsl.2009.05.008.

Guzmán-Speziale, M., Valdés-González, C., Molina, E., Gómez, J.M., 2005. Seismic activity along the Central America volcanic arc: is it related to subduction of the Cocos plate? Tectonophysics 400, 241–254. https://doi.org/10.1016/j.tecto.2005.03.006.

Hernández, E.W., 2004. Características geotécnicas y vulcanológicas de las tefras de Tierra Blanca Joven de Ilopango, El Salvador. (Tesis de maestría). Univ. Politécnica de El Salvador, San Salvador (115 pp.).

Hernández, W., 2008. Aspectos geológicos que influyen en las aguas subterráneas y en la respuesta sísmica del Area Metropolitana de San Salvador. Revista ASIA No. 162 (29-41 pp.).

Hernández, E.W., Ferrés, D., Delgado-Granados, H., Pullinger, C., Gutiérrez de Henríquez, E., 2010. The last 40 ka eruptive cycle of Ilopango caldera deposits: a settlement for the San Salvador Metropolitan Area (El Salvador). Abstract Volume, International Conference Cities on Volcanoes. Fundación Canaria ITER, Tenerife, p. 56.

Hildreth, E.W., 1981. Gradients in silicic magma chambers: implications for lithospheric magmatism. J. Geophys. Res. 86, 10,153–10,192. https://doi.org/10.1029/JB086iB11p10153.

Holohan, E.P., Van Wyk de Vries, B., Troll, V.R., 2008. Analogue models of caldera collapse in strike-slip tectonic regimes. Bull. Volcanol. 70, 773-796. https://doi.org/10.1007/s00445-007-0166-x.

Hutton, D.H.W., Reavy, R.J., 1992. Strike-slip tectonics and granite petrogenesis. Tectonics 11, 960-967.

Jacques, J.M., Reavy, R.J., 1994. Caledonian plutonism and major lineaments in the SW Scottish Highlands. J. Geol. Soc. Lond. 151, 955–969.

Koppers, A.A.P., 2002. ArArCALC—software for 40Ar/39Ar age calculations. Comput. Geosci. 28 (5), 605–619. https://doi.org/10.1016/S0098-3004(01)00095-4.

Koppers, A.A.P., Gowen, M.D., Colwell, L.E., Gee, J.S., Lonsdale, P.F., Mahoney, J.J., Duncan, R.A., 2011. New 40Ar/39Ar age progression for the Louisville hot spot trail and implications for inter–hot spot motion. Geochem. Geophys. Geosyst. 12, Q0AM02. https://doi.org/10.1029/2011GC003804.

Kuiper, K.F., Deino, A., Hilgen, F.J., Krijgsman, W., Renne, P.R., Wijbrans, J.R., 2008. Synchronizing rock clocks of Earth history. Science 320, 500–504. https://doi.org/10.1126/science.1154339.

Kutterolf, S., Freundt, A., Schacht, U., Bürk, D., Harders, R., Mörz, T., Peréz, W., 2008. Pacific offshore record of plinian arc volcanism in Central America: 3. Application to forearc geology. Geochem. Geophys. Geosyst. 9. https://doi.org/10.1029/2007GC001826.

LaFemina, P., Dixon, T.H., Govers, R., Norabuena, E., Turner, H., Saballos, A., Mattioli, G., Protti, M., Strauch, W., 2009. Fore-arc motion and Cocos Ridge collision in Central America. Geochem. Geophys. Geosyst. 10. https://doi.org/10.1029/2008GC002181.

LeBas, et al., 1986. A chemical classification of volcanic rocks based on the total alkali-silica diagram. J. Petrol. 27, 745-750.

Lexa, J., Šebesta, J., Chavez, J.A., Hernández, W., Pécskay, Z., 2011. Geology and volcanic evolution in the southern part of the San Salvador Metropolitan Area. J. Geosci. 56, 105–140. https://doi.org/10.3190/jgeosci.088.

Lipman, P.W., 1997. Subsidence of ash-flow calderas: relation to caldera size and magma-chamber geometry. Bull. Volcanol. 59, 198–218. https://doi.org/10.1007/s004450050186.

Lipman, P.W., 2000. Calderas. In: Sigurdsson, H. (Ed.), Encyclopedia of Volcanoes. Academic Press, San Francisco, pp. 643-662.

Lipman, P.W., Dungan, M.A., Brown, L.L., Deino, A., 1996. Recurrent eruption and subsidence at the Platoro caldera complex, southeastern San Juan volcanic field, Colorado: new tales from old tuffs. Bull. Geol. Soc. Am. 108, 1039–1055. https://doi.org/10.1130/0016-7606(1996)108b1039:REASATN2.3.CO;2.

Ludwig, K., 2008. Manual for isoplot 3.7. Berkeley Geochronology Center, Special Publication 4, p. 77 (rev.).

Macedonio, G., Pareschi, M.T., 1991. An algorithm for the triangulation of arbitrarily distributed points: applications to volume estimate and terrain fitting. Comput. Geosci. 17, 859–874. https://doi.org/10.1016/0098-3004(91)90086-S.

Mann, P., 2007. Overview of the tectonic history of northern Central America. In: Mann, P. (Ed.), Geologic and Tectonic Development of the Caribbean Plate Boundary in Northern Central America. Geological Society of America Special Papers vol. 428, pp. 1–19.

Marti, J., Diez-Gil, J.L., Ortiz, R., 1991. Conduction model for the thermal influence of lithic clasts in mixtures of hot gases and ejecta. J. Geophys. Res. 96 (B13) (Pages 21, 879.21, 885).

Marti, J., Ablay, G.J., Redshaw, L.T., Sparks, R.S.J., 1994. Experimental studies of collapse calderas. J. Geol. Soc. Lond. 151, 919-929.

Martínez-Díaz, J.J., Álvarez-Gómez, J.A., Benito, B., Hernández, D., 2004. Triggering of destructive earthquakes in El Salvador. Geology 32, 65-68. https://doi.org/10.1130/G20089.1.

Mason, B.G., Pyle, D.M., Oppenheimer, C., 2004. The size and frequency of the largest explosive eruptions on Earth. Bull. Volcanol. 66, 735–748.
Molina, F., Martí, J., Aguirre, G., Vega, E., Chavarría, L., 2014. Stratigraphy and structure of the Cañas Dulces caldera (Costa Rica). Bull. Geol. Soc. Am. 126, 1465-1480. https://doi.org/10.1130/B31012.1.
Molyneux, S.J., Hutton, D.H.W., 2000. Evidence for significant granite space creation by the ballooning mechanism; the example of the Ardara Pluton, Ireland. Geol. Soc. Am. Bull. 112, 1543–1558.
Montero, W., Dewey, J., 1982. Shallow-focus seismicity, composite focal mechanisms, and tectonics of the Valle Central of Costa Rica. Bull. Seismol. Soc. Am. 72, 1611–1626.
Moore, J.G., Nakamura, K., Alcaraz, A., 1966. The 1965 eruption of Taal volcano. Science 151, 955-960.
Morris, J.D., Ryan, J.G., 2004. Subduction zone processes and implications for changing composition of the upper and lower mantle. In: Holland, H.D., Turekian, K.K. (Eds.), Treatise on Geochemistry. Elsevier-Pergamon, Oxford, pp. 451–470.
Murphy, J.B., 2007. Igneous rock associations 8. Arc magmatism II: geochemical and isotopic characteristics. Geosci. Can. 34, 1.
Newhall, C.G., Dzurisin, D., 1988. Historical Unrest at Large Calderas of the World. U.S. Geological Survey (1109 pp.).
Newhall, C.G., Self, S., 1982. The volcanic explosivity index (VEI) an estimate of explosive magnitude for historical volcanism. J. Geophys. Res. Oceans 87, 1231-1238. https://doi.org/10.1029/JC087iC02p01231.
Ortega-Obregón, C., Solari, L., Gómez-Tuena, A., Elías-Herrera, M., Ortega-Gutiérrez, F., Macías-Romo, C., 2013. Permian–Carboniferous arc magmatism in southern Mexico: U–Pb dating, trace element and Hf isotopic evidence on zircons of earliest subduction beneath the western margin of Gondwana. Int. J. Earth Sci. 103 (5), 1287–1300. https://doi.org/10.1007/s00531-013-0933-1.
Pacheco-Hoyos, J.G., Aguirre-Díaz, G.J., Dávila-Harris, P., 2018. Boiling-over dense pyroclastic density currents during the formation of the ~100 km³ Huichapan ignimbrite in Central Mexico: stratigraphic and lithofacies analysis. J. Volcanol. Geotherm. Res. 349, 268-282.
Peccerillo, A., Taylor, S.R., 1976. Geochemistry of Eocene calcalkaline volcanic rocks from the Kastamonu area, Northern Turkey. Contrib. Mineral. Petrol. 58, 63–81.
Pedrazzi, D., Sunyé-Puchol, I., Aguirre-Díaz, G.J., Costa, A., Davila-Harris, P., Hernández, W., Gutierrez, E., 2018. The Ilopango Tierra Blanca Joven (TBJ) eruption, El Salvador: volcano-stratigraphy of a major Holocene event of Central America and hazards implications EGU General Assembly 2018. EGU2018-8455. vol. 20.
Pitcher, B.W., Kent, A.J.R., Grunder, A.L., Duncan, R.A., 2017. Frequency and volumes of ignimbrite eruptions following the Late Neogene initiation of the Central Oregon High Cascades. J. Volcanol. Geotherm. Res. 339, 1–22. https://doi.org/10.1016/j.jvolgeores.2017.04.019.
Pyle, D.M., 2000. Sizes of volcanic eruptions. In: Sigurdsson, H., et al. (Eds.), Encyclopedia of Volcanoes. Academic Press, pp. 263-269.
Quane, S.L., Russell, J.K., 2005. Ranking welding intensity in pyroclastic deposits. Bull. Volcanol. 67, 129–143. https://doi.org/10.1007/s00445-004-0367-5.
Rampino, M.R., Self, S., 1993. Climate-volcanism feedback and the Toba eruption of ~74,000 years ago. Quat. Res. https://doi.org/10.1006/qres.1993.1081.
Reynolds, J.H., 1987. Timing and sources of Neogene and Quaternary volcanism in south-central Guatemala. J. Volcanol. Geotherm. Res. 33, 9–22.
Richer, M., Mann, C.P., Stix, J., 2004. Mafic magma injection triggers eruption at Ilopango Caldera, El Salvador, Central America. Spec. Pap. 375 Nat. Hazards El Salvador, pp. 175–190 https://doi.org/10.1130/0-8137-2375-2.175.
Robertson, E.A.M., Biggs, J., Cashman, K.V., 2015. Influence of Regional Tectonics and Pre-existing Structures on the Formation of Elliptical Calderas in the Kenyan Rift School of Earth Sciences. University of Bristol, Wills Memorial Building, British Geological Survey, Murchison House, West Mains Road, Edinburgh EH9 3LA, UK.
Roche, O., Buesch, D.C., Valentine, G.A., 2016. Slow-moving and far-travelled dense pyroclastic flows during the Peach Spring super-eruption. Nat. Commun. 7, 10890.
Rose, W.I., Conway, F.M., Pullinger, C.R., Deino, A., McIntosh, K., 1999. An improved age framework for late Quaternary silicic eruptions in northern Central America. Bull. Volcanol. 61, 106–120. https://doi.org/10.1007/s004450050266.
Rotolo, S.G., Castorina, F., 1998. Transition from mildly-tholeiitic to calc-alkaline suite: the case of Chichontepec volcanic centre, El Salvador, Central America. J. Volcanol. Geotherm. Res. 86, 117–136. https://doi.org/10.1016/S0377-0273(98)00076-6.
Sánchez-Esquivel, I.A., 2016. Levantamiento batimétrico y medición de parámetros fisicoquímicos en el Lago de Ilopango, El Salvador (Bachelor Thesis at Facultad de Ciencias Naturales y Matemática, Escuela de Física, Universidad de El Salvador, El Salvador).
Saxby, J., Gottsmann, J., Cashman, K., Gutiérrez, E., 2016. Magma storage in a strike-slip caldera. Nat. Commun. 7, 12295. https://doi.org/10.1038/ncomms12295.
Self, S., 2006. The effects and consequences of very large explosive volcánic eruptions. Phil. Trans. R. Soc. A 364, 2073–2097. https://doi.org/10.1098/rsta.2006.1814.
de Silva, S.L., Gosnold, W.A., 2007. Episodic construction of batholiths: insights from the spatiotemporal development of an ignimbrite flare-up. J. Volcanol. Geotherm. Res. 167, 320–335. https://doi.org/10.1016/j.jvolgeores.2007.07.015.
Simkin, T., Siebert, L., 1994. Volcanoes of the World. 2nd ed. Geoscience Press, Tucson.
Sitemap, H.H., Articles, F.S., Union, A.G., 2014. The Smithsonian/NASA Astrophysics Data System Miocene Zircon Crystals in Dacite From Ilopango Caldera, El Salvador: Evidence for Recycling of Plutonic Rocks. pp. 8-9.
Smith, R.L., 1979. Ash-flow magmatism. Geological Society of America Special Paper 1749 vol. 180, pp. 5–27.
Smith, R.L., Bailey, R.A., 1968. Resurgent caldrons. Mem. Geol. Soc. Am. 116, 613–662.
Smith, R.B., Braile, L.W., 1994. The Yellowstone hotspot. J. Volcanol. Geotherm. Res. 61, 121-187.
Sofield, D., 2004. Eruptive history and volcanic hazards of Volcan San Salvador. Geol. Soc. Am. Spec. Pap. 375, 147-158.
Solari, L.A., Gómez-Tuena, A., Bernal, J.P., Pérez-Arvízu, O., Tanner, M., 2010. U-Pb zircon geochronology with an integrated LA-ICP-MS microanalytical workstation: achievements in precision and accuracy. Geostand. Geoanal. Res. 34, 5–18.
Sparks, R.S.J., Francis, P.W., Hamer, R.D., Pankhurst, R.J., O'Callaghan, L.O., Thorpe, R.S., Page, R., 1985. Ignimbrite of the Cerro Galan Caldera, NW Argentina. J. Volcanol. Geotherm. Res. 24, 205–248. https://doi.org/10.1016/0377-0273(85)90071-X.
Sparks, S., Self, S., Grattan, J.P., Oppenheimer, C., Pyle, D., Rymer, H., 2005. Supereruptions: global effects and future threats. Report of a Geological Society of London Working Group. The Geological Society, London (24 pp.).
Staller, A., Martínez-Díaz, J.J., Benito, B., Alonso-Henar, J., Hernández, D., Hernández-Rey, R., Díaz, M., 2016. Tectonophysics Present-day crustal deformation along the El Salvador Fault Zone from ZFESNet GPS network. Tectonophysics 670, 66–81. https://doi.org/10.1016/j.tecto.2015.12.017.
Sun, S.S., McDonough, W.F., 1989. Chemical and isotopic systematics of oceanic basalts: implications for mantle composition and processes. In: Saunders, A.D., Norry, M.J. (Eds.), Magmatism in the Oceanic Basins. Geological Society of London Special Publication vol. 42, pp. 313-345.
Sunye-Puchol, I., Aguirre-Díaz, G.J., Davila-Harris, P., Pedrazzi, D., Gutierrez, E., Hernanez, W., Miggins, D., Costa, A., 2017. The voluminous 1.5 Ma Olocuilta Ignimbrite: a precolapse fissure supereruption of Ilopango caldera, El Salvador. Conf. IAVCEI 2017, Portland, Oregon, USA.
Tikoff, B., de Saint Blanquat, 1997. Transpressional shearing and strike-slip partitioning in the Late Cretaceous Sierra Nevada magmatic arc, California. Tectonics 16, 442-459.
Turner, H.L., La Femina, P., Saballos, A., Mattioli, G., Jansma, P., Dixon, T., 2007. Kinematics of the Nicaraguan forearc from GPS geodesy. Geophys. Res. Lett. 34 (5 pp.).
Weber H. S., Wiesemann G., Wittek indt H., 1974. Mapa Geológico de la República de El Salvador/Geologische Übersichtskarte der Republik El Salvador 1:500,000 (after geological maps 1:100000 – 1967-74) Bundesanstalt für Geowissenschaften und Rohstoffe, Hannover; Bundesanstalt fu¨r Bodenforschung, Hannover.
Weinberg, R.E., 1992. Neotectonic development of western Nicaragua. Tectonics 11 (5), 1010–1017.
Weyl, R., 1957. Las Tobas Fundidas de la Cadena Costera. 5551. Universidad de Kiel, Alemania, DC, p. 2.
Williams, H., Meyer-Abich, H., 1955. Volcanism in the southern part of El Salvador, with particular reference to the collapse basins of Lakes Coatepeque and Ilopango. Univ. Calif. Publ. Geol. Sci.. vol. 32 (64 pp.)
Wilson, M., 1989. Igneous Petrogenesis. First edition. Springer https://doi.org/10.1007/978-94-010-9388-0.

4. Revisión estratigráfica de toda la secuencia de la caldera de Ilopango y estimación del periodo de recurrencia para grandes erupciones explosivas.

Artículo: Suñe-Puchol, I., Aguirre-Díaz, G.J., Dávila-Harris, P., Miggins, D.P., Pedrazzi, D., Costa, A., Ortega-Obregón, C., Lacan, P., Hernández, W., Gutiérrez, E., 2019. The Ilopango caldera complex , El Salvador : Stratigraphic revision of the complete eruptive sequence and recurrence of large explosive eruptions. J. Volcanol. Geotherm. Res.

Contribuciones individuales de los autores:

- **Ivan Suñé Puchol:** diseño y organización del estudio, trabajo de campo y de laboratorio, procesamiento, análisis e interpretación de datos, redacción del artículo.
- **Gerardo Aguirre Díaz:** financiamiento, concepción y plan de trabajo, supervisión, trabajo de campo, interpretación de los datos, revisión del artículo.
- **Pablo Dávila Harris:** diseño y supervisión del estudio, trabajo de campo, interpretación de datos y corrección del artículo.
- **Dan Miggins:** supervisión en laboratorio y en procesamiento e interpretación de fechamientos Ar/Ar, corrección del artículo.
- **Dario Pedrazzi:** trabajo de campo, interpretación de datos y corrección del artículo.
- **Antonio Costa:** trabajo de campo y cálculo de volumen de la ignimbritas mediante modelos numéricos.
- **Carlos Ortega Obregón:** supervisión en laboratorio y fechamientos U-Pb, procesamiento e interpretación de datos geocronológicos.
- **Pierre Lacan:** trabajo de campo e interpretación de datos vulcano-tectónicos.
- **Walter Hernández:** trabajo de campo e interpretación de la geología de la zona.
- **Eduardo Gutiérrez:** apoyo logístico y trabajo de campo.

Journal of Volcanology and Geothermal Research 374 (2019) 100-119

Contents lists available at ScienceDirect

Journal of Volcanology and Geothermal Research

jour nal homepage: www.elsevier. com/ locate/ jvolgeores

The Ilopango caldera complex, El Salvador: Stratigraphic revision of the complete eruptive sequence and recurrence of large explosive eruptions

Ivan Suñe-Puchol [a,*], Gerardo J. Aguirre-Díaz [a], Dario Pedrazzi [b], Pablo Dávila-Harris [c], Daniel P. Miggins [d], Antonio Costa [e], Carlos Ortega-Obregón [a], Pierre Lacan [a], Eduardo Gutierrez [f], Walter Hernández [f]

[a] Centro de Geociencias, Universidad Nacional Autónoma de México, Blvd. Juriquilla 3001, Campus UNAM-Juriquilla, Querétaro, 76230, Mexico
[b] ICTJA, CSIC, Group of Volcanology, SIMGEO UB-CSIC, Institute of Earth Sciences Jaume Almera, Lluis Sole i Sabaris s/n, 08028 Barcelona, Spain
[c] División de Geociencias Aplicadas, IPICYT, 78216 San Luis Potosí, Mexico
[d] College of Earth, Ocean and Atmospheric Sciences, Oregon State University, 104 CEOAS Administration Building, 101 SW 26th St, Corvallis, OR 97331, EE, UU, United States of America
[e] Instituto Nazionale di Geofisica e Vulcanologia, INGV-Bologna, Via Donato Creti, 12, 40100 Bologna, Italy
[f] Gerencia de Geología del Observatorio Ambiental, Ministerio de Medio Ambiente y Recursos Naturales MARN, San Salvador, 76230, El Salvador

a r t i c l e i n f o

Article history:
Received 13 November 2018
Received in revised form 11 February 2019
Accepted 16 February 2019
Available online 22 February 2019

Keywords:
Stratigraphy of pyroclastic deposits
Tectonic-caldera
Ignimbrite
Central America Volcanic Arc
Pull-apart graben

a b s t r a c t

Ilopango caldera erupted episodically at least 13 tuff-forming eruptions with a minimum estimate volume of 1-5 km³ DRE per eruption, reaching up to 150 km³ DRE for the first caldera-forming eruption. All tuffs are of dacitic-rhyolitic composition. The complete pyroclastic sequence spans a range in time from 1.785 to 0.0015 Ma, and based on stratigraphy and geochronology constraints can be divided into three formations: the Comalapa, Altavista and Tierras Blancas formations. In this work, we focus on the members of the newly described Altavista Formation (middle part of Ilopango caldera volcanic sequence), which consist of six consolidated pyroclastic deposits or tuffs. Each tuff corresponds to a specific eruption followed by a period of quiescence during which soil beds were developed on the deposits. The ages of the Altavista Formation ranges from 918 to 257 ka, based on new $^{40}Ar/^{39}Ar$, U/Pb-zircon, and U/Th-zircon analyses. The tuffs of this formation show similar characteristics in mineralogy and composition. They are calcalkaline, rhyodacitic tuffs, with plagioclase, clinopyroxene, and hornblende. From field mapping and descriptions of the deposits, we have inferred the eruptive styles that include pumice fallouts, pyroclastic density currents and also hydromagmatic explosions. The common vent in all tuffs was the Ilopango caldera and each member of the Altavista Formation could correspond to a caldera collapse event, except for one of the six eruptions. The volume of each member was estimated to be N30 km³ DRE, which is the same order of magnitude than that estimated for the Tierra Blanca Joven (TBJ) eruption at about 1,500 B. P, and smaller than those of the ignimbrites of the Comalapa Formation, the first three members of the Ilopango caldera reported previously. The tuffs of the Altavista Formation are visible up to 15-20 km away from the caldera's topographic margin. The recurrence interval of large explosive events at the Ilopango caldera was established by integrating the stratigraphic and geochronologic data of all 13 ignimbrites and pumice fallouts erupted from Ilopango caldera since the first one at 1.78 Ma to the last explosive event (TBJ).

1. Introduction

Ilopango Caldera (IC), located at El Salvador Volcanic Front (Fig. 1), is one of the largest active volcanoes of the Central America Volcanic Arc (CAVA). IC is 17 km × 13 km in size and it is filled by an intra-caldera lake (Fig. 1). Caldera's history includes several collapses associated to large explosive ignimbrite-forming eruptions; the initial volcanic phases of this caldera includes the Olocuilta, Colima, and Apopa ignimbrites at 1.78 -1.34 Ma (Suñe-Puchol et al., 2019). These early eruptions of the IC sequence were linked with the regional tectonics of El Salvador Fault Zone at that time (Suñe-Puchol et al., 2019), confirming the interpretation by previous authors that IC is a volcano-tectonic depression (Williams and Meyer-Abich, 1955; Golombek and Carr, 1978; Hutton and Reavy, 1992; Sofield, 2004; Saxby et al., 2016; Aguirre-Díaz and Martí, 2015; Aguirre-Díaz et al., 2016, 2017). The early ignimbrites of the IC were voluminous, for example, the Olocuilta ignimbrite, with a minimum Dense Rock Equivalent (DRE) volume of 60 km³ that could reach at least 150 km³ involving inferred covered or eroded deposits (Suñe-Puchol et al., 2019), representing so far the largest recorded from the IC.

* Corresponding author.
E-mail address: ivanbatea@gmail.com (I. Suñe-Puchol).

https://doi.org/10.1016/j.jvolgeores.2019.02.011
0377-0273/

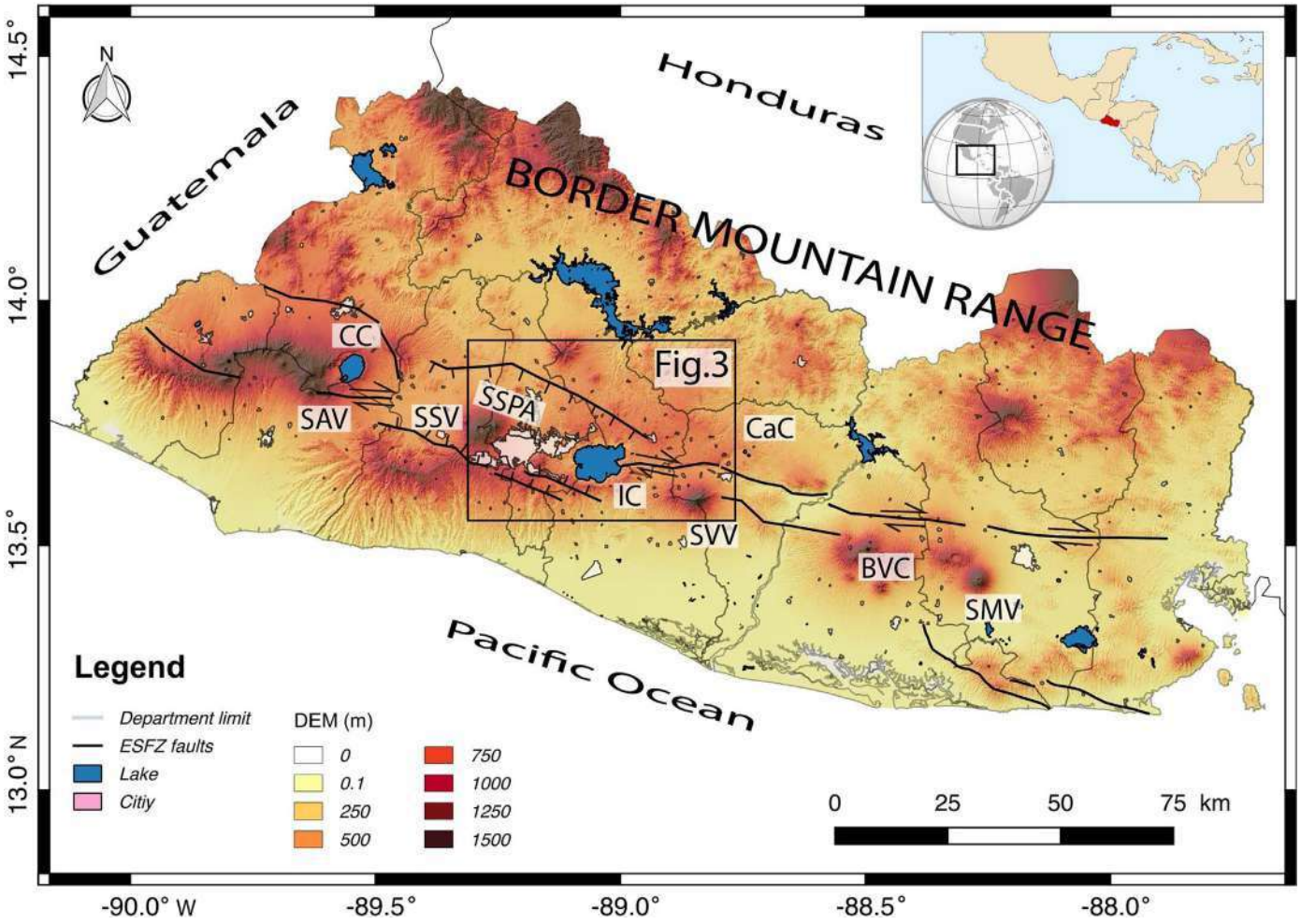

Fig. 1. Index map of El Salvador showing the El Salvador Fault Zone (ESFZ), towns, lakes and main volcanoes of El Salvador Volcanic Front. Santa Ana Volcano (SAV), Coatepeque Caldera (CC), San Salvador Volcano (SSV), Ilopango Caldera (IC), San Vicente Volcano (SVV), Carboneras caldera (CaC), Berlin Volcano Complex (BVC), and San Miguel Volcano (SMV). Inset map shows the regional location of El Salvador in Central America. The study area is outlined within the black box that represents the area of Fig. 3, which includes the San Salvador Pull-Apart (SSPA).

The most recent explosive episodes occurred during the last 57 ka and corresponded to the Tierras Blancas tuffs (or TB's), defined as TB4, TB3, TB2 and TBJ (CEL, 1992; Rose et al., 1999; Hernández, 2004; Kutterolf et al., 2008; Lexa et al., 2011; Pedrazzi et al., 2018). The youngest Tierra Blanca Joven (TBJ) occurred only ~1,500 yr ago (Dull et al., 2010) and affected significantly the Mayan population of the central part of El Salvador with ~80 km³ of erupted magma (Sheets, 1979; Dull et al., 2001, 2010; Pedrazzi et al., 2018).

The aim of this work was to identify and characterize the tuff-forming eruptions occurred between the early ignimbrites of IC (Suñe-Puchol et al., 2019), and the last Tierras Blancas tuffs (Rose et al., 1999; Kutterolf et al., 2008), that is, the eruptions occurred between 1.34 Ma to 57 ka. In addition, we provide a formal volcano-stratigraphic nomenclature to the Ilopango Group according to Martí et al. (2018). A recurrence timing of all the major explosive eruptions from IC was established by integrating the data of, 1) the Comalapa Formation (the three early ignimbrites of IC, Suñe-Puchol et al., 2019); 2) the Altavista Formation (the six tuffs presented in this work), and; 3) the Tierras Blancas Formation from published data (Weber and Wiesemann, 1974; Rose et al., 1999; Kutterolf et al., 2008).

2. Geologic and volcano-stratigraphic context of Ilopango caldera

The geology of El Salvador consists of a Jurassic - Cretaceous limestone basement mostly covered by Eocene to Holocene volcanic rocks (Appendix A; Weber and Wiesemann, 1974). Oligocene volcanism was located along the northernmost part of the country and formed the Border Mountain Range, a natural boundary between El Salvador and Honduras that includes Morazán and Chalatenango Formations (Fig. 1; Donnelly et al., 1990). Since the Miocene, volcanic activity migrated southward approaching to the Mesoamerican trench, where the active volcanoes are located forming the El Salvador Volcanic Front (Reynolds, 1987; Alonso-Henar et al., 2017; Fig. 1).

The actual magmatism of El Salvador Volcanic Front is related to the subduction of Cocos plate underneath the Caribbean plate at an average speed of 73-85 mm/year (Dixon, 1993; Mann, 2007; DeMets, 2001). The high movement rates of these plates are also responsible for the elevated regional seismic activity along the El Salvador Fault Zone (ESFZ, Martínez-Díaz et al., 2004), which is a narrow zone of *en-echelon* right-stepping dextral faults connected by transtensional pull-apart basins that crosses the country WNW-ESE (DeMets, 2001, Agostini et al., 2006; Funk et al., 2009; Canora et al., 2012; Fig. 1). IC is located along the ESZF, specifically within one of its tectonic basins: the San Salvador Pull-Apart (Fig. 1; Garibaldi et al., 2016). The active faults of the San Salvador Pull-Apart are controlling volcanism and are likely used as the preferential pathways for magma rising to the surface (Hutton and Reavy, 1992; Sofield, 2004; Saxby et al., 2016; Suñe-Puchol et al., 2019).

2.1. Volcanic stratigraphy of Ilopango caldera (IC) products

In previous studies on the IC and surroundings areas, Weber and Wiesemann (1974) grouped the oldest deposits of this caldera within the Cuscatlán Formation together with lahars and deposits from other volcanoes. The IC tuffs studied in this work (time span of 917-257 ka) and the early ignimbrites of the same caldera (1.78–1.34 Ma, Suñe-Puchol et al., 2019), belongs to this formation. The upper limit of this Cuscatlán Formation is marked by the 57 ka Congo tephra deposit (Rose et al., 1999), a Plinian fall from the Coatepeque caldera (Fig. 1). The last four tuffs of IC (TB's) are included into the San Salvador Formation (Weber and Wiesemann, 1974), together with the Upper Pliocene-Holocene eruptions from other young Salvadorian volcanoes (f. ex. from Coatepeque caldera, San Salvador volcano, Santa Ana volcano, San Miguel volcano).

In this study, a new classification for the IC products was established with the aim of a standardization, which accounts for modern volcano-stratigraphy criteria (Fig. 2). Following the formal nomenclature established by Martí et al. (2018), we grouped the IC deposits in the Ilopango Group (new name) to distinguish it from previous lithological groups not directly related to the activity of Ilopango. This Ilopango Group is subdivided into three new formations based on stratigraphy and geochronology constraints, as eruption magnitudes, quiescence periods, unconformities, volcanic processes and tectonic settings. These new formations are: 1) Comalapa Formation, which comprise the first three ignimbrites of IC (Suñe-Puchol et al., 2019); 2) Altavista Formation that includes the six tuffs studied in this work; and 3) Tierras Blancas Formation, encompassing the last four tuffs erupted by IC (Rose et al., 1999; Kutterolf et al., 2008). Fig. 2 illustrates the equivalence between the older formations classification of Weber and Wiesemann (1974) and the new classification described in this study, establishing a comparison by isochrones. As with the Comalapa Formation of IC (Suñe-Puchol et al., 2019), we define and describe here the ignimbrites and fallout deposits of the Altavista Formation.

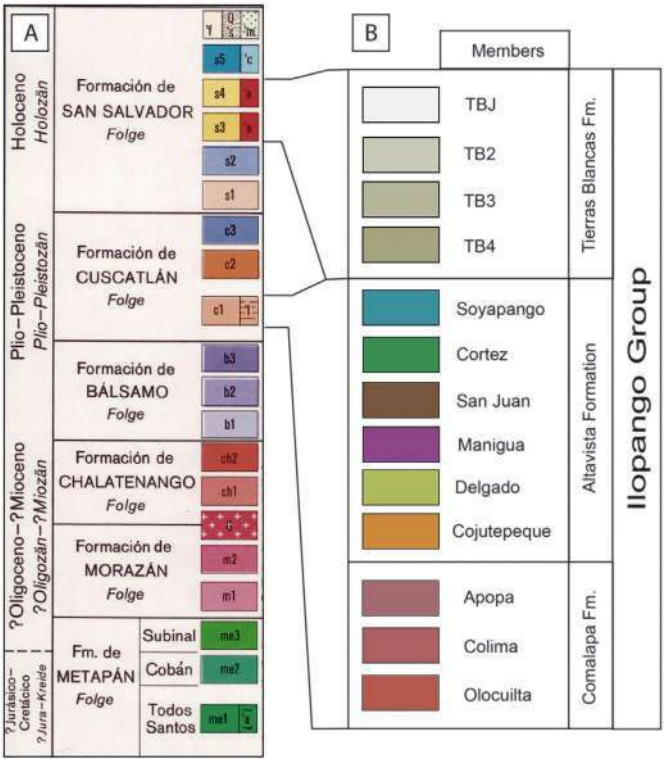

Fig. 2. Equivalence between older and the new volcano-stratigraphic classification of the Ilopango Group proposed in this study. a) Formations of El Salvador (Weber and Wiesemann, 1974). b) The new volcano-stratigraphic nomenclature that includes the Comalapa, Altavista and Tierras Blancas formations of the Ilopango Group (following the nomenclature proposed by Martí et al., 2018).

3. Methodology

A preliminary remote sensing analysis of the area was done based on satellite images and a Digital Elevation Model (DEM) of 10 m resolution. Geological fieldwork was initially based on El Salvador geological map of 1: 500,000 (Weber and Wiesemann, 1974), and also on previous maps and stratigraphy reported by other authors (Hernández, 2008; Garibaldi et al., 2016). Four fieldwork campaigns around IC between 2015 and 2017 of about 2 weeks of duration and at least 2 geologists working per campaign, allowed us to elaborate a new geologic map focused on the distribution of the Altavista Formation tuffs. This map covers about 2000 km² of the central part of El Salvador Country, from Guazapa Volcano at the north, to the Balsamo mountain range at the south; and from the San Salvador volcano at the west, and Carbonera caldera to the east (Fig. 3).

Each tuff within the Altavista Formation was sampled for laboratory analysis. Major, trace and Rare Earth-Elements (REE) were measured as whole-rock for chemical analyses. Trace and REE were carried out by means of a Thermo ICAP-Q quadruple mass spectrometer (ICP-MS), at the Laboratory of Isotopic studies (LEI), Center for Geosciences (CGEO) of the National Autonomous University of Mexico (UNAM). Analysis of major and trace elements were carried out at Institute of Geology, UNAM, with an X RIGAKU ZSX Primus II spectrometer, following standard sample preparation and analytical techniques of Bernal and Lozano-Santacruz (2005).

U/Pb, U/Th and $^{40}Ar/^{39}Ar$ geochronological analyses on each member of Altavista Formation were performed in order to support the stratigraphic correlation and constrain accuracy the IC explosive eruption ages. For deposits younger than 350 ka we used U/Th technique instead of U/Pb in zircons, because of the lack of secular equilibrium (Bernal et al., 2014). Zircon samples were separated and dated at the Laboratory of Isotopic Studies-LEI of CGEO-UNAM, using a 193 nm Resolution M50 laser ablation inductively coupled to a plasma mass spectrometer (LA-ICP-MS) Thermo ICAP Qc for U/Pb following the method described in Ortega-Obregón et al. (2013) and to a Thermo Neptune plus for U-Th ages following methodology described by Bernal et al. (2014). To obtain juvenile zircon crystals, pumice fragments were isolated, removing altered surfaces and then crushed and sieved to fractions of 74-44 μm. This fraction was then washed using a plastic pan to concentrate the heavy crystals from the lighter glass. Mineral concentrates were magnetically separated by means of a Frantz Isodynamic Separator to further concentrate the zircons. Representative zircons were handpicked under a binocular microscope and checked for purity and zoning using an ELM-3R luminoscope by cathodoluminescence (Marshall, 1988), before and after the ICP-MS laser ablation analysis. About 50 zircon grains per sample were selected in order to obtain a statistically representative age.

Samples for $^{40}Ar/^{39}Ar$ dating were prepared, irradiated and analyzed at the Argon Geochronology Laboratory of the Oregon State University (OSU), using an Argus-VI multi-collector mass spectrometer. As with zircons, clean pumice clasts were separated and crushed to obtain mineral concentrations. Crushed samples were sieved to 500-177 μm fractions and washed with deionized water using an ultrasonic bath to remove dust. Feldspars were magnetically separated from amphiboles and pyroxenes, and all phases were acid-leached following the methods of Koppers et al. (2011). The only available phases to date the members of the Altavista Formation were plagioclase and hornblende (ultra-pure separates picked clean of melt inclusion-rich crystals). Incremental heating was performed on bulk samples for each mineral phase. Mineral concentrations were used since individual grains did not yield enough radiogenic argon for accurate single-crystal total fusion analyses. To achieve the highest possible precision in the $^{40}Ar/^{39}Ar$ age determinations, a large number of heating steps (22-33 heating steps) were carried out for each sample. Plateau age chosen included as many

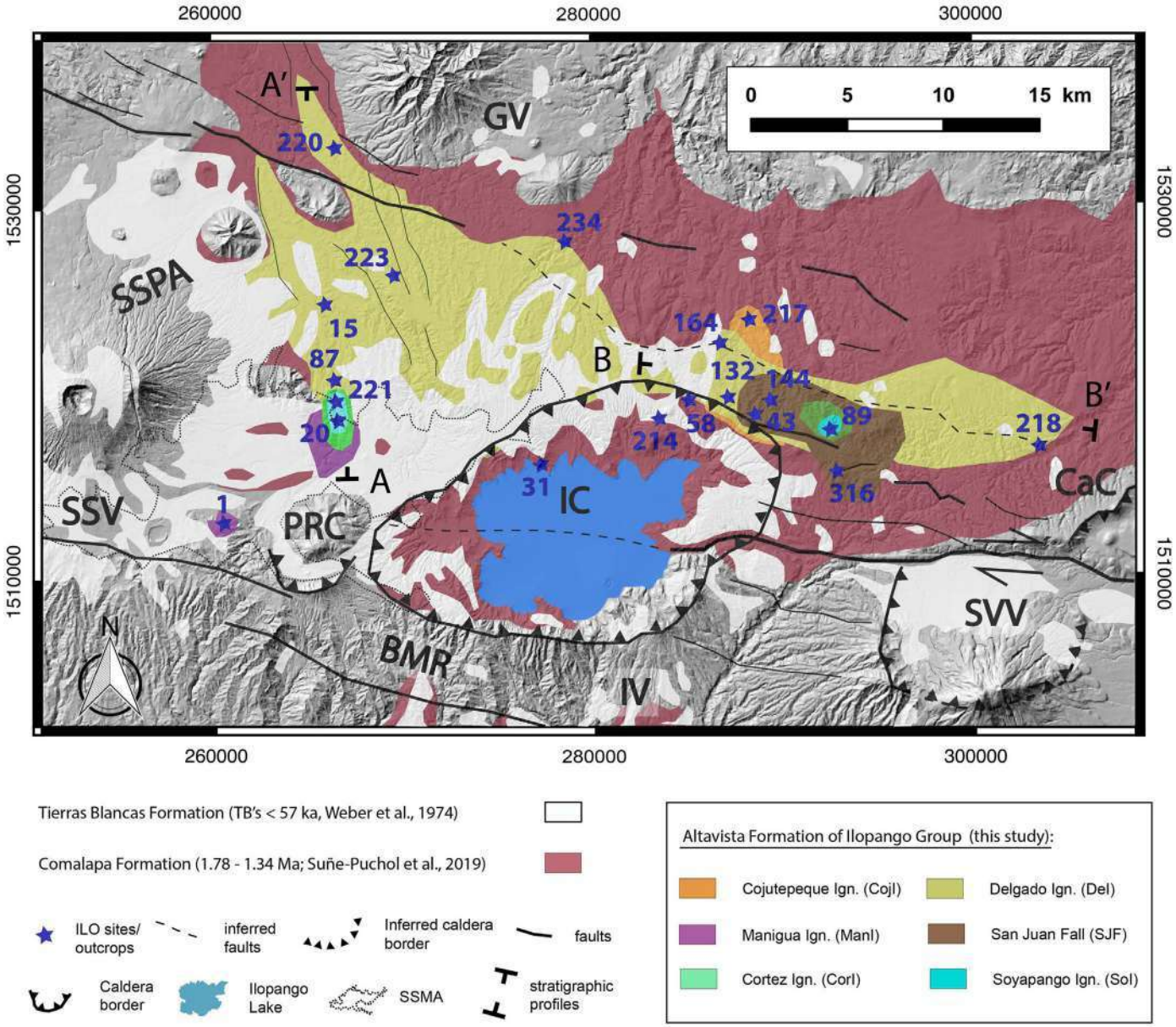

Fig. 3. Simplified geologic map of the central portion of El Salvador showing the distribution of the Altavista Formation members of Ilopango caldera. These members are stratigraphically located between the Comalapa Formation (red) and the Tierras Blancas Formation (white-pale grey). From oldest to youngest, CojI, DeI, ManI, SJF, CorI and SoI. Planes de Renderos Caldera (PRC), Guasapa Volcano (GV), old Ilopango Volcano (IV), San Vicente Volcano (SVV), Carbonera caldera (CaC), Balsamo mountain range (BMR), San Salvador Pull-Apart (SSPA). The San Salvador Metropolitan Area (SSMA) is represented by a dashed line. The geographic coordinates of the main localities (ILO localities, blue stars) are in UTM using Datum: D_WGS_1984, zone 16P. (For interpretation of the references to colour in this figure legend, the reader is referred to the web version of this article.)

contiguous and concordant step ages as possible to obtain an acceptable mean square weighted deviates (MSWD). System blanks were measured throughout the analysis. To get the appropriate eruption age it was necessary to recalculate them using the Kuiper et al. (2008) age by the Fish Canyon Tuff as flux monitor, reducing the data with the ArArCALC v2.5.1 software from Koppers (2002). All the $^{40}Ar/^{39}Ar$ age errors reported here are 2σ. More details of the techniques employed in the dating process are provided in Appendix B.

4. Results

4.1. The Altavista Formation tuffs of Ilopango Caldera: description and distribution

Six pyroclastic deposits separated by paleosols were identified in the field for the Altavista Formation. They overly the older ignimbrites of IC (Comalapa Formation) and are covered by the Tierras Blancas Formation. From oldest to youngest, these six members that conform the Altavista Formation are: the Cojutepeque Ignimbrite (CojI), Delgado Ignimbrite (DeI), Manigua Ignimbrite (ManI), San Juan pumice Fall (SJF), Cortez Ignimbrite (CorI) and Soyapango Ignimbrite (SoI). They are poorly-consolidated and unwelded deposits, and thus, are soft and easily eroded away. Their poor preservation results in the lack of lateral continuity of the Altavista Formation tuffs and scarce sites with preserved total thicknesses (Fig. 3). However, useful exposures were identified along the Panamerican Highway that crosses the San Salvador Pull-Apart along the northern sector of IC (Figs. 5, 6 and 7). In addition, several quarries and other good outcrops allowed us elaborating a composite stratigraphic section of the Altavista Formation tuffs (Fig. 4) by stratigraphic correlation (profiles A and B of Fig. 8) and supported by petrochemical and geochronological analyses (Figs. 9, 10, 11 and 12).

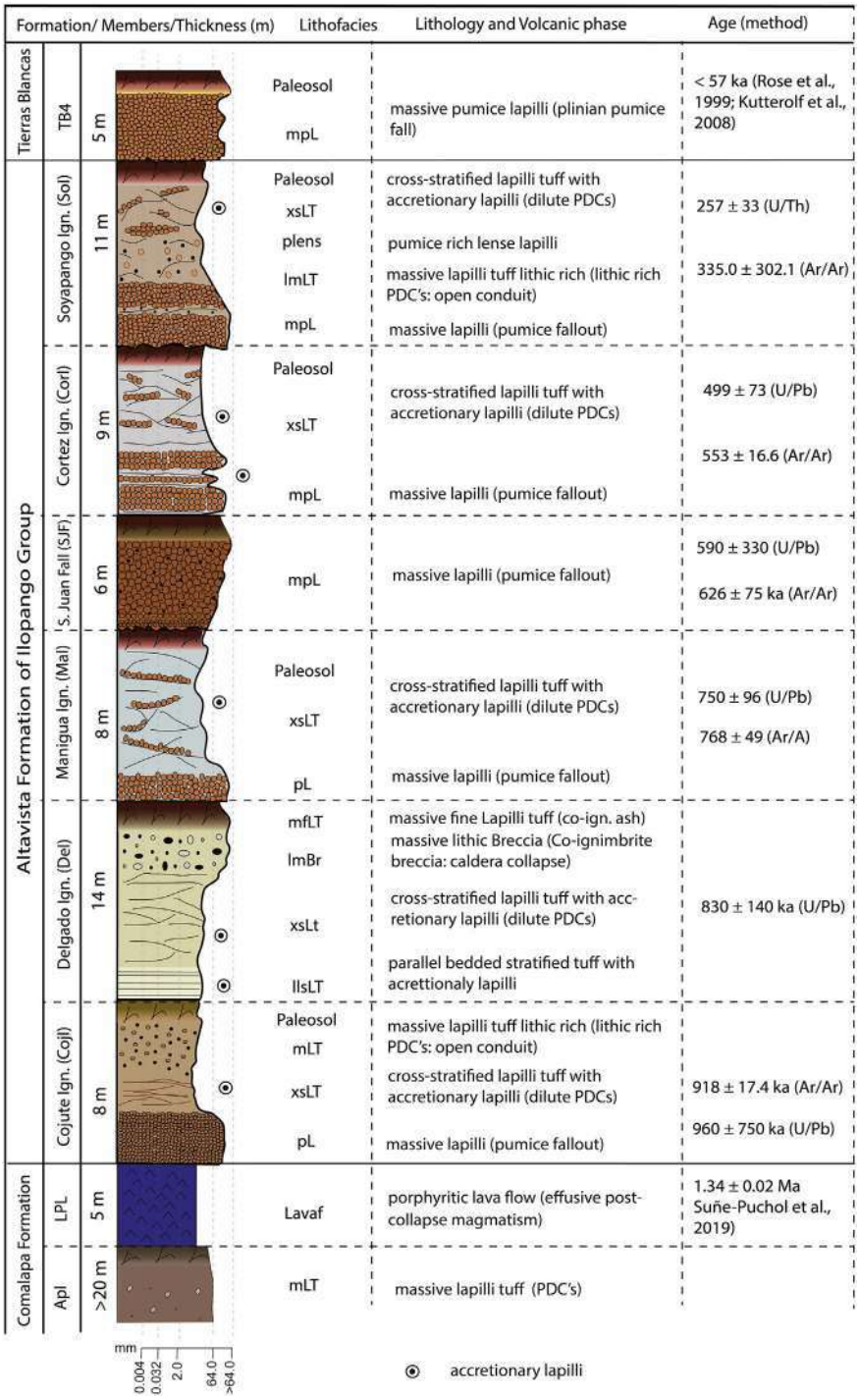

Fig. 4. Composite stratigraphic section of the Altavista Formation members, from the Comalapa Formation's youngest unit (1.32 Ma Las Pavas Lava) to the Tierras Blancas Formation (TB4, b57 ka) of IC. Figure includes the isotopic age of each unit obtained in this study. Lithofacies codes are based on nomenclature from Branney and Kokelaar (2002).

The index map (Fig. 3) shows the morphology of the study area and the spatial distribution of the six tuffs of Altavista Formation. Broadly, these members have not a generalized or radial distribution around the IC as in the older ignimbrites of the Comalapa Formation (Suñe-Puchol et al., 2019), or as the youngest TBJ (from the Tierras Blancas Formation; Fig. 3). Some deposits of the Altavista Formation have a very local distribution, such as ManI or CorI. Other deposits have an average distribution area of ~100 km², such as SJF or CojI. The DeI is the most widespread tuff and with the best exposures as far as 10-15 km from the caldera border (ILO-220, -234, and -218; Fig. 3). The tuffs of Altavista Formation were not found on the southern flank of IC mainly because of erosion.

4.1.1. Cojutepeque Ignimbrite (CojI)

CojI is not distributed radially around IC and it only crops out along the northeast border of the caldera (Fig. 3). At ILO-43 (Figs. 3 and 5) this oldest tuff of Altavista Formation overlays a thick paleosol of ~1 m thick developed at the top of the 1.32 ± 0.02 Ma Las Pavas Lava (LPL,

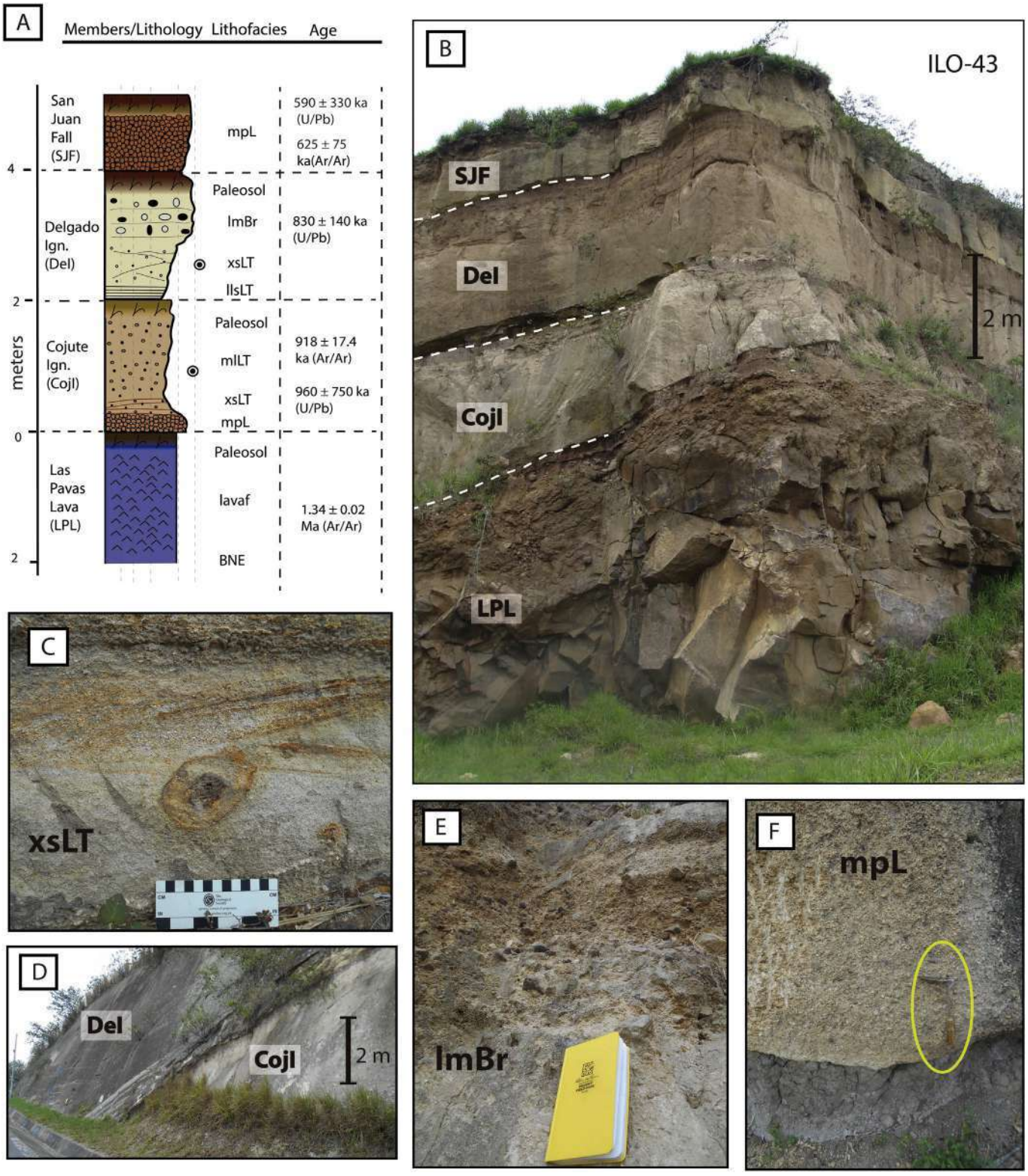

Fig. 5. Stratigraphic volcanic units and representative outcrops along the northeast border of the IC. a) Schematic stratigraphic section of ILO-43 site. For symbols refer to Fig. 4. b) Site ILO-43, a quarry near Cojutepeque City, where it is possible to observe several members of the Altavista Formation of Ilopango Group overlying Las Pavas Lava (LPL). c) Cross-stratified lapilli tuff in Cojutepeque Ignimbrite (CojI), showing oxidized levels (xsLT, ILO-144 site). d) Delgado Ignimbrite (DeI) on the top of the CojI (ILO-132 site). e) Massive lithic breccia of the DeI. f) Pumice fallout at the base of the CojI (ILO-144 site).

Suñe-Puchol et al., 2019), which corresponds to a post-collapse dome that represents the youngest unit of the Comalapa Formation of IC. The base of CojI consists of an orange-brown well-classified pumice layer, which reaches a thickness of 2 m at ILO-132 and ILO-144 (mpL; Figs. 3 and 5f). Pumices are 1–3 cm in diameter with plagioclase, hornblende, and clinopyroxene (Table 1), and smaller amounts of Fe-Ti

Table 1
Mineral percentages (%) of the Altavista Formation tuff of the Ilopango Group.

Unit	Plagioclase	Hornblende	Clinopyroxene	Quartz	Biotite	Fe-Ti oxides
Soyapango Ign.	93	0	0	0	0	7
Cortés Ign.	84	0	0	3	4	9
San Juan Fall	67	17	4	0	0	12
Manigua Ign.	72	12	0	5	0	11
Delgado Ign.	61	18	11	4	0	6
Cojutepeque Ign.	70	13	9	0	0	8

oxides and zircon (Fig. 9a and b). Above the basal pumice layer, there are ~1 m of cross-stratified layers (xsLT; Fig. 5c), composed of fine ash and abundant accretionary lapilli, with thin oxidized zones that remark the lamination of the layers. The top of this tuff is made of 4-5 m of an ash-supported massive pyroclastic deposit with pumice lenses and lithics of dacitic lava (1-2cm).

4.1.2. Delgado Ignimbrite (DeI)

DeI corresponds to the second member of the Altavista Formation, and it is the most widespread ignimbrite of this formation (Fig. 3). It is found about 20 km NW of the caldera border, next to the western flank of Guasapa Volcano and outside of the San Salvador Pull-Apart (ILO-220, Fig. 3). DeI shows a parallel-stratified base layer that ranges in thickness from a few cm to ~1 m, and consists, in the lower part, of an accretionary lapilli-rich fine ash bearing pumice deposit with lithic fragments smaller that 1 cm (llsLT; Fig. 6e). The middle part of this deposit consists of 5-6 m of cross-stratified ash-rich tuff (xsLT; Fig. 6f), with small pumice fragments and accretionary lapilli, but poorer in lithics than the basal zone. At the top, this member changes to a semi-consolidated massive lapilli tuff, about 5 m thick, with the presence, in some sites, of a lithic breccia level with diffuse parallel stratification (dslLT; Fig. 5e; ILO-43). Mineralogy includes plagioclase, hornblende, clinopyroxene and rare primary quartz (Table 1).

4.1.3. Manigua Ignimbrite (ManI)

This ignimbrite is only exposed on the western sector of IC (Fig. 3), mostly along the roadcuts of the Panamerican Highway, such as ILO-20 (Figs. 3 and 7), called as Staircase site by Garibaldi et al. (2016). At this locality, 7–8 km far away from the WNW topographic margin of the caldera, each member of Altavista Formation is affected by normal faults of the San Salvador Pull-Apart system (Fig. 3). The base of ManI consists of a layer of 0.3 m thick, well-classified, clast-supported pumice layer (mpL). The fresh pumice is white-brown, but it shows a dark patina due to oxidation (Fig. 7f). This pumice is crystal-poor, with plagioclase, hornblende and quartz, with accessory minerals of Fe\\Ti oxides, zircons and few clinopyroxene phenocrysts (Table 1). Directly above of this basal pumice fall layer, there is a 8–9m of fine-ash and accretionary lapilli rich cross-stratified tuff (xsLT, Fig. 7f and g), with few, intercalated, thin, levels rich in pumice fragments-rich levels (pLens).

4.1.4. San Juan Pumice Fall (SJF)

The SJF is a well-classified, clast-supported pumice deposit (mpL), moderately rich in lava lithics (~10-15 vol%). This member reaches 4–5 m thick in ILO-316, 5 km away from the NE margin of the caldera (Fig. 3). The pumices are 1–3 cm in diameter and contain abundant plagioclase, clinopyroxene and hornblende phenocrysts (Table 1 and Figs. 9c, d, g and h), with smaller amounts of Fe\\Ti oxides and zircons. The first 10 cm of the SJF show inverse grading, from coarse-ash to pumice lapilli. This pumice deposit overlays the paleosol formed at the top of the DeI (f. ex. in ILO-43; Fig. 5b). At ILO-89 (NE sector of the IC; Fig. 3), SJF is deposited above an angular unconformity (Figs. 6b and c). This member is not present in the NW sector of the caldera.

4.1.5. Cortez Ignimbrite (CorI)

The CorI covers the SJF at ILO-89 (Fig. 3) with a series of fine ash-rich cross-stratified tuff with accretionary lapilli (xsLT; Fig. 6). However, in the NW sector of the caldera (e.g. at ILO-20; Fig. 3), where CorI is deposited above the paleosol on ManI's top, its base consists of ~1 m of well-classified clast-supported pumice fall deposit (mpL), with two thin levels of fine-ash rich deposits intercalated (b10 cm thick, Fig. 7e). The CorI pumice clasts are very poor in crystals with sparse plagioclases, biotite and quartz phenocrysts, and Fe\\Ti oxides and zircons (Table 1). Above this pumice deposit, there is a sequence of cross-stratified fine-ash and accretionary lapilli-rich tuff (xsLT) that is very poor in lithics.

4.1.6. Soyapango Ignimbrite (SoI)

The base of SoI consists of ~2 m of well-classified, clast-supported pumice layer (mpL), deposited over an eroded surface at the top of CorI (Figs. 6 and 7). Pumice clasts of this member are crystal-poor, with few plagioclase and minor amounts of Fe\\Ti oxides and zircon (Table 1). Above the basal pumice layer there are 3–4 m of a pumice-rich tuff with heterolithological lithics (lava and plutonic fragments). The top of the SoI is represented by 4–5 m of a cross-stratified tuff with accretionary lapilli (xsLT) and pumice-rich fragments forming pumice lenses. SoI is the last member of the Altavista Formation, which is still affected by regional faults. Differently from the Altavista formation, the following Tierras Blancas Formation were not deformed by faults of the San Salvador Pull-Apart as shown for example at ILO-20 outcrop, where the TB4 pumice fall rests on an eroded surface at the top of SoI (Figs. 7a, b and c) without any evidence of tectonic deformation.

4.2. Geochemistry and petrography

Petrographic and whole-rock chemical analyses were carried out in the six pyroclastic deposits of the Altavista Formation (Table 2). All analyses were performed in pumice clasts, choosing the biggest and freshness clasts available, and discarding the small and the altered pieces. Results indicate that Altavista Formation ignimbrites are evolved felsic calcalkaline rocks from continental-margin subduction zones, confirming the tectonic setting proposed by several authors (Arculus and Curran, 1972; Morris and Ryan, 2004; Murphy, 2007). Petrography indicates a predominant presence of plagioclase, hornblende and clinopyroxene, with small presence of biotite and quartz in some deposits (Table 1 and Fig. 9). Chemical analyses indicate a rhyodacitic composition in all members, with medium to high K_2O contents (Fig. 10). The multi-element diagram (Fig. 11), which includes the REE concentrations, shows a common magmatic source for the six deposits, with marked anomalies in strontium (Sr) and europium (Eu). Evolved magmas exhibit Eu negative anomalies mainly because of plagioclase fractionation. Plagioclase is the most abundant phenocryst in calcoalkaline magmas, typically dominating over alkali feldspar (Murphy, 2007), as occurs in the IC products. The most silicic ignimbrites of the Altavista Formation are ManI and DeI, which contain primary bipyramidal quartz. Secondary quartz is common in all members of IC, and was formed during vapour phase silicification in pumice vesicles and open spaces within ash matrix.

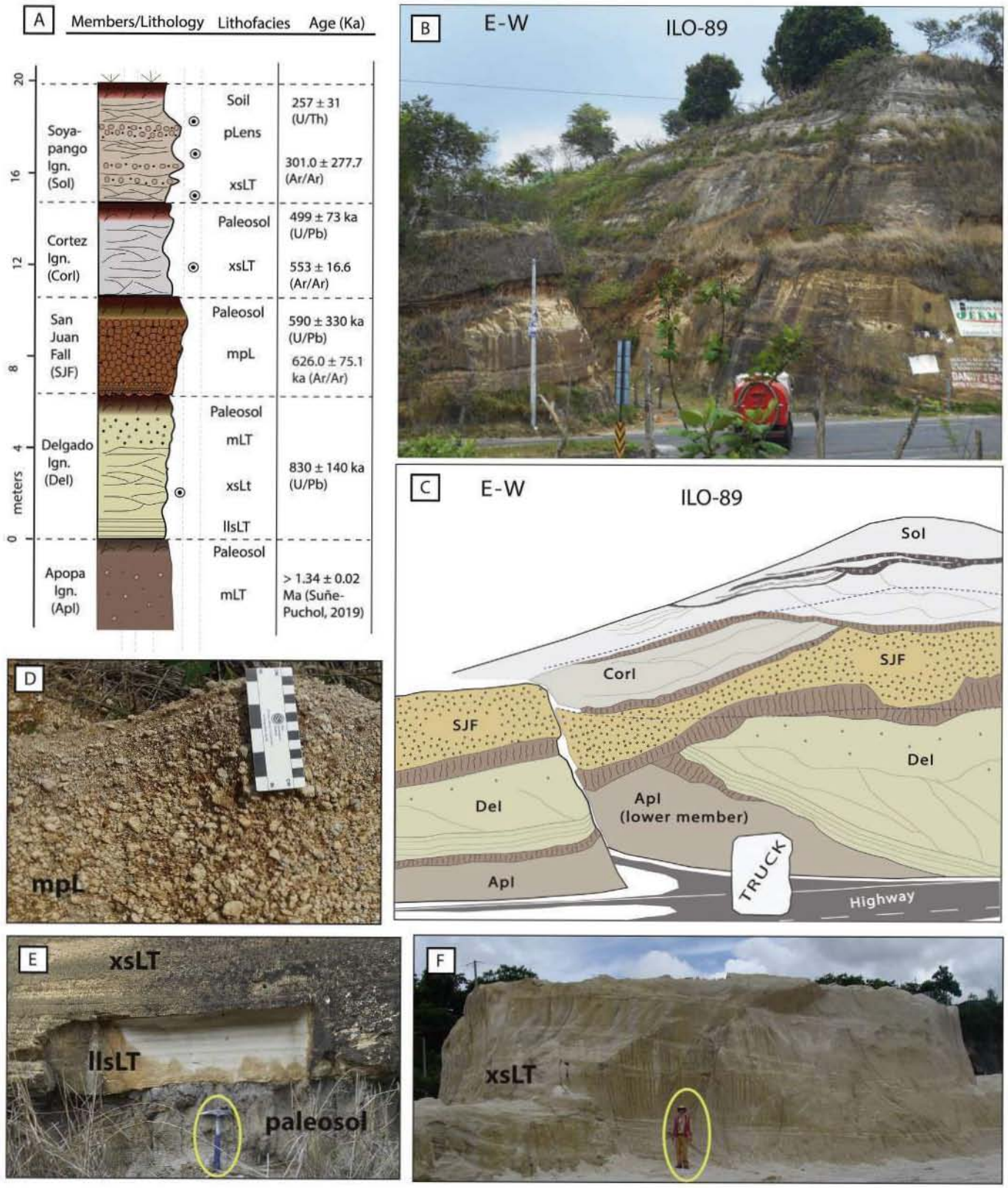

Fig. 6. Stratigraphy and representative outcrops at ILO-89 (Fig. 2). a) Schematic stratigraphic section of this site. For symbols refer to Fig. 4. b) Several members of the Altavista Formation overlying Apopa ignimbrite (ApI) at roadcuts along the Panamerican Highway on the NE flank of IC. c) Sketch of ILO-89 outcrop including paleosols between ignimbrites. d) Detail photo of the well-classified SJF pumice fall. e) Parallel-stratified base of Delgado Ignimbrite (llsLT). f) Cross-stratified lapilli tuff rich in accretionary lapilli and fine ash of DeI (xsLT).

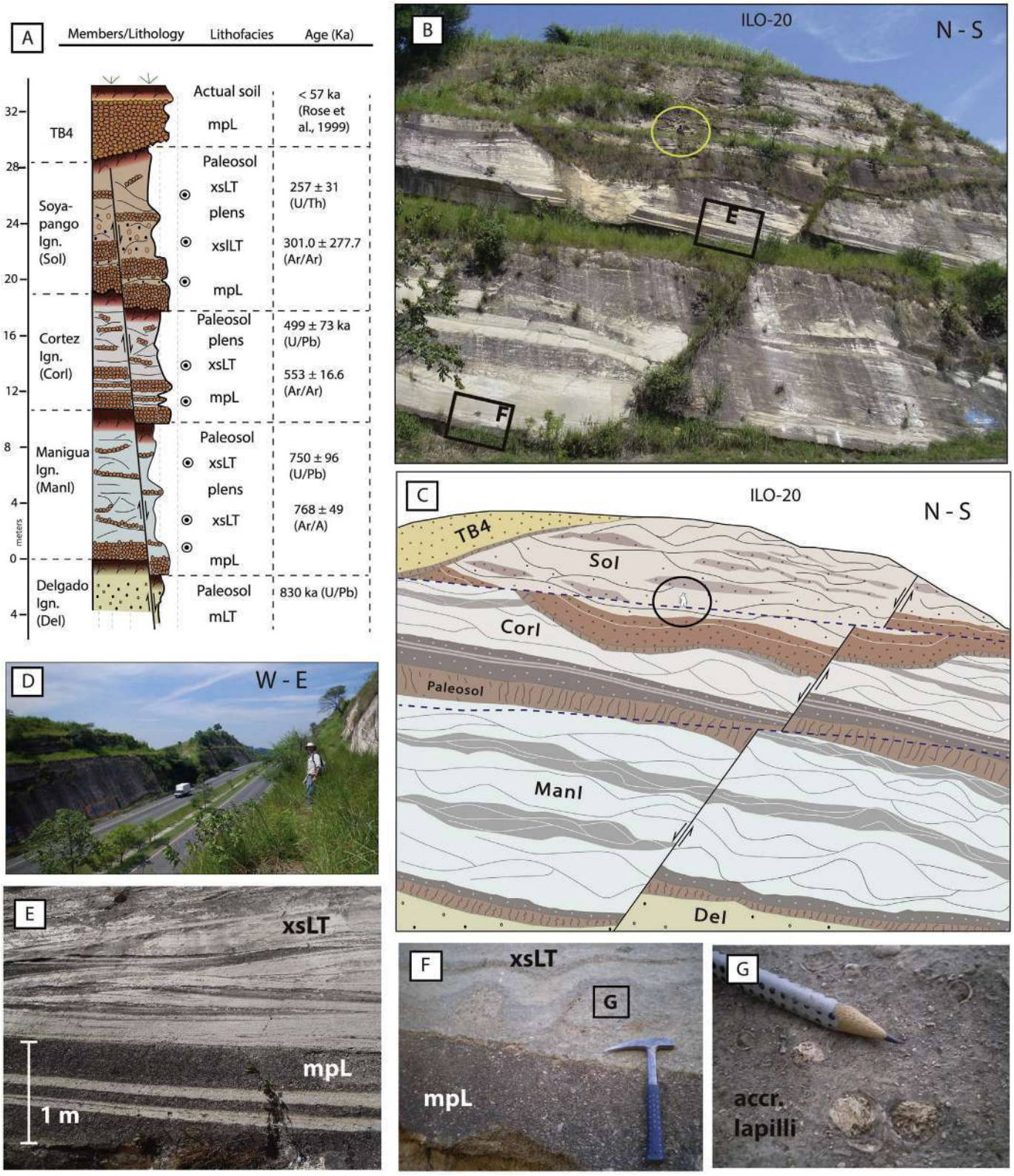

Fig. 7. Stratigraphy and representative outcrops of ILO-20 (Fig. 2). a) Schematic stratigraphic section of this site. b) ILO-20 site at roadcut in Panamericana Highway on the NW flank of IC (note the person to scale, yellow circle). c) Sketch of ILO-20 outcrop including paleosols between ignimbrites and the regional faults affecting the deposits of Altavista Formation (note the person to scale, yellow circle). d) Oblique view of ILO-20 outcrop showing the terraces of the Staircase site. e) Detail photo of pumice fall at the base of CorI with two interbedded surges and cross-stratified lapilli tuff (xsLT) deposited from dilute PDCs. f) Detail of the pumice fall at the base of ManI with hydromagmatic overlying surge PDCs deposit, and g) detail photo of accretionary lapilli from the xsLT of Manigua Ignimbrite (ManI). (For interpretation of the references to colour in this figure legend, the reader is referred to the web version of this article.)

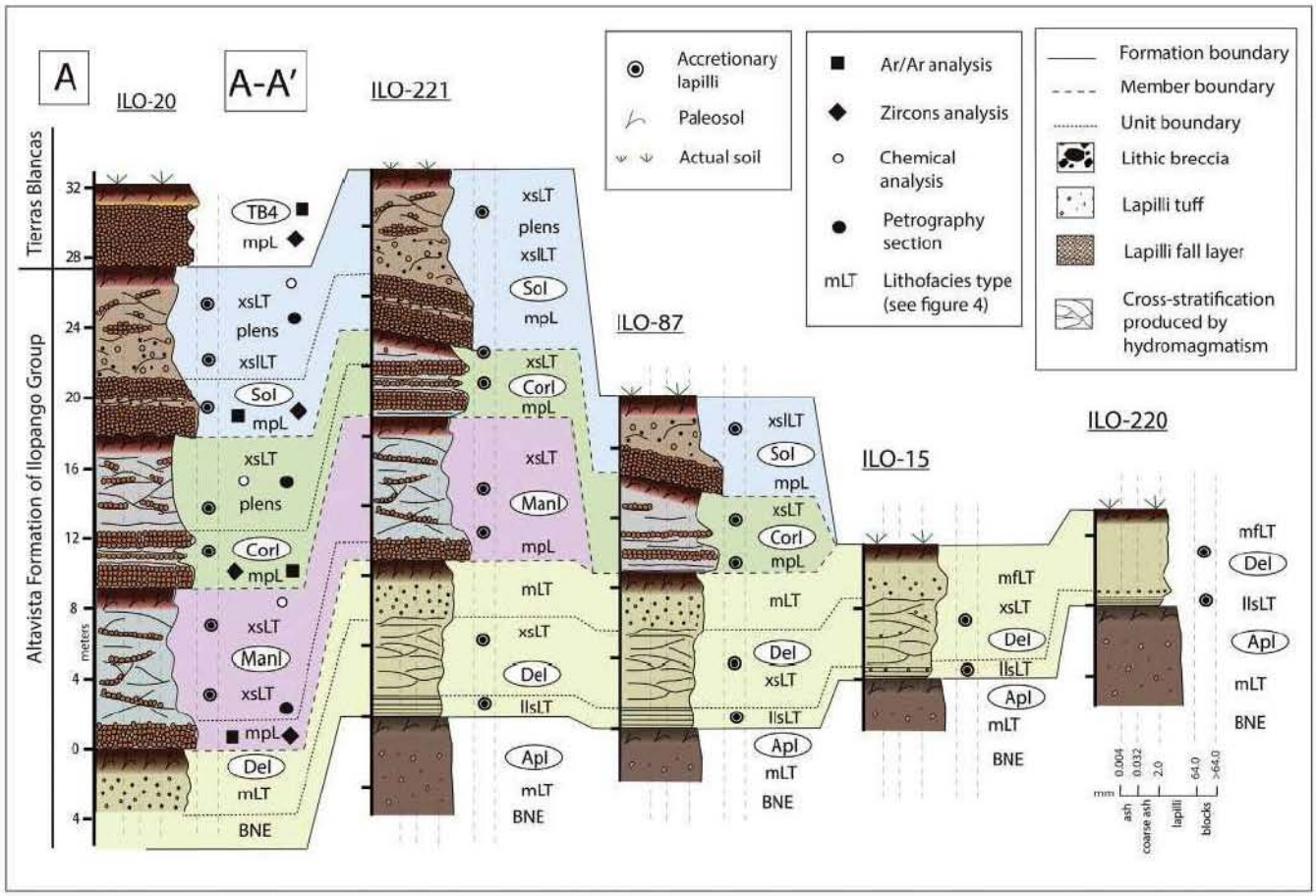
A
A-A′
ILO-20
ILO-221
ILO-87
ILO-15
ILO-220
Tierras Blancas
Altavista Formation of Ilopango Group
meters
Accretionary lapilli
Paleosol
Actual soil
Ar/Ar analysis
Zircons analysis
Chemical analysis
Petrography section
mLT Lithofacies type (see figure 4)
Formation boundary
Member boundary
Unit boundary
Lithic breccia
Lapilli tuff
Lapilli fall layer
Cross-stratification produced by hydromagmatism
TB4
mpL
xsLT
plens
xslLT
Sol
Corl
Manl
Del
IlsLT
Apl
mLT
BNE
mfLT
ash
coarse ash
lapilli
blocks
mm

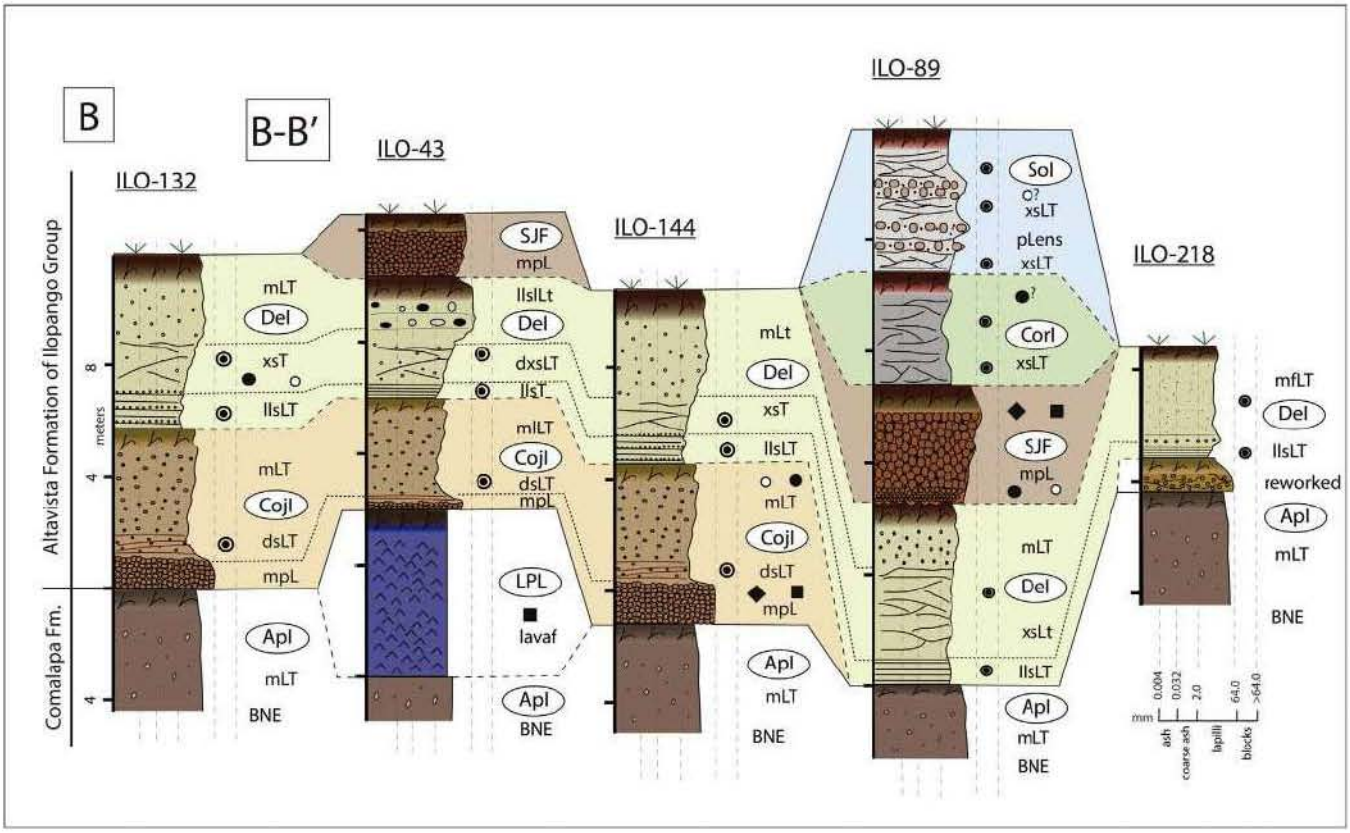
B
B-B′
ILO-132
ILO-43
ILO-144
ILO-89
ILO-218
Altavista Formation of Ilopango Group
Comalapa Fm.
meters
SJF
mpL
IlslLt
Del
dxsLT
IlsT
mlLT
Cojl
dsLT
LPL
lavaf
Apl
mLT
BNE
Sol
xsLT
plens
Corl
mLt
xsT
mLT
reworked
ash
coarse ash
lapilli
blocks
mm

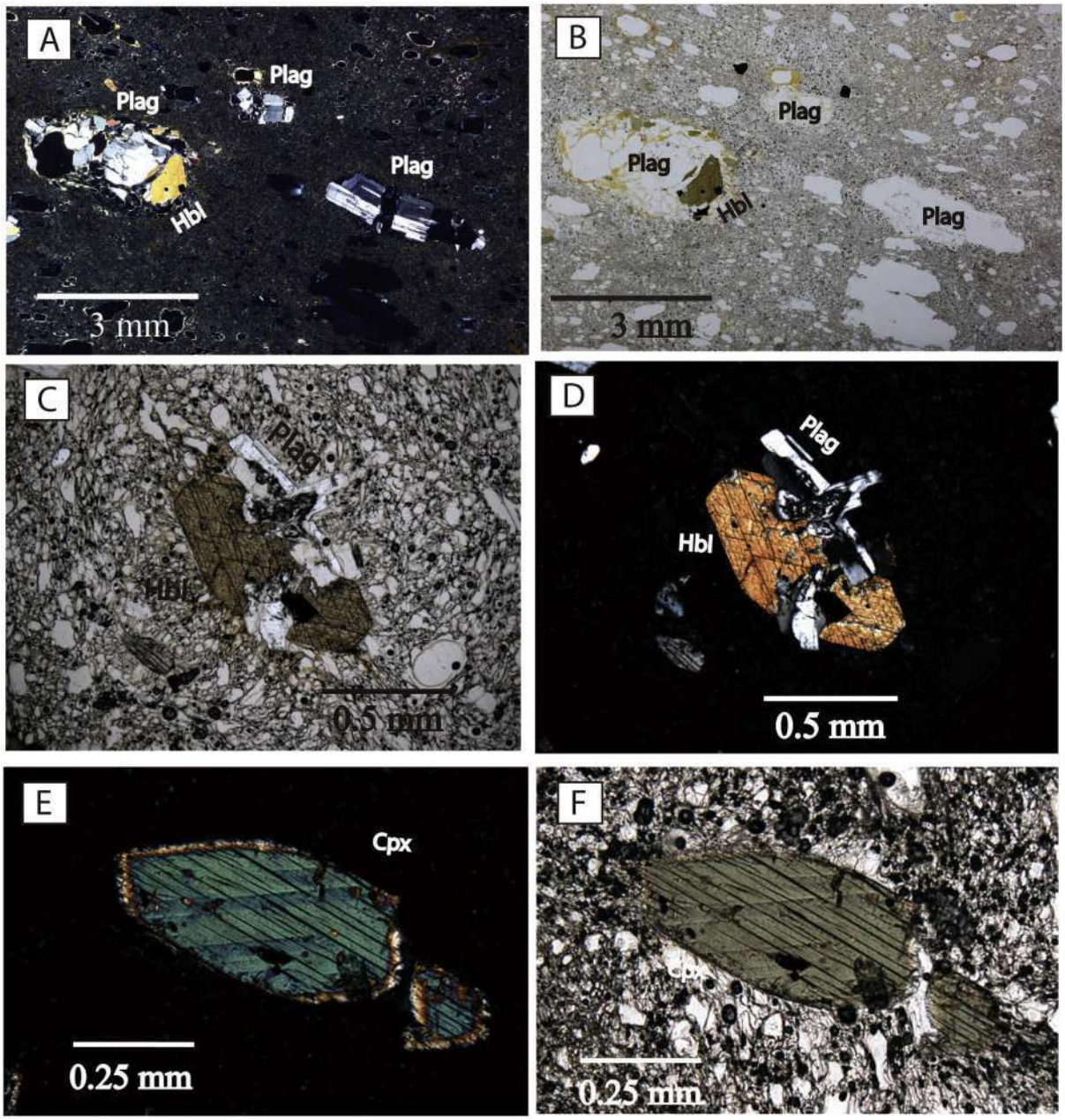

Fig. 9. Micro-photographs of polished thin sections of pumice clasts from the Altavista Formation tuffs of Ilopango caldera. a) Image in crossed Nichols of pumices from Cojutepeque Ignimbrite, with phenocrysts of plagioclase (plag) and hornblende (hbl) in a vesicular texture. b) The same micro-photograph that in a) but in parallel light. c) Pyramidal section of a hornblende phenocryst from San Juan Fall showing glomeroporphydic texture together with plagioclase crystals. d) Same image than c) in crossed Nichols. e) Tabular clinopyroxene (cpx) of egirine from San Juan Fall (image in crossed Nichols). f) The same egirine of e) in parallel light.

4.3. Geochronology of the Altavista Formation

A complete set of new isotopic ages of the Altavista Formation is provided in this study in order to have, for the first time, a more detailed volcanic history of IC.

4.3.1. Results of U/Pb and U/Th analysis

Six samples of zircon-separates that encompass the entire stratigraphic section of Altavista Formation were prepared to determine the age of each tuff-forming eruption. The first five members of the Altavista Formation were analyzed by U/Pb methods and only the last member was done by U/Th. Ages of the first five deposits were calculated with the intersection of the Concordia curve and the normal isochron (Figs. 12a, b, d and e), using the Isoplot software v. 3. 7, and following methods of Ludwig (2008). For ManI, the age was obtained as the average of the non-inherited zircons ages (Fig. 11c). SoI age (Figs. 12f) was calculated using IntCal09 software (Reimer et al., 2009), to calibrate U/Th ages (Bernal et al., 2014).

The first member of the Altavista Formation, CojI, is dated at 960 ± 750 ka (Fig. 12a). The large error is caused probably because most

Fig. 8. Representative stratigraphic sections of the six members of Altavista Formation. a) SW-N profile along the Panamerican Highway at NW of IC and b) W-E profile along the same road on the NE flank of the caldera. ILO localities and stratigraphic sections are shown in Fig. 2.

Table 2
Whole-rock chemistry of the Altavista Formation tuffs of Ilopango caldera.

Sample	ILO-20-P	ILO-20-E	ILO-89-C	ILO-20-F	ILO-132-A	ILO-144-A
Unit	SoI(TB5)	CorI (TB6)	SJF (TB7)	ManI (TB8)	DeI (TB9)	CojI (TB10)
SiO_2	70.4	72.2	69.0	75.0	74.6	70.8
TiO_2	0.28	0.23	0.40	0.25	0.21	0.33
Al_2O_3	18.5	17.5	17.8	14.8	13.9	16.2
FeO*	3.63	2.83	4.42	2.09	2.31	3.18
MnO	0.11	0.09	0.13	0.09	0.09	0.09
MgO	0.58	0.61	0.77	0.69	0.65	0.74
CaO	1.50	1.52	2.52	1.58	2.00	1.98
Na_2O	1.27	1.02	2.52	1.54	2.89	2.42
K_2O	3.48	3.99	2.51	3.94	3.29	4.31
P_2O_5	0.04	0.04	0.05	0.03	0.04	0.03
LOI	7.29	8.62	5.29	6.80	3.81	5.08
SUM	99.8	100.1	100.0	100.2	99.9	100.1
Rb	69	115	47	74	66	132
Sr	139	242	245	152	216	202
Ba	1009	864	1121	1147	1171	1091
Y	20	34	15	13	15	17
Zr	151	301	137	159	110	193
Nb	4	14	4	3	4	4
V	27	31	32	21	14	29
Cr	b3	12	b3	b3	b3	b3
Co	5	8	7	6	b4	8
Ni	7	13	8	8	7	10
Cu	23	11	15	13	8	20
Zn	48	58	44	41	31	45
Th	6	19	4	6	6	10
Pb	9	22	9	8	8	11
X (m)	266,586	266,586	292,473	266,586	287,416	289,231
Y (m)	1,518,661	1,518,661	1,517,803	1,518,661	1,518,785	1,518,825

OI: Olocuilta Ignimbrite, CoI: Colima Ignimbrite, ApI: Apopa Ignimbrite.
Major elements in wt% and trace elements in ppm.
Samples analyzed by X-Ray Fluorescence in the Instituto de Geología (UNAM) by Patricia Girón.
Coordinates in WGS84 system (zone 16P).
FeO*-total iron; LOI: lost of ignition.

analyzed zircons were too small (b80 μm), with xenocrystic cores and concentric zoning, and also due to the limitations of the U\Pb method in such young zircons (all the errors of U/Pb reported in this study refer to 2σ standard deviation). To obtain the best possible results, we discarded the most discordant zircons (largest ellipsoids in the isochron diagram, Fig. 12). The second member of this formation, the widespread DeI, is dated at 830 ± 140 ka (Fig. 12b). The third member, ManI, is dated at 750 ± 96 ka (Fig. 12c). The fourth member of this formation, SJF, yielded an U/Pb age of 590 ± 330 ka (Fig. 12d). The fifth member, CorI, yielded an age of 499 ± 73 ka (Fig. 12d). SoI, the youngest member of Altavista Formation, yielded an U/Th age of 257 ± 33 ka (Fig. 12f). All zircons age data are compiled in Appendix C.

4.3.2. Results of $^{40}Ar/^{39}Ar$ analyses

Five new $^{40}Ar/^{39}Ar$ ages were performed to obtain a second set of results for comparison and to get more precise age constraints (Table 3 and Fig. 13). Four high-purity plagioclase and one hornblende separates were analyzed. Plagioclase of CojI (sampled at ILO-144, Fig. 3) yielded a flat plateau with an age of 918.8 ± 17.4 ka (Fig. 13a). This $^{40}Ar/^{39}Ar$ age for CojI improves the U\Pb results presented above showing a smaller error. Plagioclase and hornblende separates of DeI did not yield meaningful $^{40}Ar/^{39}Ar$ ages due to the large abundance of atmospheric argon; thus, the U\Pb age is the best one we have for this member, although with a large analytical error (Fig. 12b). The plagioclase concentrate analyzed for ManI pumice yielded a $^{40}Ar/^{39}Ar$ age of 768.3 ± 49.4 ka. The age spectrum was discordant whose shape is classic "shaddle-shaped" type (Fig. 13c), which probably represents a mix of excess and atmospheric argon. This $^{40}Ar/^{39}Ar$ age agrees with the U\Pb results obtained with zircons (Fig. 11c). SJF's age was calculated on hornblende phenocrysts because the plagioclase contained numerous melt inclusions throughout 99% of the grains, yielding a $^{40}Ar/^{39}Ar$ plateau age of 626.0 ± 75.1 ka (Fig. 13d). CoI's age was obtained from the analysis of a plagioclase separate, yielding a plateau age of 553.0 ± 16.6 ka (Fig. 13e). The $^{40}Ar/^{39}Ar$ analyses of this fifth member constrain better the age obtained by U\Pb (Fig. 12e). SoI's age includes only few small plagioclase crystals, which resulted in low quantities of gas and higher uncertainties for many of the heating steps. We chose the upper heating steps that were the most concordant that yielded a weighted mean age of 335 ± 302.1 ka (Fig. 13f). A list of all $^{40}Ar/^{39}Ar$ age (plateau, mini-plateau, total fusion, normal and inverse isochron ages), as well as MSWD's and K/Ca ratios are given in Table 3.

5. Discussion

5.1. Volcanic phases and eruptive styles of the Altavista Formation tuffs

The style and eruption dynamics within the Altavista Formation are very diversified. Eruption processes for each one of the six members of

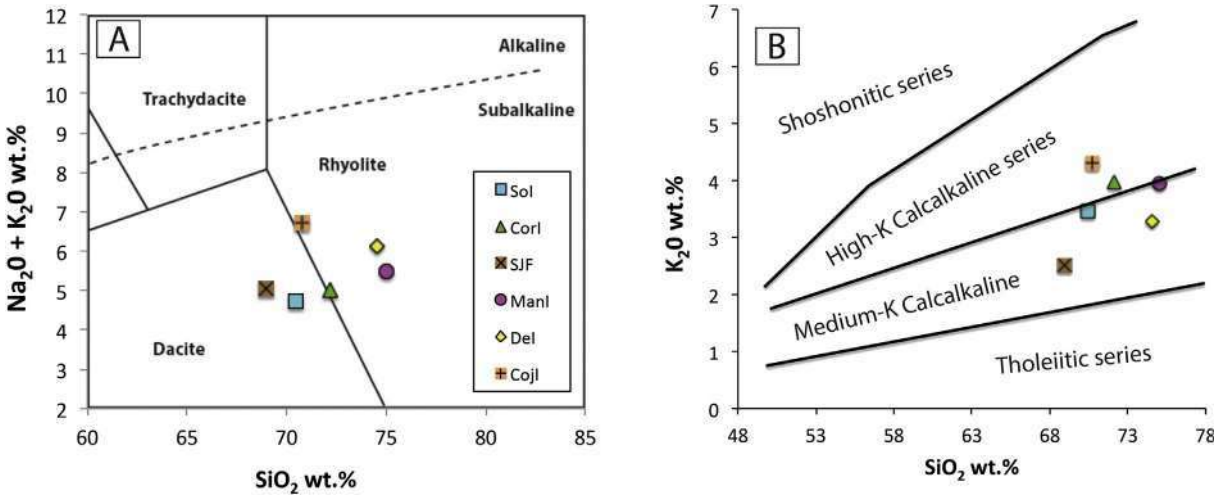

Fig. 10. Major element chemical classification plots for the Altavista Formation tuffs. a) Total Alkali Silica (TAS) diagram (after Le Bas et al., 1986). b) K_20 vs SiO_2 diagram (after Peccerillo and Taylor, 1976), where is remarkable the High-K content of the Altavista Formation. See Table 2 for chemical data.

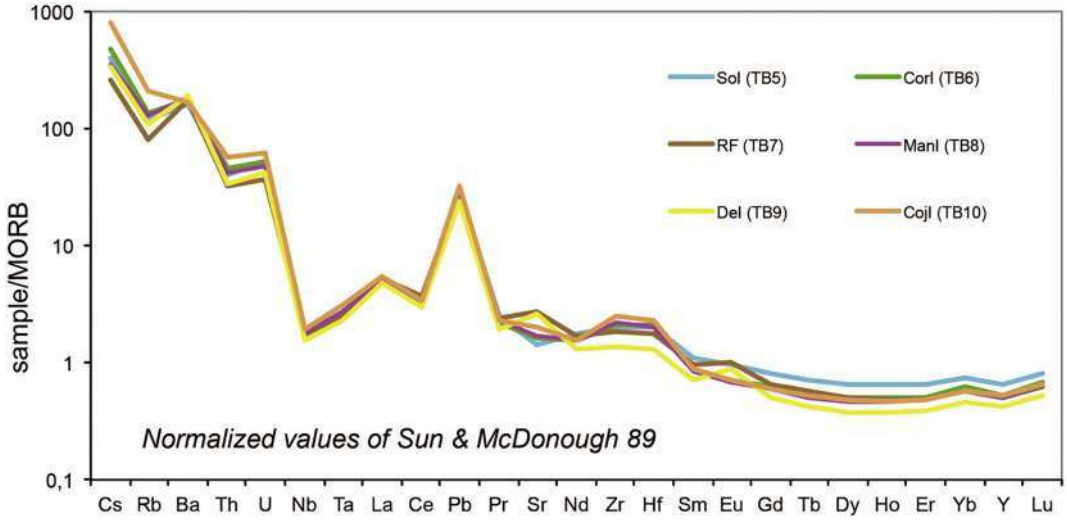

Fig. 11. N-MORB normalized multi-element diagram including of REE abundances of the Altavista Formation tuffs (normalizing values of Sun and McDonough, 1989).

this formation were interpreted from their deposits (Fig. 15) and are described below.

1. Cojutepeque Ignimbrite (CojI; ~918 ka). The vent of the first eruption of the Altavista Formation that produced the CojI was localized in the NE sector of the caldera, inferred by the distribution of the associated ignimbrite (Fig. 3). The CojI eruption started with a Plinian or Sub-Plinian column (Fig. 14a) that deposited a 2 m thick pumice fall layer up to 2 km to the NE of the caldera rim (Fig. 5f). Later, as the sharp contact between this pumice-fallout and the overlying cross-bedded PDC deposit indicates (Fig. 5c), a drastic change in the eruptive style occurred (Fig. 14b). The initial eruptive column collapsed, probably due to the widening of the conduit or by an increase of the mass eruption rate (MER; Costa et al., 2018). This MER increasing could be produced by the beginning of a caldera collapse, which would start the rapid evacuation of magma from the subcaldera magma chamber. The presence of accretionary lapilli (Fisher and Schmincke, 1984), suggests a water-rich environment, likely resulting for the interaction of magma with water from the Ilopango caldera lake. But later, the eruption returned to a magmatic style (Fig. 14c), as inferred by the presence of a massive tuff deposited at the top of CojI, formed by a series of lithic-rich PDCs deposits without accretionary lapilli. In fact, the caldera collapse onset likely coincides with the appearance of a lithic-rich PDC. This shift from hydromagmatic to magmatic style could be caused by a high magma/water ratio due to an increase of the magma eruption rate (Wohletz, 1986; Wohletz et al., 2013), probably caused by the caldera collapse. This collapse may have been as trap-door type (Aguirre-Díaz, 2008), due the limited distribution of the associated ignimbrite only present in the NE sector of the caldera (Fig. 3). This interpretation matches with the models of Aguirre-Díaz and Martí (2015); Aguirre-Díaz et al. (2016) and Saxby et al. (2016), who suggest this kind of collapse mechanism in the past and current IC.
2. Delgado Ignimbrite (DeI; ~830 ka). The second eruption of Altavista Formation apparently started with hydromagmatic explosions. This early activity was inferred from the parallel-stratified, fine-rich deposit with accretionary lapilli at the base of DeI (Fig. 6e), probably produced by very dilute PDC's (Fig. 14d). Later on, the hydromagmatic eruption produced highly turbulent PDCs distributed in all directions (Fig. 14e), depositing a widespread cross-stratified tuff, which is richer in solid components and thus apparently derived from denser PDCs than those that formed during the initial blasts (Figs. 3 and 6f). The last phase of this eruption apparently marks a possible change to a magmatic eruptive style, indicated by a lithic-rich level within a massive ignimbrite deposited on the top of this member (Fig. 5e). This kind of lithic-rich zones can be interpreted as a coignimbritic lag breccia suggesting the moment of a caldera collapse (Fig. 14f). Roof collapse of the magma chamber causes a massive and rapid evacuation of magma (Folch and Martí, 2009) that makes less effective the magma-water interactions necessary to carry out hydromagmatic explosions. The caldera collapse could have been the cause of the generation of dry magmatic PDCs at the end of the DeI eruption. The result is a massive and widely distributed ignimbrite sheet (DeI).
3. Manigua Ignimbrite (ManI; ~768 ka). The eruption associated to ManI began as purely magmatic, producing likely an eruptive column (Fig. 14g) that deposited a 30 cm thick layer of pumice fallout in the NW sector of IC (Fig. 7f). Later, the eruption became hydromagmatic, probably due to the input of water from the paleo-Ilopango lake into the vent, drastically increasing the explosivity of the eruption. The resulting product is a sequence of dilute and cross-bedded PDCs deposits, ~8 m thick, composed of ash matrix and accretionary lapilli, with some thin lens-shape layers rich in pumice fragments (pLens, Fig. 7), which serve as cross-stratification markers. This eruption apparently was laterally directed towards the W-NW flank of the caldera, since the ignimbrite is only observable in this sector of IC (Fig. 3). ManI eruption could be also linked to a partial collapse event, probably with a trap-door collapse style (Fig. 14h) due to the limited distribution of ManI in the eastern sector of the caldera (Fig. 3).
4. San Juan Fall (SJF; ~625 ka). This member was produced completely by a single eruptive column, probably Plinian or Sub-Plinian type (e.g., Bonadonna and Costa, 2013; Fig. 14i), which formed a thick pumice fallout of 5-6 m (Figs. 6d). This eruption was most likely purely magmatic, as no evidence of hydromagmatic processes were found in field exposures. This observation suggests that the vent of the SJF eruption was located outside the paleo-Ilopango lake, and probably in the northeast sector of IC because SJF is only observable in this direction, near Cojutepeque City (ILO-43, 89 and 316; Fig. 3). This eruption may not have produced a caldera collapse, because there is no associated widespread ignimbrite or other evidence of caldera roof subsidence. As in Las Pavas Lava and other IC products,

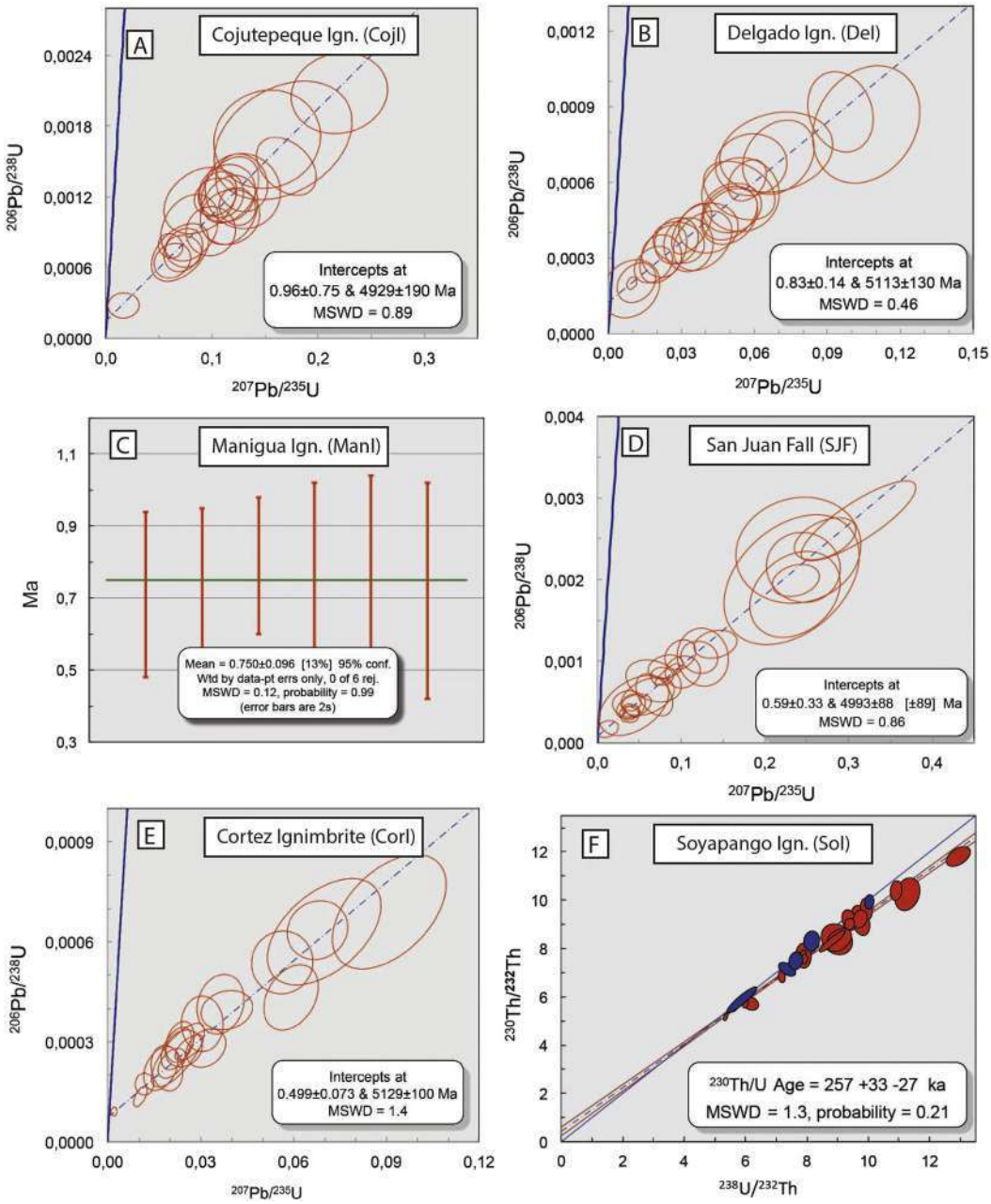

Fig. 12. Results of zircons analyses from the members of Altavista Formation. a) Concordia diagrams with normal isochron to calculate the ages of CojI, and b) DeI by U/Pb methodology. c) Average ages of the most concordant zircons from ManI (U/Pb). d) Concordia diagrams with normal isochron to calculate the ages of SJF, and e) CorI respectively (by U/Pb). f) Age calculation by U/Th of SoI (the blue spheres are zircons in secular equilibrium, see Bernal et al., 2014). (For interpretation of the references to colour in this figure legend, the reader is referred to the web version of this article.)

SJF may have erupted from the outer margin of the caldera, probably from vents controlled by the faults of the pull-apart system that have been linked to previous caldera eruptions of the Comalapa and Altavista Formations (Saxby et al., 2016; Suñe-Puchol et al., 2019).

5. Cortez Ignimbrite (CorI; ~553 ka). The eruptive processes associated to CorI are very similar to those of the previous ManI member. This eruption started with an eruptive column that deposited a thin layer of pumice fallout (b1 m; Fig. 7e). The vent of this eruption may be localized at the northwest sector of the caldera (Fig. 14j), inferred by the distribution of the associated pumice deposit, which is absent at the base of CorI on the northeast flank of IC. The initial eruptive column was suddenly interrupted by hydromagmatic explosions, which deposited a fine-ash tuff with accretionary lapilli derived probably from dilute PDCs (Fig. 14k). We suggest that this eruption was linked to a caldera collapse event based on the relatively large distribution of CorI, which it is still preserved at both flanks of IC (ILO-87, ILO-221 and ILO-20 in the NW sector, and in ILO-89 in the NE sector; Fig. 3).
6. Soyapango Ignimbrite (SoI; ~257 ka). The last eruption of the Altavista Formation also started with a sustained eruptive column in the NW sector of IC (Fig. 14l), which deposited N2 m of pumice fallout as far as 5 km from the caldera's topographic margin (Figs. 7 and 14l). This phase depressurized the subcaldera magma chamber and could have caused another caldera collapse. In this case, the possible collapse may have been complete along the caldera structure. The

Table 3
Summary of Incremental Heating 40Ar/39Ar Analyses on Altavista Formation tuffs of Ilopango Caldera.

Sample information					Age spectrum						Total fusion		Inverse isochron analyses		
Unit	Sample	X (m)	Y (m)	Material	Age ± 2σ (Ka)	39Ar (%)	K/Ca	MSWD	n	N	Age ± 2σ (Ka)	K/Ca	Age ± 2σ (Ka)	40/36 intercept	MSWD
Soyapango Ign.	ILO-20-P	266,586	1,518,661	Plagioclase	335.4 ± 302.1	33.74	0.0232	0.81	5	18	2858.0 ± 512.3	0.0234	509.9 ± 341.8	294.53 ± 1.44	0.86
Cortez Ign.	ILO-20-E	266,586	1,518,661	Plagioclase	553.0 ± 16.6	92.40	0.0428	0.92	15	20	538.0±20.2	0.0445	559.5 ± 23.3	295.06 ± 1.21	1.11
San Juan Fall	ILO-89-C	292,473	1,517,803	Hornblende	626.0 ± 75.1	99.94	0.0246	0.33	24	25	599.8±88.6	0.0247	679.0 ± 89.4	291.83 ± 3.49	0.18
Manigua Ign.	ILO-20-F	266,586	1,518,661	Plagioclase	768.3 ± 49.4	55.76	0.0327	1.32	9	24	691.2 ± 190.7	0.0340	768.2 ± 87.6	297.93 ± 2.16	2.14
Cojutepeque Ign.	ILO-144-A	289,231	1,518,825	Plagioclase	918.8 ± 17.4	76.10	0.0261	0.46	13	24	907.2±15.7	0.0264	910.2 ± 32.7	316.77 ± 69.32	0.46

K/Ca values are calculated as weighted means for the age spectra or as total fusion K/Ca values by combining the gas analyses. Both the number of steps (n) included in the age plateau and isochron calculations and the total number of incremental heating steps (N) have been listed. MSWD values for the age plateaus and inverse isochrons are calculated using n-1 and n-2 degrees of freedom, respectively. All samples from this study where monitored against FCT-FM sanidine (28.03 ± 0.18 Ma) as calibrated by Kuiper et al. (2008). Reported errors on the 40Ar/39Ar ages are at the 95% confidence level (2σ) including 0.3–0.4% standard deviation in the J-value.

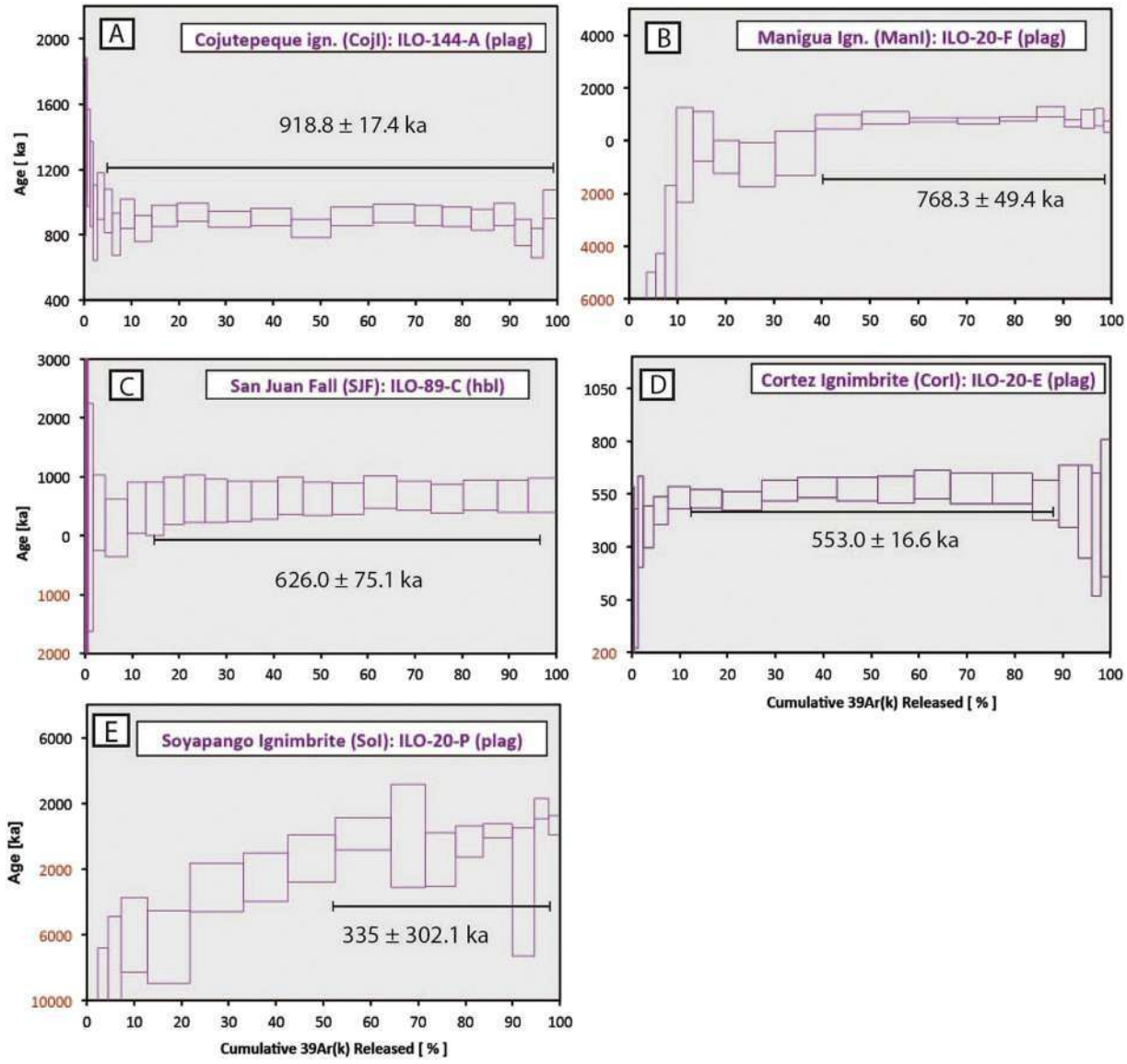

Fig. 13. High-resolution incremental heating $^{40}Ar/^{39}Ar$ age spectra for the members of Altavista Formation. The weighted average age (±2σ) is shown above a black bar that indicates the heating steps used in the calculation of a) CojI, b) ManI, c) SJF, d) CorI, and e) SoI ages.

eruption style changed from vertical column to low pyroclastic fountaining and radial ejection of dense PDCs (Fig. 14m), overflowing the crater rim and forming a widespread ignimbrite, ~5 m thick, and observed up to 10 km from the caldera margin. This ignimbrite is rich in pumice lenses and lithics (heterolitologic). At the final stage, this eruption became slightly hydromagmatic as suggested by the presence of fine-ash particles (higher magma fragmentation) and accretionary lapilli in detriment of larger components, such as pumices and coarser ash matrix, as well as the change from a massive deposit to cross-stratified laminated deposit, although still with pumice-rich lenses. This member crops out on both northern sectors of the caldera (NW and NE), but as in CorI, the pumice-fall layer at the base of the SoI is not evident around the northeast of IC.

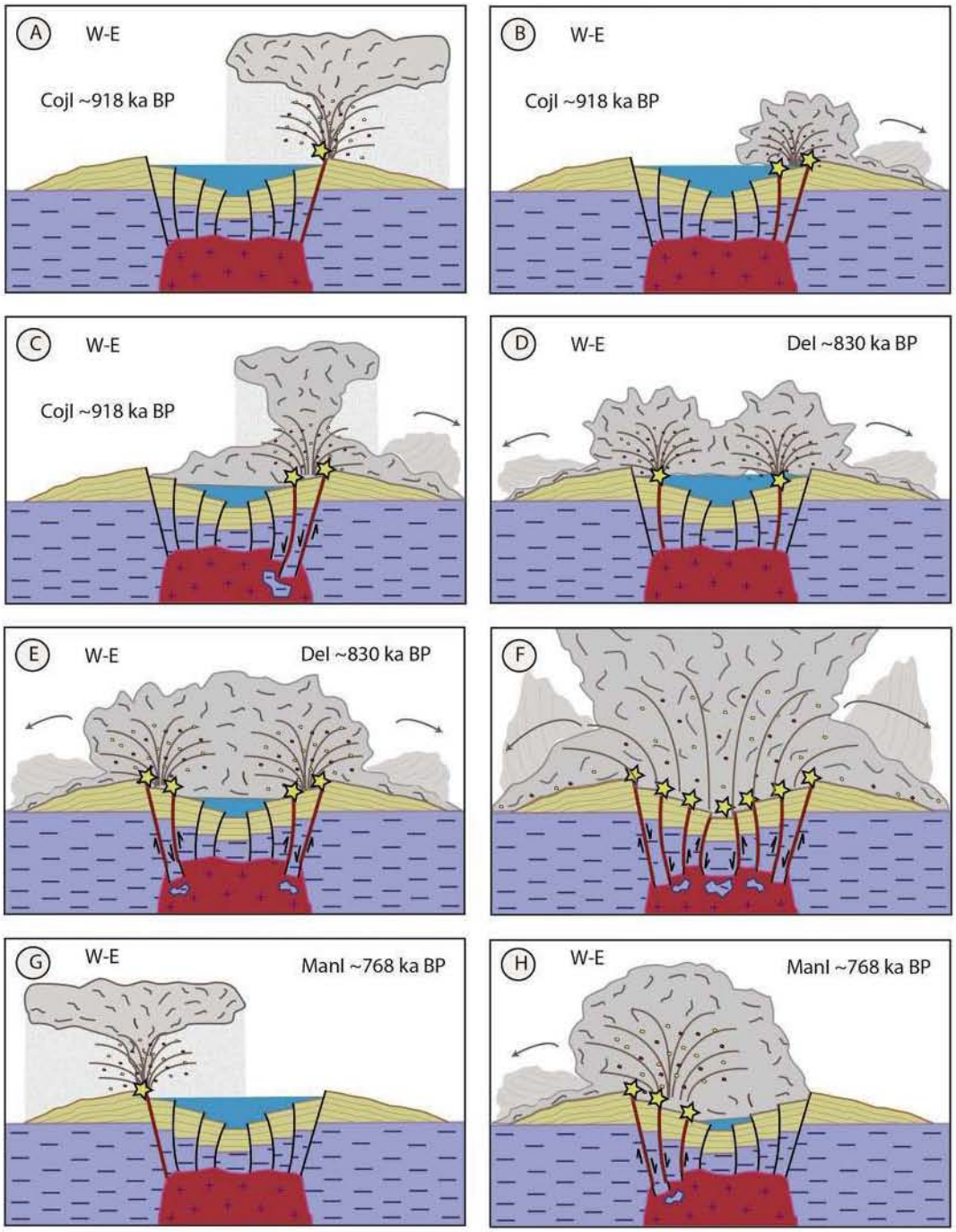

Fig. 14. Sketch (not to scale) illustrating the eruptive processes that formed the deposits of the Altavista Formation, since ~918 to ~257 ka BP. a) Eruptive column and associated pumice fallout at the beginning of Cojutepeque Ignimbrite (CojI), followed by b) dilute PDCs generated from hydromagmatic explosions, and c) denser PDCs formed during a possible partial collapse with trap-door style. d) "Blast-type" explosions at the beginning of Delgado Ignimbrite (DeI), followed by e) dilute and turbulent hydromagmatic PDCs and by f) total caldera collapse that generated a lithic-rich ignimbrite. g) Brief eruptive column at the beginning of the Manigua Ignimbrite (ManI) followed by h) hydromagmatic and dilute PDCs erupted from a partial collapse at the east. i) Eruptive column that deposited the fallout unit of San Juan Fall (SJF). j) Initial phase of eruptive column with intercalated blast-type explosions at the initial stage of Cortez Ignimbrite (CorI) eruption, followed by k) caldera collapse and massive generation of dilute PDCs. l) Eruptive column during the first phase of Soyapango Ignimbrite (SoI)'s eruption followed by m) lithic-rich PDCs produced by caldera collapse.

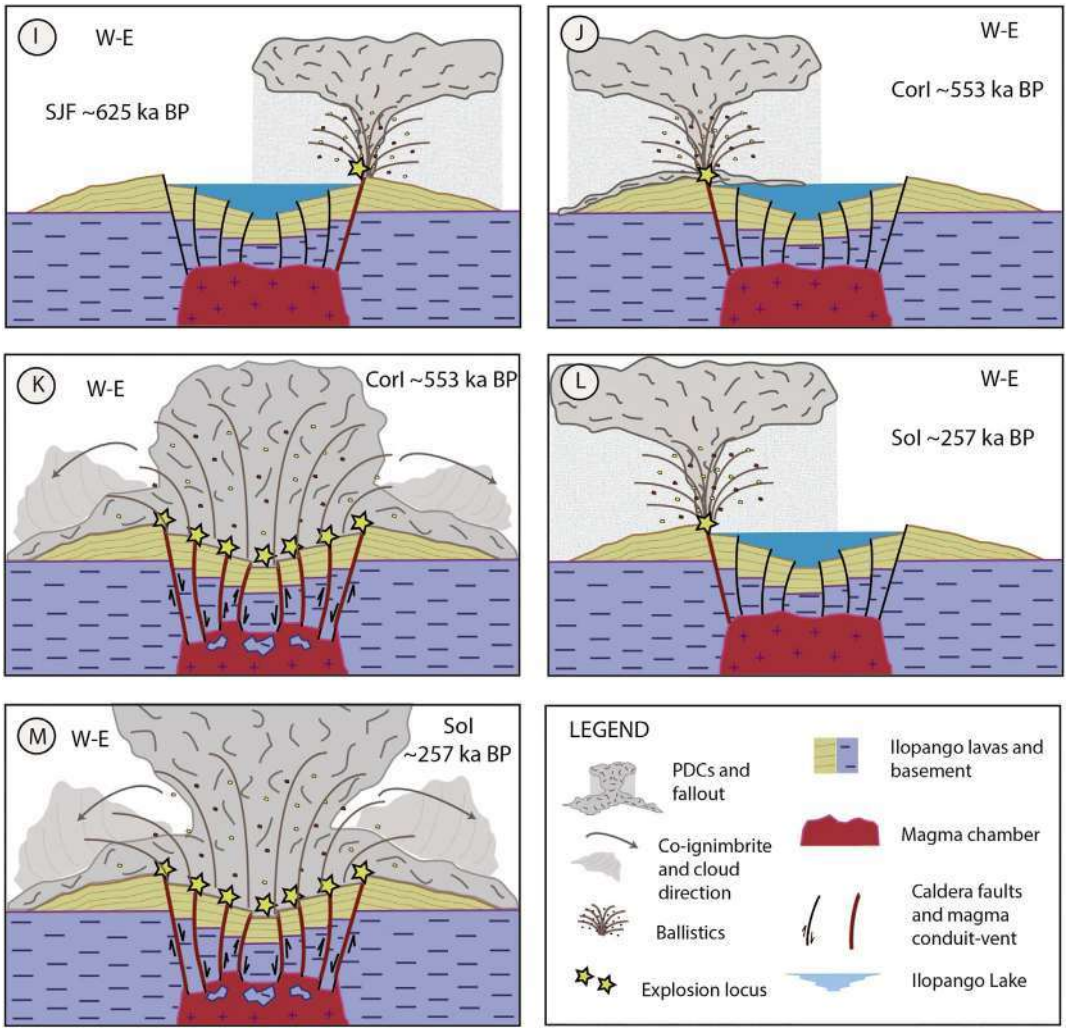

Fig. 14 (*continued*).

5.2. Volume and eruption magnitude of the Altavista Formation tuffs

Deposit volumes were calculated applying the Delaunay triangulation method (Macedonio and Pareschi, 1991), by using the thicknesses measured in the field. All data was imported, managed and processed into an attribute table within ArcGIS 10.2 by ESRI ©, following methods described in Pitcher et al. (2017). Because of the poor preservation of the Altavista Formation deposits, mainly due to erosion, the corresponding volumes are underestimated. The Delgado Ignimbrite (DeI) was the best member for volume estimation due to its widespread distribution and preservation (Fig. 3). A minimum volume of 5 km³ DRE was estimated for the DeI. This value corresponds to a magnitude of 6 (Pyle, 2000). This estimation ignores distal ash-fall facies, caldera fill and eroded material over the Balsamo Mountain Range (BMR, southern flank of IC, Fig. 3). Considering that DeI deposits are thicker and more widespread than the TBJ ignimbrite (see Fig. 3), DeI may have had a volume similar to TBJ or even N40 km³ DRE, reaching a magnitude of 7.

For the other five members of the Altavista Formation, we have established a minimum and conservative estimate, using the thicknesses and distribution of sparse incomplete outcrops, resulting in the order of 1 to 5 km³ DRE volume for each, which could reach around 30 km³, as those reported for the recent Tierras Blancas tuff-eruptions (CEL, 1992), if the eroded parts are also considered in the estimate.

5.3. Recurrence period of the Ilopango Caldera explosive eruptions

The IC has generated at least thirteen explosive eruptions during the Quaternary, most of them ignimbrite-forming events. According to Suñe-Puchol et al. (2019), the first three explosive phases, grouped as the Comalapa Formation, occurred in a time span of 440 ka, from 1.78 Ma (1st eruption) to 1.34 Ma (3rd eruption). Those three ignimbrite-forming eruptions had a similar recurrence period of around 220 ka (blue dashed square in Fig. 15). The $^{40}Ar/^{39}Ar$ ages presented in this study indicate a long quiescence period between the Comalapa Formation and the first eruption of the Altavista Formation (the CojI eruption, at ~918 ka). This volcanic hiatus was as large as ~ 420 ka (Fig. 15). Furthermore, the recurrence period of explosive eruptions within the Altavista Formation is quite shorter than the return time of the first eruptions. This lasted about 100 ka (Fig. 15), which is practically half the time of the frequency of the Comalapa Formation eruptions.

The chronogram of Fig. 15 shows all the IC major explosive eruptions recorded from the stratigraphy and geochronology, by integrating the data of Suñe-Puchol et al. (2019) for the Comalapa

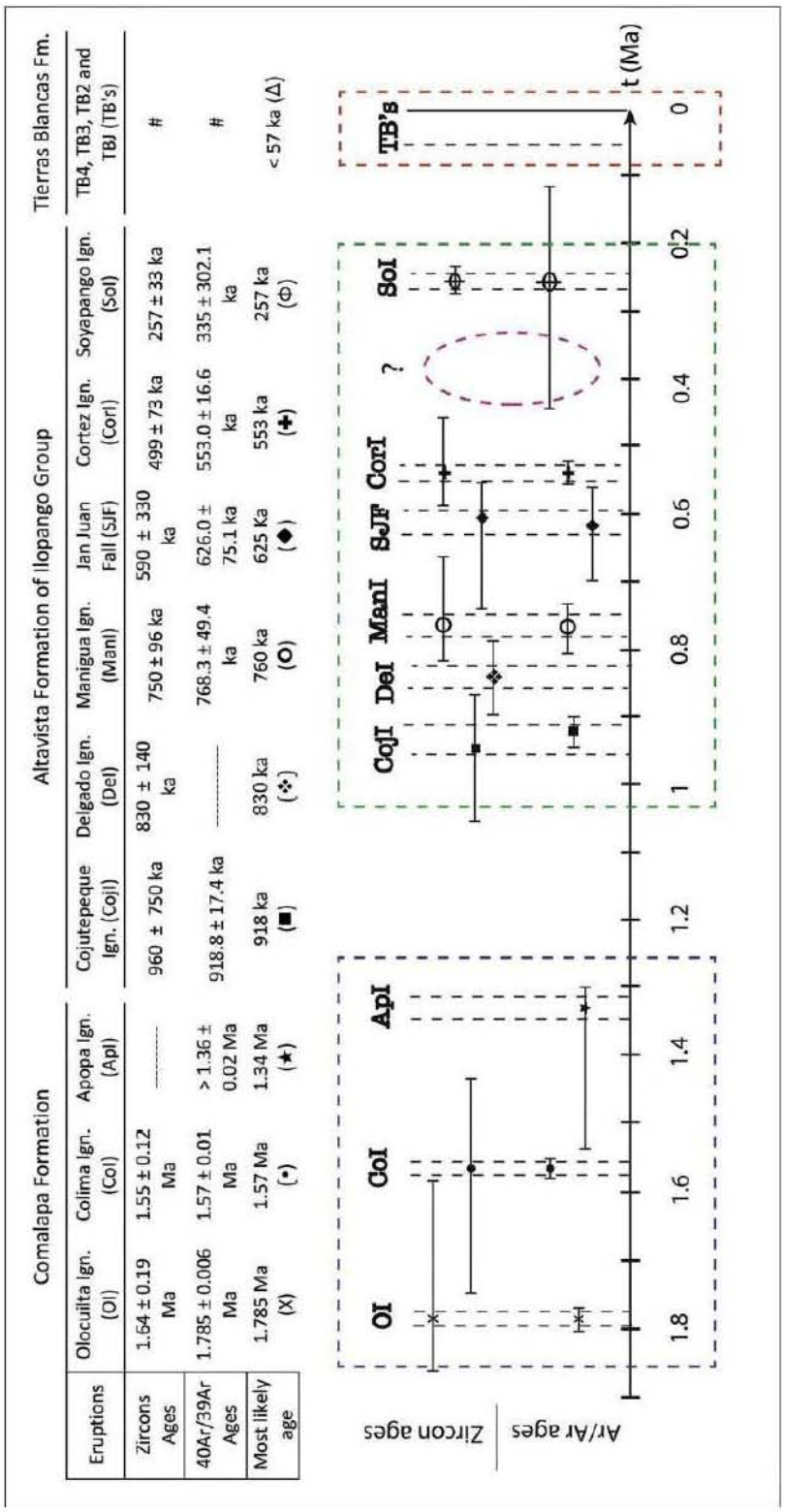

15. Chronogram of Ilopango caldera ignimbrite-forming eruptions during its activity, from the first ignimbrite at 1.785 Ma, to the last one, Tierra Blanca Joven ignimbrite at about 1.5 ka. The chronogram ılights the long period of quiescence between Comalapa and Altavista Formations, and also the long hiatus in volcanic activity between Altavista and Tierras Blancas Formations. The recurrence period ıin the Comalapa Formation eruptions (~220 ka, blue dashed rectangle) are twice longer than the Altavista Formation eruptions (~100 ka, green dashed rectangle), and much higher than the Tierras cas Formation eruptions (~20 ka, red dashed rectangle). The fuchsia dashed ellipsoid highlights an anomalous long volcanic hiatus (~300 ka) within the Altavista Formation, which may indicate that e eruptions could have happened between Cortez and Soyapango eruptions (CorI and, SoI). (For interpretation of the references to colour in this figure legend, the reader is referred to the web ion of this article.)

Formation, the data of the present work for the Altavista Formation tuffs, and published data elsewhere for the Tierras Blancas Formation (Rose et al., 1999; Kutterolf et al., 2008). Eruption ages of U-Pb, U-Th and $^{40}Ar/^{39}Ar$ from our database are positioned along a timescale bar with the corresponding analytical error bars. This chronogram shows a regular periodicity along the Altavista Formation eruptions, except for the time span between CorI (~553 ka) and SoI (~257 ka), which had a hiatus in the activity of ~300 ka (Fig. 15). In addition, it is evident another relatively long period of volcanic inactivity of ~200 ka between the Altavista and Tierras Blancas formations of IC (Fig. 15).

The most notorious observation from this chronologic chart is the relatively large quiescence periods between each formation, in the order of 200-400 ka each. The meaning of these quiet periods is still not clear, but we assume that the tectonic factor and the magma input rate are the two principal reasons. During the whole IC activity, from 1.78 to present, there was also intense tectonic activity in the area, and a seismogenically active period related to the ESFZ (Garibaldi et al., 2016). As previously reported in Aguirre-Díaz et al. (2016), Saxby et al. (2016), and Suñe-Puchol et al. (2019), the IC volcanic activity was in close relationship with the transtensive tectonic regime of the region, and IC is the result of several episodes of pull-apart-related caldera collapses that were linked to the strike-slip faults of the ESFZ.

IC volcanism, since the initial eruptions to the last one of TBJ (1.5 ka), was, and is tied to the Neogene activity of the regional faults of the central El Salvador region. The recurrence of large explosive eruptions could be linked to tectonic slips and the corresponding displacements between blocks, and probably, these tectonic events were the triggers for large explosive eruptions at IC, if the magma of the subcaldera chamber was close to eruptive conditions.

6. Conclusions

Ilopango Caldera (IC) has had at least 13 large Quaternary explosive eruptions, mostly ignimbrite-forming events, which were grouped into three formations, Comalapa Formation (1.78-1.32 Ma), Altavista Formation (918-257 ka) and Tierras Blancas Formation (b57 ka).

The Altavista Formation, presented in this study for the first time, consists of ryhodacitic pyroclastic deposits that are the product of six explosive eruptions, including eruptive columns and dense and dilute PDCs of magmatic and hydromagmatic type. The largest member of the Altavista Formation is the Delgado Ignimbrite (DeI), with a minimum DRE volume N 30 km^3 if eroded deposits are considered. The recurrence period of the Altavista Formation eruptions is ~100 ka, except between the two last events (553 ka CorI and 257 ka SoI). This is half the time of the Comalapa Formation explosive eruptions recurrence period (~220 ka).

A chronostratigraphic chart of all IC eruptions since the initial large Olocuilta ignimbrite (1.78 Ma; N150 km^3 DRE) to the latest TBJ (~1.5 ka; 30 km^3 DRE) shows large quiescence gaps of nearly 200 to 400 ka between major eruptive members. These long quiet gaps and intense activity within each formation are apparently linked with the transtensive tectonic activity of the ESFZ. IC is the result of several caldera collapse episodes, each for a major ignimbrite eruption, which were probably triggered by tectonic events, although this complex relation needs to be investigate further.

Supplementary data to this article can be found online at https://doi.org/10.1016/j.jvolgeores.2019.02.011.

AcknowledgeThents

This study was financed by CONACYT-CB grant 240447 to GJAD. We appreciate the logistical support of the Ministerio de Medio Ambiente y Recursos Naturales – MARN, and of the Policia Nacional Civil – PNC, of El Salvador. We thank the doctoral scholarship grant to the first author from CONACYT-Mexico. We acknowledge to Anthony Koppers for his help and support in the Ar/Ar geochronology laboratory at Oregon State University (OSU). We want to be grateful to Juan Vazquez for thin section elaboration, to Lozano Santacruz and Patricia Girón for XRF analyses, and Ofelia Perez for the REE and trace elements analyses. We also want to thank Victor Noll for his rappel training to sample the ignimbrites of Ilopango caldera. This manuscript was greatly improved by comments and suggestions from the editors Joan Martí and James Gardner, and also from two experts reviewers.

References

Agostini, S., Corti, G., Doglioni, C., Carminati, E., Innocenti, F., Tonarini, S., Manetti, P., Di Vincenzo, G., Montanari, D., 2006. Tectonic and magmatic evolution of the active volcanic front in El Salvador: insight into the Berlín and Ahuachapán geothermal areas. Geothermics 35, 368–408. https://doi.org/10.1016/j.geothermics.2006.05.003.

Aguirre-Díaz, G.J., 2008, Types of collapse calderas: Collapse calderas Workshop 19-25 October 2008, Querétaro, Mexico "Reconstructing the Evolution of Collapse Calderas: Magma Storage, Mobilization and Eruption". IOP Conference Series: Earth and Environmental Science, 3 012021 (5pp) doi:https://doi.org/10.1088/1755-1307/3/1/012021 (http://www.iop.org/EJ/toc/1755-1315/3/1

Aguirre-Díaz, G.J., Martí, J., 2015. Graben Calderas: Examples from Mexico, Central America, and the Andes: 26th IUGG General Assembly, Prague, Czech Republic, June 22–July 2, 2015. Abstracts. https://www.czech-in.org/cm/IUGG/.

Aguirre-Díaz, G.J., Suñe-Puchol, I., Dávila-Harris, P., Pedrazzi, D., Hernández, W., 2016. The Ilopango Caldera: A Long-Lived Caldera System of Central America: 6th International Workshop on Collapse Calderas, IAVCEI, Hokkaido, Japan; June 2016 (Abstracts).

Aguirre-Díaz, J.G., Suñe-Puchol, I., Davila-Harris, P., Pedrazzi, D., Hernandez, W., Gutierrez, E., 2017. Volcanic History of the Ilopango Caldera, Central American Volcanic Arc. 113th Annual Meeting. GSA Cordilleran Section, Hawaii, USA, p. 2017.

Alonso-Henar, J., Álvarez-Gõmez, J.A., Martinez-Díaz, J.J., 2017. Neogene-quaternary evolution from transpressional to transtesional tectonics in Northern Central America controlled by cocos: Caribbean subduction coupling change. J. Iber. Geol. https://doi.org/10.1006/s415113-017-0034-2.

Arculus, R.J., Curran, E.B., 1972. The genesis of the calc-alkaline rock suite. Earth Planet. Sci. Lett. 15, 255-262.

Bernal, J.P., Lozano-Santacruz, R., 2005. Characterization of a new set of eight geochemical reference materials for XRF major and trace element analysis. Revista Mexicana de Ciencias Geológicas 22 (3), 329-344.

Bernal, J.P., Solari, L.A., Gómez-Tuena, A., Ortega-Obregón, C., Mori, L., Vega- González, M., Espinosa-Arbeláez, D.G., 2014. In-situ230Th/U dating of Quater- nary zircons using LA-MCICPMS. Quat. Geochronol. 23, 46-55. https://doi.org/10.1016/j.quageo.2014.06.003.

Bonadonna, C., Costa, A., 2013. Plume height, volume, and classification of explosive volcanic eruptions based on the Weibull function. Bull. Volcanol. 75 (8), 1–19.

Branney, M.J., Kokelaar, P., 2002. Pyroclastic density currents and the sedimentation of ignimbrites: Geol Soc London. Memoirs 27 (152 pp).

Canora, C., Villamor, P., Martínez-Díaz, J.J., Berryman, K.R., Álvarez-Gómez, J.A., Capote, R., Hernández, W., 2012. Paleoseismic analysis of the San Vicente segment of the El Salvador Fault Zone, El Salvador, Central America. Geol. Acta 10, 103-123. https://doi.org/10.1344/105.000001700.

CEL (Comision Ejecutiva Hidroelectrica del Rio Lempa), 1992. Desarrollo de los Recursos Geotermicos del Area Centro-Occidental de El Salvador. Prefactibilidad Geotermica del Area de Coatepeque. Reconocimiento Geotermico. Informe Final. Internal report.

Costa, A., Suzuki, Y.J., Koyaguchi, T., 2018. Understanding the plume dynamics of explosive super-eruptions. Nat. Commun. 9, 654. https://doi.org/10.1038/s41467-018-02901-0.

DeMets, C., 2001. A new estimate for present-day Cocos-Caribbean plate motion: Implications for slip along the Central American volcanic arc. Geophys. Res. Lett. 28, 4043–4046. https://doi.org/10.1029/2001GL013518.

Dixon, T.H., 1993. GPS measurement of relative motion of the Cocos and Caribbean plates and strain accumulation across the Middle America Trench. Geophys. Res. Lett. 20, 2167–2170. https://doi.org/10.1029/93GL02415.

Donnelly, T.W., Horne, G.S., Finch, R.C., Lopez-Ramos, E., 1990. Northern Central America: the Maya and Chortis blocks. In: Dengo, G., Case, J.E. (Eds.), The Geology of North America: The Caribbean Region, pp. 37–76.

Dull, R.A., Southon, J.R. and Sheets, P., 2001. Volcanism, Ecology and Culture: A Reassessment of the Voclán Ilopango TBJ eruption in the Southern Maya Realm, v. 12, No. 1, pp. 25–44.

Dull, R.A., Southon, J.R., Kutterolf, S., Freundt, a., Wahl, D., Sheets, P., 2010. Did the TBJ Ilopango eruption cause the AD 536 event? AGU fall Meet. Abstr. 1, 2370.

Fisher, R.V., Schmincke, H.-U., 1984. Pyroclastic Rocks: Berlin. Springer Verlag (472 p).

Folch, A., Martí, J., 2009. Time-dependent chamber and vent conditions during explosive caldera-forming eruptions. Earth Planet. Sci. Lett. https://doi.org/10.1016/j.epsl.2009.01.035.

Funk, J., Mann, P., McIntosh, K., Stephens, J., 2009. Cenozoic tectonics of the Nicaraguan depression, Nicaragua, and Median Trough, El Salvador, based on seismic-reflection profiling and remote-sensing data. Bull. Geol. Soc. Am. 121, 1491–1521. https://doi.org/10.1130/B26428.1.

Garibaldi, N., Tikoff, B., Hernández, W., 2016. Neotectonic deformation within an extensional stepover in El Salvador magmatic arc, Central America: Implication for the interaction of arc magmatism and deformation. Tectonophysics 693, 327–339. https://doi.org/10.1016/j.tecto.2016.05.015.

Golombek, M.P., Carr, M.J., 1978. Tidal triggering of seismic and volcanic phenomena during the 1879-1880 eruption of Islas Quemadas volcano in El Salvador, Central America. J. Volcanol. Geotherm. Res. 3, 299–307. https://doi.org/10.1016/0377-0273(78)90040-9.

Hernández, E.W., 2004, Características geotécnicas y vulcanológicas de las tefras de Tierra Blanca Joven de Ilopango, El Salvador: Tesis de maestría, Univ. Politécnica de El Salvador, San Salvador, 115 p.

Hernández, W., 2008, Aspectos geológicos que influyen en las aguas subterráneas y en la respuesta sísmica del Area Metropolitana de San Salvador. Revista ASIA No. 162. 29-41p.

Hutton, D.H.W., Reavy, R.J., 1992. Strike-slip tectonics and granite petrogenesis. Tectonics 11, 960-967.

Koppers, A.A.P., 2002. ArArCALC–Software for 40Ar/39Ar age calculations. Comput. Geosci. 28 (5), 605–619. https://doi.org/10.1016/S0098-3004(01)00095-4.

Koppers, A.P., Gowen, M.D., Colwell, L.E., Gee, J.S., Lonsdale, P.F., Mahoney, J.J., Duncan, R.A., 2011. New 40Ar/39Ar age progression for the Louisville hot spot trail and implications for inter-hot spot motion. Geochem. Geophys. Geosyst. 12: Q0AM02. doi: https://doi.org/10.1029/2011GC003804.

Kuiper, K.F., Deino, A., Hilgen, F.J., Krijgsman, W., Renne, P.R., Wijbrans, J.R., 2008. Synchronizing rock clocks of Earth history. Science 320, 500–504. https://doi.org/10.1126/science.1154339.

Kutterolf, S., Freundt, A., Schacht, U., Bürk, D., Harders, R., Mörz, T., Peréz, W., 2008. Pacific offshore record of plinian arc volcanism in Central America: 3. Application to forearc geology. Geochem. Geophys. Geosyst. 9. https://doi.org/10.1029/2007GC001826.

LeBas, et al., 1986. A chemical classification of volcanic rocks based on the total alkali-silica diagram. J. Petrol. 27, 745-750.

Lexa, J., Šebesta, J., Chavez, J.A., Hernández, W., Pécskay, Z., 2011. Geology and volcanic evolution in the southern part of the San Salvador Metropolitan Area. J. Geosci. 56, 105–140. https://doi.org/10.3190/jgeosci.088.

Ludwig, K. 2008. Manual for Isoplot 3.7. Berkeley Geochronology Center, Special Publication 4, rev. p. 77.

Macedonio, G., Pareschi, M.T., 1991. An algorithm for the triangulation of arbitrarily distributed points: applications to volume estimate and terrain fitting. Comput. Geosci. 17, 859–874. https://doi.org/10.1016/0098-3004(91)90086-S.

Mann, P., 2007. Overview of the tectonic history of northern Central America. In: Mann, P. (Ed.), Geologic and Tectonic Development of the Caribbean Plate Boundary in Northern Central America. 428. Geological Society of America Special Papers, pp. 1–19.

Marshall, D.J., 1988. Cathodoluminescence of Geological Materials. Unwin Hyman, p. 181.

Martí, J., Groppelli, G., & da Silveira, A. B., 2018. Volcanic stratigraphy: a review. J. Volcanol. Geotherm. Res. Volume 357, 15 May 2018, Pages 68–91.

Martínez-Díaz, J.J., Álvarez-Gómez, J.A., Benito, B., Hernández, D., 2004. Triggering of destructive earthquakes in El Salvador. Geology 32, 65-68. https://doi.org/10.1130/G20089.1.

Morris, J.D., and Ryan, J.G, 2004, Subduction zone processes and implications for changing composition of the upper and lower mantle, in Treatise on Geochemistry, ed., H.D. Holland and K.K. Turekian, Elsevier-Pergamon, Oxford, p. 451-470.

Murphy, J.B., 2007. Igneous Rock Associations 8. Arc Magmatism II: Geochemical and Isotopic Characteristics. Geosci. Can. 34, 1.

Ortega-Obregón, C., Solari, L., Gómez-Tuena, A., Elías-Herrera, M., Ortega-Gutiérrez, F., Macías-Romo, C., 2013. Permian–Carboniferous arc magmatism in southern Mexico: U–Pb dating, trace element and Hf isotopic evidence on zircons of earliest subduction beneath the western margin of Gondwana. Int. J. Earth Sci. 103 (5), 1287–1300. https://doi.org/10.1007/s00531-013-0933-1.

Peccerillo, A., Taylor, S.R., 1976. Geochemistry of Eocene calcalkaline volcanic rocks from the Kastamonu area, Northern Turkey. Contrib. Mineral. Petrol. 58, 63–81.

Pedrazzi, D., Sunyé-Puchol, I., Aguirre-Díaz, G.J., Costa, A., Davila-Harris, P., Hernández, W., Gutierrez, E., 2018. The Ilopango Tierra Blanca Joven (TBJ) eruption, El Salvador: volcano-stratigraphy of a major Holocene event of Central America and hazards implications EGU General Assembly 2018. Vol. 20, EGU2018–8455.

Pitcher, B. W., Kent, A.J.R, Grunder, A.L. and Duncan, R.A., Frequency and volumes of ignimbrite eruptions following the Late Neogene initiation of the Central Oregon High Cascades. J Volcanol Geotherm Res 339: 1-22, doi:10.1016/j.jvolgeores.2017.04.019.

Pyle, D.M., 2000. The sizes of volcanic eruptions. In: Sigurdsson, H., Houghton, B., McNutt, S.R., Rymer, H., Stix, J. (Eds.), Encyclopedia of Volcanoes. Academic Press, London, UK, pp. 263-269.

Reimer, P.J., Baillie, M.G.L., Bard, E., Bayliss, A., Beck, J.W., Blackwell, P.G., Ramsey, C.B., Buck, C.E., Burr, G.S., Edwards, R.L., Friedrich, M., Grootes, P.M., Guilderson, T.P., Hajdas, I., Heaton, T.J., Hogg, A.G., Hughen, K.A., Kaiser, K.F., Kromer, B., McCormac, F.G., Manning, S.W., Reimer, R.W., Richards, D.A., Southon, J.R., Talamo, S., Turney, C.S.M., van der Plicht, J., Weyhenmeyer, C.E., 2009. IntCal09 and Marine09 radiocarbon age calibration curves, 0e50,000 years cal BP. Radiocarbon 51 (4), 1111e1150.

Reynolds, J.H., 1987. Timing and sources of Neogene and Quaternary volcanism in south-central Guatemala. J. Volcanol. Geotherm. Res. 33, 9–22.

Rose, W.I., Conway, F.M., Pullinger, C.R., Deino, A., McIntosh, K., 1999. An improved age framework for late Quaternary silicic eruptions in northern Central America. Bull. Volcanol. 61, 106–120. https://doi.org/10.1007/s004450050266.

Saxby, J., Gottsmann, J., Cashman, K., Gutiérrez, E., 2016. Magma storage in a strike-slip caldera. Nat. Commun. 7, 12295. https://doi.org/10.1038/ncomms12295.

Sheets, P.D., 1979. Environmental and cultural effects of the Ilopango eruption in Central America. Volcan. Act. Hum. Ecol. 525-564, ill. https://doi.org/10.1016/B978-0-12-639120-6.50022-4.

Sofield, D., 2004. Eruptive history and volcanic hazards of Volcan San Salvador. Geol. Soc. Am. Spec. Pap. 375, 147-158.

Sun, S.S., McDonough, W.F., 1989. Chemical and isotopic systematics of oceanic basalts: implications for mantle composition and processes. In: Saunders, A.D., Norry, M.J. (Eds.), Magmatism in the Oceanic Basins. 42. Geological Society of London Special Publication, pp. 313-345.

Suñe-Puchol, I., Aguirre-Díaz, G.J., Dávila-Harris, P., Miggins, D.P., Pedrazzi, D., Costa, A., Ortega-Obregón, C., Lacan, P., Hernández, W., Gutiérrez, E., 2019. The Ilopango caldera complex, El Salvador: origin and early ignimbrite-forming eruptions of a graben/pull-apart caldera structure. J. Volcanol. Geotherm. Res. 371, 1–19. https://doi.org/10.1016/j.jvolgeores.2018.12.004.

Weber HS, Wiesemann G, Wittek indt H (1974), Mapa Geológico de la República de El Salvador/Geologische Übersichtskarte der Republik El Salvador 1:500,000 (after geological maps 1:100000 – 1967-74) Bundesanstalt für Geowissenschaften und Rohstoffe, Hannover; Bundesanstalt fu¨r Bodenforschung, Hannover.

Williams, H., Meyer-Abich, H., 1955. Volcanism in the southern part of El Salvador, with particular reference to the collapse basins of Lakes Coatepeque and Ilopango. Geol. Sci. Univ. Calif. Publ. 32 (64 p).

Wohletz, K.H., 1986. Explosive magma-water interactions: Thermodynamics, explosion mechanisms, and field studies. Bull. Volcanol. 48 (5), 245-264.

Wohletz, K.H., Zimanowski, B., Büttner, R., 2013. Magma-water Interactions. Modeling volcanic processes. Cambridge University Press, New York, pp. 230–257.

5. Estudio vulcano-estratigráfico de la erupción Tierra Blanca Joven (TBJ): caracterización física del mayor evento Holoceno en Centro America.

Artículo: Pedrazzi, D., Suñe-Puchol, I., Aguirre-Díaz, G., Costa, A., Smith, V. C., Poret, M., Dávila-Harris, P., Miggins, D. P., Hernández, W. and Gutiérrez, E., 2019. The Ilopango Tierra Blanca Joven (TBJ) eruption, El Salvador: volcano-stratigraphy and physical characterization of the major Holocene event of Central America. J. Volcanol. Geotherm. Res.

Contribuciones individuales de los autores:

- **Dario Pedrazzi:** diseño y organización del estudio, trabajo de campo, de laboratorio, modelado numérico, procesamiento, análisis e interpretación de datos, redacción del artículo.
- **Ivan Suñé Puchol:** organización y trabajo de campo, análisis en laboratorio, interpretación de datos, apoyo en la redacción del artículo.
- **Gerardo Aguirre Díaz:** financiamiento, supervisión, trabajo de campo, interpretación de los datos, revisión del artículo.
- **Antonio Costa:** estimación de parámetros físicos eruptivos.
- **Victoria C. Smith**: análisis químicos del vidrio de la TBJ
- **Matthieu Poret:** Modelado numérico para dispersión de ceniza
- **Pablo Dávila Harris:** trabajo de campo, interpretación de datos y corrección del artículo.
- **Dan Miggins:** análisis de laboratorio, interpretación de datos y corrección del artículo.
- **Walter Hernández:** trabajo de campo e interpretación de la geología de la zona.
- **Eduardo Gutiérrez:** apoyo logístico y trabajo de campo.

Journal of Volcanology and Geothermal Research 377 (2019) 81-102

Contents lists available at ScienceDirect

Journal of Volcanology and Geothermal Research

jour nal homepage: www.elsevier. com/ locate/ jvolgeores

The Ilopango Tierra Blanca Joven (TBJ) eruption, El Salvador: Volcano-stratigraphy and physical characterization of the major Holocene event of Central America

Dario Pedrazzi [a,*], Ivan Sunye-Puchol [b], Gerardo Aguirre-Díaz [b], Antonio Costa [c], Victoria C. Smith [d], Matthieu Poret [c], Pablo Dávila-Harris [e], Daniel P. Miggins [f], Walter Hernández [g], Eduardo Gutiérrez [g]

[a] ICTJA, CSIC, Group of Volcanology, SIMGEO UB-CSIC, Institute of Earth Sciences Jaume Almera, Lluis Sole i Sabaris s/n, 08028 Barcelona, Spain
[b] Centro de Geociencias, Universidad Nacional Autónoma de México, Blvd. Juriquilla 3001, Campus UNAM, Querétaro 76230, Mexico
[c] Istituto Nazionale di Geofisica e Vulcanologia, INGV-Bologna, Via Donato Creti, 12, 40100 Bologna, Italy
[d] Research Laboratory for Archaeology and the History of Art, University of Oxford, 1-2 South Parks Road, Oxford OX1 3TG, UK
[e] División de Geociencias Aplicadas, IPICYT, San Luis Potosí 78216, Mexico
[f] College of Earth, Ocean and Atmospheric Sciences, Oregon State University, 104 CEOAS Administration Building, 101 SW 26th St, Corvallis, OR 97331, United States of America
[g] Gerencia de Geología del Observatorio Ambiental, Ministerio de Medio Ambiente y Recursos Naturales MARN, San Salvador 76230, El Salvador

a r t i c l e i n f o

Article history:
Received 29 August 2018
Received in revised form 7 March 2019
Accepted 8 March 2019
Available online 16 March 2019

Keywords:
Pyroclastic Density Currents
Co-ignimbrite
Tephra fallout
Tephra dispersal modelling
Ilopango caldera

a b s t r a c t

The Ilopango caldera is the source of the large Tierra Blanca Joven (TBJ) eruption that occurred about 1.5 ka years ago, between ca. AD270 and AD535. The eruption dispersed volcanic ash over much of the present territory of El Salvador, and pyroclastic density currents (PDCs) extended 40 km from the volcano. In this study, we document the physical characteristics of the deposits from all over El Salvador to further constrain the eruption processes and the intensity and magnitude of the different phases of the eruption. The succession of deposits generated by the TBJ eruption is made of 8 units. The eruption started with PDCs of hydromagmatic origin (Unit A_0), followed by fallout deposits (Units A and B) that are b15 cm thick and exposed in sections close to the Ilopango caldera (within 10–15 km). The eruption, then, transitioned into a regime that generated further PDCs (Units C–F), these range from dilute to dense and they filled the depressions near the Ilopango caldera with thicknesses up to 70 m. Deposits from the co-ignimbrite plume (Unit G) are the most widespread, the deposits are found in Guatemala, Honduras, Nicaragua, Costa Rica and the Pacific Ocean and cm-thick across El Salvador. Modelling of the deposits suggests that column heights were 29 km and 7 km for the first two fallout phases, and that the co-ignimbrite phoenix plume rose up to 49 km. Volumes estimated for the fallout units are 0.15, 0.8 and 16 km^3 dense rock equivalent (DRE) for Unit A, B and G respectively. The PDCs deposits volumes were estimated to be ~0.5, ~3.3, ~0.3 and ~9.1 km^3 DRE for Units C, D, E and F, respectively. The combined volume of TBJ deposits is ~30 km^3 DRE (~58 km^3 bulk rock), indicating that it was one of largest Holocene eruptions from Central America. This eruption occurred while Mayan populations were living in the region and it would have had a significant impact on the areas within tens of kilometres of the vent for many years to decades after the eruption.

1. Introduction

Large caldera volcanoes pose a significant hazard to populations that surround them. In order to understand the likelihood and type of further activity it is key that the deposits of previous eruptions are well studied. This study focuses on the thick deposits of the Tierra Blanca Joven (TBJ) eruption from Ilopango Caldera, El Salvador.

Ilopango Caldera (IC; Fig. 1), is a 13 by 17 km volcano-tectonic structure filled by an intra-caldera lake (Mann et al., 2004), recently interpreted as a strike-slip caldera by Saxby et al. (2016). The IC belongs to the San Salvador Extensional Step-over in the central part of the country (SSES; Fig. 1b; Garibaldi et al., 2016), which is in turn part of the El Salvador Fault Zone-ESFZ (Montero and Dewey, 1982; Siebert and Simkin, 2002; LaFemina et al., 2009; Corti et al., 2005; Turner Henry et al., 2007). The IC was formed and shaped by various eruptions, and older (pre-57 ka) pyroclastic deposits are related to previous caldera collapse episodes (Lexa et al., 2011; Aguirre-Díaz et al., 2017; Suñe-Puchol et al., 2019a, 2019b). There are only a few publications that detail the eruptions in the last 57 ka, i.e. the TB4, TB3 and TB2 eruptions (Rose et al., 1999; Kutterolf et al., 2008a, 2008b; Hernández, 2004; Hernández et al., 2012; Mann et al., 2004) and some recent studies have been carried out on the pre-57 ka

* Corresponding author.
E-mail address: dpedrazzi@ictja.csic.es (D. Pedrazzi).

https://doi.org/10.1016/j.jvolgeores.2019.03.006
0377-0273/

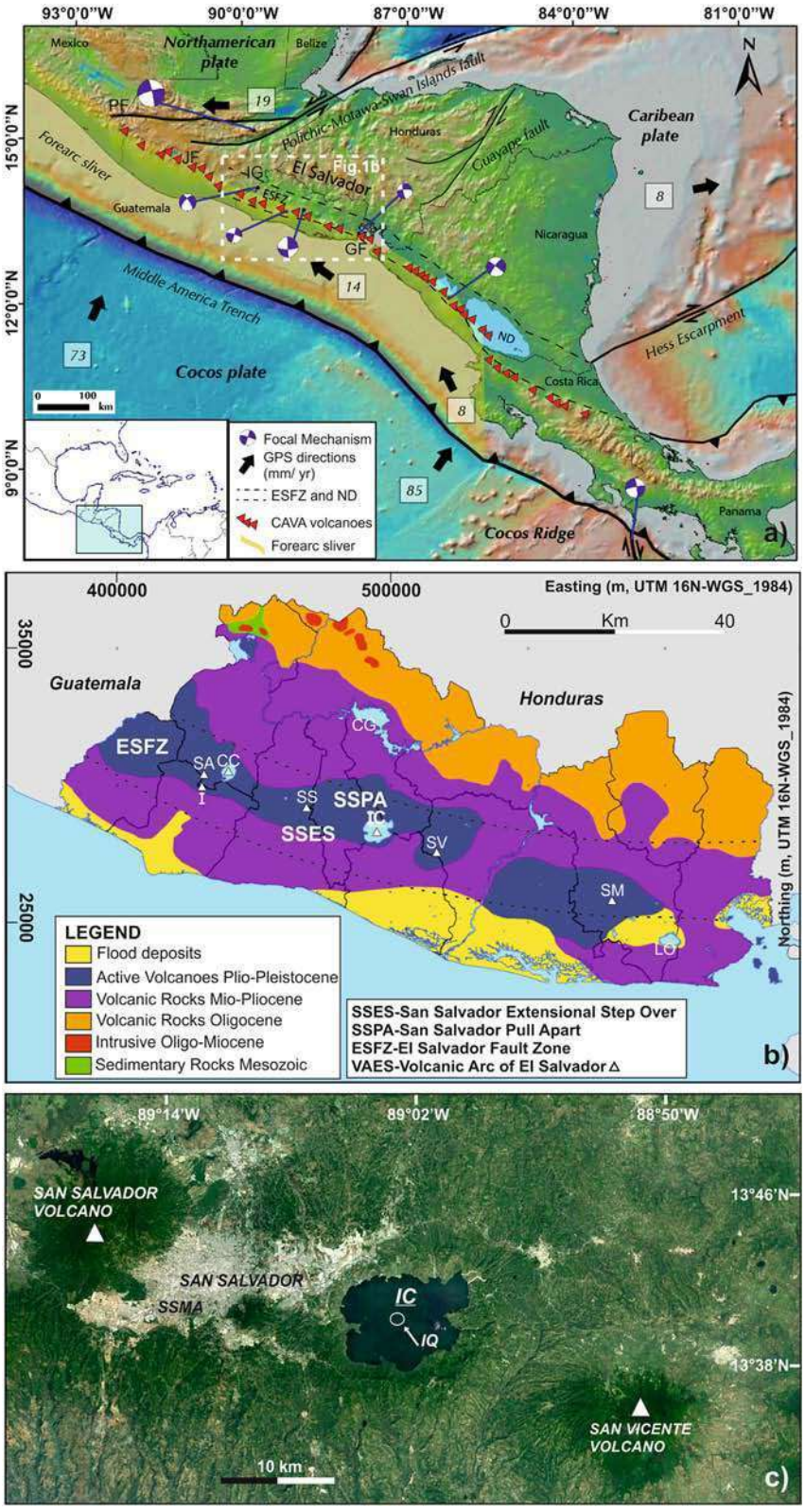

Fig. 1. a) Geological setting of northern Central America; ESFZ: El Salvador Fault Zone; GF: Gulf of Fonseca; IG: Ipala Graben; JF: Jalpatagua Fault; ND: Nicaraguan Depression; PF: Polochic fault; b) simplified geological map showing all the major geological formations of El Salvador (Hernández, 2004). CC: Coatepeque Caldera; CG: Cerrón Grande dump; I: Izalco Volcano; IC: Ilopango Caldera; LO: Laguna Olomega; SA: Santa Ana Volcano; SM: San Miguel Volcano; SS: San Salvador Volcano; SV: San Vicente Volcano; c) Google Earth image of Ilopango caldera (IC) (US Depth of State Geographer 2018); SSMA: San Salvador Metropolitan area; IQ: Islas Quemadas.

ignimbrites of Ilopango (Hernández, 2004; Hernández et al., 2010; Lexa et al., 2011; Aguirre-Díaz et al., 2017; Suñe-Puchol et al., 2019a, 2019b). More studies focused respectively on the eruption of a dacitic dome that formed the Islas Quemadas in Ilopango Lake (IQ; Fig. 1c) in 1879 (Richer et al., 2004), and a subaquatic eruption in this lake (Mann et al., 2004).

The last large explosive eruption of Ilopango volcano was the TBJ (*Tierra Blanca Joven* – white young earth), which is estimated to have erupted ~30 km³ DRE of magma about 1.5 ka years ago, between AD270 and AD535 (Dull et al., 2001, 2010). The TBJ was a cataclysmic eruption (Rolo et al., 2004) and is considered to be the largest in Central America since the ca. 84 ka Los Chocoyos-Guatemala eruption (Dull et al., 2010). Outside of the zone of devastation by the TBJ eruption, there was a much larger area of prolonged depopulation (10-150 years) following the TBJ eruption (Dull et al., 2001).

Presently, the area around IC is densely populated with about 3,000,000 people living within 30 km of the caldera. The population density during most of the late Holocene in El Salvador has been the greatest of any mainland country in the Americas (Daugherty, 1969; Denevan, 1992; Lovell and Lutz, 1995; Wilkie and Guadalupe Ortega, 1997). Since the last eruption was in AD1879, IC is still considered active and, it poses a major risk for El Salvador and neighbouring countries. In order to contribute to the hazard assessment at IC, we conducted a detailed field mapping to further investigate the TBJ deposits with the aim of building on the previous work and accurately reconstructing the eruption sequence.

There have been several publications about the TBJ eruption deposits. They were first documented by Williams and Meyer-Abich (1955) and called "white earth" due to their peculiar white colour, although they were thought to originate from San Salvador Volcano. Further studies of IC deposits were carried out by the German Geological Mission (MGA) whilst they completed the 1:500,000 scale El Salvador Geological Map (Weber et al., 1974). They defined IC and divided the proximal deposits into Units s4 (TBJ deposits) and s3'a (TB4, TB3 and TB2 eruptions) as part of the San Salvador Formation. Later, Hart (1981) worked on the detailed stratigraphy of the TBJ deposits and identified two important eruptive stages; T1 and T2, whose products are subdivided into six units and associated with different eruptive phases. Subsequently, Hart and Steen-McIntyre (1983) described the stratigraphy and distribution of the TBJ tephra and Vallance and Houghton (1998) revised the stratigraphy of Hart and Steen-McIntyre (1983) and labelled the stratigraphic units, characterizing them lithologically and refining associated eruptive processes. Recent works on TBJ by Hernández (2004) identified new ignimbrites (Alpha, Beta, and Grey) and detailed the characteristics of each unit in more detail.

Despite all this studies, a detailed stratigraphic survey including mapping and reconstruction of eruptive dynamics was still lacking. This study presents new field descriptions, petrographic observations, major element glass geochemistry, granulometric data for the TBJ deposits, and uses these data to further understand transport/depositional mechanisms and the corresponding eruption dynamics of the TBJ eruption. Moreover, the physical parameters of the eruption were determined, including the total erupted mass, the height of the eruptive columns, the emission rate and, above all, reconstruct the distribution of the TBJ deposit using models and field observations. In particular, the stratigraphic and granulometric data obtained in the field were used to model the distribution of the TBJ tephra, including the dispersion of the finest ash that covered vast areas (thousands of km²).

2. Geological setting

2.1. Central America and El Salvador geodynamic and geology

El Salvador is located in North Central America, on the Pacific margin of the Caribbean Plate (Fig. 1a). To the north, this plate interacts with the North American plate with a relative velocity between plates of 19 mm/year (DeMets et al., 2000; Guzmán-Speziale et al., 2005; Funk and Mann, 2009). Towards the west of El Salvador, the relatively young Cocos Plate (b25 Ma; Protti et al., 1995; Barckhausen et al., 2001) subducts towards the NE under the Caribbean plate along the Middle America Trench, at a speed of 73-85 mm/year (Dixon, 1993; DeMets, 2001).

The highest rate of continental tectonic deformation in El Salvador occurs in the El Salvador Fault Zone (ESFZ), a narrow E-W zone of right lateral faulting connected by pull-aparts, that extends for N150 km (Martínez-Díaz et al., 2004; Fig. 1a) from Guatemala, where it is known as the Jalpatagua Fault (JF), to the Nicaragua Depression (ND) (Canora et al., 2012). These faults are sub-parallel and affect volcanic products of Pleistocene-Holocene age (Corti et al., 2005). Geological and seismological analyses suggest that ESFZ is not laterally continuous and it has been subdivided into different sections (Martínez-Díaz et al., 2004; Corti et al., 2005).

The chain of volcanoes along the Central American Volcanic Arc (CAVA; Fig. 1a) has been developing since the Tertiary (DeMets, 2001; Mann, 2007; Carr et al., 2007) and is part of the Pacific Ring of Fire (Simkin and Siebert, 1994; Carr et al., 2007; Saxby et al., 2016). The CAVA extends for N1000 km from the southeast of Mexico to the central valley of Costa Rica and defines an abrupt continental volcanic front located between 165 and 190 km from the Middle America Trench (Fig. 1a). Volcanoes of Panama are excluded from the CAVA as they are associated with the subduction of the Nazca Plate below the Caribbean, which makes them distinct in composition and activity relative to those in the CAVA (Carr et al., 2007).

Volcanism of the Volcanic Arc of El Salvador (VAES) constitutes one of the most active segments of the CAVA. VAES includes 21 active volcanoes, three of which have erupted in the last century: Santa Ana-SA, Izalco-I, San Salvador-SS and San Miguel-SM (Fig. 1b; Siebert and Simkin, 2002). Deposits from these volcanoes, together with volcanic rocks of ages ranging from the Cenozoic to the present, constitute most of the geology of El Salvador (Fig. 1b)

2.2. Ilopango caldera

The IC (Fig. 1c) is located b10 km from San Salvador City and it forms part of the same eruptive lineament as the San Salvador and San Vicente volcanoes (Fig. 1b). IC is located directly above faults in the San Salvador and San Vicente ESFZ segments within the San Salvador Pull-Apart (SSPA; Garibaldi et al., 2016), which is a tectonic structure-oriented NW-SE, with right trans-tensive dynamics, parallel to the Mesoamerican trench. The transforming faults of the graben/pull-apart seem to control the morphology of IC, its formation and its volcanic eruptions (Sofield, 2004; Suñe-Puchol et al., 2019a), as described for other Graben Calderas (Aguirre-Díaz, 2008). Several authors, in their study of volcanism in southern El Salvador, noticed that the IC was a volcanic-tectonic depression controlled by the faults of an ancient graben (Williams and Meyer-Abich, 1955; Golombek and Carr, 1978; Hutton and Reavy, 1992; Sofield, 2004; Aguirre-Díaz and Martí, 2015; Aguirre-Díaz et al., 2016, 2017). Recently, Saxby et al. (2016) interpreted IC as a strike-slip caldera. IC was the result of several collapses associated to large explosive ignimbrite-forming eruptions (Suñe-Puchol et al., 2019a, 2019b) as previously suggested by Williams and Meyer-Abich (1955). The topographic edge of IC has several semicircular bays (Fig. 1c), which are evidence for multiple collapse events (Lexa et al., 2011).

3. Methods

Field mapping was carried out over an area of about 20,000 km² across El Salvador to reconstruct the stratigraphy of the TBJ deposits and the stratigraphic relationships with other eruptive deposits. The characteristics of the deposits were recorded including grading, colour, sorting, apparent component content (juvenile and lithic fragments), and primary sedimentary structures. The nomenclature used in this study for the bed thickness, grain size and sorting of the pyroclastic deposits follows that proposed by Sohn and Chough (1989). The classification of the primary volcaniclastic deposits follows White and Houghton (2006) and the nomenclature for volcanic stratigraphy is based on Martí et al. (2018), adopting the same criteria as Suñe-Puchol et al. (2019a, 2019b) for the previous Ilopango eruptions. A total of 82 stratigraphic sections were measured, but we focus here on 21 outcrops that we

consider representative of the whole succession, and its spatial variations and preservation of deposits.

The geographical coordinates of the locations, stratigraphic sections and sampling points were recorded using a portable Garmin Dakota-20 GPS (precision of ~3 m) and quoted on the UTM projection Datum: D_WGS_1984, zone 16 N. All this local information is reported in Supplementary Material 1. All the georeferenced data were managed and processed using the open source software Quantum GIS (Las Palmas; https://www.qgis.org/en/site/).

Thicknesses of the deposits and specific units were measured to create a database (see Supplementary Material 1) for tephra dispersal simulations (Macedonio et al., 2005). Tephra dispersal from virtual sources in an eruption column was simulated using the HAZMAP model, which solves equations for advection, diffusion and sedimentation of tephra particles in two dimensions (Macedonio et al., 2005). We followed an approach similar to Matthews et al. (2012) but used the Total Grain Size Distributions (TGSDs) (Bonadonna and Houghton, 2005) phases determined through the Voronoi Tessellation method, that we estimated for the different phases using data collected in this study. The granulometry data used to generate the TGSDs are available in Supplementary Material 2. Isopach maps were generated by modelling the ash deposition in terms of mass loading (kg/m^2) and these were converted into thicknesses using a bulk density of 1000 kg/m^3. In addition to the volumes, the solution of the inverse problem (Costa et al., 2009; Matthews et al., 2012) allowed us to estimate column heights, from which, by using the results of Mastin et al. (2009) and Bonadonna and Costa (2013), we assessed the corresponding Mass Eruption Rates (MER) for each unit. The volume estimations of the PDCs units were determined using the Delaunay triangulation method (Macedonio and Pareschi, 1991) that is particularly suitable for the reconstruction of volume between geological horizons and the interpolation of bivariate data, when function values are available at irregularly-spaced data points, as in the case of geological outcrops.

A binocular microscope was used to determine the main petrographic and textural characteristics of the juvenile components. In addition, petrographic analyses were carried out in order to identify the mineralogy and general composition of the studied deposits. Thin sections were produced at Wagner Petrographic LLC, a professional company of Lindon, Utah (USA).

Granulometric analyses were performed at the MARN (Ministerio de Medio Ambiente y Recursos Naturales) facilities of El Salvador Government and the Physical Volcanology Laboratory of Centro de Geociencias, Universidad Nacional Autonoma de Mexico (UNAM) in Juriquilla-Querétaro (Mexico). Representative levels of each stratigraphic unit were sampled and analysed (141 samples in total; Fig. 2 and Supplementary material 2) for grain-size distribution and componentry. Grain-size analysis were performed by dry sieving at 1 phi (Φ) intervals through sieves with aperture sizes ranging from 64 to 0.25 mm (−6 Φ to 3 Φ, where $\Phi = -\log_2 d$ with d is the diameter in mm) and by wet sieving through a MicroTec Analisette22 Fritsch from 0.125 mm to Þ0.01 mm (4 Φ to Ñ10 Φ). The weight percentages of the sieved fractions were calculated and then plotted as cumulative curves to give grain-size distribution. All data from grain-size analysis are reported in Supplementary Materials 2, 3 and 4. The proportion of juveniles from −5 Φ to 0 Φ was defined by hand picking and from 0 Φ to 2 Φ using a binocular microscope and image analysis techniques (e.g. ImageJ software; https://imagej.nih.gov/ij/). This point-counting method allows identifying the different components of each particle-size class using binocular microscope pictures. Modal proportions of juvenile pumice and accidental lithic fragments are reported in Supplementary Material 5.

Whole rock pumice geochemical analyses for major elements, trace and rare earth-elements (REE) (Table 2) were measured at the CGEO LEI laboratory (trace and REE, with an ICP-MS) and at Instituto de Geología of UNAM (major and trace elements, X *RIGAKU ZSX Primus II* spectrometer), following standard sample preparation and analytical techniques (Bernal and Lozano-Santacruz, 2005).

Electron probe X-ray microanalysis for mineralogy was performed using a JEOL JXA-8230 electron microprobe at the Scientific and Technological Centers (Universitat de Barcelona). Wavelength-dispersive analyses of silicates were conducted using a 20 kV accelerating voltage and 15 nA current and with a focused beam. Glasses were analysed using a 6 nA current with a defocused 5-10 μm spot. Counting times were 10 s peak and 10 s background. A range of natural and synthetic standards was used for calibration. The correction model XPP was used to convert X-ray intensity ratios into concentrations. Data are included in Supplementary Material 6.

The major element compositions of the matrix glass of the TBJ were determined using wavelength-dispersive electron probe microanalysis (EPMA) in the Research Laboratory for Archaeology and the History of Art (RLAHA) at the University of Oxford. Analyses were carried out on samples from all units, A to G, and distal deposits located up to 130 km from the caldera. The EPMA of the TBJ glasses were acquired using an accelerating voltage of 15 kV, beam current of 6 nA, and 10-μm-diameter beam. The count times on peak were: 30 s for Si, Al, Fe, Ca, K and Ti; 50 s for Cl and Mn; 60 s for P; and 12 s for Na, and background counts were collected for the same amount of time but split to positions either side of the peak. The PAP absorption correction method was used for quantification and the oxide compositions quoted assume stoichiometry. The electron probe was calibrated for each element using well-characterized mineral standards, which was verified by analysing MPI-DING reference glasses (Jochum Klaus et al., 2006). These MPI-DING glasses were used as secondary standards during each analytical run, and this data is included in the Supplementary Material 7 as they demonstrate the accuracy and precision of the TBJ datasets. All the glass analyses presented have been normalized to 100% to account for variable hydration and allow different samples to be compared, and all the raw compositional data can be accessed in Table 3.

4. Characteristics of the pyroclastic succession

Proximal TBJ member products (0-10 km from the caldera) are exposed inside and close to the caldera with a maximum observed thickness of ~60 m (Supplementary Material 1). The TBJ member can be divided in 8 units that were labelled alphabetically from base to top (A_0-G; Fig. 2). Due to differences in dispersal patterns, lateral facies variations and surface erosion, the complete stratigraphy was reconstructed from a large number of individual outcrops. Simplified stratigraphic logs of 21 localities are shown in Fig. 2. The TBJ member consists of initial pumice lapilli-supported grain deposits and later of several units made of a coarse and fine ash, matrix-supported massive deposits with pumice lapilli and lithics interbedded with laminated levels of lapilli (i.e. ILO 18 and ILO22; Fig. 2). All these deposits were mapped across several dozens of km from the caldera rim. The medial succession can be observed up to 30-40 km from the caldera rim, where the best exposures are found on the southern slopes of IC (i.e. ILO 8 and ILO130; Fig. 2). The last unit, which comprises massive fine-grained deposits, is observed in medial exposures and distal ones that are Ñ100 km from the caldera (i.e. ILO289 and ILO302; Fig. 2). Deposits from the TBJ eruption are characterized as being white soft and easily erodible, generating "badlands" type scarps (Šebesta, 2007). Most of the San Salvador Metropolitan Area (Fig. 1c) has been built on the TBJ tephra deposits.

4.1. Unit A_0

A_0 is the first unit in the TBJ succession of deposits (stratigraphic log 22 in Fig. 2), which is observed in medial (10–40 km from the vent) outcrops mainly to the south of the caldera. Thickness ranges from 2 to 4 cm (Supplementary Material 1) and the deposits are characterized by poorly-sorted, thinly bedded or laminated, moist beds of rounded dense, glassy coarse and fine pumice ash with accidental lithic fragments. The deposit usually rests directly upon a paleosol or older,

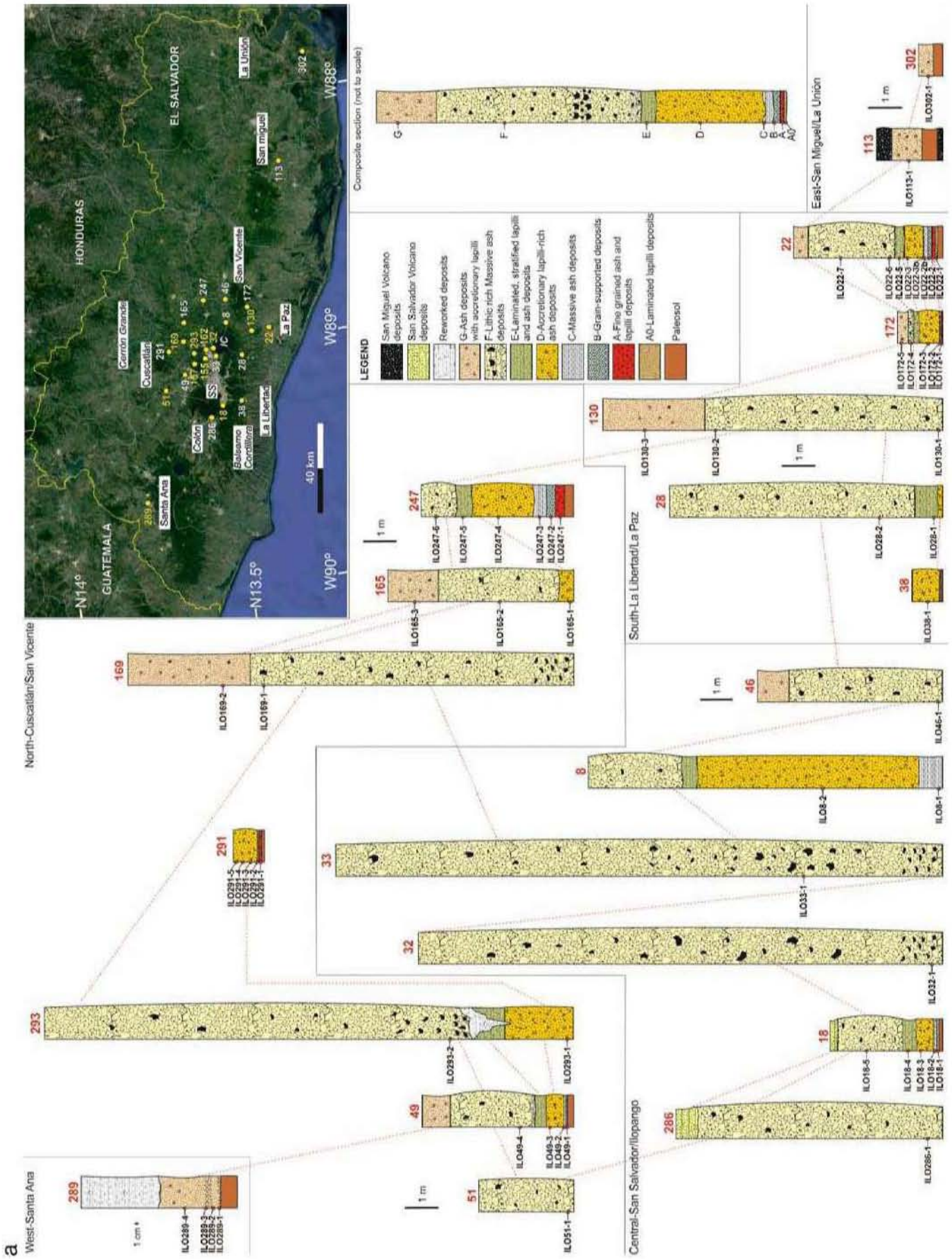
a
West-Santa Ana
North-Cuscatlán/San Vicente
South-La Libertad/La Paz
East-San Miguel/La Unión
Central-San Salvador/Ilopango
Composite section (not to scale)
LEGEND
San Miguel Volcano deposits
San Salvador Volcano deposits
Reworked deposits
G-Ash deposits with accretionary lapilli
F-Lithic rich Massive ash deposits
E-Laminated, stratified lapilli and ash deposits
D-Accretionary lapilli-rich ash deposits
C-Massive ash deposits
B-Grain-supported deposits
A-Fine grained ash and lapilli deposits
A0-Laminated lapilli deposits
Paleosol
HONDURAS
EL SALVADOR
GUATEMALA
Santa Ana
Cuscatlán
Cerron Grande
San Vicente
La Paz
La Libertad
Balsamo Cordillera
Colón
San miguel
La Unión
40 km
W90°
W89°
W88°
N14°
N13.5°

b

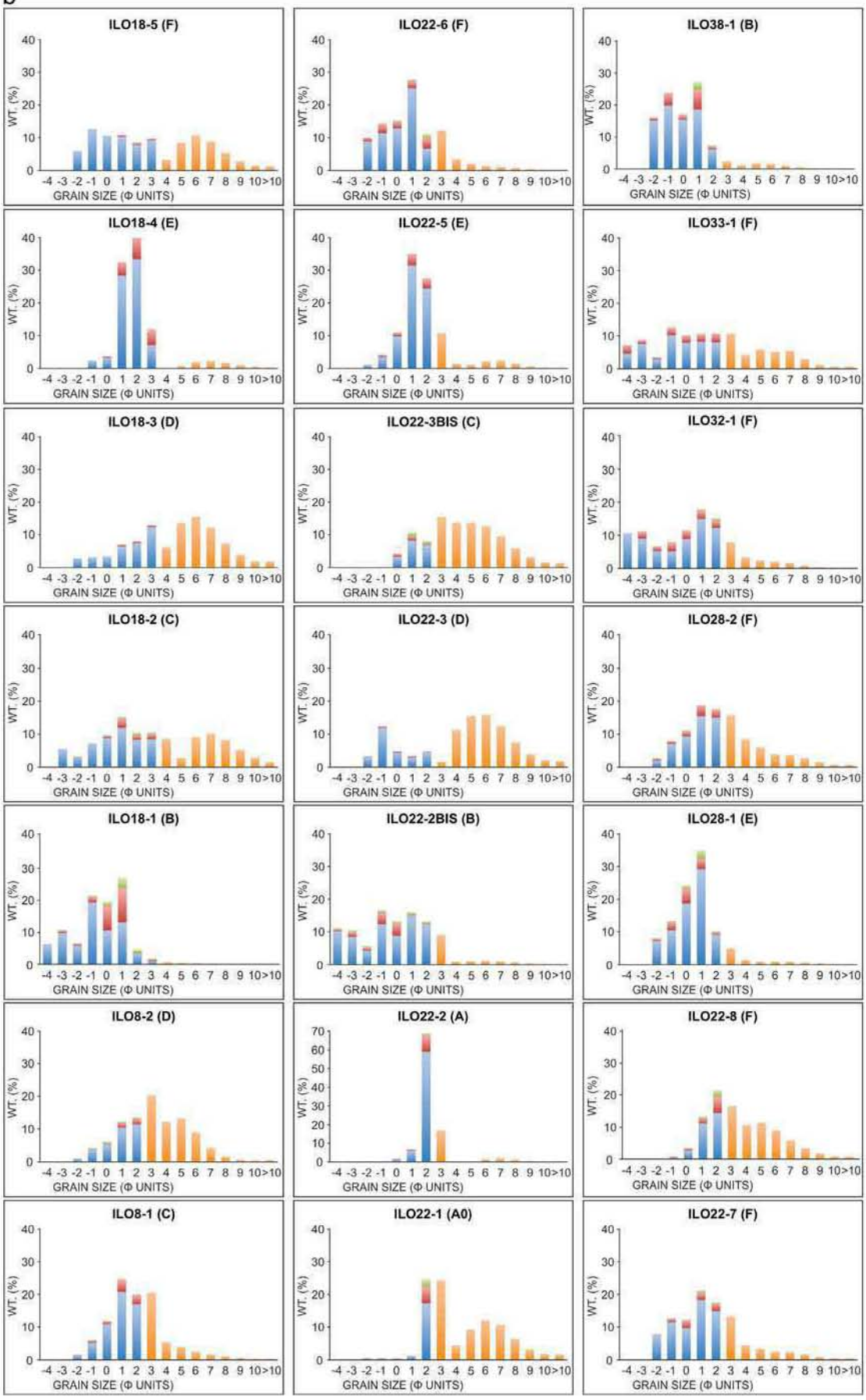
ILO18-5 (F)
ILO22-6 (F)
ILO38-1 (B)
ILO18-4 (E)
ILO22-5 (E)
ILO33-1 (F)
ILO18-3 (D)
ILO22-3BIS (C)
ILO32-1 (F)
ILO18-2 (C)
ILO22-3 (D)
ILO28-2 (F)
ILO18-1 (B)
ILO22-2BIS (B)
ILO28-1 (E)
ILO8-2 (D)
ILO22-2 (A)
ILO22-8 (F)
ILO8-1 (C)
ILO22-1 (A0)
ILO22-7 (F)
WT. (%)
GRAIN SIZE (Φ UNITS)
-4 -3 -2 -1 0 1 2 3 4 5 6 7 8 9 10>10

C

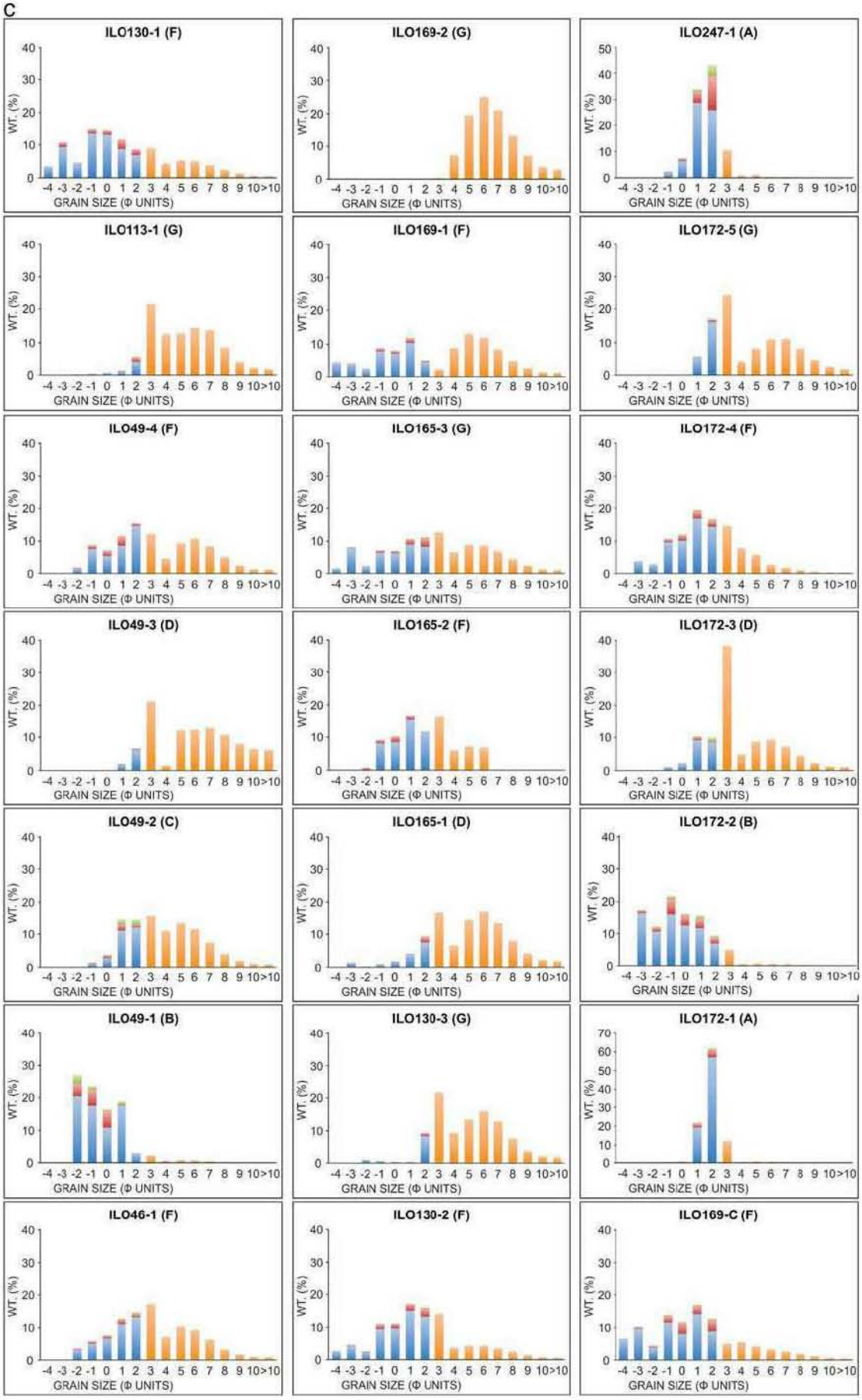
ILO130-1 (F)
ILO169-2 (G)
ILO247-1 (A)
ILO113-1 (G)
ILO169-1 (F)
ILO172-5 (G)
ILO49-4 (F)
ILO165-3 (G)
ILO172-4 (F)
ILO49-3 (D)
ILO165-2 (F)
ILO172-3 (D)
ILO49-2 (C)
ILO165-1 (D)
ILO172-2 (B)
ILO49-1 (B)
ILO130-3 (G)
ILO172-1 (A)
ILO46-1 (F)
ILO130-2 (F)
ILO169-C (F)
WT. (%)
GRAIN SIZE (Φ UNITS)
-4 -3 -2 -1 0 1 2 3 4 5 6 7 8 9 10>10

d

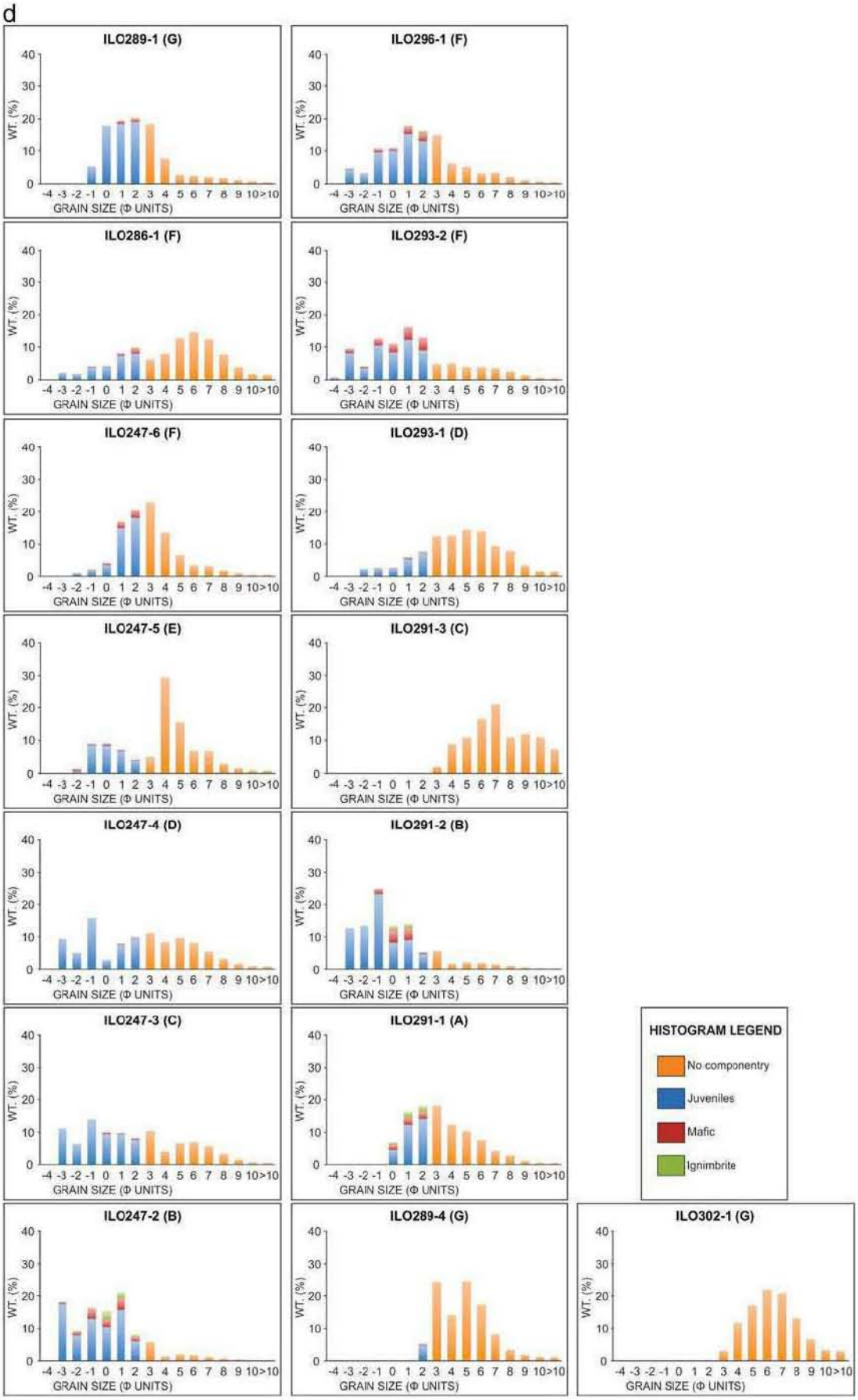
ILO289-1 (G)
ILO296-1 (F)
ILO286-1 (F)
ILO293-2 (F)
ILO247-6 (F)
ILO293-1 (D)
ILO247-5 (E)
ILO291-3 (C)
ILO247-4 (D)
ILO291-2 (B)
ILO247-3 (C)
ILO291-1 (A)
ILO247-2 (B)
ILO289-4 (G)
ILO302-1 (G)
WT. (%)
GRAIN SIZE (Φ UNITS)
-4 -3 -2 -1 0 1 2 3 4 5 6 7 8 9 10>10
HISTOGRAM LEGEND
No componentry
Juveniles
Mafic
Ignimbrite

weathered pre-caldera lavas. At the outcrop scale, there are lateral variations in the thickness and number of beds, with pinch and swell structures and locally erosive basal contacts (Fig. 3a,b).

4.2. Unit A

Unit A (stratigraphic logs 22, 172, 247, 291 in Fig. 2) outcrops in different points around IC, but mainly in the eastern and southern sectors at medial locations. It shows thicknesses from 3 to 14 cm (Supplementary Material 1) and is characterized by massive well-sorted thin to medium coarse angular pumice ash beds (Fig. 3a,b) with ash-sized lithic fragments. A planar contact separates it from the underlying Unit A_0.

4.3. Unit B

Unit B (stratigraphic logs 18, 22, 38, 49, 172, 247, 291 in Fig. 2) is characterized by moderately sorted, massive thin beds of angular pumice lapilli and lithics with no ash (Fig. 3c). Thicknesses vary from 1 to ~5 cm (Supplementary Material 1). This deposit shows sometimes yellowish colour due to the pigmentation and cementing of iron oxides by contact with the underlying paleosol. It appears in several outcrops at proximal and medial locations.

4.4. Unit C

Unit C (stratigraphic logs 8, 18, 22, 49, 247 in Fig. 2) is only preserved at a few outcrops in proximal and medial locations. It has a peculiar grey-yellowish colour (Fig. 3a) and is a well-sorted, matrix-supported deposit with light stratification of pumice fragments with scattered accretionary lapilli and hydrothermally altered lithics. Observed thicknesses range from a few cm up to 10 m in some depressions (Supplementary Material 1).

4.5. Unit D

Well-sorted, massive, lithic-poor ash rich deposit (Fig. 3d). Unit D outcrops at proximal and medial locations (stratigraphic log 8, 18, 22, 28, 38, 49, 172, 247, 291, 293 in Fig. 2). The intermediate and distal (N40 km from the caldera) facies of this unit are quite unconsolidated with a fine ash matrix and dispersed pumice juvenile fragments (Fig. 3ei) and with slight variations between one horizon and another. At proximal locations the deposits are more cemented with a coarse ash matrix and containing beds that show a strong enrichment of millimetric accretionary lapilli (Fig. 3eii). At some outcrops, the deposit shows planar stratification. The maximum measured thickness of the Unit D is about 8 m (Supplementary Material1).

4.6. Unit E

Unit E consists of doublets of thin to medium thick massive and laminated beds of rounded lapilli and coarse ash pumice (Fig. 3d,f). The unit outcrops at proximal and medial locations from the caldera (stratigraphic logs 8, 18, 22, 28, 49, 172, 247, 293 in Fig. 2). It represents a good stratigraphic marker of the TBJ eruption and to differentiate between Units D and F (Fig. 3d). The massive deposits are light coloured and composed of unconsolidated thick ash with pumice thin lapilli and lithics. The laminated deposits constitute very fine, well-sorted ash, that is light brown and dark brown when wet. It is commonly quite consolidated and rich in glass fragments and crystals. Locally, these deposits show folding that is characteristic of soft sediments (Fig. 3g). The maximum measured thickness is 1 m (Supplementary Material 1).

4.7. Unit F

Unit F is composed of chaotic, massive, poorly-sorted, non-welded, light-coloured to light beige (Fig. 3d) with thickness up to about 60-70 m thick (Supplementary Material 1). Unit F outcrops at both proximal and medial locations (stratigraphic logs 8, 18, 22, 28, 32, 33, 46, 49, 51, 130, 165, 169, 172, 247, 286, 293 in Fig. 2) and found up to 40 km from the caldera. To the north, the deposits extend away from the caldera for at least ~35 km and outcrop close to Cerrón Grande (Fig. 2). To the west, deposits cover part of San Salvador Volcano (Fig. 2), reaching a maximum height of 930 m (1,740 m a.s.l.). Deposits were also found close to the Municipality of Colón (Fig. 2), where they achieve a distance of ~40 km. Towards the southern part (Balsamo Cordillera; Fig. 2), deposits outcrop along the old channels of rivers and streams reaching distances of N30 km. East of IC, Unit F was recognized up to 30-35 km away, close to the San Vicente Volcano (Fig. 2). The deposits in the proximal outcrops show a coarse ash matrix with abundant centimeter- and decimeter-sized pumice and lithic fragments (Fig. 3h,i). Visibly mingled pumice with dark to light grey bands within the white pumice are found in unit F at very proximal sites within the caldera, e.g. ILO-32 (Fig. 3h). The abundance of mingled clasts at this site is ~5–10% and the clasts range from around 5 to 20 cm in length.

Some decimeter-sized lithic-rich beds are observed close to the caldera edge (Fig. 3j). Medial outcrops show the same massive, lithic-rich deposits with a fine ash matrix, and lithic and juvenile pumice up to few centimetres in size (Fig. 3k). Most of the outcrops show a lower layer with higher particle concentrations. Degassing pipes are seen in this unit at some outcrops (Fig. 3l). In some cases, Unit F is found directly above Unit D or with a reworked lower part (Fig. 3m).

4.8. Unit G

It is an unconsolidated, massive, well-sorted, coarse to fine ash deposit with millimeter-sized accretionary lapilli (Fig. 3n). In some outcrops, a slight stratification is observed, with a transitional contact with Unit F below. Deposits were described mainly at medial and distal outcrops (stratigraphic logs 22, 46, 49, 113, 130, 165, 169, 172, 289, 302 in Fig. 2) and found up to 100 km from the vent (Fig. 3o). Maximum measured thicknesses are ~6 m (Supplementary Material 1).

5. Physical paraTheters

5.1. Grain-size distribution

Data from Supplementary Material 3 was plotted in Supplementary Material 4 in order to show variation of TBJ grain-size at proximal (0-10 km), medial (10-40 km) and distal locations (N40 km) from IC. Data include Medium Diameter (MdΦ), Sorting (σΦ) and Skewness (αΦ) parameters (Supplementary Material 4a-f) as well as F1 [wt% b1 mm diameter (0Φ)] and F2 [wt% b1/16 mm diameter (4Φ)] (Supplementary Material 4 g-i). Granulometric data of the local distributions characterized up to phi 10 were used to reconstruct the Total Grain Size Distributions (Fig. 4).

Figures j-ac of Supplementary Material 4 illustrate the grain-size distribution of the TBJ samples depending on distance from the caldera. Both A_0 and A samples show a bimodal trend. Conversely, samples from Unit A are characterized by a unimodal trend. No proximal and distal samples were found for both Units A_0 and A. Only two samples from

Fig. 2. Stratigraphic logs of TBJ succession of deposits and their locations. Granulometric analysis and lithics content are shown as well. The TBJ eruption can be divided in 8 units from base to top; Units A_0 to G. Stratigraphic logs are arranged from west (left) to east (right) and from south to north, and cover most of the El Salvador. Inset figure show the locations respectively of samples and outcrops of Figs. 2 and 3.

Unit B were collected at proximal locations, and only one of the two samples shows a unimodal trend. Medial samples from Unit B seem no show a clear relationship between distance and grain size trend similarly to the only sample from a distal outcrop that only shows a slight shift to finer classes. Two samples from Unit C at proximal locations show a polymodal trend, similarly to the ones at medial outcrops.

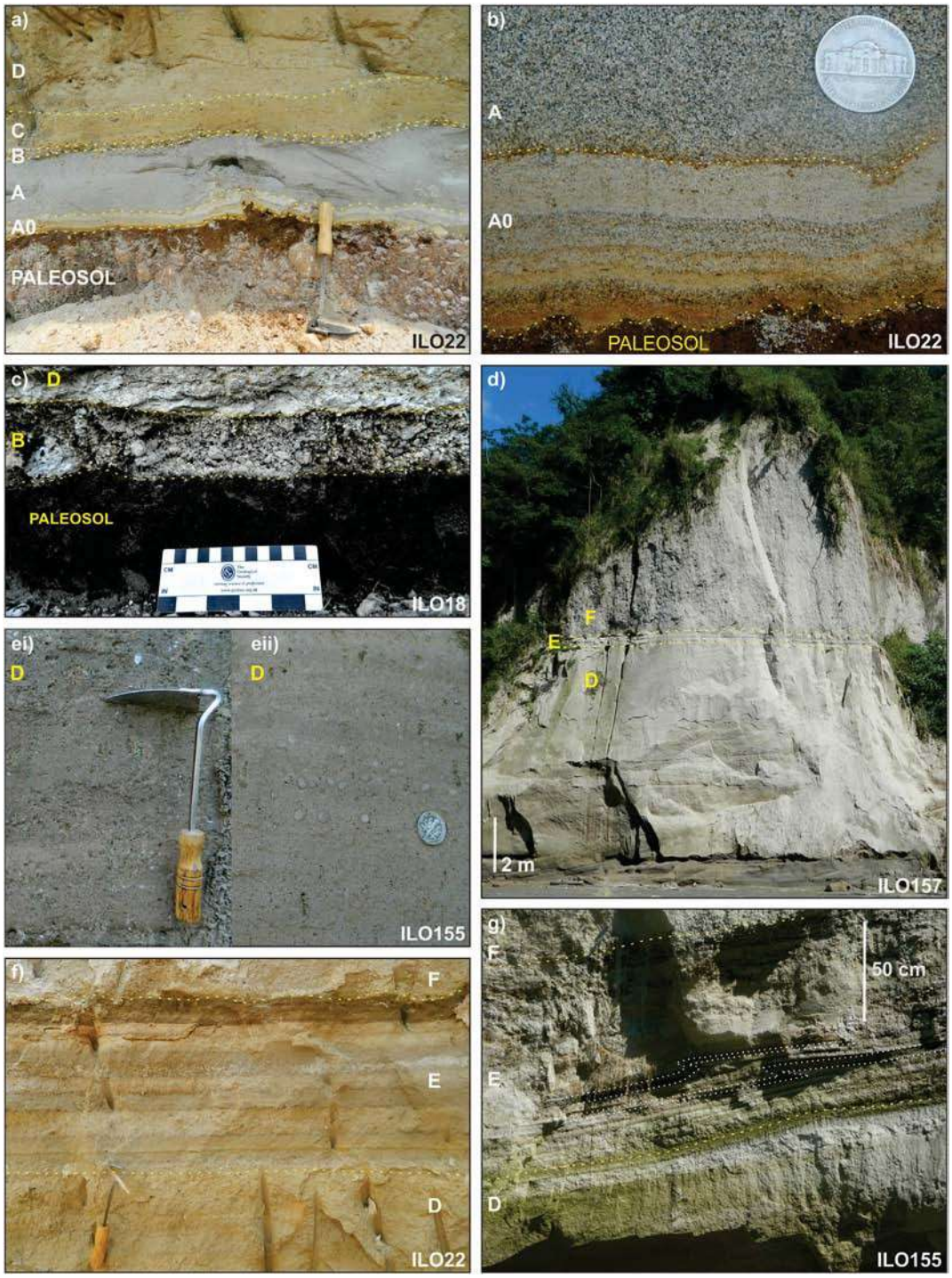

Fig. 3. Field photographs of the TBJ units with views of details. a) Units A_0-D resting on a paleosol, see the scraper for scale; b) features of Units A_0 and A: the former is characterized by poorly-sorted thinly, laminated beds of rounded pumice lapilli and coarse ash, and the latter by lithic-rich, massive, well-sorted thin to medium coarse angular pumice ash beds; c) Unit B, it shows massive thin beds of angular pumice lapilli with no ash; d) Units D, E, F. Unit D is an ash rich deposit whilst Unit F is characterized by a coarse ash matrix with abundant centimeter- and decimeter-size pumice and lithic fragments. Unit E has laminated beds; e) photographs of Unit D showing ei) ash matrix and dispersed pumice juvenile fragments with slight variations between one horizon and another and eii) strong enrichment of millimeter-size accretionary lapilli. Photographs of the characteristics feature of Unit E; f) doublets of thin to medium thick massive and laminated beds lapilli and coarse ash pumice; g) soft-sediments deformation structures: folding; Unit F with h) coarse ash matrix with abundant centimeter-size and decimeter-size pumice and lithic fragments at proximal outcrops, in the inset figure a mingled pumice is shown as well i) chaotic massive poorly-sorted, non-welded, light-coloured deposits; j) some decimeter-size lithic-rich levels; k) at distal outcrop; l) degassing pipes; m) reworked (RW) lower part of Unit F; n) Unit G, unconsolidated massive ash deposits with dispersed accretionary lapilli (AL); o) distal outcrops of Unit G reach thicknesses of 40-50 cm at Tazumal Archaeological Site (Chalchuapa). Outcrops numbers are shown in yellow in the inset in Fig. 2. Yellow dotted lines divide different units of the TBJ Member. White dotted lines outline details of the field picture. (For interpretation of the references to color in this figure legend, the reader is referred to the web version of this article.)

Fig. 3 (*continued*).

Only one sample was collected from distal outcrops showing a shift towards finer classes. However, unlike Unit C, samples from Unit D at proximal and medial outcrops have a clear polymodal trend. Therefore not a clear relationship between distance and grain size trend was observed for sample from this unit. Only one distal sample from Unit D indicates a shift towards finer classes similar to the samples from Unit C. Two proximal samples from Unit E show different tendencies with a unimodal trend but towards coarser and finer classes. The same is observed at medial distance. Only one distal outcrop from Unit E was found in the field. It shows a clear shift towards finer classes. Proximal and medial samples from Unit F show a polymodal trend with coarser classes being more representative. Distal samples from Unit F seem to show a slight bimodal trend without any substantial change in the granulometrical distribution. Only one sample from Unit G was collected at one proximal outcrop. Medial and distal samples from Unit G are characterized by a bimodal trend.

5.2. Componentry analysis

Componentry of individual beds is presented in Fig. 2 and Supplementary Material 5. The modal proportions of juvenile pumice and accidental lithic fragments (mafic clasts and pre-TBJ eruption ignimbrites)

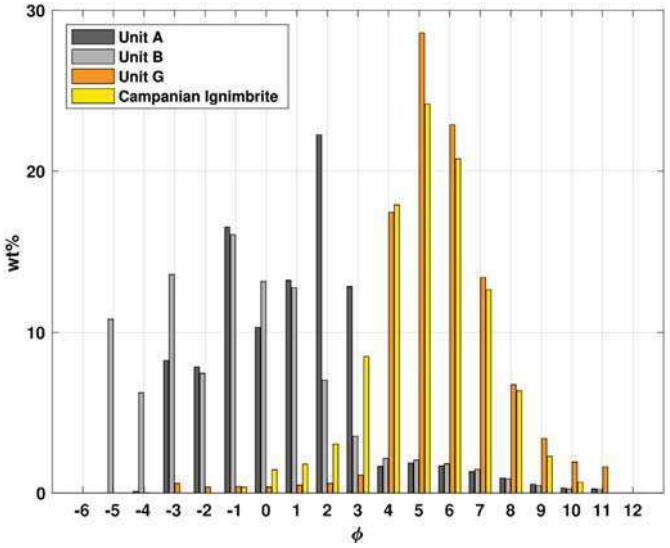

Fig. 4. Total Grain Size Distributions of fallout units (A, B and G). For the sake of comparison TGSDs associated to the co-ignimbrite phase of the Campanian Ignimbrite are also reported (Marti et al., 2016).

are given for each grain-size fraction (or class) until 2Φ and their distribution among grain-size fractions, as well as units is not constant. Unit A_0, which is only present at few scattered medial outcrops, has a lithic content of ~8–8.5%. The following Unit A shows variable values from ~10–11% up to ~22–23% at medial locations. Unit B, at medial locations, shows values between ~15 and ~19% up to 28%. At distal outcrops, lithics are ~12%. Unit C at proximal outcrops contains total lithic values of ~9%. Medial outcrops are characterized by lithic values of ~5–8.5%. Unit D shows a constant lithic content from proximal to distal outcrops with values ~1–4%. Unit E shows values comprised between ~8% and ~16% although several samples show a considerable decrease with only lithics of ~3%. Unit F at proximal outcrops shows values ~15% of lithics whilst at medial outcrops values are generally around 5–15%. Unit G is characterized by lithics values at medial and distal outcrops of ~1–3%.

5.3. Product distribution and volume of the different eruptive phases

The distribution of outcrops and the thickness data (reported in the Supplementary Material 1) from each unit is shown in Fig. 5. Combining these field observations and dispersal models for each phase, we estimate the corresponding mass of erupted material (in terms of DRE) and intensity (in terms of discharge rate).

Concerning the fallout units, which includes Units A and B from sustained eruption columns, and G from a co-ignimbrite plume, we computed the tephra transport and sedimentation by solving an inverse problem (Pfeiffer et al., 2005; Costa et al., 2009) using the tephra dispersal model Hazmap (Macedonio et al., 2005). The results are summarized in Table 1, where the Total Erupted Mass (TEM), the column height, maximum wind intensity, and other physical parameters are reported for the different units. Furthermore, for Unit A we estimated a TEM of ~3.5×10^{11} kg (i.e. 0.15 km^3 DRE assuming a constant magma density of 2300 kg/m^3), and an eruptive column height of ~29 km, corresponding MER of ~10^8 kg/s (Bonadonna and Costa, 2013). TEM for Unit B is of ~2×10^{12} kg (i.e. 0.8 km^3 DRE), with an eruptive column height of ~7 km, corresponding MER of ~10^5-10^6 kg/s (Bonadonna and Costa, 2013). For the fallout unit G from the co-ignimbrite column, we adopted a first order approach similar to Matthews et al. (2012). Results of the inverse problem for the co-ignimbrite phase suggest a TEM of ~4×10^{13} kg (i.e. 16 km^3 DRE) with a co-ignimbrite plume that reached a height of ~49 km (corresponding to a MER of ~10^{10} kg/s). For the co-ignimbrite plume the source of ash is not "point source" but rise from all the surface of ignimbrite sheet, which can have a radius N 30-50 km (Costa et al., 2018). For this reason, the validity of the tephra dispersal model, which assumes virtual sources along an eruption column, is not fully appropriate for points at distances smaller than 30-50 km and simulation results should be considered simply as model extrapolations. However, in our case most of the available outcrops were at larger distances (see Supplementary Material 1). The individual grain-size distributions of the samples of each unit at several locations (Fig. 2 and Supplementary Material 2) were used to generate the TGSDs (Total Grain Size Distributions) reported in Fig. 4. These TGSDs were estimated using the Voronoi tessellation method of Bonadonna and Houghton (2005). For the sake of comparison, the volumes of Units A, B, and G were also assessed by adopting empirical integrations of the deposit thinning (Bonadonna and Costa, 2012).

The dispersal of the different units as isopachs is shown in Fig. 5. From these maps, we can see that Units A (Fig. 5a) and B (Fig. 5b) were mainly dispersed to the west and west-south-west areas, respectively. In contrast, Unit G (Fig. 5g) was dispersed towards the south by weak winds.

Taking into account that PDC of Unit F had a runout distance of ~50 km (Fig. 5f), from the results of Costa et al. (2018) we can estimate a MER of order of 10^{10} kg/s, which is consistent with the value estimated for the co-ignimbrite phase (Unit G) on the basis of the height of the co-ignimbrite plume (see Table 1). The volume of PDC Units C, D, and F were calculated using the Delaunay triangulation method (Macedonio and Pareschi, 1991), which is, as mentioned in the Methods Section, suitable for assessing the volume between geological horizons from irregularly-spaced data points. We obtained the following volume estimations:

1. ~0.7 km^3 (i.e. ~0.5 km^3 DRE) for Unit C;
2. ~5.0 km^3 (i.e. ~3.3 km^3 DRE) for Unit D;
3. ~0.5 km^3 (i.e. ~0.3 km^3 DRE) for Unit E;
4. ~14 km^3 (i.e. ~9.1 km^3 DRE) for Unit F.

DRE volumes were calculated using an assumed deposit density of ~1500 kg/m^3 (Quane and Russell, 2005) and a magma density of 2300 kg/m^3. These volumes indicate that 30 km^3 of magma was ejected during the TBJ eruption.

6. Petrography, geocheThistry and glass coThpositions of the TBJ deposits

Pumice clasts from the TBJ units are moderately crystal-rich (up to 10–15%) and highly vesicular. Mineralogy assemblage consists of 70–75% euhedral to subhedral plagioclase (andesine and labradorite; Figs. 6a–d and Fig. 7a), about 20% of magnesio-hornblende (Figs. 6a,b, e,f and 7b), and 10 vol% of crystal content is made of pyroxene (Figs. 6g,h and 7c,d), Fe-Ti oxides and apatite. Plagioclase crystals often have sieve-textured cores and contain apatite inclusions, Fe-Ti oxides and clinopyroxene (Fig. 6a-d). The hornblende crystals (Fig. 6e, f) have pristine rims with abundant inclusions of apatite (Fig. 6a) and orthopyroxene.

Whole-rock compositions of the TBJ pumices are dacitic to rhyolitic (Fig. 8a and Table 2), and glass compositions are typically rhyolitic with the exception of mingled pumices found in the upper sequence (Unit F; see above) that extend to basalt (Fig. 8a). The glass compositions were determined for individual shards using an electron

Fig. 5. Distribution maps (in cm) of each unit of TBJ eruption: a) Unit A, b) Unit B, C) Unit C, d) Unit D, E) Unit E, F) Unit F, g) and gi) Unit G. Latitude and longitude are expressed in degreees. Thicknesses reported in Fig. c, d, e, f only refer to the main outcrops.

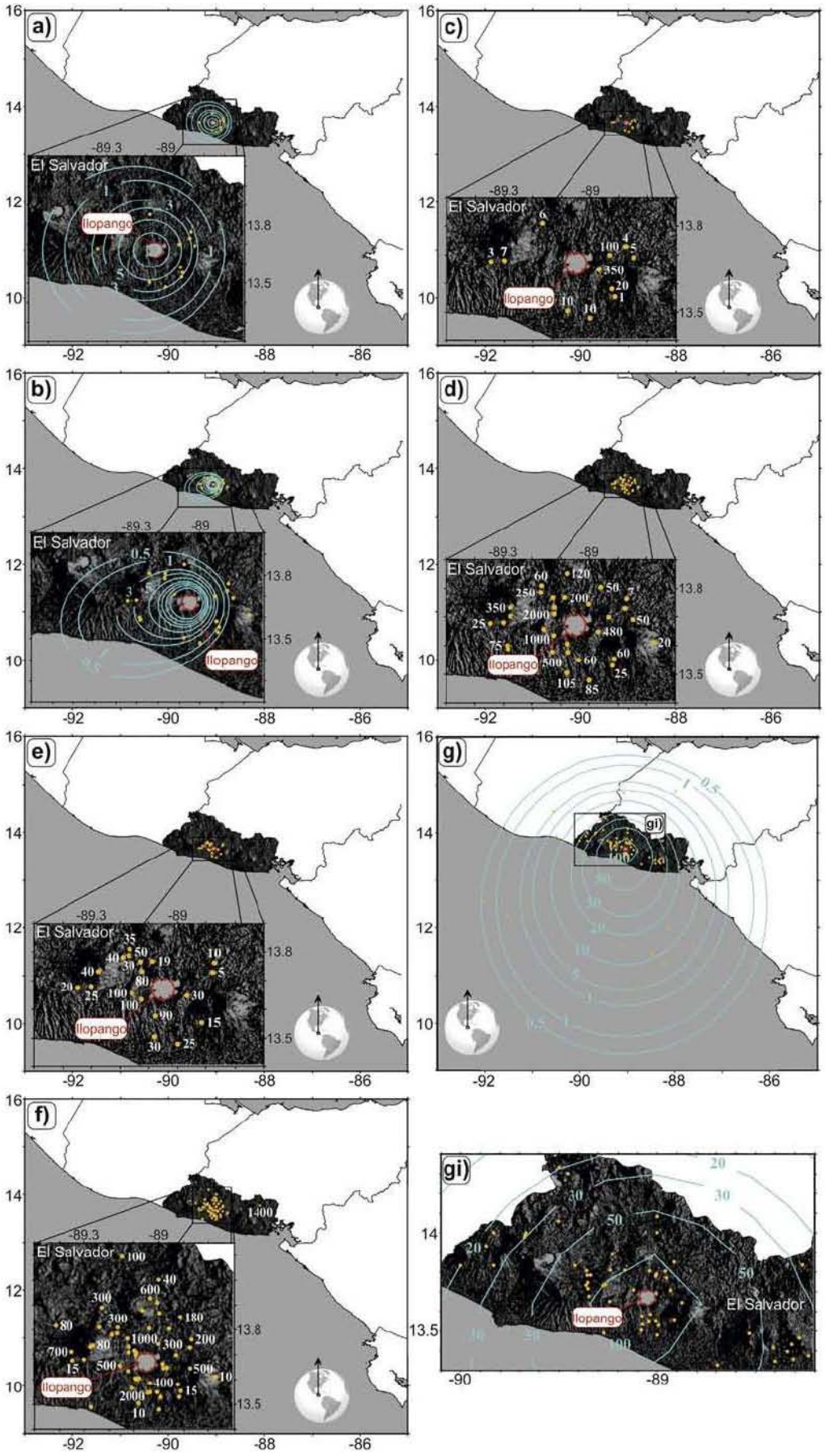
a)
b)
c)
d)
e)
f)
g)
gi)
El Salvador
Ilopango
-89.3
-89
13.8
13.5
16
14
12
10
-92
-90
-88
-86

Table 1
Summary of the physical parameters of the deposits from the TBJ eruption.

Physical parameters	Unit A0	Unit A	Unit B	Unit C	Unit D	Unit E	Unit F	Unit G	Total TBJ	
Bulk Volume (km^3)	<0.1	0.35	1.84	0.7	5	0.5	14	36.80	69.35	"+ caldera filling"
Total Erupted Mass (kg)	<0.1	3.5×10^{11}	2×10^{12}	1.2×10^{12}	8.2×10^{12}	0.7×10^{12}	2.3×10^{13}	4×10^{13}	7.5×10^{13}	"+ caldera filling"
DRE volume (km^3)	<0.1	0.15	0.8	0.5	3.3	0.3	9.1	16	30	"+ caldera filling"
Mass Eruption Rate (kg/s)	~10^9	~10^8	~ 10^5-10^6	~10^9	~10^9	~10^9	~10^{10}	~10^{10}	-	
Runout PDC (km)	20	-	-	25	25	20	50	-	-	
Column Height (km)	-	29	7	-	-	-	-	49	-	
Magnitude	-	-	-	-	-	-	-	-	6.8	

microprobe from samples through the entire succession of deposits, and from both proximal and distal sites. Excluding the rare mingled clasts in Unit F, other deposits display homogenous, rhyolitic major element compositions with SiO_2 = 75.3–78.1 wt%, Al_2O_3 = 11.9–13.8 wt%, Total FeO = 0.99-1.53 wt%, MgO = 0.12-0.33 wt%, CaO = 0.9-1.6 wt %, NaO_2 = 3.78-4.88 wt% and K_2O = 2.38-3.37 wt% (n = 239; Table 3; Fig. 8a–d). The darkest material within the mingled pumice is basaltic and ranges down to 48.63 wt% SiO_2, 7.91 wt% Al_2O_3, 12.42 wt % Total FeO, 12.03 wt% MgO, and 15.02 wt% CaO (Table 3; Fig. 8a-d). These grey bands are heterogenous in composition and extend from the least evolved composition to SiO_2 concentrations up to 68.5 wt%. The whole-rock XRF data plot between this dacitic composition and the dominant rhyolite (Fig. 8a–d).

7. Discussion

The volume of material erupted during the TBJ eruption was ~58 km^3 of bulk rock, equivalent to ~30 km^3 DRE of magma and corresponding to a magnitude of 6.8 (Pyle, 2000) (Table 1). Eight units can be identified in the deposits that provide evidence for distinct eruptive styles. The sedimentological and lithological characteristics of these deposits suggest that the TBJ eruption included phases associated with pure magmatic activity and those characterized by magma–water interaction, which are also seen in older intra-caldera deposits (Mann et al., 2004; Suñe-Puchol et al., 2019a, 2019b). Paleosols separate the TBJ from previous eruption deposits at several outcrops (Fig. 2). The repose period before the TBJ was of a sufficient length for this pedogenesis to occur, and the caldera was probably quiescent for around 8 ka, i.e. since TB2 (Kutterolf et al., 2008a, 2008b).

Unit A_0 (b0.1 km^3 total DRE volume - Table 1) represents the onset of the TBJ eruption. The field characteristics (Fig. 3a,b) and granulometric analysis (poorly sorted deposit, positive grain-size skewness values and a bimodal trend; Supplementary material 4b, e, j) suggest that this unit was deposited by dilute PDCs (Branney and Kokelaar, 2002; Dellino et al., 2004a, 2004b; Brand and White, 2007; Brand and Clarke, 2009). The high proportion of mafic lithic fragments is consistent with explosive excavation of the conduit and vent (Fig. 9a), as described in other studies e.g. Vesuvius, Italy (Barberi et al., 1989) and the AD1630 eruption of Furnas volcano, San Miguel, Azores (Cole et al., 1995). These surge clouds had a high momentum as they travelled at least up to 15-20 km from the vent. The deposits show similar field characteristics to the ones of the Layer LM1 from the Lower Member of the Neapolitan Yellow Tuff that represented the onset of the eruption (Orsi et al., 1992). Grain size and componentry (fine-grained deposits; Supplementary Material 4h and high mafic lithic content - Fig. 2), as well as ash deposits suggest that there was magma-water interaction (Self and Sparks, 1978; Barberi et al., 1989; Houghton and Schmincke, 1989; Houghton and Smith, 1993; Cole et al., 1995; Dellino and La Volpe, 1995; De Rita et al., 2002). The opening phases of volcanic eruptions present favourable conditions for magma-water interaction, similar to other case studies such as the Minoan, Santorini Island, Greece, AD79 Vesuvius, Italy (Cioni et al., 2000), Etna 122 BCE, Italy (Coltelli et al., 1998), and Tarawera AD1886, New Zealand (Houghton et al., 2004) eruptions.

The explosive eruptions that formed Unit A (Fig. 9b) produced an eruptive column that rose to 29 km (Table 1) and it spread mainly westwards in the proximal and medial area. Field evidence (Fig. 3a,b) and granulometric data (well-sorted deposit and a unimodal trend; Supplementary material 4b, e and k) of samples are consistent with a tephra fallout deposit (0.15 km^3 total DRE volume - Table 1). Unit A was most likely hydromagmatic, due to the high lithic content (Fig. 2) and fine grain size at medial locations (Supplementary Material 4h) and a distribution mainly to the south of the caldera (Fig. 5a). Passing from dilute PDCs of Unit A_0 to fallout deposits of Unit A is probably related to changes in magma-water mass ratio, which has been observed at several historical hydromagmatic eruptions, e.g. Kilauea volcano, Hawaii, AD1790 (McPhie et al., 1990) or Capelinhos (1957-1958) in Faial, Azores (Cole et al., 2001).

Concerning the first two phases (A_0 and A), the magma-water mass ratio promoted a more or less high explosive efficiency, from wet PDCs and fallout deposits towards drier lapilli fall (Unit B), so the magmatic fragmentation became progressively more dominant. Then, the eruption entered a magmatic fall-dominated phase (Fig. 9c) that formed Unit B (Fig. 3c), which is characterized by highly vesiculated juvenile products released through a ~7-km-high column (Table 1) with a grain-supported deposit mainly oriented southwestwards from the source (Fig. 5b). This eruption phase produced a coarse, generally medium sorted (Supplementary Material 4a,b,d,e), pumice fall deposit with a 0.22 km^3 total DRE volume (Table 1). General drier conditions can be related to any factors such as, for example, the variations in magma flux or availability of water in the system, or in some cases, some batches of magma can reach the surface without explosive interaction with water, similarly to maar-diatreme eruptions (Valentine and White, 2012). Similar activity was observed for the C11 deposits of Caldeira Volcano, Faial Island, Azores (Pimentel et al., 2015). The eruption was characterized at the beginning by a series of hydromagmatic eruptions with fallout and PDCs deposits and a subsequent more dominant magmatic fragmentation, due to the rapid draining of magma from the conduit, with the establishment of a sub-Plinian column. The increase in the dispersal area and grain size features in the deposits (Supplementary Material 4g, h, i, l, m, n) indicates steady growth of the eruption column. The column reached its climax without major fluctuations, as there are internal bedding features and the deposits lack normal or inverse grading. This was probably facilitated by the gradual stabilization of the conduit walls associated with increasing vent diameter and magma discharge rate.

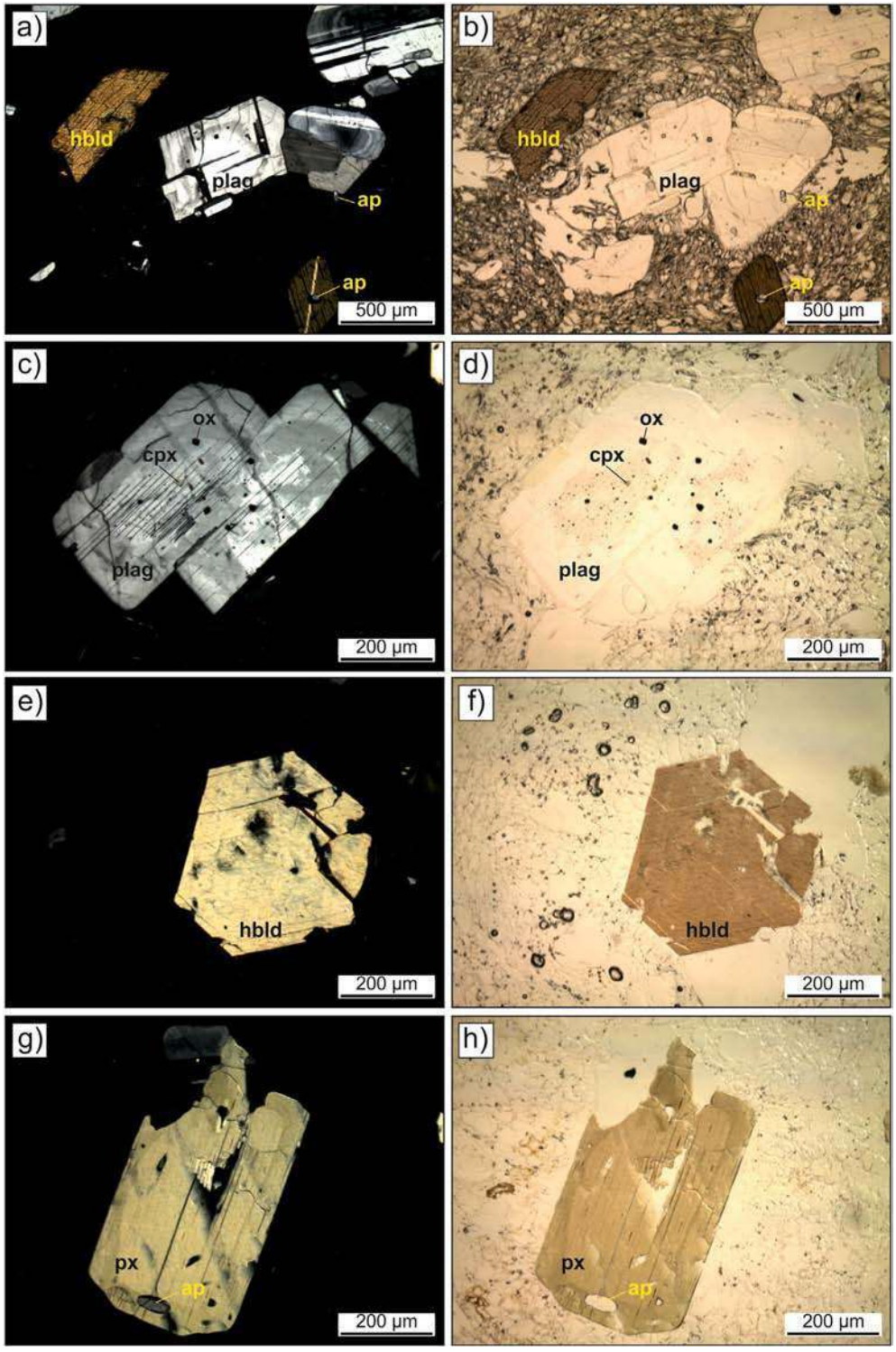

Fig. 6. Petrographic features of the TBJ eruption products: parallel and crossed polarized nichols: a) and b) mineralogy assemblage with euhedral to subhedral plagioclase and hornblende with apatite inclusions; c) and d) detailed picture of plagioclase with pyroxene and oxide inclusions; e) and f) euhedral hornblende; g) and h) subhedral pyroxene with apatite inclusions.

Unit C (0.5 km^3 total DRE volume - Table 1) represents an abrupt change in the eruption dynamics (Fig. 9d). This well-sorted (Supplementary Material 4a–c), massive, lithic-poor and ash-rich deposit (Supplementary Material 4d–f and g–i), with few dispersed pumice fragments and accretionary lapilli indicate deposition from PDCs (Fig. 3a) that flowed mainly to the south-east part of the IC (Fig. 5c). These dynamics were probably due to the shift of the vent location and a subsequent interaction of magma with external water that led to an enhanced magma fragmentation, as well as a greater explosivity of the eruption that contributed to the generation of fine ash (Supplementary Material 4o–q). The stratigraphic position of these hydromagmatic deposits immediately above the magmatic deposits suggests a subsequent access of the lake water to the column of rising magma. However, we cannot discount the role of hydrothermal and groundwater in the hydromagmatic episode that lead to the emplacement of Unit C. The presence of

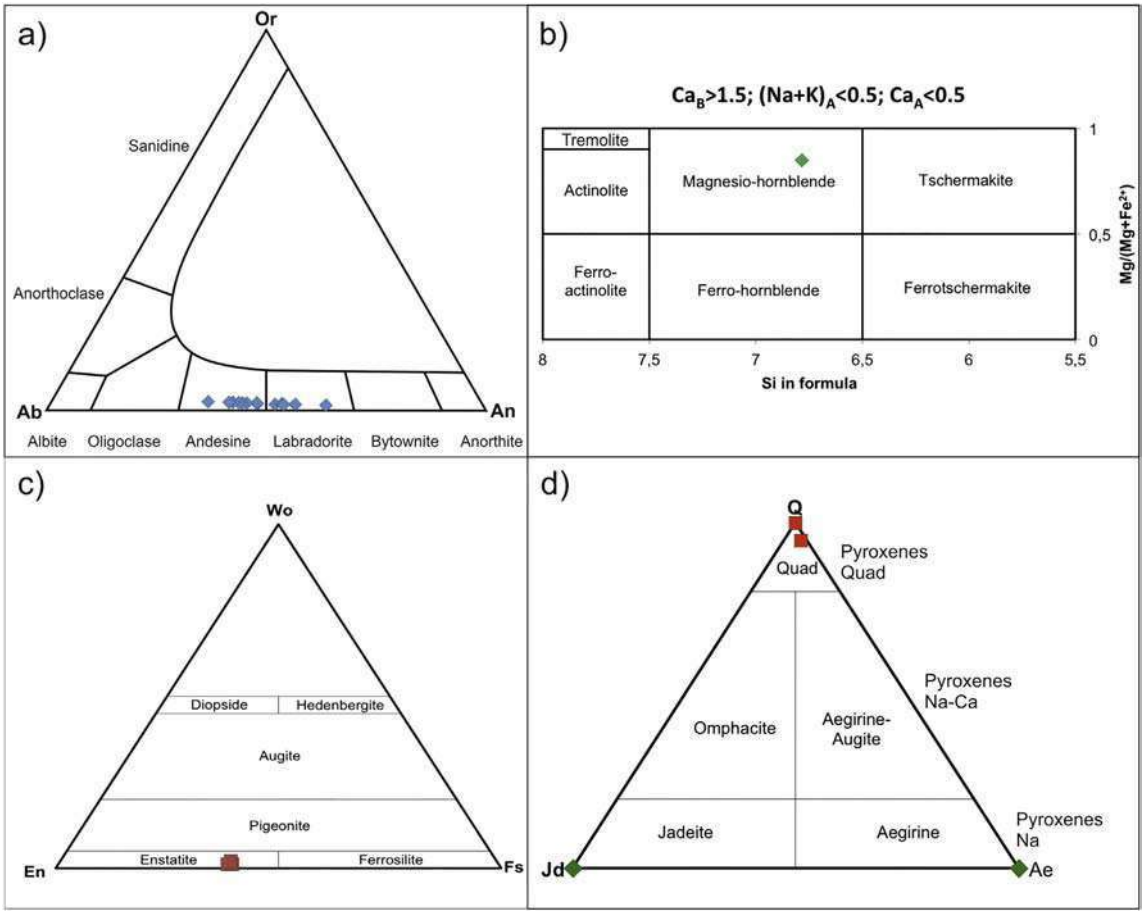

Fig. 7. Microprobe data of a) feldspars (classification of Smith and Brown, 1988); b) amphiboles (classification of Leake et al., 1997); and c) sodium and d) calcium, magnesium, iron pyroxenes (classification of Morimoto, 1989) diagrams.

hydrothermally altered lithic fragments suggests the occurrence of an extensive hydrothermal system within the caldera at the time of the eruption (Saxby et al., 2016).

Unit D (3.3 km³ total DRE volume - Table 1) shows similar field characteristics (Fig. 3d,e) and granulometric data (Supplementary Material 4a-c and r-t) to the previous unit C (Fig. 3d), and suggest it was emplaced from PDCs of hydromagmatic origin (Fig. 9d). The hydrothermally altered lithic fragments observed in Unit C are not recognized in the Unit D, so the ongoing magma-water interaction was most likely fuelled by surface water. A shallow lake seems to have been present in the IC at ≥43.670 ka years ago as proposed by Mann et al. (2004) although the last study of Suñe-Puchol et al. (2009a) suggests the presence of a paleolake already at 1.5 Ma. As proposed by Aravena et al. (2018), natural aquifers appear unlikely to be sources of enough water to significantly affect the eruptive dynamics of an event with high mass discharge rate; conversely, evidence for magma-water interaction are probably related to the involvement of surface water or the injection of groundwater by high-magnitude collapse mechanisms. The same type of activity was also reported for Taal caldera lake, Philippines in 1991 (Delmelle and Bernard, 2000), the hydromagmatic eruption of Kilauea Volcano, Hawaii, in 1970 (Mastin, 1997), or the Nari Caldera at Ulleung Island, Korea (Kim et al., 2014). Changes from dry to wet conditions in such eruptions were also observed for the Askja 1875 eruption, Iceland (Sparks et al., 1981; Carey et al., 2010) and the AD232 Taupo eruption, New Zealand (Houghton et al., 2000). The absence of any fall deposits at the base of Units C and D rules out the possibility of a sustained eruptive column phase (Fig. 5d).

During the course of the eruption, there was another change in the eruptive dynamics, with a switch to drier conditions (Fig. 9e). Unit E (0.3 km³ total DRE volume - Table 1) was deposited by alternation of dilute PDCs and fallout, which is based on plane-parallel and low-angle cross laminations and grain-supported layers without traction structures (Fig. 3f; Chough and Sohn, 1990; De Rosa et al., 1992; Dellino et al., 2004b; Solgevik et al., 2007), alternation of well and poorly sorted deposits (Supplementary Material 4 a-c) of ash and lapilli (Supplementary Material 4 g–i), and a clear polymodal trend of the grain size distribution (Supplementary Material 4u–w). Soft sediment folding (Fig. 3g) might indicate that some of the layers were deposited wet as consequence of magma-water interaction, thus characterizing the whole unit as alternation of dry and wet deposits that were deposited around the IC (Fig. 5e). At this time, due to structural faults that characterize IC, the magma might have had interaction with the almost empty Ilopango Lake after Unit D phase, thus allowing an intermittent magma-water interaction with the formation of short-lived columns and lateral blast.

It is important to consider how, not only a change in the water-magma ratio might have led to the emplacement of fallout and PDCs deposits, but also the scaled depth (ratio between depth of explosion and energy) can have huge effects on deposit characteristics, grain size and deposit morphology (see Taddeucci et al., 2013; Graettinger et al., 2014, 2015; Valentine et al., 2014, 2015; Sonder et al., 2015). As suggested in Graettinger et al. (2015), when scaled depth is constant, the crater focuses the jet and results in decreasing overall volumes of coarse ejecta and the potential occurrence of fine-grained dilute density current deposits. Progressively increasing scaled depth results in an overall decrease in ejecta volume to the point where the explosion is confined and no ejecta are produced. A progressive decrease in scaled depth will result in an increase in ejecta volume and in the grain size of ejecta

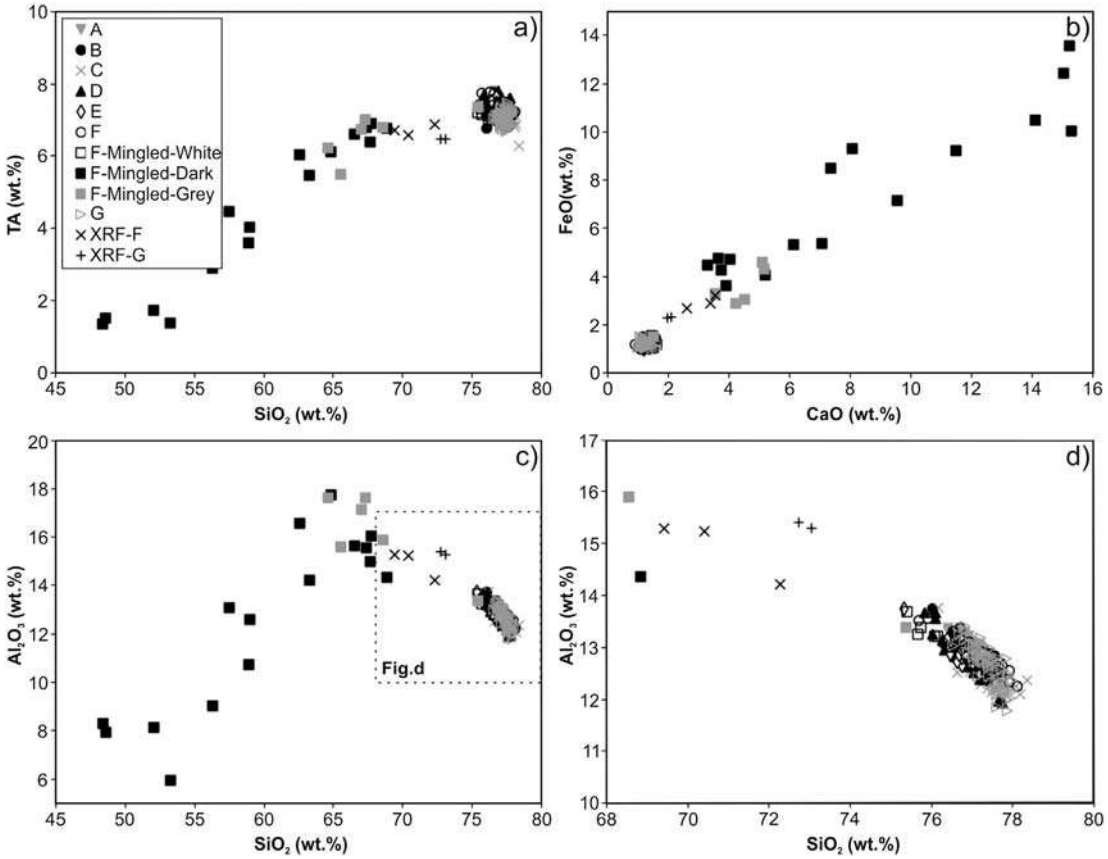

Fig. 8. a) Plot of TBJ juvenile samples (i.e. pumice clasts) and mingled pumices of Unit F in the TAS (SiO_2-Na_2O+ K_2O) classification diagram of Le Bas et al. (1986). Glass compositions from the entire composition succession of deposits, and from both proximal and distal sites: b) CaO vs FeO; c) and d) SiO_2 vs Al_2O_3.

deposits and low occurrence of fine-grained dilute density currents as the jet is larger than the previous crater and therefore does not exhibit significant focusing.

The final phase (Fig. 9f) of the eruption was marked by a dramatic change in eruptive style with deposition of chaotic, massive, poorly-sorted (Supplementary Material 4a–c), non-welded dry thick PDC deposits (Fig. 3h, i). The lag-breccia deposits of Unit F are observed only close to the caldera topographic edge (Fig. 3j). This might be related to the strong control exerted by the paleotopography on facies architecture as observed, for example, for the Abrigo Ignimbrite in Tenerife, Canary Islands (Pittari et al., 2006) or the Acatlán ignimbrite, Mexico (Branney and Kokelaar, 1997). This is a lithic-rich ignimbrite that represents continued clearing from fissure vents along the main bounding caldera faults (Fig. 9f). The sharp, erosive lower contact with underlying units, coarse, up to meter-sized lithic clasts and juveniles in a poorly sorted matrix (Fig. 3h–k), together with granulometric analyses (Supplementary Material 4g-i and x-z), suggest eruptive dynamics that were dominated by vigorous and prolonged pyroclastic fountaining that produced sustained quasi-steady PDCs, as the eruption waxed and stabilized. Both basal high-particle concentrations in the PDCs and the long runout distances were maintained because of the continuous supply of dense currents at the vent (Roche et al., 2016). These deposits formed an ignimbrite sheet, Unit F (9.3 km^3 total DRE volume-Table 1) that reached the sea on southern sectors of the caldera and was widespread around IC (Fig. 5f). At this point, the increase in the magma eruption rate could have been produced by the start of the caldera collapse, which would have commenced the rapid evacuation of magma from the sub-caldera magma chamber, leading to a subsequent inefficient magma-water interaction during F eruptive phase. Similar mechanisms from wet to drier conditions were also observed during the Neapolitan Yellow Tuff eruption (Orsi et al., 1992). The mingled pumice clasts that extend to basaltic compositions are also found in deposits from this phase of the eruption suggesting that additional melts were erupted. Since these distinctive less evolved compositions are restricted to the clasts in the very proximal outcrops it implies that the erupted volume of this melt was incredibly small. It is quite common for additional melts to be erupted during caldera formation (cf. Smith et al., 2016).

As for Units C and D, no fallout layers were recognized at the base of Unit F, thus, suggesting that an initial buoyant Plinian eruption column-building phase was not produced. This feature is similar to other ignimbrites such as Campanian (Marti et al., 2016) and Ora in Italy (Willcock et al., 2013), or Huichapan in Mexico (Pacheco-Hoyos et al., 2018). The occurrence of fines-poor elutriation pipes (Fig. 3l) indicates that following deposition, vigorous gas escape occurred elutriating fines. These pipes are interpreted as evidence of rapid emplacement involving particle segregation and vigorous, post emplacement fluid (dusty gas) escape (Branney and Kokelaar, 2002), thus suggesting that at the time of deposition Unit F deposits were hot.

Unit G (Fig. 3n) represents the final co-ignimbritic deposit of the TBJ eruption (Fig. 9g). Deposits were found at medial and distal locations that are N100 km from the caldera (Fig. 3o). This unit is made of moderately to poorly sorted (Supplementary Material 4a-c) ash (Supplementary Material 4g-i) with a clear bimodality grain-size distribution trend (Supplementary Material 4aa-ac) that highlights the significance of ash aggregation processes in the transport and deposition.

The absence of Plinian pumice fall deposits preceding the dense PDC deposits of TBJ is a typical characteristic of graben-type calderas as Ilopango (Aguirre-Díaz and Martí, 2015; Aguirre-Díaz et al., 2016, 2017; Saxby et al., 2016; Suñe-Puchol et al., 2019a) or fissure ignimbrite eruptions related to local/regional faults (Aguirre-Díaz and Labarthe-

Table 2
Whole rock analyses of representative TBJ samples.

Sample	ILO-32-2	ILO-128-1	ILO-169-A	ILO-302-1	ILO-303-1
TBJ Unit	F (base)	F (base)	F (base)	G	G
Site	Apulo	S. Anton. Masahuat	Oratorio	La Union	Santa Elena
Distance	Proximal	Medial	Medial	Distal	Distal
Latitude	N13°42.504'	N13°32.826'	N13°48.382'	N13°16.263'	N13°24.965'
Longitude	W89°05.365'	W89°02.510'	W89°02.301'	W87°54.421'	W88°24.560'
Major and minor elements (oxides, wt.%)					
SiO_2	67.34	70.325	68.631	70.45	70.081
TiO_2	0.408	0.301	0.34	0.247	0.25
Al_2O_3	14.833	13.826	14.846	14.744	14.835
Fe_2O_3	3.475	2.913	3.142	2.431	2.495
MnO	0.122	0.109	0.113	0.099	0.101
MgO	1.216	0.873	0.995	0.557	0.597
CaO	3.453	2.528	3.311	1.9	2.01
Na_2O	4.317	4.263	4.295	3.623	3.64
K_2O	2.188	2.433	2.122	2.621	2.595
P_2O_5	0.133	0.097	0.105	0.06	0.067
Total	99.975	99.888	99.99	99.932	99.891
LOI	2.49	2.22	2.09	3.2	3.22
Trace elements (ppm)					
Li	14	15	8	20	20
Be	1	1	1	1	1
B	43	73	41	39	31
P	0	0	0	0	0
Sc	5	3	7	2	3
Ti	0	0	0	0	0
V	40	27	34	20	22
Cr	3	3	3	3	3
Co	5	4	4	3	4
Ni	2	2	3	2	2
Cu	9	6	8	14	16
Zn	47	44	44	40	41
Ga	14	13	13	14	14
Rb	37	48	27	56	55
Sr	308	242	284	191	213
Y	17	17	15	17	17
Zr	144	149	149	139	143
Nb	3	4	3	4	4
Mo	2	2	2	2	2
Sn	1	1	1	3	3
Sb	1	1	1	1	1
Cs	2	2	2	3	3
Ba	997	1111	974	1271	1199
La	12	13	10	14	13
Ce	24	26	19	28	28
Pr	3	3	3	3	3
Nd	13	13	11	13	13
Sm	3	3	2	3	3
Eu	1	1	1	1	1
Tb	0	0	0	0	0
Gd	3	3	2	3	3
Dy	3	3	2	3	3
Ho	1	1	1	1	1
Er	2	2	2	2	2
Yb	2	2	2	2	2
Lu	0	0	0	0	0
Hf	4	4	4	4	4
Ta	0	0	0	0	0
W	0	1	0	1	1
Tl	0	0	0	0	0
Pb	6	7	6	8	8
Th	3	3	2	4	4
U	1	2	1	2	2

Samples analysed by X-Ray Fluorescence in the Insituto de Geología (UNAM) by Patricia Girón.
Coordinates in WGS84 system (zone 16P).
LOI: Lost of ignition.

Hernández, 2003; Aguirre-Díaz et al., 2008). This is due to the significant control of tectonic stress on mass discharge rate (Costa et al., 2011; Costa and Martí, 2016), with graben-type calderas tending to generate large MER larger that are too high to sustain a Plinian column (see Costa et al., 2018).

The TBJ deposits highlight that a single eruption can produce a complex sequence of eruption styles and depositional processes. The magnitude of this eruption means that Mayan populations living in the region would have been considerably affected (Dull et al., 2001; Hernández, 2004; Hernández et al., 2015). The human populations directly affected

Table 3
Representative glass analyses of the TBJ eruption units.

Sample	ILO-122-1	ILO-122-2	ILO-123-3	ILO-8-1	ILO-122-4	ILO-2-1	ILO-122-6	ILO-8-3	ILO-8-2	ILO-8-4	ILO-32	ILO-32	ILO-32	ILO-9-1	ILO-122-9	ILO-288
TBJ Unit	A (base)	A (top)	B (top)	C	C	D	Da (top)	Db	Dc	E	F	F-Mingled-White	F-Mingled-Grey	F	G	G (distal)
Site	Comalapa	Comalapa	Comalapa	E San Emigdio	Comalapa	San Marcos	Comalapa	E San Emigdio	E San Emigdio	E San Emigdio	Utb. La Selva	Utb. La Selva	Utb. La Selva	E Ilopango	Comalapa	Tacumal
Distance	Medial	Medial	Medial	Proximal	Medial	Proximal	Medial	Proximal	Proximal	Proximal	Proximal	Proximal	Proximal	Proximal	Medial	Distal
Latitude	N13°30.283'	N13°30.283'	N13°30.283'	N13°38.876'	N13°30.283'	N13°36.361'	N13°30.283'	N13°38.876'	N13°38.876'	N13°38.876'	N13°42.504'	N13°42.504'	N13°42.504'	N13°39.807'	N13°30.283'	N13°58.769
Longitude	W89°04.805'	W89°04.805'	W89°04.805'	W88°58.097'	W89°04.805'	W89°9.517'	W89°04.805'	W88°58.097'	W88°58.097'	W88°58.097'	W89°05.365'	W89°05.365'	W89°05.365'	W89°59.099'	W89°04.805'	W89°40.397'
Analysis label	ILO-123-1_17	ILO-122-2_13	ILO-123-3_12	TBJ_8-1_6	ILO-122-4_15	TBJ_2-1_8	ILO-122-6_4	TBJ_8-3_16	TBJ_8-2_9	TBJ_8-4_19	ILO-32_13	ILO-32_white-4	ILO-32_grey-2	TBJ_9-1_13	ILO-122-9_12	ILO-288_6
SiO_2	76.42	76.85	77.22	77.31	77.38	77.05	76.79	76.11	77.04	76.76	78.12	78.16	66.55	52.09	77.58	77.22	77.40
TiO_2	0.19	0.24	0.19	0.17	0.17	0.19	0.17	0.18	0.20	0.15	0.16	0.21	0.49	1.17	0.15	0.19	0.19
Al_2O_3	13.30	13.09	12.63	12.84	12.84	12.68	13.14	13.66	12.51	13.12	12.24	13.20	15.60	8.12	12.47	12.74	12.80
FeO	1.23	1.09	1.06	0.99	1.17	1.18	1.10	1.06	1.23	1.07	1.06	1.19	4.58	10.02	1.00	1.26	1.02
MnO	0.13	0.12	0.12	0.02	0.07	0.11	0.10	0.03	0.05	0.05	0.00	0.10	0.20	0.30	0.03	0.09	0.09
MgO	0.18	0.22	0.22	0.20	0.23	0.19	0.23	0.19	0.23	0.17	0.16	0.26	2.63	11.14	0.19	0.18	0.18
CaO	1.38	1.22	1.21	1.23	1.21	1.22	1.27	1.50	1.19	1.24	1.00	1.60	5.09	15.26	1.14	1.28	1.24
Na_2O	4.30	4.32	4.54	4.44	4.43	4.59	4.34	4.44	4.50	4.62	4.26	4.07	3.82	1.24	4.41	4.31	4.36
K_2O	2.87	2.84	2.82	2.80	2.71	2.80	2.86	2.81	3.06	2.83	2.97	2.95	1.68	0.50	3.03	2.71	2.72
P_2O_5				0.01		0.02		0.02	0.02	0.09		0.03	0.17	0.08	0.02		
Cl				0.17		0.19		0.18	0.21	0.17		0.22	0.17	0.05	0.20		
Analytical total	98.08	99.00	97.35	95.65	97.41	96.13	95.01	95.76	96.84	99.43	97.36	94.46	92.68	97.85	94.78	98.59	99.52

EPMA of individual glass shards acquired at 15 kV and 6 nA using a 10 μm defocused beam. Data are normalized to 100% to account for variable hydration and facilitate comparison.

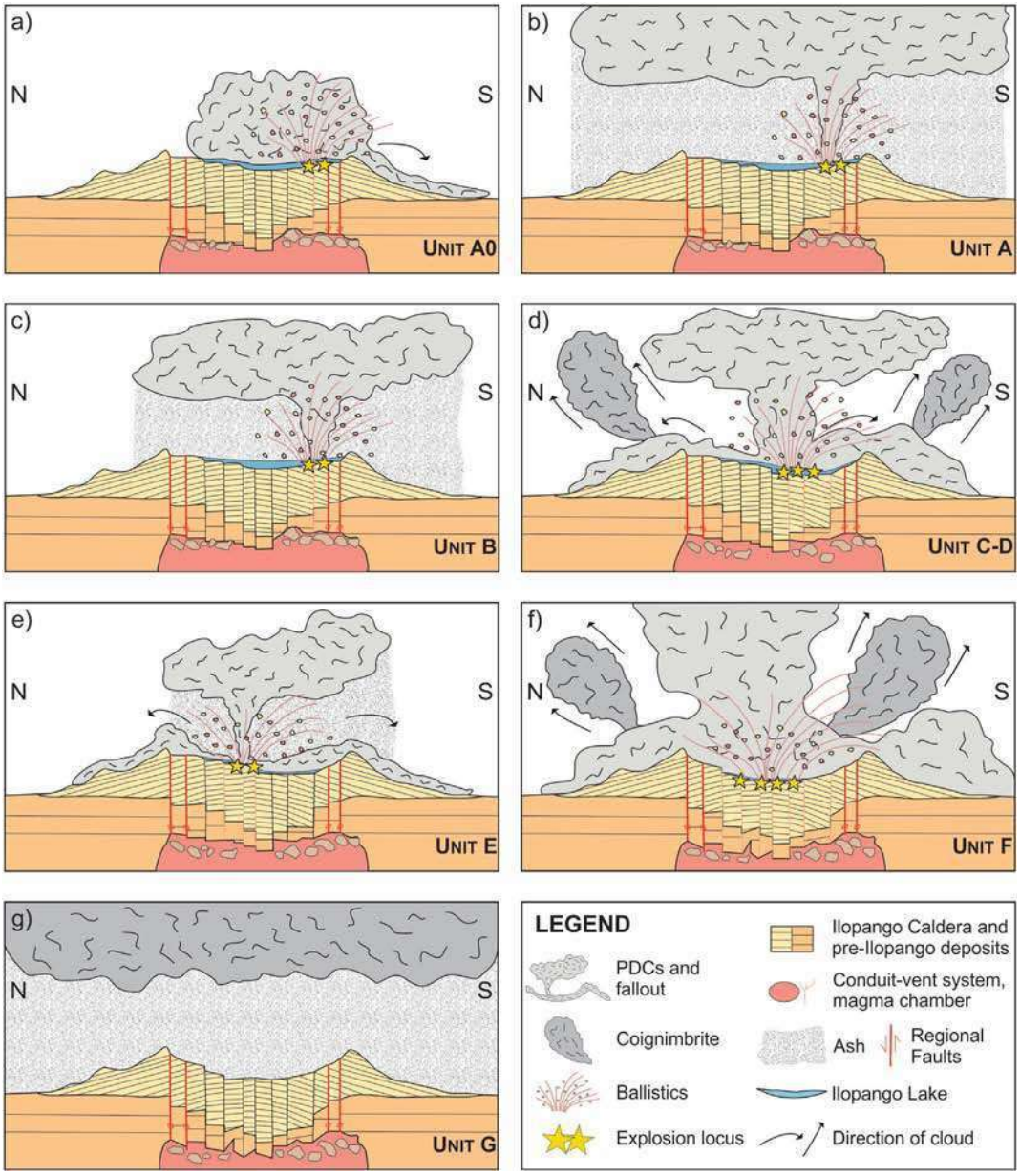

Fig. 9. Sketch (not to scale) illustrating the evolution of the TBJ eruption: a) rise of magma and interaction with a shallow aquifer or water lake and formation of the directional dilute PDCs that spread mainly southward (Unit A_0); fallout phases represented by b) hydromagmatic Unit A and c) magmatic Unit B; d) PDCs of hydromagmatic origin, due to a renewed magma-water interaction, with formations of Unit C and Unit D; e) PDCs and fallout deposits from the transitional Unit E due to the alternation of dry and wet phases; f) main phase of the TBJ eruption with deposition of Unit F by dense PDCs associated to the caldera collapse; g) co-ignimbrite deposits.

by the TBJ eruption would have been those living in the territory within 50 km of the IC. However, the indirect effects on social, economic, and political systems probably affected a much wider area of Mesoamerica (Dull et al., 2001). It has also been suggested that the sulphate peak, typically associated with volcanic eruptions, in the both Greenland and Antarctic ice cores at 539-540 CE could be associated with the TBJ eruption (Sigl et al., 2015). These peaks are associated with the H_2SO_4 aerosols that are injected into the high atmosphere during large volcanic eruptions, which increase the albedo and potentially produce a volcanic winter period (Robock, 2000). However, the date of the eruption has not been sufficiently resolved to establish if these sulphate peaks in the polar ice cores are in fact associated with the TBJ eruption as the ^{14}C dates fall on a plateau in the radiocarbon calibration curve (e.g., Reimer et al., 2013), which results in an imprecise eruption range of AD270-AD400 (Lohse et al., 2018) to AD440-550 (Dull et al., 2010).

The examination of this eruption sheds light on a number of important implications for hazard assessment when considered within the framework of the volcanism associated with IC and Country of El Salvador. The detailed study of the TBJ eruption together with the ones of Suñe-Puchol et al. (2019a, 2019b) about the older eruptions of IC, represent the first and necessary step towards improved volcanic hazard assessments for the region. These are essential to mitigate volcanic risk for the large number of communities, including the City of San Salvador, that are expanding around this active volcano.

8. Conclusion

In this study, we conducted a detailed stratigraphic and lithological study of the dacitic pumice Tierra Blanca Joven (TBJ) deposit. The TBJ is the last explosive eruption of Ilopango Caldera, representing a singular eruptive episode and constitutes the last eruptive cycle of the Tierra

Blanca sequence that starts with the TB4 eruption deposit. The TBJ eruption erupted ~58 km³ of bulk volume rock or ~30 km³ DRE of magma, corresponding to a 6.8 magnitude eruption.

The eruption was characterized by eight phases (A_0-G) with distinct eruptive styles without major pauses in between. The eruption started with dilute PDCs followed by two fallout phases that left only few cm of deposits, found mainly close to the IC. Subsequently, dense and dilute PDCs of hydromagmatic and magmatic origin filled the depressions near the Ilopango Lake. Deposits thicknesses are up to 70 m and reached distances of at least 40 km from the vent, covering the area where the city of San Salvador is now located. Finally, coignimbritic ash deposits of the last stage of the eruption were found all over El Salvador with significant thicknesses, and also found dispersed into neighbouring countries.

The TBJ was a cataclysmic event and is considered to be one of the largest Quaternary eruptions in Central America. TBJ eruptive products would have considerably affected the Mayan populations living in Salvadorian and nearby territories at that time. Consequently, long- and short-term hazard assessments for IC should take into account all possible scenarios including those described for the TBJ eruption.

Supplementary data to this article can be found online at https://doi.org/10.1016/j.jvolgeores.2019.03.006.

AcknowledgeThents

This study was financed by CONACYT-CB grant 240447 to GJAD and logistically supported by MARN-El Salvador and PNC-El Salvador. We thank Caterina Muñoz Torres, Academic Technician of CGEO and the students Karina Rodríguez García and Katia Jasso Torres for their help during the survey. This manuscript was greatly improved by comments and suggestions from the chief-editor Joan Martí and an anonymous reviewer.

References

Aguirre-Díaz, G.J., 2008. Types of collapse calderas. Collapse Calderas Workshop 19-25 October 2008, Querétaro, Mexico "Reconstructing the Evolution of Collapse Calderas: Magma Storage, Mobilization and Eruption". IOP Conference Series: Earth Environ. Sci., 3 012021 (5pp).

Aguirre-Díaz, G.J., Labarthe-Hernández, G., 2003. Fissure ignimbrites: Fissure-source origin for voluminous ignimbrites of the Sierra Madre Occidental and its relationship with Basin and Range faulting. Geology 31 (9), 773–776.

Aguirre-Díaz, G.J. and Martí, J., 2015. Graben calderas: examples from Mexico, Central America, and the Andes. 26th IUGG General Assembly, Prague, Czech Republic, June 22-July 2, 2015.

Aguirre-Díaz, G.J., Labarthe-Hernández, G., Tristán-González, M., Nieto-Obregón, J., Gutiérrez-Palomares, I., 2008. The ignimbrite flare-up and graben calderas of the Sierra Madre Occidental, Mexico. Dev. Volcanol. 10, 143-180.

Aguirre-Díaz, G.J., Suñe-Puchol, I., Dávila-Harris, P., Pedrazzi, D., Hernández, W. and Gutiérrez, E., 2016. Volcanic history of the Ilopango caldera, Central American Volcanic Arc: Cities on Volcanoes 9, IAVCEI; Puerto Varas, Chile, (November 2016).

Aguirre-Díaz, J.G., Suñe-Puchol, I., Davila-Harris, P., Pedrazzi, D., Hernandez, W. and Gutierrez, E., 2017 Volcanic history of the Ilopango caldera, Central American Volcanic Arc. 113th Annual Meeting, 2017 GSA Cordilleran Section, Hawaii, USA.

Aravena, A., Vitturi, M., Cioni, R., Neri, A., 2018. Physical constraints for effective magma-water interaction along volcanic conduits during silicic explosive eruptions. Geology 46 (10), 867–870.

Barberi, F., Cioni, R., Rosi, M., Santacroce, R., Sbrana, A., Vecci, R., 1989. Magmatic and phreatomagmatic phases in explosive eruptions of Vesuvius as deduced by grain-size and component analysis of the pyroclastic deposits. J. Volcanol. Geotherm. Res. 38 (3), 287-307.

Barckhausen, U., Ranero Cesar, R., Huene, R., Cande Steven, C., Roeser Hans, A., 2001. Revised tectonic boundaries in the Cocos Plate off Costa Rica: Implications for the segmentation of the convergent margin and for plate tectonic models. J. Geophys. Res. Solid Earth 106 (B9), 19207-19220.

Bernal, J.B., Lozano-Santacruz, R., 2005. Characterization of a new set of eight geochemical reference materials for XRF major and trace element analysis. Revista Mexicana de Ciencias Geológicas 22 (3), 329-344.

Bonadonna, C., Costa, A., 2012. Estimating the volume of tephra deposits: a new simple strategy. Geology 40 (5), 415–418.

Bonadonna, C., Costa, A., 2013. Plume height, volume, and classification of explosive volcanic eruptions based on the Weibull function. Bull. Volcanol. 75 (8), 742.

Bonadonna, C., Houghton, B.F., 2005. Total grain-size distribution and volume of tephra-fall deposits. Bull. Volcanol. 67 (5), 441–456.

Brand, B.D., Clarke, A.B., 2009. The architecture, eruptive history, and evolution of the Table Rock complex, Oregon: from a Surtseyan to an energetic maar eruption. J. Volcanol. Geotherm. Res. 180 (2), 203–224.

Brand, B.D., White, C.M., 2007. Origin and stratigraphy of phreatomagmatic deposits at the Pleistocene Sinker Butte Volcano, Western Snake River Plain, Idaho. J. Volcanol. Geotherm. Res. 160 (3), 319–339.

Branney, M.J., Kokelaar, P., 1997. Giant bed from a sustained catastrophic density current flowing over topography: Acatlan ignimbrite, Mexico. Geology 25 (2), 115–118.

Branney, M.J., Kokelaar, P., 2002. Pyroclastic Density Currents and the Sedimentation of Ignimbrites (Geological Society of London).

Canora, C., Villamor, P., Martínez-Díaz, J.J., Berryman, K.R., Álvarez-Gómez, J.A., Capote, R., Hernández, W., 2012. Paleoseismic analysis of the San Vicente segment of the El Salvador Fault Zone, EL Salvador, Central America. Geol. Acta 10, 103-123.

Carey, R.J., Houghton, B.F., Thordarson, T., 2010. Tephra dispersal and eruption dynamics of wet and dry phases of the 1875 eruption of Askja Volcano, Iceland. Bull. Volcanol. 72 (3), 259-278.

Carr, M.J., Patino, L.C. and Feigenson, M.D., 2007. Petrology and geochemistry of lavas. Central America: geology, resources and hazards. 1 565-577.

Chough, S.K., Sohn, Y.K., 1990. Depositional mechanics and sequences of base surges, Songaksan tuff ring, Cheju Island, Korea. Sedimentology 37 (6), 1115–1135.

Cioni, R., Gurioli, L., Sbrana, A., Vougioukalakis, G., 2000. Precursory phenomena and destructive events related to the late Bronze Age Minoan (Thera, Greece) and AD 79 (Vesuvius, Italy) Plinian eruptions; inferences from the stratigraphy in the archaeological areas. Geol. Soc. Lond., Spec. Publ. 171 (1), 123-141.

Cole, P.D., Queiroz, G., Wallenstein, N., Gaspar, J.L., Duncan, A.M., Guest, J.E., 1995. An historic subplinian/phreatomagmatic eruption: the 1630 AD eruption of Furnas volcano, São Miguel, Azores. J. Volcanol. Geotherm. Res. 69 (1–2), 117–135.

Cole, P.D., Guest, J.E., Duncan, A.M., Pacheco, J.-M., 2001. Capelinhos 1957-1958, Faial, Azores: deposits formed by an emergent surtseyan eruption. Bull. Volcanol. 63 (2–3), 204.

Coltelli, M., Del Carlo, P., Vezzoli, L., 1998. Discovery of a Plinian basaltic eruption of Roman age at Etna volcano, Italy. Geology 26 (12), 1095-1098.

Corti, G., Carminati, E., Mazzarini, F., Garcia, M.O., 2005. Active strike-slip faulting in El Salvador, Central America. Geology 33 (12), 989-992.

Costa, A., Martí, J., 2016. Stress Field Control during Large Caldera-Forming Eruptions. Front. Earth Sci. 4 (92).

Costa, A., Dell'Erba, F., Di Vito, M.A., Isaia, R., Macedonio, G., Orsi, G., Pfeiffer, T., 2009. Tephra fallout hazard assessment at the Campi Flegrei caldera (Italy). Bull. Volcanol. 71 (3), 259.

Costa, A., Gottsmann, J., Melnik, O., Sparks, R.S.J., 2011. A stress-controlled mechanism for the intensity of very large magnitude explosive eruptions. Earth Planet. Sci. Lett. 310 (1–2), 161–166.

Costa, A., Suzuki, J.Y., Koyaguchi, T., 2018. Understanding the plume dynamics of explosive super-eruptions. Nat. Commun. 9 (1), 654.

Daugherty, H.E., 1969 Man-Induced Ecological Change in El Salvador. Ph.D. dissertation, University of California, Los Angeles. University Microfilms, Ann Arbor.

De Rita, D., Giordano, G., Esposito, A., Fabbri, M., Rodani, S., 2002. Large volume phreatomagmatic ignimbrites from the Colli Albani volcano (Middle Pleistocene, Italy). J. Volcanol. Geotherm. Res. 118 (1–2), 77–98.

De Rosa, R., Frazzetta, G., La Volpe, L., 1992. An approach for investigating the depositional mechanism of fine-grained surge deposits. The example of the dry surge deposits at "La Fossa di Vulcano". J. Volcanol. Geotherm. Res. 51 (4), 305-321.

Dellino, P., La Volpe, L., 1995. Fragmentation versus transportation mechanisms in the pyroclastic sequence of Monte Pilato-Rocche Rosse (Lipari, Italy). J. Volcanol. Geotherm. Res. 64 (3–4), 211–231.

Dellino, P., Isaia, R., La Volpe, L., Orsi, G., 2004a. Interaction between particles transported by fallout and surge in the deposits of the Agnano-Monte Spina eruption (Campi Flegrei, Southern Italy). J. Volcanol. Geotherm. Res. 133 (1), 193-210.

Dellino, P., Isaia, R., Veneruso, M., 2004b. Turbulent boundary layer shear flows as an approximation of base surges at Campi Flegrei (Southern Italy). J. Volcanol. Geotherm. Res. 133 (1), 211-228.

Delmelle, P., Bernard, A., 2000. Downstream composition changes of acidic volcanic waters discharged into the Banyupahit stream, Ijen caldera, Indonesia. J. Volcanol. Geotherm. Res. 97 (1), 55–75.

DeMets, C., 2001. A new estimate for present-day Cocos-Caribbean Plate motion: Implications for slip along the central American Volcanic Arc. Geophys. Res. Lett. 28 (21), 4043-4046.

DeMets, C., Jansma, P.E., Mattioli, G.S., Dixon, T.H., Farina, F., Bilham, R., Calais, E., Mann, P., 2000. GPS geodetic constraints on Caribbean-North America Plate Motion. Geophys. Res. Lett. 27 (3), 437-440.

Denevan, W.M., 1992. Introduction. In: The Native Population of the Americas in 1492. 2nd (Ed.), Edited by William M. Denevan. University of Wisconsin Press, Madison, pp. xv–xli.

Dixon, T.H., 1993. GPS measurement of relative motion of the Cocos and Caribbean Plates and strain accumulation across the Middle America Trench. Geophys. Res. Lett. 20 (20), 2167–2170.

Dull, R.A., Southon, J.R., Sheets, P., 2001. Volcanism, ecology and culture: a reassessment of the Volcán Ilopango TBJ eruption in the southern Maya realm. Lat. Am. Antiq. 12 (1), 25–44.

Dull, R., Southon, J., Kutterolf, S., Freundt, A., Wahl, D., Sheets, P., 2010. Did the Ilopango TBJ Eruption Cause the AD 536 Event. AGU Fall meeting, Abstracts.

Funk, J., Mann, P., 2009. Cenozoic tectonics of the Nicaraguan depression, Nicaragua, and median Trough, El Salvador, based on seismic-reflection profiling and remote-sensing dataCenozoic tectonics of the Nicaraguan depression. GSA Bull. 121 (11−12), 1491-1521.

Garibaldi, N., Tikoff, B., Hernández, W., 2016. Neotectonic deformation within an extensional stepover in El Salvador magmatic arc, Central America: Implication for the interaction of arc magmatism and deformation. Tectonophysics 693, 327-339.
Golombek, M.P., Carr, M.J., 1978. Tidal triggering of seismic and volcanic phenomena during the 1879-1880 eruption of Islas Quemadas volcano in El Salvador, Central America. J. Volcanol. Geotherm. Res. 3 (3–4), 299–307.
Graettinger, A.H., Valentine, G.A., Sonder, I., Ross, P.S., White, J.D.L., Taddeucci, J., 2014. Maar-diatreme geometry and deposits: Subsurface blast experiments with variable explosion depth. Geochem. Geophys. Geosyst. 15 (3), 740-764.
Graettinger, A.H., Valentine, G.A., Sonder, I., Ross, P.-S., White, J.L., 2015. Facies distribution of ejecta in analog tephra rings from experiments with single and multiple subsurface explosions. Bull. Volcanol. 77 (8), 66.
Guzmán-Speziale, M., Valdés-González, C., Molina, E., Gómez, J.M., 2005. Seismic activity along the Central America volcanic arc: is it related to subduction of the Cocos plate? Tectonophysics 400 (1–4), 241–254.
Hart, W.J.E., 1981. The Panchimalco tephra, El Salvador. New Brunswick, New Jersey, Rutgers University, Central America. M.S. thesis (101 p).
Hart, W.J.E., Steen-McIntyre, V., 1983. Tierra Blanca Joven Tephra from the AD 260 eruption of Ilopango caldera. Archeology and Volcanism in Central America—The Zapotitán Valley of El Salvador, pp. 15–34.
Hernández, E.W., 2004. Características geotécnicas y vulcanológicas de las tefras de Tierra Blanca Joven de Ilopango, El Salvador. Tesis de maestría, Univ. Politécnica de El Salvador, San Salvador (115 p).
Hernández, E.W., Ferrés, D., Delgado-Granados, H., Pullinger, C. and Gutiérrez de Henríquez, E., 2010. The last 40 ka eruptive cycle of Ilopango caldera deposits: a settlement for the San Salvador Metropolitan Area (El Salvador). A. Abstract volume, International Conference Cities on Volcanoes, Fundación Canaria ITER, Tenerife: pp 56.
Hernández, W., Delgado-Granados, H., Nieto, J., 2012. La erupción Tierra Blanca 4 (TB4), Caldera de Ilopango, El Salvador. Ministerio de Medio Ambiente y Recursos Naturales, Informe inédito (36 p).
Hernández, W., Aguirre-Díaz, G. and Ayala, P., 2015. La erupción Tierra Blanca Joven y la diáspora de los Mayas. Museo Nacional de Antropología David J. Guzmán, V Congreso Centroamericano de Arqueología en El Salvador. José Erquicia y Shione Shibata editores. 238p. ISBN 978-99961-958-0-8: 227-237.
Houghton, B.F., Schmincke, H.-U., 1989. Rothenberg scoria cone, East Eifel: a complex Strombolian and phreatomagmatic volcano. Bull. Volcanol. 52 (1), 28–48.
Houghton, B.F., Smith, R.T., 1993. Recycling of magmatic clasts during explosive eruptions: estimating the true juvenile content of phreatomagmatic volcanic deposits. Bull. Volcanol. 55 (6), 414-420.
Houghton, B.F., Smith, R.T., Gilbert, J.S., 2000. Phreatoplinian eruptions. Encyclopedia of Volcanoes, pp. 513-525.
Houghton, B.F., Wilson, C.J.N., Del Carlo, P., Coltelli, M., Sable, J.E., Carey, R.J., 2004. The influence of conduit processes on changes in style of basaltic Plinian eruptions: Tarawera 1886 and Etna 122 BC. J. Volcanol. Geotherm. Res. 137 (1–3), 1–14.
Hutton, D.H.W., Reavy, R.J., 1992. Strike-slip tectonics and granite petrogenesis. Tectonics 11 (5), 960-967.
Jochum Klaus, P., Stoll, B., Herwig, K., Willbold, M., Hofmann, A.W., Amini, M., Aarburg, S., Abouchami, W., Hellebrand, E., Mocek, B., Raczek, I., Stracke, A., Alard, O., Bouman, C., Becker, S., Dücking, M., Brätz, H., Klemd, R., de Bruin, D., Canil, D., Cornell, D., de Hoog, C.J., Dalpé, C., Danyushevsky, L., Eisenhauer, A., Gao, Y., Snow, J.E., Groschopf, N., Günther, D., Latkoczy, C., Guillong, M., Hauri, E.H., Höfer, H.E., Lahaye, Y., Horz, K., Jacob, D.E., Kasemann, S.A., Kent, A.J.R., Ludwig, T., Zack, T., Mason, P.R.D., Meixner, A., Rosner, M., Misawa, K., Nash, B.P., Pfänder, J., Premo, W.R., Sun, W.D., Tiepolo, M., Vannucci, R., Vennemann, T., Wayne, D., Woodhead, J.D., 2006. MPI-DING reference glasses for in situ microanalysis: New reference values for element concentrations and isotope ratios. Geochem. Geophys. Geosyst. 7 (2).
Kim, G.B., Cronin, S.J., Yoon, W.S., Sohn, Y.K., 2014. Post 19 ka BP eruptive history of Ulleung Island, Korea, inferred from an intra-caldera pyroclastic sequence. Bull. Volcanol. 76 (4), 802.
Kutterolf, S., Freundt, A., Perez, W., Mörz, T., Schacht, U., Wehrmann, H. and Schmincke, H.U., 2008a. Pacific offshore record of plinian arc volcanism in Central America: 1. Along-arc correlations. Geochemistry, Geophysics, Geosystems, 9(2).
Kutterolf, S., Freundt, A. and Perez, W., 2008b. Pacific offshore record of plinian arc volcanism in Central America: 2. Tephra volumes and erupted masses. Geochemistry, Geophysics, Geosystems, 9(2).
LaFemina, P., Dixon Timothy, H., Govers, R., Norabuena, E., Turner, H., Saballos, A., Mattioli, G., Protti, M., Strauch, W., 2009. Fore-arc motion and Cocos Ridge collision in Central America. Geochem. Geophys. Geosyst. 10 (5).
Le Bas, M.J., Le Maitre, R.W., Streckeisen, A., Zanettin, B., Rocks, I.S.o.t.S.o.I., 1986. A chemical classification of volcanic rocks based on the total alkali-silica diagram. J. Petrol. 27 (3), 745–750.
Leake, B.E., Woolley, A.R., Arps, C.E., Birch, W.D., Gilbert, M.C., Grice, J.D., Hawthorne, F.C., Kato, A., Kisch, H.J., Krivovichev, V.G., 1997. Report. Nomenclature of amphiboles: report of the subcommittee on amphiboles of the international mineralogical association commission on new minerals and mineral names. Mineral. Mag. 61 (2), 295-321.
Lexa, J., Sebesta, J., Chávez, J.A., Hernández, W., Pecskay, Z., 2011. Geology and volcanic evolution in the southern part of the San Salvador Metropolitan Area. J. Geosci. 56 (1), 106–140.
Lohse, J.C., Hamilton, W.D., Brenner, M., Curtis, J., Inomata, T., Morgan, M., Cardona, K., Aoyama, K., Yonenobu, H., 2018. Late Holocene volcanic activity and environmental change in Highland Guatemala. Quat. Sci. Rev. 191, 378–392.
Lovell, W.G. and Lutz, C.H., 1995 Demography and Empire. Dellplain Latin American Studies, Number 33. Westview Press, Boulder.
Macedonio, G., Pareschi, M.T., 1991. An algorithm for the triangulation of arbitrarily distributed points: applications to volume estimate and terrain fitting. Comput. Geosci. 17 (7), 859-874.
Macedonio, G., Costa, A., Longo, A., 2005. A computer model for volcanic ash fallout and assessment of subsequent hazard. Comput. Geosci. 31 (7), 837–845.
Mann, P., 2007. Overview of the tectonic history of northern Central America. Geol. Soc. Am. Spec. Pap. 428, 1–19.
Mann, C.P., Stix, J., Vallance, J.W., Richer, M., 2004. Subaqueous intracaldera volcanism, Ilopango Caldera, El Salvador, Central America. In: Rose, W.I., Bommer, J.J., López, D.L., Carr, M.J., Major, J.J. (Eds.), Natural Hazards in El Salvador: Boulder. Colorado, Geological Society of America Special Paper vol. 375, pp. 159-174.
Marti, A., Folch, A., Costa, A., Engwell, S., 2016. Reconstructing the plinian and co-ignimbrite sources of large volcanic eruptions: a novel approach for the Campanian Ignimbrite. Sci. Rep. 6, 21220.
Martí, J., Groppelli, G., Brum da Silveira, A., 2018. Volcanic stratigraphy: a review. J. Volcanol. Geotherm. Res. 357, 68–91.
Martínez-Díaz, J.J., Álvarez-Gómez, J.A., Benito, B., Hernández, D., 2004. Triggering of destructive earthquakes in El Salvador. Geology 32 (1), 65–68.
Mastin, L.G., 1997. Evidence for water influx from a caldera lake during the explosive hydromagmatic eruption of 1790, Kilauea volcano, Hawaii. J. Geophys. Res. Solid Earth 102 (B9), 20093-20109.
Mastin, L.G., Guffanti, M., Servranckx, R., Webley, P., Barsotti, S., Dean, K., Durant, A., Ewert, J.W., Neri, A., Rose, W.I., Schneider, D., Siebert, L., Stunder, B., Swanson, G., Tupper, A., Volentik, A., Waythomas, C.F., 2009. A multidisciplinary effort to assign realistic source parameters to models of volcanic ash-cloud transport and dispersion during eruptions. J. Volcanol. Geotherm. Res. 186 (1), 10–21.
Matthews, N.E., Smith, V.C., Costa, A., Durant, A.J., Pyle, D.M., Pearce, N.J.G., 2012. Ultra-distal tephra deposits from super-eruptions: examples from Toba, Indonesia and Taupo Volcanic Zone, New Zealand. Quat. Int. 258, 54–79.
McPhie, J., Walker, G.P.L., Christiansen, R.L., 1990. Phreatomagmatic and phreatic fall and surge deposits from explosions at Kilauea volcano, Hawaii, 1790 AD: Keanakakoi Ash Member. Bull. Volcanol. 52 (5), 334-354.
Montero, W., Dewey, J., 1982. Shallow-focus seismicity, composite focal mechanism, and tectonics of the Valle Central of Costa Rica. Bull. Seismol. Soc. Am. 72 (5), 1611-1626.
Morimoto, N., 1989. Nomenclature of pyroxenes. Mineral. J. 14 (5), 198–221.
Orsi, G., D'Antonio, M., Vita, S.d., Gallo, G., 1992. The Neapolitan Yellow Tuff, a large-magnitude trachytic phreatoplinian eruption: eruptive dynamics, magma withdrawal and caldera collapse. J. Volcanol. Geotherm. Res. 53 (1), 275–287.
Pacheco-Hoyos, J.G., Aguirre-Díaz, G.J., Dávila-Harris, P., 2018. Boiling-over dense pyroclastic density currents during the formation of the ~100km3 Huichapan ignimbrite in Central Mexico: Stratigraphic and lithofacies analysis. J. Volcanol. Geotherm. Res. 349, 268-282.
Pfeiffer, T., Costa, A., Macedonio, G., 2005. A model for the numerical simulation of tephra fall deposits. J. Volcanol. Geotherm. Res. 140 (4), 273-294.
Pimentel, A., Pacheco, J., Self, S., 2015. The~1000-years BP explosive eruption of Caldeira Volcano (Faial, Azores): the first stage of incremental caldera formation. Bull. Volcanol. 77 (5), 42.
Pittari, A., Cas, R.A.F., Edgar, C.J., Nichols, H.J., Wolff, J.A., Marti, J., 2006. The influence of palaeotopography on facies architecture and pyroclastic flow processes of a lithic-rich ignimbrite in a high gradient setting: the Abrigo Ignimbrite, Tenerife, Canary Islands. J. Volcanol. Geotherm. Res. 152 (3–4), 273–315.
Protti, M., Guendel, F. and McNally, K., 1995. Correlation between the age of the subducting Cocos plate and the geometry of the Wadati-Benioff zone under Nicaragua and Costa Rica. Special Papers Geological Society of America: 309-309.
Pyle, D.M., 2000. Sizes of volcanic eruptions. In the Encyclopaedia of Volcanoes, (Sigurdsson, H.; Houghton, B.; McNutt, SR; Rymer, H.; Stix, J., editors). Academic Press, London.
Quane, S.L., Russell, J.K., 2005. Ranking welding intensity in pyroclastic deposits. Bull. Volcanol. 67 (2), 129-143.
Reimer, P.J., Bard, E., Bayliss, A., Beck, J.W., Blackwell, P.G., Ramsey, C.B., Buck, C.E., Cheng, H., Edwards, R.L., Friedrich, M., 2013. IntCal13 and Marine13 radiocarbon age calibration curves 0–50,000 years cal BP. Radiocarbon 55 (4), 1869–1887.
Richer, M., Mann, C.P. and Stix, J., 2004. Mafic magma injection triggers eruption at Ilopango Caldera, El Salvador, Central America. Spec. Pap. 375 Nat. Hazards El Salvador 175-190.
Robock, A., 2000. Volcanic eruptions and climate. Rev. Geophys. 38 (2), 191-219.
Roche, O., Buesch, D.C., Valentine, G.A., 2016. Slow-moving and far-travelled dense pyroclastic flows during the Peach Spring super-eruption. Nat. Commun. 7, 10890.
Rolo, R., Bommer, J.J., Houghton, B.F., Vallance, J.W., Berdousis, P., Mavrommati, C. and Murphy, W., 2004. Geologic and engineering characterization of Tierra Blanca pyroclastic ash deposits. Special Papers Geological Society of America: 55–68.
Rose, W.I., Conway, F.M., Pullinger, C.R., Deino, A., McIntosh, W.C., 1999. An improved age framework for late Quaternary silicic eruptions in northern Central America. Bull. Volcanol. 61 (1), 106-120.
Saxby, J., Gottsmann, J., Cashman, K., Gutiérrez, E., 2016. Magma storage in a strike-slip caldera. Nat. Commun. 7, 12295.
Šebesta, J., 2007. Geomorfología del AMSS y su relación con los movimientos de ladera. Open file report, Czech Geological Survey Prague Oficina de Planificación del Área Metropolitana de San Salvador (OPAMSS): pp 1–40.
Self, S., Sparks, R.S.J., 1978. Characteristics of widespread pyroclastic deposits formed by the interaction of silicic magma and water. Bull. Volcanol. 41 (3), 196.
Siebert, L., Simkin, T., 2002. Volcanoes of the World: an Illustrated Catalogue of Holocene Volcanoes and their Eruptions. Smithsonian Institution, Global Volcanism Program Digital Information Series, GVP-3. http://www.volcano.si.edu/world/.

Sigl, M., Winstrup, M., McConnell, J.R., Welten, K.C., Plunkett, G., Ludlow, F., Büntgen, U., Caffee, M., Chellman, N., Dahl-Jensen, D., 2015. Timing and climate forcing of volcanic eruptions for the past 2,500 years. Nature 523 (7562), 543.

Simkin, T., Siebert, L., 1994. Volcanoes of the. World2nd Ed. Geoscience Press, Tucson.

Smith, J.V., Brown, W.L., 1988. Spectroscopy–IR, Raman, NMR, NQR, EPR, NGR (Mössbauer), XAS, EXAFS, ESCA, XPS, Feldspar Minerals. Springer 244-267.

Smith, V.C., Isaia, R., Engwell, S.L., Albert, P.G., 2016. Tephra dispersal during the Campanian Ignimbrite (Italy) eruption: implications for ultra-distal ash transport during the large caldera-forming eruption. Bull. Volcanol. 78 (6), 45.

Sofield, D., 2004. Eruptive history and volcanic hazards of Volcan San Salvador. Geol. Soc. Am. Spec. Pap. 375, 147-158.

Sohn, Y.K., Chough, S.K., 1989. Depositional processes of the Suwolbong tuff ring, Cheju Island (Korea). Sedimentology 36 (5), 837-855.

Solgevik, H., Mattsson, H.B., Hermelin, O., 2007. Growth of an emergent tuff cone: Fragmentation and depositional processes recorded in the Capelas tuff cone, São Miguel, Azores. J. Volcanol. Geotherm. Res. 159 (1), 246-266.

Sonder, I., Graettinger, A.H., Valentine, G.A., 2015. Scaling multiblast craters: General approach and application to volcanic craters. J. Geophys. Res. Solid Earth 120 (9), 6141–6158.

Sparks, R.S.J., Wilson, L., Sigurdsson, H., 1981. The pyroclastic deposits of the 1875 eruption of Askja, Iceland. Philosophical transactions of the Royal Society of London. Series A, Math. Phys. Sci. 299 (1447), 241-273.

Suñe-Puchol, I., Aguirre-Díaz, G.J., Dávila-Harris, P., Miggins, D.P., Pedrazzi, D., Costa, A., Ortega-Obregón, C., Lacan, P., Hernández, W., Gutiérrez, E., 2019a. The Ilopango caldera complex, El Salvador: Origin and early ignimbrite-forming eruptions of a graben/pull-apart caldera structure. J. Volcanol. Geotherm. Res. 371, 1–19.

Suñe-Puchol, I., Aguirre-Díaz, G.J., Pedrazzi, D., Dávila-Harris, P., Miggins, D.P., Costa, A., Ortega-Obregón, C., Lacan, P., Gutierrez, E., Hernández, W., 2019b. Stratigraphic revision of the complete eruptive sequence and recurrence of large explosive eruptions. The Ilopango Caldera Complex. J. Volcanol. Geotherm. Res. 374, pp. 100-119 (El Salvador).

Taddeucci, J., Valentine, G.A., Sonder, I., White, J.D.L., Ross, P.S., Scarlato, P., 2013. The effect of pre-existing craters on the initial development of explosive volcanic eruptions: an experimental investigation. Geophys. Res. Lett. 40 (3), 507-510.

Turner Henry, L., LaFemina, P., Saballos, A., Mattioli Glen, S., Jansma Pamela, E., Dixon, T., 2007. Kinematics of the Nicaraguan forearc from GPS geodesy. Geophys. Res. Lett. 34 (2).

Valentine, G.A., White, J.D.L., 2012. Revised conceptual model for maar-diatremes: Subsurface processes, energetics, and eruptive products. Geology 40 (12), 1111–1114.

Valentine, G.A., Graettinger, A.H., Sonder, I., 2014. Explosion depths for phreatomagmatic eruptions. Geophys. Res. Lett. 41 (9), 3045-3051.

Valentine, G.A., Graettinger, A.H., Macorps, É., Ross, P.-S., White, J.D.L., Döhring, E., Sonder, I., 2015. Experiments with vertically and laterally migrating subsurface explosions with applications to the geology of phreatomagmatic and hydrothermal explosion craters and diatremes. Bull. Volcanol. 77 (3), 15.

Vallance, J., Houghton, B., 1998. The AD 260 Eruption at Lake Ilopango. A complex explosive eruption through a caldera lake. National Science Foundation, Research Proposal, El Salvador.

Weber, H.S., Wiesemann, G. and Wittekindt, H., 1974. Mapa Geológico de la República de El Salvador/Geologische Übersichtskarte der Republik El Salvador 1: 500,000 (after geological maps 1:100000 – 1967-74) Bundesanstalt für Geowissenschaften und Rohstoffe, Hannover; Bundesanstalt fu¨r Bodenforschung, (Hannover).

White, J.D.L., Houghton, B.F., 2006. Primary volcaniclastic rocks. Geology 34 (8), 677–680.

Wilkie, J.W. and Guadalupe Ortega, J., 1997 Statistical Abstracts of LatinAmerica. 33, the Regents of the University of California, Los Angeles.

Willcock, M.A.W., Cas, R.A.F., Giordano, G., Morelli, C., 2013. The eruption, pyroclastic flow behaviour, and caldera in-filling processes of the extremely large volume (N1290 km^3), intra- to extra-caldera, Permian Ora (Ignimbrite) Formation, Southern Alps, Italy. J. Volcanol. Geotherm. Res. 265, 102-126.

Williams, H., Meyer-Abich, H., 1955. Volcanism in the Southern Part of El Salvador: With Particular Reference to the Collapse Basins of Lakes Coatepeque and Ilopango. University of California Press.

6. Discusiones y trabajos futuros

La caldera de Ilopango, considerada como poligenética, ha sufrido múltiples colapsos caldéricos a lo largo de su historia que han provocado grandes erupciones explosivas. Por ahora se han identificado 13 erupciones piroclásticas cuaternarias emitidas por esta caldera, las cuales están casi todas relacionadas a colapsos caldéricos totales o parciales. Todos estos materiales piroclásticos forman parte del Grupo Ilopango, introducido en este trabajo siguiendo la metodología actual de estratigrafía volcánica publicada por Martí et al. (2018). El Grupo Ilopango se subdivide en tres Formaciones, de la más antigua a la más reciente son: 1) Formación Comalapa (1.78 – 1.32 Ma); 2) Formación Altavista (918 – 257 ka), y 3) Formación Tierras Blancas (< 57 ka). Cada formación del Grupo Ilopango está constituida por varios miembros, formados por los depósitos asociados a diferentes erupciones explosivas. Estas erupciones han sido muy variadas, desde columnas eruptivas que han depositado espesas capas de pómez, a flujos piroclásticos densos y diluidos, tanto de origen magmático como hidromagmático.

La Fm. Comalapa la constituyen las tres primeras grandes erupciones explosivas de la caldera de Ilopango, las cuales han generado las ignimbritas más voluminosas emitidas por esta caldera. Éstas son: 1) la Ignimbrita soldada de Olocuilta (OI, 1.785 ± 0.006 Ma), que cubrió un área de ~3,000 km^2 con un volumen mínimo de 50 km^3 DRE, pero que podría llegar a considerarse como el producto de una Supererupción (más de 350 km^3 DRE; Miller y Wark, 2008) si tenemos en cuenta la ceniza coignimbrítica distal, el relleno caldérico, el material erosionado y los piroclastos que llegaron al océano. 2) La Ignimbrita Colima (CoI, 1.56 ± 0.01 Ma) y 3) la Ignimbrita Apopa (ApI~1.34 Ma), fueron de menor magnitud que la primera erupción, pero mucho mayores que la TBJ (> 40 km^3), pudiendo llegar a superar el VEI 7 (100 km^3 de tefra emitida). Estas dos últimas erupciones, marcan un cambio en los procesos eruptivos provocados por la interacción del magma con el agua del lago de Ilopango formado a raíz de los dos primeros colapsos de la caldera. La interacción hidrovolcánica genera un aumento en la explosividad de la erupción y la fragmentación de los piroclásticos, lo que produce depósitos mucho menos consolidados como los de la Colima y la Apopa, provocando una mayor susceptibilidad a la erosión y complicando una estimación más real de su volumen original.

Los depósitos de las siguientes seis erupciones explosivas forman parte de la Fm. Altavista. Sus miembros son: 1) la Ignimbrita Cojutepeque (CojI, 918.8 ± 17.4 ka), 2) la Ignimbrita Delgado (DeI, 830 ± 140 ka), 3) la Ignimbrita Manigua (ManI, 768.3 ± 49.4 ka), 4) la caída de pómez San Juan (SJF, 625.0 ± 75.1 ka), 5) la Ignimbrita Cortez (CorI, 553.0 ± 16.6 ka), y 6) la Ignimbrita Soyapango (SoI, 257 ± 33 ka). Estas tobas están muy mal preservadas y tienen muy poca continuidad lateral debido a la poca consolidación de los materiales piroclásticos de origen mayormente hidrovolcánico. Los depósitos de la Fm. Altavista solamente se exhiben en el flanco norte de la caldera, sobretodo en cortes profundos de carretera. Aun así, se ha podido hacer una estimación aproximada del volumen de estas tobas, las cuales tienen todas de 1-5 km^3 DRE como mínimo, siendo la ignimbrita Delgado la mayor de todas, la cual podría llegar a superar los 40 km^3 DRE si consideramos los depósitos erosionados.

Los depósitos de las cuatro erupciones explosivas más recientes de la caldera de Ilopango (TB4, TB3, TB2 y TBJ), constituyen la Fm. Tierras Blancas (TB's), siendo las únicas que se habían identificado y caracterizado antes de esta investigación. El estudio geocronológico realizado para fechar todas las otras erupciones explosivas más viejas que las TB's (< 57 ka; Rose et al., 1999), ha permitido detallar una historia volcánica más completa de la caldera de Ilopango. El diagrama de la **Fig. 13** ilustra las edades de estas erupciones explosivas antiguas. Como se aprecia en este cronograma, las erupciones de la Fm. Comalapa tienen un tiempo de recurrencia el doble de largo que las erupciones de la Fm. Altavista. Mientras las tres primeras Ignimbritas (OI, CoI y ApI; recuadro punteado azul de la **Fig. 13**), tienen hiatos de hasta 220 ka entre erupciones, las siguientes seis erupciones (CojI, DeI, ManI, SJF, CorI y SoI; recuadro punteado verde de la **Fig. 13**) tienen periodos de inactividad inter-eruptivos sobre los 100 ka. Mucho más corto es el periodo de retorno para las erupciones explosivas de la Fm. Tierras Blancas (recuadro punteado rojo de la **Fig. 13**). Además, destacan los periodos largos de inactividad que hay entre las diferentes formaciones, con más de 400 ka de quietud entre la Fm. Comalapa y la Altavista (elipsoide punteada naranja de la **Fig.13**), o los 200 ka entre la Altavista y las Tierras Blancas (elipsoide punteada amarilla de la **Fig. 13**).

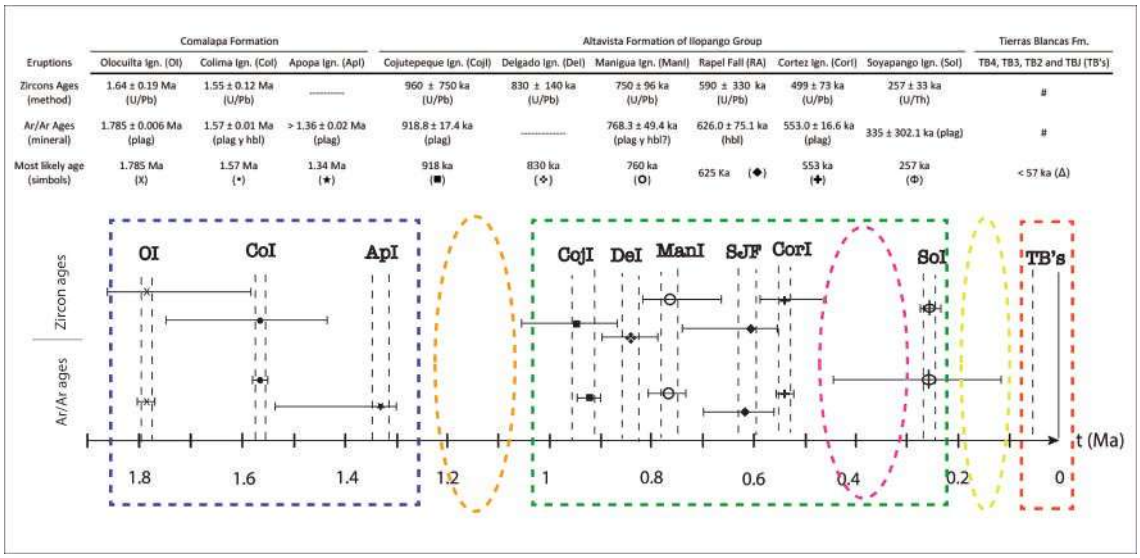

Fig. 13: Cronograma de las erupciones explosivas de la caldera de Ilopango, desde la formación de la primera ignimbrita hace 1.785 Ma (OI), hasta las últimas tobas (TB's). El cronograma resalta el largo período de inactividad entre las Formaciones Comalapa y Altavista (elipsoide de puntos naranjas), y también el largo hiato volcánica entre las Formaciones de Altavista y Tierras Blancas (elipsoide de puntos amarillos). El período de recurrencia dentro de las erupciones de la Formación Comalapa (~ 220 ka, rectángulo de puntos azules) es dos veces más largo que las erupciones de la Formación Altavista (~ 100 ka, rectángulo de puntos verdes), y mucho más alto que las erupciones de la Formación Tierras Blancas (~20ka). El elipsoide discontinuo fucsia representa un hiato volcánico >200 ka dentro de las erupciones de la Formación Altavista, entre las ignimbritas de Cortez y Soyapango (CorI y, SoI).

Estos periodos de recurrencia similares para las erupciones de una misma formación, pero tan variables entre erupciones de diferentes formaciones, así como los largos intervalos de inactividad volcánica que hay entre formaciones, podrían ser causados por cambios en el régimen tectónico a lo largo de la Zona de Falla de El Salvador (ZFES), y más concretamente al origen y evolución del *Pull-Apart* de San Salvador. Parece ser que la génesis de la caldera de Ilopango estuvo estrechamente ligada a la tectónica regional de El Salvador, colapsando primero en una caldera tipo graben durante un periodo extensional en la ZFES, para posteriormente transformarse en una caldera tipo *pull-apart* al mismo tiempo que la ZFES evolucionaba hacia un régimen más transtensivo, el cual continúa hasta el presente, en donde la actividad volcánica sigue vinculada a las fallas regionales, tal y como lo demuestra la erupción de las Islas Quemadas en 1879, emplazadas justo después de un terremoto tectónico provocado por la falla San Vicente.

En los últimos años varios autores han realizado trabajos sobre las Tierras Blancas, sobretodo en la TBJ, la última gran erupción explosiva de la caldera de

Ilopango. Durante esta investigación y en colaboración con otros participantes del proyecto Ilopango, se condujo un trabajo estratigráfico detallado y un análisis granulométrico del depósito piroclástico TBJ, a partir del cual se pudieron identificar ocho fases distintas de la erupción, caracterizadas por estilos y procesos eruptivos diversos, cada uno con sus propias características y sin pausas mayores de actividad entre ellas. La erupción TBJ inició con una explosión tipo "blast", seguida de dos fases de caída de tefra producidas por columnas eruptivas. Posteriormente la erupción se desarrolló con una interacción del magma con el agua del lago Ilopango y la formación de flujos piroclásticos (PDCs) densos y diluidos del tipo hidrovolcánico, dando lugar al colapso caldérico y la consecuente evacuación rápida de la ignimbrita paroximal. Como última fase, la ceniza fina elutriada durante la erupción de los PDCs en forma de nube coignimbritica se deposita, distribuyendose a lo largo y ancho de todo el país, con alturas estimadas de hasta 45 km sobre la superficie terrestre. El depósito de la TBJ llegó a acumular hasta 70 m de espesor en las cercanias de la caldera y nuevos cálculos en desarrollo por el equipo del Proyecto Ilopango estiman un volumen mínimo de ~58 km^3 de tefras expulsados durante esta erupción (~30 km^3 DRE). En colaboración con los participantes del proyecto se elaboraron nuevos mapas de isopacas en base a la estratigrafía, distribución de los depósitos y datos granulométricos detallados, mediate los cuales se calcularon parámetros físicos como la altura de la columna, la duración de la erupción, y la tasa de emisión. La erupción TBJ fue cataclismica y está considerada la mayor erupción explosiva del Holoceno en Centroamérica.

Todos los productos piroclásticos de la CI son calcoalcalinos ricos en sílice, de composición riolítica a dacítica, con contenido medio-alto en potasio, típico de los magmas producidos en zonas de subducción en márgenes continentales, como es el caso del Arco Volcánico Centroamericano. La mineralogía que presentan son mayormente plagioclasas y hornblendas, con presencia de piroxenos, con cuarzo para las unidades más riolíticas y con pequeñas cantidades de biotita en algunos depósitos. Todas las ignimbritas y caídas de pómez presentan minerales accesorios como los circones, apatitos o óxidos de Fe-Mg. Las unidades de CI no contienen ningún sanidino.

Trabajos futuros

Todavía siguen en curso otros trabajos de este proyecto de investigación, como por ejemplo el estudio tefro-estratigráfico sobre los depósitos de las últimas erupciones explosivas de la caldera de Ilopango (las TB's de la Fm. Tierras Blancas). Por ahora se ha realizado ya el mapeo geológico y el levantamiento estratigráfico en campo para caracterizar estas erupciones, y se han descrito con más detalle y elaborado estimaciones de magnitud y volumen para conocer el alcance de estas erupciones. Falta terminar el estudio geocronológico por medio de técnicas $^{238}U/^{230}Th$ y Ar^{39}/Ar^{40}, y en particular de radiocarbono en la unidad TBJ. De esta manera se podrían integrar estos nuevos datos más precisos con las edades de los paleoterremotos registrados a lo largo de la traza de la falla San Vicente (Canora et al., 2012), y hacer una reevaluación del peligro considerando esta relación vulcano-tectónica. La de San Vicente es una falla principal del Pull-Apart de San Salvador que afecta la caldera de Ilopango y que parece estar controlando la actividad actual de este volcán, es por eso que creemos que se debe considerar a estas dos estructuras (falla + caldera) como un único sistema natural.

Otro trabajo específico es el que se está realizando sobre la TBJ, la erupción explosiva más reciente de la caldera y ocurrida hace tan solo ~1500 años (Dull et al., 2010). Una vez determinados los procesos eruptivos, la distribución y el volumen de sus productos, así como otros parámetros físicos de la erupción, el enfoque de la investigación se centra ahora en evaluar en el impacto que tuvo esa erupción sobre las poblaciones Mayas contemporáneas y en el medio ambiente.

7. Conclusiones

- La caldera de Ilopango se originó hace 1.785 ± 0.006 Ma y ha tenido una formación cíclica, con múltiples colapsos caldéricos asociados a las estructuras tectónicas de la Zona de Falla de El Salvador. Primero colapsó en una caldera tipo graben, que evolucionó a una caldera tipo *pull-apart*, régimen que continua hasta el presente con un aumento paulatino de la componente lateral.
- A lo largo de su historia, la caldera de Ilopango ha generado al menos 13 erupciones explosivas de gran magnitud, con un volumen mínimo por evento de 1-5 km^3 DRE, y pudiendo llegar hasta los 350 km^3 DRE para la primera ignimbrita (VEI ~ 8, parámetros de supererupción), la cual se soldó y ocupó un área de ~3,000 km^2. Se propone una nueva nomenclatura estratigráfica donde todas las tobas de la caldera de Ilopango se han incluyen en el Grupo Ilopango, el cual comprende las formaciones Comalapa, Altavista y Tierras Blancas.
- La Fm. Comalapa (1.78 – 1.34 Ma) está formada por los miembros Olocuilta, Colima y Apopa. La Fm. Altavista (918 – 257 ka) por los miembros Cojutepeque, Delgado, Manigua, San Juan, Cortez y Soyapango. La Fm. Tierras Blancas (<57ka) por lo miembros TB4, TB3, TB2 y TBJ. Las erupciones que formaron todos estos miembros fueron muy diversas: columnas eruptivas puramente magmáticas, flujos piroclásticos diluidos de origen hidromagmático (interacción con el lago de Ilopango) o PDC's magmáticos eyectados sostenida y radialmente desde la caldera.
- Los periodos de recurrencia para grandes erupciones explosivas en la caldera de Ilopango son variables, con ~220 ka durante las primeras tres erupciones (Fm. Comalapa), ~100 ka para las 6 erupciones intermedias (Fm. Altavista), y ~20 ka para las últimas 4 erupciones (Fm. Tierras Blancas). Entre las erupciones de las diferentes formaciones, hay intervalos de inactividad muy largos, hasta 400 ka entre la Fm. Comalapa y la Fm. Altavista, o 200 ka entre Fm. Altavista y Fm. Tierras Blancas. Esta distribución de la actividad volcánica en el tiempo, podría estar

determinada por cambios en el contexto tectónico regional, el cual controla el ascenso de magma a la superficie con las fallas profundas strike-slip y las cuencas pull-apart de la ZFES.

- Los productos piroclásticos de la caldera de Ilopango son riolitas y riodacitas calcoalcalinas, con contenidos medio-alto en K, ricas en plagioclasa y hornblenda, con biotita ocasional y piroxeno. No contiene sanidino. Características químicas típicas de magmas de subducción en márgenes continentales, como es el caso del Arco Volcánico de Centroamérica.

- La última erupción explosiva de la caldera de Ilopango generó un extenso depósito blanco de pómez y ceniza (la TBJ) que cubrió todo El Salvador y parte de los países vecinos de Guatemala, Honduras y Nicaragua. La TBJ fue una gran erupción hidrovolcánica con 8 fases diferentes (columnas eruptivas y flujos piroclásticos), con un volumen eyectado de hasta 30 km^3 DRE, y dispersión de cenizas hasta los 45 km de altura que quedaron por años en la estratosfera pudiendo afectar el clima global terrestre. Con dataciones dendrocronológicas aún por terminar, se sabe que la TBJ ocurrió hace unos 1500 años, la cual afectó catastróficamente a las poblaciones Mayas de la zona y es considerada la mayor erupción del Holoceno en Centroamérica. Si hoy en día ocurriera una erupción similar a las TB's, provocaría un desastre incalculable para la población metropolitana de San Salvador que con más de 3 millones de personas, es el núcleo urbano más habitado de Centroamérica.

- La presente investigación sobre la caldera de Ilopango presentada en esta tesis de doctorado, ha dado como resultado la publicación de tres artículos publicados en revistas indexadas, los cuales representan en los Capítulos 3, 4 y 5.

8. Referencias

Acocella, V., Korme, T., Salvini, F., Funiciello, R., 2002. Elliptic calderas in the Ethiopian Rift: the control of pre-existing structures. J. Volcanol. Geotherm. Res. 119, 189– 203.

Acocella, V. 2007. Understanding caldera structure and development: an overview of analogue models compared to natural calderas. Earth-Sciences Reviews, 85, 125–160.

Acocella, V. 2008. Structural development of calderas: a synthesis from analogue experiments. In:

Agostini, S., Corti, G., Doglioni, C., Carminati, E., Innocenti, F., Tonarini, S., Manetti, P., Di Vincenzo, G., Montanari, D., 2006. Tectonic and magmatic evolution of the active volcanic front in El Salvador: insight into the Berlín and Ahuachapán geothermal areas. Geothermics 35, 368–408. doi:10.1016/j.geothermics.2006.05.003

Aguirre-Díaz, G.J., Labarthe-Hernández, G., 2003. Fissure ignimbrites: fissure source origin for voluminous ignimbrites of the Sierra Madre Occidental and its relationship with Basin and Range faulting. Geology, 31, 773–776.

Aguirre-Díaz, G.J., Labarthe-Hernández, G., Tristán-González, M., Nieto-Obregón, J., Gutiérrez- Palomares, I., 2007. Graben-calderas. Volcano-tectonic explosive collapse structures of the Sierra Madre Occidental, Mexico. European Geosciences Union Annual Meeting at Viena, Geophysical Research Abstracts, 9, 04704.

Aguirre-Díaz, G.J., Labarthe-Hernández, G., Tristán-González, M., Nieto-Obregón, J., Gutiérrez-Palomares, I., 2008. Ignimbrite Flare-up and graben-calderas of the Sierra Madre Occidental, Mexico: in J. Gottsmann, and J. Martí, eds., "Caldera Volcanism: Analysis, Modelling and Response", Developments in Volcanology 10, Elsevier, Amsterdam, 492 p., (143-180 pp.), ISBN 978-0-444-53165-0, doi: 10.1016/S1871-644X(07)00004-6.

Aguirre-Díaz, J.G., Suñe-Puchol, I., Davila-Harris, P., Pedrazzi, D., Hernandez, W. and Gutierrez, E., 2017. Volcanic history of the Ilopango caldera, Central American

Volcanic Arc. 113th Annual Meeting, 2017 GSA Cordilleran Section, Hawaii, USA.

Alonso-Henar, J., Schreurs, G., Martinez-Díaz, J.J., Álvarez-Gõmez, J.A., Villamor, P., 2015. Neotectonic development of the El Salvador Fault Zone and implications for deformation in the Central America Volcanic Arc: Insights from 4-D analog modeling experiments. Tectonics 34, 133–151. doi:10.1002/2014TC003723

Alonso-Henar, J., Álvarez-Gõmez, J.A. and Martinez-Díaz, J.J., 2017. Neogene-quaternary evolution from transpressional to transtesional tectonics in Northern Central America controlled by cocos: Caribbean subduction coupling change. J Iber Geol. DOI 10.1006/s415113-017-0034-2.

Alvarado, D., DeMets, C., Tikoff, B., Hernandez, D., Wawrzyniec, T.F., Pullinger, C., Mattioli, G., Turner, H.L., Rodriguez, M., Correa-Mora, F., 2011. Forearc motion and deformation between El Salvador and Nicaragua: GPS, seismic, structural, and paleomagnetic observations. Lithosphere 3, 3–21. doi:10.1130/L108.1

Alvarenga, E.R., Hernández, D.A., Hernández-Flores, D.A., 2001, Cronología de sismos destructivos en El Salvador: Servicio Geológico Nacional, Área de Sismología.

Arqueología Mexicana, 2010, Culturas prehispánicas de México, Edición Especial 34, pp. 44-49

Authemayou, C., Brocard, G., Teyssier, C., Simon-Labric, T., Guttiérrez, A., Chiquín, E.N., Morn, S., 2011. The Caribbean-North America-Cocos Triple Junction and the dynamics of the Polochic-Motagua fault systems: Pull-up and zipper models. Tectonics 30, 1–23. doi:10.1029/2010TC002814

Bacon, C.R., 1983. Eruptive history of Mount Mazama and Crater Lake Caldera, Cascade Range, USA. J. Volcanol. Geotherm.Res. 18, 57–115.

Beresford, S.W., Cole, J.W., 2000. Kaingaroa Ignimbrite, Taupo Volcanic Zone, New Zealand: evidence for asymmetric caldera subsidence of the Reporoa Caldera. N.Z. J. Geol. Geophys 43, 471– 481.

Bernal, J.P. and Lozano-Santacruz, R., 2005. Characterization of a new set of eight geochemical reference materials for XRF major and trace element analysis. Revista Mexicana de Ciencias Geológicas, 22(3): 329-344.

Bernal, J.P., Solari, L.A., Gómez-Tuena, A., Ortega-Obregón, C., Mori, L., Vega-González, M., Espinosa-Arbeláez, D.G., 2014. In-situ230Th/U dating of Quaternary zircons using LA-MCICPMS. Quat. Geochronol. 23, 46–55. doi:10.1016/j.quageo.2014.06.003

Bibby, H.M., Caldwell, T.G., Davey, F.J., Webb, T.H., 1995. Geophysical evidence on the structure of the Taupo Volcanic Zone and its hydrothermal circulation. J. Volcanol. Geotherm. Res. 68, 29–58.

Bonadonna, C. and Costa, A., 2012. Estimating the volume of tephra deposits: A new simple strategy. Geology, 40(5): 415-418.

Bonadonna, C. and Costa, A., 2013. Plume height, volume, and classification of explosive volcanic eruptions based on the Weibull function. Bulletin of Volcanology, 75(8): 742.

Branney MJ, Kokelaar P (1994) Volcanotectonic faulting, softstate deformation, and rheomorphism of tuffs during development of a piecemeal caldera, English Lake District. Geol Soc Am Bull 106: 507–530

Canora, C., Villamor, P., Martínez-Díaz, J.J., Berryman, K.R., Álvarez-Gómez, J.A., Capote, R. y Hernández, W., 2012, Paleoseismic analysis of the San Vicente segment of the El Salvador Fault Zone, EL Salvador, Central America. Geologica Acta, Vol. 10, Nº 2, DOI: 10. 1344/105.000001700

Canora, C., Martínez-Díaz, J.J., Villamor, P., Staller, A., Berryman, K., Álvarez-Gómez, J.A., Capote, R., Diaz,M., 2014. Structural evolution of the El Salvador Fault Zone: an evolving fault system within a volcanic arc. J. Iber. Geol. 40, 471–488.

Carr, M.J., 1976. Underthrusting and Quaternary faulting in northen Central America. Geol. Soc. Am. Bull. 87, 825–829. doi:10.1130/0016-7606(1976)87<825:UAQFIN>2.0.CO;2

Carr, M., Patiño, L., Feingenson, M., 2007. Chapter 22: Petrology and geochemistry of lavas. Cent. Am. Geol. Resour. hazards 1–26.

Cas, R.A.F. and Wright, J.V., 1987, Volcanic Successions. Modern and ancient. Allen & Unwin, London, 528 p.

CEL (Comision Ejecutiva Hidroelectrica del Rio Lempa), 1992. Desarrollo de los

Recursos Geotermicos del Area Centro-Occidental de El Salvador. Prefactibilidad Geotermica del Area de Coatepeque. Reconocimiento Geotermico. Informe Final. Internal report.

Cole, J.W., Milner, D.M., and Spinks, K.D., 2005. Calderas and caldera structures: a review. Earth Science Reviews, v. 69, p. 1–96.

Corti, G., Carminati, E., Mazzarini, F., Garcia, M.O., 2005. Active strike-slip faulting in El Salvador, Central America. Geology, 33, 989-992.

Costa, A., Dell'Erba, F., Di Vito, M.A., Isaia, R., Macedonio, G., Orsi, G. and Pfeiffer, T., 2009. Tephra fallout hazard assessment at the Campi Flegrei caldera (Italy). Bulletin of Volcanology, 71(3): 259.

Costa A., Smith V., Macedonio G., Matthews N., 2014. The magnitude and impact of the Youngest Toba Tuff super-eruption, Front. Earth Sci., 2, 16, doi:10.3389/feart.2014.00016.

DeMets, C., 2001. A new estimate for present-day Cocos-Caribbean plate motion:Implications for slip along the Central American volcanic arc. Geophys. Res. Lett. 28, 4043–4046. doi:10.1029/2001GL013518

de Silva, S.L., and Gosnold, W.A., 2007. Episodic construction of batholiths: Insights from the spatiotemporal development of an ignimbrite flare-up: Journal of Volcanology and Geothermal Research, v. 167, p. 320–335, doi: 10.1016/j.jvolgeores.2007.07.015

Dixon, T.H., 1993, GPS measurement of relative motion of the Cocos and Caribbean plates and strain accu- mulation across the Middle America Trench: Geo- physical Research Letters, v. 20, p. 2167–2170, doi: 10.1029/93GL02415.

Donnelly T.W., Horne G.S., Finch R.C., Lopez-Ramos E., 1990. Northern Central America: the Maya and Chortis blacks. In: Dengo G, Case JE (eds) The geology of North America: the Caribbean region, pp :37–76

Dull, R.A., Southon, J.R. and Sheets, P., 2001. Volcanism, Ecology and Culture: A Reassessment of the Voclán Ilopango TBJ eruption in the Southern Maya Realm, v. 12, No. 1, pp. 25-44.

Dull, R.A., Southon, J.R., Kutterolf, S., Freundt, a., Wahl, D., Sheets, P., 2010. Did the

TBJ Ilopango eruption cause the AD 536 event? AGU Fall Meet. Abstr. 1, 2370.

Druitt, T.H. and Sparks, R.S.J., 1984, On the formation of calderas during ignimbrite eruptions. Nature, v. 310, p. 679–681.

Dvorak, J.J., Dzurisin, D., 1997. Volcano geodesy: the search for magma reservoirs and the formation of eruptive vents. Rev. Geophys. 35, 343–384.

Francis, P.W., O'Callaghan, L., Kretzschmar, G.A., Thorpe, R.S., Sparks, R.S.J., Page, R.N., 1983. The Cerro Galan ignimbrite. Nature 301, 51– 53.

Funk, J., Mann, P., McIntosh, K., Stephens, J., 2009. Cenozoic tectonics of the Nicaraguan depression, Nicaragua, and Median Trough, El salvador, based on seismic-reflection profiling and remote-sensing data. Bull. Geol. Soc. Am. 121, 1491–1521. doi:10.1130/B26428.1

Garibaldi, N., Tikoff, B., Hernández, W., 2016. Neotectonic deformation within an extensional stepover in El Salvador magmatic arc, Central America: Implication for the interaction of arc magmatism and deformation. Tectonophysics 693, 327–339. doi:10.1016/j.tecto.2016.05.015

Geyer, A. & Martí, J. 2008. The new worldwide collapse caldera database (CCDB): a tool for studying and understanding caldera processes. Journal of Volcanology and Geothermal Research, 175, 334–354.

Golombek, M.P., Carr, M.J., 1978. Tidal triggering of seismic and volcanic phenomena during the 1879-1880 eruption of Islas Quemadas volcano in El Salvador, Central America. J. Volcanol. Geotherm. Res. 3, 299–307. doi:10.1016/0377-0273(78)90040-9

Gottsmann, J. and Martí, J., 2008, Caldera Volcanism: Analysis, Modelling and Response, Developments in Volcanology 10, Elsevier, Amsterdam, 492 p.

Grube, N. (ed.) 2006, Los mayas. Una civilización milenaria: Tandem Verlag GmbH: Ullmann & Könemann. ISBN 978-3-8331-1959-0.

Guillou - Frottier, L., Burov, E. B. & Milé SI, J.-P. 2000. Genetic links between ash-flow calderas and associated ore deposits as revealed by large scale thermo-mechanical modeling. Journal of Volcanology and Geothermal Research, 102, 339–361

Guzmán-Speziale, M., Valdés-González, C., Molina, E., Gómez, J.M., 2005. Seismic

activity along the Central America volcanic arc: Is it related to subduction of the Cocos plate? Tectonophysics 400, 241–254. doi:10.1016/j.tecto.2005.03.006

Hansen, J., Sato, M., Ruedy, R. y 27 otros, 1996. A Pinatubo climate modelling investigation. In: Fiocco G, Fua D, Visconti G (eds) The Mount Pinatubo Eruption: Effects on the Atmosphere and Climate. NATO Advanced Study Institute Series 14, Springer-Verlag Heidelberg, pp 233-272

Hallinan, S., 1993. Nonchaotic collapse at funnel calderas: gravity study of the ring fractures at Guayabo caldera, Costa Rica. Geology 21,367–370.

Hart, W.J., and Steen McIntyre, V., (1983). Tierra Blanca Joven Tephra from the AD 260 Eruption of Ilopango Caldera: in Archeology and Volcanism in Central America. University of Texas Press, Austin, Texas, p. 14-34.

Heiken, G., Goff, F., Stix, J., Tamanyu, S., Shafiqullah, M., Garcia, S., 1986. Intracaldera volcanic activity, Toledo Caldera and embayment, Jemez Mountains, New Mexico. J. Geophys. Res. 91B, 1799– 1815.

Hernández, E.W., 2004. Características geotécnicas y vulcanológicas de las tefras de Tierra Blanca Joven de Ilopango, El Salvador: Tesis de maestría, Univ. Politécnica de El Salvador, San Salvador, 115 p.

Hildreth, W., Christiansen, R.L., O'Neil, J.R., 1984. Catastrophic isotopic modification of rhyolitic magma at times of caldera subsidence, Yellowstone plateau volcanic field. J. Geophys. Res. 89B, 8339–8369.

Holohan, E.P., Van Wyk de Vries, B., Troll, V.R., 2008. Analogue models of caldera collapse in strike-slip tectonic regimes. Bull. Volcanol. 70, 773–796. doi:10.1007/s00445-007-0166-x

Hutton D.H.W., Reavy R.J., 1992. Strike-slip tectonics and granite petrogenesis. Tectonics 11:960–967

Jochum Klaus, P., Stoll, B., Herwig, K., Willbold, M., Hofmann, A.W., Amini, M., Aarburg, S., Abouchami, W., Hellebrand, E., Mocek, B., Raczek, I., Stracke, A., Alard, O., Bouman, C., Becker, S., Dücking, M., Brätz, H., Klemd, R., de Bruin, D., Canil, D., Cornell, D., de Hoog, C.J., Dalpé, C., Danyushevsky, L., Eisenhauer, A., Gao, Y., Snow, J.E., Groschopf, N., Günther, D., Latkoczy, C., Guillong, M., Hauri, E.H., Höfer, H.E., Lahaye, Y., Horz, K., Jacob, D.E., Kasemann, S.A., Kent, A.J.R., Ludwig, T., Zack, T., Mason, P.R.D., Meixner, A.,

Rosner, M., Misawa, K., Nash, B.P., Pfänder, J., Premo, W.R., Sun, W.D., Tiepolo, M., Vannucci, R., Vennemann, T., Wayne, D. and Woodhead, J.D., 2006. MPI-DING reference glasses for in situ microanalysis: New reference values for element concentrations and isotope ratios. Geochemistry, Geophysics, Geosystems, 7(2).

Koppers, A. A. P., 2002. ArArCALC—Software for 40Ar/39Ar age calculations, Comput. Geosci., 28(5), 605–619, doi:10.1016/S0098-3004(01)00095-4.

Koppers, A.A.P., Gowen, M.D., Colwell, L.E., Gee, J.S., Lonsdale, P.F., Mahoney, J.J., Duncan, R.A., 2011. New 40Ar/39Ar age progression for the Louisville hot spot trail and implications for inter–hot spot motion. Geochem. Geophys. Geosyst. 12:Q0AM02. http:// dx.doi.org/10.1029/2011GC003804.

Kuiper, K.F., Deino, A., Hilgen, F.J., Krijgsman, W., Renne, P.R., Wijbrans, J.R., 2008. Synchronizing rock clocks of Earth history. Science 320:500–504. http://dx.doi.org/10. 1126/science.1154339.

Kutterolf, S., Freundt, A., Schacht, U., Bürk, D., Harders, R., Mörz, T., Peréz, W., 2008. Pacific offshore record of plinian arc volcanism in Central America: 3. Application to forearc geology. Geochemistry, Geophys. Geosystems 9. doi:10.1029/2007GC001826

La Femina, P., Dixon, T., and Strauch, W., 2002, Bookshelf faulting in Nicaragua: Geology, v. 30, p. 751–754, doi: 10.1130/0091-7613(2002)030<0751:BFIN>2.0.CO;2.

LaFemina, P., Dixon, T.H., Govers, R., Norabuena, E., Turner, H., Saballos, A., Mattioli, G., Protti, M., Strauch, W., 2009. Fore-arc motion and Cocos Ridge collision in Central America. Geochemistry, Geophys. Geosystems 10. doi:10.1029/2008GC002181

LeBas et al. 1986. A chemical classification of volcanic rocks based on the total alkali-silica diagram: Journal of Petrology, v. 27, p. 745-750.

Lexa, J., Šebesta, J., Chavez, J.A., Hernández, W., Pécskay, Z., 2011. Geology and volcanic evolution in the southern part of the San Salvador Metropolitan Area. J. Geosci. 56, 105–140. doi:10.3190/jgeosci.088

Lipman PW (1984) The roots of ash-flow calderas in North America: windows into the tops of granitic batholiths. J Geophys Res 89 :8801–8841

Lipman, P.W., 1995. Subsidence of ash-flow calderas; role of magma chamber geometry. IUGG Gen. Assem. 21 (Week A), 452.

Lipman, P.W., Dungan, M.A., Brown, L.L., Deino, A., 1996. Recurrent eruption and subsidence at the Platoro caldera complex, southeastern San Juan volcanic field, Colorado: New tales from old tuffs. Bull. Geol. Soc. Am. 108, 1039–1055. doi:10.1130/0016-7606(1996)108<1039:REASAT>2.3.CO;2

Lipman, P.W., 1997. Subsidence of ash-flow calderas: relation to caldera size and magma-chamber geometry. Bull. Volcanol. 59, 198–218. doi:10.1007/s004450050186

Lipman, P.W., 2000. Calderas. In: Sigurdsson, H. (Ed.), Encyclopedia of Volcanoes. Academic Press, San Francisco, pp. 643– 662.

Lipman, P. and Mullineaux, D., 1981, The 1980 eruptions of Mount St. Helens, Washington. U.S. geological survey professional paper 1250, 844 p;

Ludwig, K. 2008. Manual for Isoplot 3.7. Berkeley Geochronology Center, Special Publication 4, rev. p. 77

Macedonio, G. and Pareschi, M.T., 1991. An algorithm for the triangulation of arbitrarily distributed points: Applications to volume estimate and terrain fitting. Comput. Geosci. 17, 859–874. doi:10.1016/0098-3004(91)90086-S

Macedonio, G., Costa, A. and Longo, A., 2005. A computer model for volcanic ash fallout and assessment of subsequent hazard. Computers & Geosciences, 31(7): 837-845.

Mann, P., 2007. Overview of the tectonic history of northern Central America: In: Mann, P., ed., Geologic and Tectonic Development of the Caribbean Plate Boundary in Northern Central America, Geological Society of America Special Papers 428, pp. 1–19.

Marshall, D. J. 1988. Cathodoluminiscence of geological materials. Unwin Hyman, 181 pp.

Marti J., Ablay G. J., Redshaw L. T., Sparks R. S. J., 1994. Experimental studies of collapse calderas. J Geol Soc Lond 151 :919–929

Marti, J., Gudmundsson, A., 2000. The Las Canadas caldera (Tenerife, Canary Islands): an overlapping collapse caldera generated by magma-chamber migration. J.

Volcanol. Geo- therm. Res. 103, 161–173.

Martí, J., Groppelli, G., & da Silveira, A. B., 2018. Volcanic stratigraphy: a review. *Journal of Volcanology and Geothermal Research*. Volume 357, 15 May 2018, Pages 68-91.

Martínez-Díaz, J.J., Álvarez-Gómez, J.A., Benito, B., Hernández, D., 2004. Triggering of destructive earthquakes in El Salvador. Geology 32, 65–68. doi:10.1130/G20089.1

Mastin, L.G., Guffanti, M., Servranckx, R., Webley, P., Barsotti, S., Dean, K., Durant, A., Ewert, J.W., Neri, A., Rose, W.I., Schneider, D., Siebert, L., Stunder, B., Swanson, G., Tupper, A., Volentik, A. and Waythomas, C.F., 2009. A multidisciplinary effort to assign realistic source parameters to models of volcanic ash-cloud transport and dispersion during eruptions. Journal of Volcanology and Geothermal Research, 186(1): 10-21.

Miles, D H, 1997 The interpretation, presentation, and use of tree-ring dates, *Vernacular Architect*, **28**, 40-56

Moore, I., Kokelaar, P., 1997. Tectonic influences in piecemeal caldera collapse and Glencoe volcano, Scotland. J. Geol. Soc. (Lond) 154, 765– 768.

Moore, I., Kokelaar, P., 1998. Tectonically controlled piecemeal caldera collapse: a case study of Glencoe volcano, Scotland. Geol. Soc. Am. Bull. 110, 1446–1466.

Montero, W., and Dewey, J., 1982. Shallow-focus seismicity, composite focal mechanisms, and tectonics of the Valle Central of Costa Rica: Bulletin of the Seismological Society of America, v. 72, p. 1611–1626.

Nairn, I.A., Wood, C.P., Bailey, R.A., 1994. The Reporoa caldera, Taupo volcanic zone: source of the Kaingaroa Ignimbrites. Bull. Volcanol. 56, 529– 537.

Newhall, C.G., Dzurisin, D., 1988. Historical unrest at large calderas of the world. U.S. Geological Survey. 1109 pp.

Newhall, C.G., Self, S., 1982. The volcanic explosivity index (VEI) an estimate of explosive magnitude for historical volcanism. Journal of Geophysical Research: Oceans 87: 1231–1238 http://dx.doi.org/10.1029/JC087iC02p01231.

Ninkovich, D. Y Heezen, B., C., 1965. Santorini tephra. Colston Pap. (Bristol University), 17, 413.

Peccerillo, A., and Taylor, S. R., 1976. Geochemistry of Eocene calcalkaline volcanic rocks from the Kastamonu area, Northern Turkey. Contrib. Mineral. Petrol., 58:63-81.

Pedrazzi, D., Sunyé-Puchol, I., Aguirre-Díaz, G. J., Costa, A., Davila-Harris, P., Hernández, W. and Gutierrez, E., 2018. The Ilopango Tierra Blanca Joven (TBJ) eruption, El Salvador: volcano-stratigraphy of a major Holocene event of Central America and hazards implications EGU General Assembly 2018, Vol. 20, EGU2018-8455.

Pratt, S.E., 2012, Eruption of El Salvador's Ilopango explains…A.D. 536 global cooling: Earth Magazine, February 25, 2012 issue, 5 p.

Quane, S.L., Russell, J.K., 2005. Ranking welding intensity in pyroclastic deposits. Bull. Volcanol. 67, 129–143. doi:10.1007/s00445-004-0367-5

Rampino, M.R., Self, S., 1993. Climate-Volcanism Feedback and the Toba Eruption of ~74,000 Years Ago. Quat. Res. doi:10.1006/qres.1993.1081

Reimer, P.J., Baillie, M.G.L., Bard, E., Bayliss, A., Beck, J.W., Blackwell, P.G., Ramsey, C.B., Buck, C.E., Burr, G.S., Edwards, R.L., Friedrich, M., Grootes, P.M., Guilderson, T.P., Hajdas, I., Heaton, T.J., Hogg, A.G., Hughen, K.A., Kaiser, K.F., Kromer, B., McCormac, F.G., Manning, S.W., Reimer, R.W., Richards, D.A., Southon, J.R., Talamo, S., Turney, C.S.M., van der Plicht, J., Weyhenmeyer, C.E., 2009. IntCal09 and Marine09 radiocarbon age calibration curves, 0e50,000 years cal BP. Radiocarbon 51 (4), 1111e1150.

Reynolds J., H., 1987. Timing and sources of Neogene and Quaternary volcanism in south–central Guatemala. J Volcanol Geotherm Res 33: 9–22

Richer, M., Mann, C.P., Stix, J., 2004. Mafic magma injection triggers eruption at Ilopango Caldera, El Salvador, Central America. Spec. Pap. 375 Nat. Hazards El Salvador 175–190. doi:10.1130/0-8137-2375-2.175

Rose, W.I., Conway, F.M., Pullinger, C.R., Deino, A., McIntosh, W.C., 1999. An improved age framework for late Quaternary silicic eruptions in northern Central America. Bull. Volcanol. 61, 106–120. doi:10.1007/s004450050266

Saxby, J., Gottsmann, J., Cashman, K., Gutiérrez, E., 2016. Magma storage in a strike-

slip caldera. Nat. Commun. 7, 12295. doi:10.1038/ncomms12295

Schmincke, H.-U., 1967. Cone sheet warm, resurgence of Tejeda caldera, and early geologic history of Gran Canaria. Bull. Volcanol. 31, 153–162.

Sheets, P.D., 1979. Environmental and cultural effects of the Ilopango eruption in Central America. Volcan. Act. Hum. Ecol. 525–564, ill. doi:http://dx.doi.org/10.1016/B978-0-12-639120-6.50022-4

Self, S., 2006. The effects and consequences of very large explosive volcánic eruptions. Phil. Trans. R. Soc. A, 364, 2073-2097. Doi: 10.1098/rsta.2006.1814.

Self, S. y Blake, S., 2008. Consequences of Explosive Supereruptions. Elements, 4, 41-46. DOI: 10.2113/GSELEMENTS.4.1.41

Sigurdsson, H., et al., 2006. Marine Investigations of Greece's Santorini Volcanic Field. Eos 87 (34): 337–348.

Siebert, L., Simkin, T., 2002. Volcanoes of the World: an Illustrated Catalogue of Holocene Volcanoes and their Eruptions. Smithsonian Institution, Global Volcanism Program Digital Information Series, GVP-3, (http://www.volcano.si.edu/world/).

Simkin, T., and Siebert, L., 1994. Volcanoes of the World, 2nd ed., Geoscience Press, Tucson

Smith, R.L., 1979. Ash-flow magmatism: Geological Society of America Special Paper 1749, 180, p. 5–27.

Smith, R.L., Bailey, R.A., 1968. Resurgent caldrons. Mem. Geol. Soc. Am. 116, 613–662.

Smithsonian Global Volcanism Program, 2013, Natural Museum of Natural History, Smithsonian Institution, Washington, U.S. http://www.volcano.si.edu.

Sofield, D., 2004. Eruptive history and volcanic hazards of Volcan San Salvador. Geol. Soc. Am. Spec. Pap. 375, 147–158

Solari, L.A., Gómez-Tuena, A., Bernal, J.P., Pérez-Arvízu, O., and Tanner, M., 2010. U-Pb zircon geochronology with an integrated LA-ICP-MS microanalytical workstation: Achievements in precision and accuracy: Geostandards and Geoanalytical Research, v. 34, p. 5–18.

Sparks, R., S., J., 1979. The Santorini eruption and its consequences. Endeavour, New Series, Volume 3, No. 1.

Sparks, R., S., J., Self, S., Grattan, J.,P., Oppenheimer, C., Pyle, D.,M. y Rymer, H., 2005. Supereruptions: global effects and future threats. Report of a Geological Society of London Working Group, The Geological Society, London, 24 pp

Sun S.S, and McDonough W.F., 1989. Chemical and isotopic systematics of oceanic basalts: implications for mantle composition and processes, in Saunders A.D., and Norry, M.J.,eds ., Magmatism in the Oceanic Basins: Geological Society of London Special Publication 42, p. 313-345.

Suñe-Puchol, I., Aguirre-Díaz, G.J., Dávila-Harris, P., Miggins, D.P., Pedrazzi, D., Costa, A., Ortega-Obregón, C., Lacan, P., Hernández, W., Gutiérrez, E., 2019. The Ilopango caldera complex , El Salvador : Origin and early ignimbrite-forming eruptions of a graben / pull-apart caldera structure. J. Volcanol. Geotherm. Res. 371, 1–19. doi:10.1016/j.jvolgeores.2018.12.004

Stix, J., Kennedy, B. et al. 2003. Caldera-forming processes and the origin of submarine volcano- genic massive sulfide deposits. Geology, 31, 375 – 378.

Tikoff, B., de Saint Blanquat, 1997. Transpressional shearing and strike-slip partitioning inthe Late Cretaceous Sierra Nevada magmatic arc, California. Tectonics 16, 442–459.

Turner, H.L., La Femina, P., Saballos, A., Mattioli, G., Jansma, P., and Dixon, T., 2007. Kinematics of the Nicaraguan forearc from GPS geodesy: Geophysical Research Letters, v. 34, 5 p.

Vallance J., and Houghton B. (1998). The AD 260 eruption at Lake Ilopango, El Salvador: A complex explosive eruption through a caldera lake. National Science Foundation, Research Proposal.

Walker GPL (1988) Three Hawaiian calderas: an origin through loading by shallow intrusions? J Geophys Res 93:14773–14784

Weber H. S., Wiesemann G., Wittek indt H., 1974. Mapa Geológico de la República de El Salvador / Geologische Übersichtskarte der Republik El Salvador 1 : 500,000 (after geological maps 1:100000 – 1967-74) Bundesanstalt für Geowissenschaften und Rohstoffe, Hannover ; Bundesanstalt fu¨r Bodenforschung, Hannover.

Weinberg, R. E., 1992. Neotectonic development of western Nicaragua: Tectonics, 11(5), 1010–1017.

Weyl, R., 1957. Las Tobas Fundidas de la Cadena Costera. Universidad de Kiel, Alemania, DC 5551.2

Williams, H., Meyer-Abich, H., 1955. Volcanism in the southern part of El Salvador, with particular reference to the collapse basins of Lakes Coatepeque and Ilopango. Univ. Calif. Publ. Geol. Sci. 32, 64 p.